DIAGNOSTICS OF MECHANICAL AND ELECTRICAL FAULTS IN INDUCTION MOTORS BASED ON SUPPORT VECTOR MACHINE ALGORITHMS

A Thesis Submitted in Partial Fulfillment of the requirements

for the degree of

DOCTOR OF PHILOSOPHY

by

PURUSHOTTAM GANGSAR

(Roll No. 146103011)

DEPARTMENT OF MECHANICAL ENGINEERING

INDIAN INSTITUTE OF TECHNOLOGY GUWAHATI

GUWAHATI 781039 INDIA

APRIL 2018

Department of Mechanical Engineering
Indian Institute of Technology Guwahati
Guwahati-781039, INDIA

CERTIFICATE

It is certified that the work contained in this thesis titled "**Diagnostics of Mechanical and Electrical Faults in Induction Motors Based on Support Vector Machine Algorithms"** submitted by **Mr. Purushottam Gangsar** (Roll no. 146103011) to the Indian Institute of Technology Guwahati for the award of the degree of Doctor of Philosophy has been carried out under my supervision in the Department of Mechanical Engineering, Indian Institute of Technology Guwahati. This work has not been submitted elsewhere for the award of any other degree or diploma.

April 2018

Dr. Rajiv Tiwari

Professor

Department of mechanical Engineering

Indian institute of Technology Guwahati

Guwahati-781039, INDIA

Acknowledgements

As it is rightly said - “A good teacher can inspire hope, ignite the imagination and instill a love of learning” and I am fortunate to find an inspirer, a task master and a wholesome guru in my supervisor, Professor Rajiv Tiwari, who played a pivotal role in accomplishing my research. Without his time and supervision, it would have been impossible to realize a task as this. I am grateful to him for enabling me to understand, explore, and perform both in the course work and the thesis work during M.Tech and PhD. I wish to place on record the patience with which Professor dealt with me even in the most difficult times of my research. The great virtues of him are etched on my character and molded me to whoever I am today. I wish to collaborate and correspond with him in the future as well.

I found a team of mentors in my doctoral committee comprising of, Prof. Sashindra K. Kakoty, Dr. Karuna Kalita, and Prof. Sudip Talukdar. They periodically assessed my work and gave constructive feedback and inputs for the improvement of this research. I specially would like to thank Dr. Dhruba Jyoti Bordoloi for helping me in the smooth conduct of the laboratory experiments at the Vibration and Acoustic laboratory of Department of Mechanical Engineering, IIT Guwahati. I also would like to thank the anonymous reviewers for taking time off their busy schedule in giving my work the beneficial responses necessary to improve its quality. I would fail in my duties if I would not thank the infrastructure and facilities provided by Indian Institute of Technology Guwahati for the completion of this thesis work.

I am indebted to Department of Mechanical Engineering, IIT Guwahati for the financial support provided to me to felicitate my participation in various prestigious national and international conferences. Thus providing me with enormous opportunities to meet and interact with some of the veteran researchers in my field, especially at the 11th Vibrations in Rotating Machinery (VIRM-11) Conference at University of Manchester, Manchester, UK.

I will cherish the fond memories of my friends who let fun into my research and also gave me technical provisions when necessary. My friends, Mrutyunjay, Uttam, Dipendra, Shruti, Nilakshi, Gyaan, Shivam, Shashi, Rajendra, Sumit, Sunil, Siddesh, Anand Sir, Shyam Sir, Kishore sir, Ashish Sir and Dip Sir will remain close to my heart forever. It would be incomplete if I would not thank the faculty, staff, and students of IIT Guwahati who have actively or passively supported me during my stay here. My parents Shree Bala Prasad Gangsar and Krishna Gangsar, stood as my pillars of support and never let me lose my focus. They gave me all the emotional backing necessary during my crucial years of research and stay at IIT Guwahati.

Last but not the least, I would like to thank the Almighty God for giving me the mental strength and taking care of my near and dear, so that I could dedicate myself completely to this research.

April, 2018

Guwahati

Purushottam Gangsar

Abstract

Continuous and trouble-free operation of induction motors (IMs) is an essential part of the modern power and production plants. Accordingly, this study presents fault diagnostics of the mechanical and electrical faults in IMs through an artificial intelligence (AI) methodology, i.e. the support vector machine (SVM) algorithm. Ten IM fault conditions are considered for the diagnosis, i.e. four mechanical fault conditions (i.e., the bearing fault, the unbalanced rotor, the bowed rotor and the misaligned rotor), five electrical fault conditions (i.e., the broken rotor bar, the stator winding fault with two severity levels, and phase unbalance with two severity levels), and a healthy IM. In order to generate relevant fault signatures of IM faults, vibration signals in three orthogonal directions and current signals of all three phases have been acquired for a wide range of operating conditions (i.e., the speed and the load) using an experimental test rig.

The fault diagnostics of IMs have been performed through the SVM based on the time domain, frequency domain and time-frequency domain features. A comparative investigation of the vibration and current signals have been done in time domain in order to find out which signal(s) (i.e., vibration or/and current) is/are required for an effective SVM based diagnosis of the mechanical and/or electrical faults in IMs. The effect of adjusted sampling rate and data points on the fault diagnostic performances has also been checked using time domain data. The frequency domain data are obtained from time domain data based on the fast Fourier transform (FFT). The time-frequency domain data are obtained by transforming the time domain data based on the continuous wavelet transform (CWT) and the wavelet packet transform (WPT). A number of useful statistical features are extracted from time domain data, frequency domain data, CWT data

and WPT data. These features are further used as input to the SVM classifier. The grid-search technique along with the cross-validation is performed to select optimal SVM parameters, which is required to build an optimal SVM model. This model is used for fault predictions. If a defect exists at any stage, the classifier identifies it, then isolates and finds its severity.

As the prediction accuracy highly depends on features, the wrapper model is used to select the most suitable features for the present fault diagnosis. In the case of wavelet transform, several mother wavelets are considered to study the effects of these on the fault diagnosis. In order to check the robustness of the proposed methodology, the fault diagnosis is performed for various operating conditions of IMs. From the industrial perspective, the fault diagnosis in this study is extended to the intermediate load as well as speed cases in order to perform the diagnosis when database is not available at all the required operating conditions of IMs. The diagnosis based on intermediate operating conditions is a work of practical significance because often fault symptoms' database may not be available at all operating conditions of IMs.

The investigation based on the SVM concludes that to diagnose mechanical faults alone, the vibration signal is good and sufficient. To diagnose electrical faults alone, the current signal is sufficient; however, when the current signal is not available, the diagnosis can be performed successfully with the vibration signal alone. Moreover, when the mechanical and the electrical faults are considered simultaneously for the diagnosis, both the vibration as well as the current signals are required for the effective fault diagnosis. It is also observed that the performance of the SVM based fault diagnosis of IM improves significantly with the low sampling rate data.

Moreover, in all three domains, the fault diagnosis for the same speed and load case is found to be nearly perfect. The fault diagnosis in case of the intermediate speed are found to be satisfactory. However, the fault diagnosis in the case of intermediate load are found to be effective. In all three domains, the most of the considered features have performed the fault diagnosis successfully. The highest prediction performance is achieved with the set of standard deviation, skewness and kurtosis in the time as well as frequency domain, the standard deviation alone in the case of CWT, and the combination of standard deviation and mean in the case of the WPT. In the case of CWT and WPT, all considered mother wavelets with appropriate features are effectively performed the IM fault diagnosis. However, the Shannon wavelet using the standard deviation in the case of CWT, and the discrete Meyer wavelet using the combination of standard deviation and mean in the case of WPT showed the highest prediction.

It is also observed that for the same speed and load case, and the intermediate load case in all three domains, the performance of the fault diagnosis does not depend on the load. However, for the intermediate speed case in all domains, the performance of fault diagnosis reduces at higher load. This may be due to unavoidable fluctuation of speeds under loading conditions. In addition, for all the cases in the time and time-frequency domain, the performance of fault diagnosis does not depend over the speed. However, for all the cases in frequency domain, the diagnosis reduces at lower speeds. This may be due to low signal-to-noise levels at lower speeds in frequency domain signals.

Contents

List of Figures

List of Tables

Nomenclature

C	Soft margin or penalty parameter for support vector machine
$C_{n,j}$	Wavelet coefficient
CF	Crest factor
$E_{overall}$	Overall energy
f_s	Supply frequency
f_r	Rotational frequency of rotor
$g(k)$	High pass filter
$h(k)$	Low pass filter
$k(x, x_i)$	Kernel function
k	Number of classes
L	Langarngian
P_m	Probability distribution of energy
R_{msd}	Mean to standard deviation ratio
R_{pp}	Peak to peak ratio
s	Scale of wavelet
S_i	Spectrum data points
T_1	No load
T_2	Light load
T_3	High load
$\mathbf{w}$	A normal vector to the hyperplane

$W_{j,k}^{m}$	Wavelet packet function
$x(t)$	Time domain signal or data
$\mathbf{x_i}$	Training vector
y_i	Fault's class or label

Greek

α_i	Langrange multiplier
γ	Kernel parameter
κ	Kurtosis
μ_r	*r*-th Statistical moment
μ_1	Mean or first moment
ξ_i	Slack variable for support vector machine
σ	Standard deviation
σ_b	Width of the RBF kernel
τ	Translation parameter of wavelet
$\phi(\mathbf{x})$	Transformation function
χ	Skewness
$\psi^*(t)$	Window function

Abbreviations

AC	Alternate current
AI	Artificial intelligence
ANN	Artificial Neural Network
ART	adaptive resonance theory
BBS	Best basis selection
BEF	Ball element fault
BF	Bearing fault
BP	Back propagation
BR	Bowed rotor
BRB	Broken-rotor bar
CART	Classification and regression tree
CBM	Condition based maintenance
CWT	Continues wavelet transform
CV	Cross validation
CVA	Common vector approach
DAG	Direct acyclic graph
DAQ	Data acquisition system
DC	Direct current
DWT	Discrete wavelet transform
EOP	Emergency operating procedure
ERM	Empirical risk minimization

EWN	Evolving wavelet network
FL	Fuzzy logic
FFT	Fast Fourier transform
FNN	Fuzzy neural network
GA	Genetic algorithm
GDA	Generalized discrimination analysis
HMM	Hidden Morkov model
HHT	Hilbert-Huang transform
HOS	Higher order statistics
HT	Hilbert transform
ORF	Outer race fault
IACO	Improved ant colony optimization
ICA	Independent component analysis
IR	Infrared
IRF	Inner race fault
LDA	Linear discriminant analysis
LDB	Local discriminant basis
LIBSVM	A library for support vector machine
MCSA	Motor current signature analysis
MFS	Machine fault simulator
MLBS	Multi-level basis selection
MLP	Multilayer perception
MR	Misaligned Rotor

MRA	Multi resolution analysis
MUSIC	Multiple signal classification
ND	No defect condition of induction motor
OASYS	On-line operator aid system
ORF	Outer race fault
OVA	One versus all
OVO	One versus one
PCA	Principal component analysis
PD	Partial discharge
PDF	Probability distribution function
PSWT	Pitch synchronous wavelet transform
PUF	Phase unbalance fault
PUF1	Phase unbalance fault level-1
PUF2	Phase unbalance fault level-2
PVM	Park vector machine
RBF	Radial basis function
RFE	Recursive feature elimination
RMS	Root mean square
RUWPT	Recursive un-decimated wavelet packet transform
RWE	Relative wavelet energy
SFAM	Simplified fuzzy ARTMAP
SLBS	Single-level basis selection
SOM	Self-organizing map

SRM	Structural risk minimization
STFT	Short time Fourier transform
SVM	Support vector machine
SWF	Stator winding fault
SWF1	Stator winding fault level-1
SWF2	Stator winding fault level-2
SVs	Support vectors
TDA	Time domain averaging
UMP	Unbalanced magnetic pull
UR	Unbalanced rotor
VFD	Variable frequency drive
WPT	Wavelet packet transform
WT	Wavelet transform
WVD	Wigner-Ville distribution

CHAPTER 1

Introduction and Literature Survey

1.1 Introduction

This chapter presents an overview of the existing literature on the condition monitoring and fault diagnosis of rotating machineries, mainly induction motors (IMs). Initially, the importance of the present study is discussed in brief. Then the condition monitoring and fault diagnosis of rotating machines are discussed. The importance of the condition based maintenance (CBM) in the industry is also added in the same section. After that, various problems in IMs and their identification techniques available in the literature are described. The outcome of the literature survey is described next. Then the aims and objectives of this thesis are presented. The chapter concludes with a brief description of various chapters in the thesis.

1.2 Importance of Study

Rotating machineries become the backbone of the industrial world, since they play a vital role in the power generation, manufacturing and transportation industries. The most commonly used rotating machines are turbines, generators, electric motors, rotary engines, pumps, compressors and fans. Rotating machines reliability and availability are crucial to ensure a trouble free and continuous operation in the industry. These machines are subjected to various unavoidable stresses such as the mechanical, electrical, thermal and environmental, throughout the operation due to the variable loading, unbalanced power supply, dusty environment and natural aging. This leads to creation of some modes of unexpected faults in different components of the machines. These faults

are usually left unnoticed in its primary stage; and this ends up with the catastrophic machine failure. Consequently, an industry has to bear a huge financial loss due to process shutdown or sometimes serious human wounds. Therefore, for early fault detection of the machine component that begin to degrade and to avoid the likelihoods of catastrophic machine failure, condition monitoring of rotating machines, is gaining importance in industry. Condition monitoring provides continuous evaluation of the health of the machines and its components throughout its serviceable life. Early detection of machine faults, offers adequate warning of imminent failures, condition based maintenance and minimum downtime (El-Shafei and Rieger, 2003; Jardine et al. 2006).

1.3 Condition Monitoring and Fault Diagnosis of Rotating Machines

The condition monitoring is a continuous process of monitoring of certain machine parameters related to the operation and structural condition of the machinery. It helps to judge whether the machines are in normal or deteriorating condition, which could prevent otherwise unforeseen damages. In order to retain or restore a machine to a specified operable condition or to achieve its maximum useful life, various maintenance strategies have been developed. The maintenance strategies mainly divide into three groups as shown in Figure 1.1.

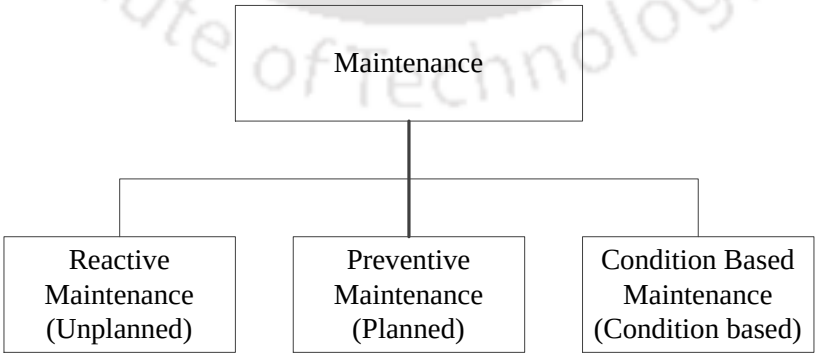

Figure 1.1 Maintenance strategies

The reactive maintenance is the earliest maintenance technique. It is basically a breakdown maintenance, which takes place only at the breakdowns. It is also called unplanned maintenance, or run-to-failure maintenance. After that, another maintenance technique, i.e. time-based preventive maintenance was introduced, which sets a periodic interval to perform preventive maintenance regardless of the health status of a machine. It is also called planned or scheduled maintenance. However, with the rapid development of modern technology, products have become more and more complex while better quality and higher reliability are required. This makes the cost of preventive maintenance higher and higher. Eventually, the preventive maintenance has become a major expense of many industrial companies. Therefore, more efficient maintenance approaches such as the condition-based maintenance (CBM) also called predictive maintenance are being developed to handle the situation (Martin, 1994).

CBM is a maintenance program that recommends maintenance actions based on the information collected through condition monitoring. CBM attempts to avoid unnecessary maintenance tasks by taking maintenance actions only when there is evidence of abnormal behaviors of a machine. A CBM program, if properly established and effectively implemented, can significantly reduce maintenance cost by reducing the number of unnecessary scheduled preventive maintenance operations (Jardine et al. 2006; Randall, 2011). The procedure of CBM is as shown in Figure 1.2.

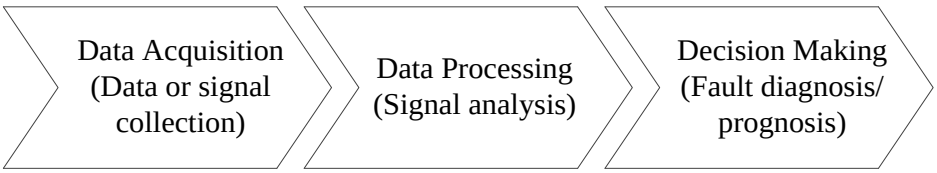

Figure 1.2 Components of the condition based maintenance

The data acquisition is a process of CBM of collecting and storing useful data or information from the targeted physical assets. The condition monitoring data are very versatile. It may be the vibration, current, acoustic, temperature, pressure, oil analysis data, etc., depending upon the machine. In order to acquire the data, various sensors such as the accelerometer, current probes, acoustic emission sensors, ultrasonic sensors, thermocouples, pressure sensors, etc. have been developed.

The data processing includes the process of feature extraction of different faults of a machine. The feature extraction is used to reduce the dimension of data by selecting the important features. The accuracy and effectiveness of signal processing techniques depend on the feature characteristics that can be obtained from the time, frequency, and time-frequency domain (Jardine et al. 2006). The simplest form of signal processing is that the magnitude of the raw incoming signal is examined on a regular basis in the time domain. The signal processing in such cases may consist of a comparison of the current record with the previous value or with some preset or predetermined threshold. The earlier example of magnitude detection implies that the motor condition information is seeded in the change of signals obtained from the motor. The variation of signals usually tells us the change of condition. Many techniques can be used for time-domain analysis. Traditional time domain calculates characteristic features from time waveform signal as descriptive statistics such as the mean, peak, peak-to-peak interval, standard deviation, skewness, kurtosis, and higher order statistics, etc. These features are usually called time domain features. Time domain averaging (TDA) is a traditional and typical method to detect fault signals in rotating machines. It extracts a periodic component of interest from a noisy compound signal. Data-clustering techniques are used to extract an average pattern that serves as the mechanical imbalance indicator (Lin, 2009)

Frequency-domain analysis is more attractive than time domain analysis because it can provide more detailed information about the status of the machine. In the frequency domain, spectral analysis is a very useful technique of signal processing used in the fault diagnosis. Spectral analysis is effective when applied to steady-state periodic signals, which is usually the case with monitoring machine faults that gradually develop. To improve the data processing, methods based on fast Fourier transform (FFT), Hilbert transform (HT) and high resolution spectrum analysis have been applied (Mehrjou et al., 2011). The FFT is the most widely used technique in the frequency domain. The concept of FFT based techniques relies on analyzing the whole spectrum or identifying certain fault frequencies or harmonics related to a particular fault and thus extracting features from the signals. The nature of the signals of rotating machines may be stationary or non-stationary. For stationary signals, the FT provides an ideal candidate for feature extraction. However, FT suffers from the problem of frequency band resolution and is not suitable for the transient and non-stationary signals. Many factors, including the change of the environment and the faults from the machine itself, often make the output signals (of the running motor) transient and non-stationary (Thomson and Orpin, 2002). These signals often contain inherent information of the faults that cannot be revealed by the traditional FFT based technique.

For non-stationary signals, features reflecting machine faults do not consist of regular frequency components with respect to time. They often demonstrate a transient nature, and carry small components embedded in larger repetitive signals. Thus, to handle the transient and non-stationary signals, and the problem of frequency resolution various time-frequency analysis have been developed such as the Wigner-Ville distribution (WVD), short-time Fourier transform (STFT), and wavelet transform (WT) (Peng and Chu, 2004). However, the WT is preferred over other time-

frequency analysis because it uses varying window (called mother wavelet) for different frequency signals that make it suitable for de-noising and extraction of weak signals, singularity detection, and, the system and parameter identification (Peng and Chu, 2004).

Three variants of WT, i.e. continuous wavelet transform (CWT), discrete wavelet transform (DWT) and wavelet packet transform (WPT) have been developed and used for the fault diagnosis. The ability to examine the local behavior of the signal with reasonably precise frequency information is one of the most important features of the WT. Due to its good properties in time-frequency domain analysis the wavelet analysis has gained much attention from many engineering fields. The WT technique has been developed to reveal the hidden information that is not readily available in the raw signals (Chow and Hai, 2004; Antonino-Daviu et al. 2006). Whereas the CWT and DWT provide the signal analysis with more flexible time-frequency resolution, their drawback is that they cannot split the high frequency band where the modulation information of machine fault always exist. The expansion of classical WT, i.e. the WPT can overcome this difficulty of frequency resolution in the high frequency region (Yan et al. 2014).

The third step of CBM, i.e. the maintenance decision making is an essential step in implementing a CBM program for the machine fault diagnosis and prognosis. The diagnosis deals with the fault detection, isolation and identification when it occurs. The fault detection indicates whether something is going wrong in the machine; the fault isolation locates the machine component that is faulty; and the fault identification determines the severity of the fault when it is detected. The prognosis deals with the machine fault prediction before it occurs. Obviously, the prognosis is superior to diagnosis in the sense that it can prevent faults or failures, and if impossible, be ready

(with prepared spare parts and planned human resources) for the problems, and thus save extra unplanned maintenance cost. Nevertheless, the prognosis cannot completely replace the diagnosis since in practice, there are always some machine faults and failures that are not predictable. Besides, the prognosis, like any other prediction techniques, cannot be 100% sure to predict faults and failures. In the case of unsuccessful prediction, the diagnosis can be a complementary tool for providing a maintenance decision support. In addition, the diagnosis is also helpful in improving the prognosis in the way that the diagnostic information can be useful for preparing more accurate event data and hence building better CBM model for the prognosis. Furthermore, the diagnosis information can be used as useful feedback information for the system redesign (Jardine, 2006).

Machine fault diagnostics is a procedure of mapping the information obtained in the measurement space and/or features in the feature space to machine faults in the fault space. This mapping process is also called the pattern recognition. Different conventional pattern recognition methods are available which can identify certain faults in machines, such as the power spectrum graph, phase spectrum graph, cepstrum graph, AR spectrum graph, spectrogram, wavelet scalogram, wavelet phase graph, etc. However, these techniques often present several problems in terms of complexity and cost. The conventional signal based methods are not always reliable as they depend over the operating conditions of the motors (Lee et al., 2006). In addition, other fault diagnosis methods are also available based on mathematical modelling of machines (Rong and Xiuhe, 2007). Based on the explicit model, residual generation methods such as the Kalman filter, parameter estimation (or system identification) and parity relations are used to obtain signals, called residuals, which is an indicative of the fault presence in the machine. Finally, the residuals are evaluated to arrive at the fault detection, isolation and identification. The model based diagnosis can be more effective

than other model free approaches, if accurate model is developed. However, several assumptions must be made to develop a mathematical model to take care of the nonlinear and stochastic machine dynamics, still it is not robust enough in the presence of perturbation and noise (Bilski, 2014). In addition, explicit modelling may not be possible and feasible for complex systems because it is not easy to consider the disturbances and the uncertainty in the models.

The conventional signal based method is more accurate and preferred than the model based method because it does not require any assumptions and complex mathematical models (Da-Silva et al., 2008). The machine fault diagnosis based on conventional methods, mathematical models require practice engineers to have sufficient knowledge and experience. As the number of rotating machines is increasing steadily in all types of industries, so it is not practical to fulfill the demand of required expertise. The increasing economic pressure requires the development of a cost-effective maintenance system to guarantee machine operating reliability and at relatively low cost. Therefore, during the last decade, in order to automate, improve the reliability and sensitivity, and reduce the cost of the fault monitoring and diagnosis technique, a more sophisticated technique, called intelligent fault diagnosis, is developing and growing popularity in the field of mechanical engineering (Siddique et al. 2003).

The intelligent fault diagnosis is possible by incorporating artificial intelligence (AI) into the online machine condition monitoring. The AI based diagnoses have shown improved performance over the conventional signal and modelling based approaches. This reduces the direct human-machine interaction for the diagnosis. Moreover, these are data based techniques; therefore they do not require any detailed knowledge of the IM model and parameters. These techniques use

association, reasoning and decision making processes as would the human brain in solving diagnostic problems. These diagnostic techniques involve signal processing methods and classification tools such as the neural network (NN), fuzzy logic (FL), fuzzy neural network (FNN), genetic algorithm (GA), Hidden Morkov model, Bayesian classifier and SVM (Baccarini et al. 2011; Zhou et al. 2016).

The development of AI based diagnostic system in the machine condition monitoring is summarized here. For example, Chang et al. (1995) developed the on-line operator aid system (OASYS) to support the operator's decision making process and to ensure the safety of a nuclear power plant by providing operators with proper guidelines in a timely manner, according to the plant operation mode. The OASYS uses a rule-based expert system and fuzzy logic. The rule-based expert system is used to classify the predefined events and track the emergency operating procedures (EOPs) through data processing, and the fuzzy logic is used to generate the conceptual high-level alarms for the prognostic diagnosis and to evaluate the qualitative fuzzy criteria used in the EOPs. Evaluation results show that the OASYS is capable of diagnosing plant abnormal conditions and providing operators appropriate guidelines with fast response time and consistency. Liu et al. (1996) applied the fuzzy expert system for the fault detection in bearing. Ayoubi and Isermann (1997) gave an overview of integration techniques for the fuzzy expert system and the adaptive neural network. A special focus was given to develop a hybrid neuro-fuzzy network for monitoring the air pressure in vehicle tires. Mechefske (1998) applied fuzzy logic techniques to classify various rolling element bearing faults based on frequency spectra. Li et al. (2000) performed the fault diagnosis of rolling bearings of motors using neural networks and time/frequency-domain vibration analysis.

Qingling et al. (2001) used the fuzzy back propagation (BP) network to diagnose various faults in rotating machines (such as the unbalance, misalignment, hydraulic and aerodynamics forces, rotational disconnection, surge and film whirling motion). Huang and Huang (2002) developed evolving wavelet networks (EVNs) for the condition monitoring and fault diagnosis of power transformers. They compared the results with the fuzzy diagnostic system and the ANN, and concluded that the EWNs have a better capability for generalization than the fuzzy system and the ANN. Jack et al. (2002) illustrated the fault detection of roller bearings using the SVM and the ANN. They defined and estimated statistical features based on moments and cumulants, and selected the optimal features using the GA. Zhang et al. (2003) applied fuzzy neural networks (FNN) in fault diagnosis of rotary machines, especially to water pump sets of oil plants, and concluded that the FNN improves the recognition rate of the pattern recognition even when the sample data are similar.

Samanta et al. (2003) performed ANN based fault diagnostics of rolling element bearings using time domain features. In other work, Samanta et al. (2003) used ANN and SVM with genetic algorithm for bearing fault detection. Samanta (2004) performed the gear fault detection using the ANN and the SVM, and concluded that the SVM can perform well in comparison with the ANN even with the smaller number of samples and also the training time is less in case of SVM. Rojas and Nandi (2005) proposed the development of SVM for the detection and classification of rolling bearing faults. The training of SVM was done using sequential minimal optimization algorithm, and a mechanism for selecting adequate training parameter was also proposed. This makes the classification procedure fast and effective.

Widodo and Yang (2007) summarized and reviewed the recent research and developments of the SVM in the machine condition monitoring and diagnosis. They showed that various intelligent systems such as the ANN, fuzzy logic, condition based reasoning and random forest have been developed for the machine fault diagnosis; however, the use of SVM is rare in the same field. The SVM has excellent performance in generalization, so it can produce high accuracy in the classification for machine condition monitoring and diagnosis. Until 2006, the use of SVM in the machine condition monitoring and fault diagnosis was tending to develop towards the expertise orientation and problem-oriented domain. Finally, they concluded that the ability to continually change and obtain an idea for the machine condition monitoring and fault diagnosis using the SVM will have lots of scope in near future.

After that, in a work Hu et al. (2007) performed the fault diagnosis in rolling element bearings based on an improved WPT and the SVM ensemble, and achieved a high prediction rate even in the presence of noise. Yu et al. (2007) illustrated a fault diagnosis approach for roller bearing based on the intrinsic mode function (IMF) envelope spectrum and the SVM. Sui et al. (2009) illustrated rolling element bearings fault classification based on the feature evaluation with the SVM. The feature evaluation based on the class separatibility criterion was discussed in this work. Yang et al. (2007) applied a fault diagnosis approach for roller bearing based on IMF envelope spectrum and SVM. Sugumaran et al. (2008) presented fault diagnostics of roller bearing using kernel based neighborhood score multi-class support vector machine. Xian and Zeng (2009) performed an intelligent fault diagnosis of the rotating machinery based on the WPT and the SVM. In, addition, they compared the performance of the hybrid SVM and the back-propagation (BP) network. They

concluded that the accuracy of SVM is better than those of the BPN, and the SVM spent less time than the BPN in classification.

Meng et al. (2010) performed a comparison between the RBF neural network and the SVM for cases where only limited training samples were available for the fault diagnosis of rolling bearing. The result showed that the SVM had better performance than the RBF neural network both in the training time and the prediction accuracy. Saravanan and Ramachandran (2010) performed incipient gear box fault diagnosis using DWT and ANN. Sugumaran et al. (2010) illustrated the effect of number of features on the classification of roller bearing faults using the SVM and the proximal support vector machine (PSVM). A set of statistical features and histogram features were extracted from time domain signals and the order of importance was found using decision tree. In other work, Kankar et al. (2011) presented fault identification in ball bearings based on the CWT and the AIs (i.e. the ANN, Self-Organizing Map (SOM) and SVM). Six different wavelets were considered in the study. Finally, they concluded that Meyer and complex Meyer wavelet with the SVM gives the best performance for the bearing fault diagnosis.

Li et al. (2012) successfully used the WPT feature and the SVM for the fault diagnosis of the gearbox and gasoline engine valve trains. Zheng et al. (2012) illustrated the rolling element bearing fault diagnosis based on the SVM. In this paper, the wavelet packet analysis was used to extract the features from the vibration signal and the principal component analysis (PCA) was performed for features reduction. Liu et al. (2012) illustrated the multi-fault classification based on the wavelet SVM (WSVM) with the particle swarm optimization (PSO) algorithm to analyze vibration signals from rolling element bearings. Li et al. (2013) performed the fault diagnosis of rolling

element bearings by the SVM. Improved ant colony optimization (IACO) algorithm was used for the optimization of SVM parameters. Zhu et al. (2014) illustrated the roller bearing fault diagnosis method based on the hierarchical entropy and the SVM with the PSO algorithm. Gangsar and Tiwari (2014) successfully applied SVM for bearing fault diagnosis at interpolated speed and extrapolated speed using vibration signals. Bordoloi and Tiwari (2014) performed the optimum multiclass classification of gears with integration of the evolutionary and SVM algorithms. In another work, Bordoloi and Tiwari (2014) attempted the fault classification of gears using wavelet based features and the SVM. The genetic algorithm, grid-search method and artificial bee colony algorithms were used for optimizing SVM parameters.

As the condition monitoring and diagnosis of rotary machines has moved from traditional techniques to AI techniques, so there is much scope of research in this field. The AI based diagnostic systems still have several challenging tasks to accomplish in regards to its efficiency, reliability, computational time, sufficient database, and robustness. Nowadays, the SVM is extensively gaining popularity in machine fault diagnosis owing to their best prediction performance, and less training and testing time. In addition, SVM has advantages of handling large amount of data with several classes. It can effectively classify this data into classes using feature spaces. The best property of SVM algorithms is that it can perform well even with the small number of training and testing data; hence, reduces the computational load. The basics of SVM have been developed by Vladimir Vapnik in 1994, which is based on binary class classification. Later, the SVM has been extended to the multiclass-classification from the binary class classification in order to classify the multi-fault in machines (Hsu and Lin, 2002). In order to compare multiclass SVM techniques, Hsu and Lin (2002) and Hsu et al. (2003) presented a

comparison among different methods of multiclass SVM through different kernels, and concluded that one-versus-one method is most effective for the classification, among the one-versus-one (OVO), one-versus-all (OVA) and direct-acyclic graph SVM (DAGS) methods. In addition, various kernel function such as, the linear, polynomial and sigmoid, have been developed to handle nonlinear problem through the SVM. However, the RBF kernel produced better result, among other kernels. The research on fault diagnosis based on the SVM is still continuing on different rotating machines. On consideration of focus of the present work, the literature review on the condition monitoring and fault diagnosis of induction motors is presented in the subsequent section.

1.4 Condition Monitoring and Fault Diagnosis of Induction Motors

Various rotating machineries such the pumps, compressors, blowers, fans, etc., and industrial machineries such as the machine tools, cranes, conveyors, motor vehicles, etc. operate with the help of electric motors. Over 50% of the total electrical energy generated globally is utilized by motors, mainly induction motors (IMs), which consumed around 60% of the industrial electricity (Bazzi and Krein, 2010). Deployment of IMs in all types of industries is increasing day by day owing to their low cost, ruggedness, high power to weight ratio, and adaptability to a wide variety of operational conditions (Zhang et al., 2011). In spite of their reliability, they usually fall out of service due to following reasons: unusual mechanical load, power supply deviation, improper or inadequate lubrications, more heat and ineffectual sealing, dusty environment and manufacturing defect. Hence, the early detection of faults in IMs is very important in order to prevent the complete failure of motor and unexpected huge production losses in the industry (Henao et al. 2014).

An IM consists of three main components called the stator, rotor and bearings (as shown in Figure 1.3). The stator, as its name indicates, is a stationary component of an IM. It consists of a stator frame, stator core and stator winding or field winding. The stator frame is used to support the stator core and windings. It provides protection and mechanical strength to all inner components of the IM. The stator core is constructed from insulated laminations which are stamped together in order to reduce the eddy current loss. They are generally made of silicon steel, which helps to reduce the hysteresis loss occurring in the motor. The slots on the periphery of the stator core carry three-phase windings. Three-phase winding is supplied by three-phase AC supply that produces a rotating magnetic field.

The rotor is a rotating component of an IM, which is connected to the mechanical load through the shaft. Two types of rotors are used in three phase IM, i.e. squirrel cage rotor and slip ring (or wound) rotor. The squirrel cage rotor consists of aluminum, copper or brass bars, which is also called the rotor conductors. These conductors are placed in slots on the periphery of the rotor and permanently shorted by the end ring. In order to provide the mechanical strength these conductors are braced to the end ring and hence form a complete closed circuit resembling like a cage, and hence it got its name as the squirrel cage rotor. IMs with this kind of rotor is called squirrel cage IMs. Unlike the squirrel cage rotor, the slip ring (or wound) rotor consists of numbers of slots and rotor winding are placed in these slots. As its name indicates, the slip ring rotor consists of slip rings, which are permanently connected to three-phase winding. In this study, three-phase IMs with the squirrel cage rotor is used. The bearing is one of the main components of IM that support the rotating shaft. A fan is used for cooling the IM.

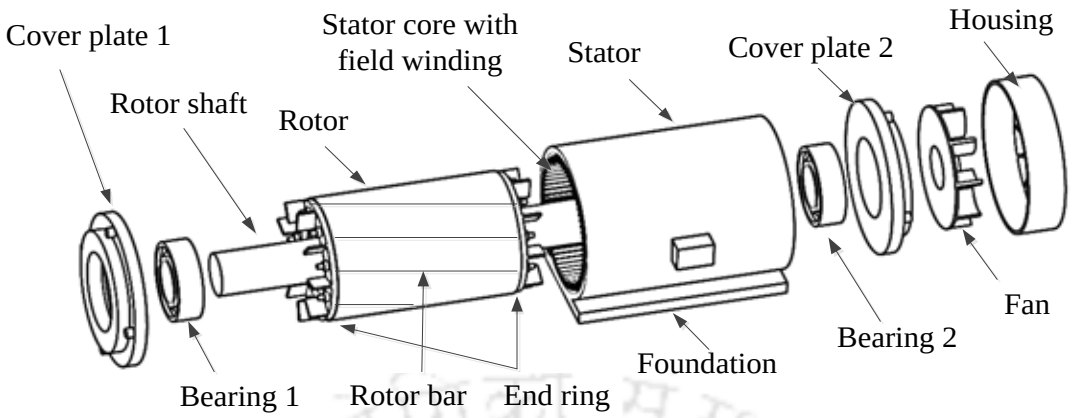

Figure 1.3 The schematic exploded view of an induction motor

1.4.1 Various Types of Faults in Induction Motor

The IM fails due to damage in any of the IM components, i.e. the stator, rotor and bearing. The true percentage of failure of IM components is described as (Albrecht et al., 1987; Benbouzid, 2000).

1. Bearing faults; 41-42 %
2. Stator winding faults; 28-36 %
3. Rotor related faults; 8-9 %
4. Other faults; 14-28 %

The bearing fault and the stator winding fault together account for more than at least 69 % of the total motor faults. Though, the rotor and shaft damages appear less significant, the most of bearing damages are produced due to the rotor eccentricity, shaft unbalance and misalignment, and sometimes winding damage are also produced due to rubbing of the broken and misaligned rotor. The majority of winding failure occurs due to unbalanced supply. If the fault coverage is extended

to include rotor related faults (such as the broken rotor bar, unbalanced rotor, and misaligned and bowed rotor) and other IM faults (such as, the phase unbalance and single phasing), more than 90% of all fault modes are covered.

The IM faults can be broadly classified as either mechanical or electrical faults, as shown in Figure 1.4 (Zhang et al., 2011).

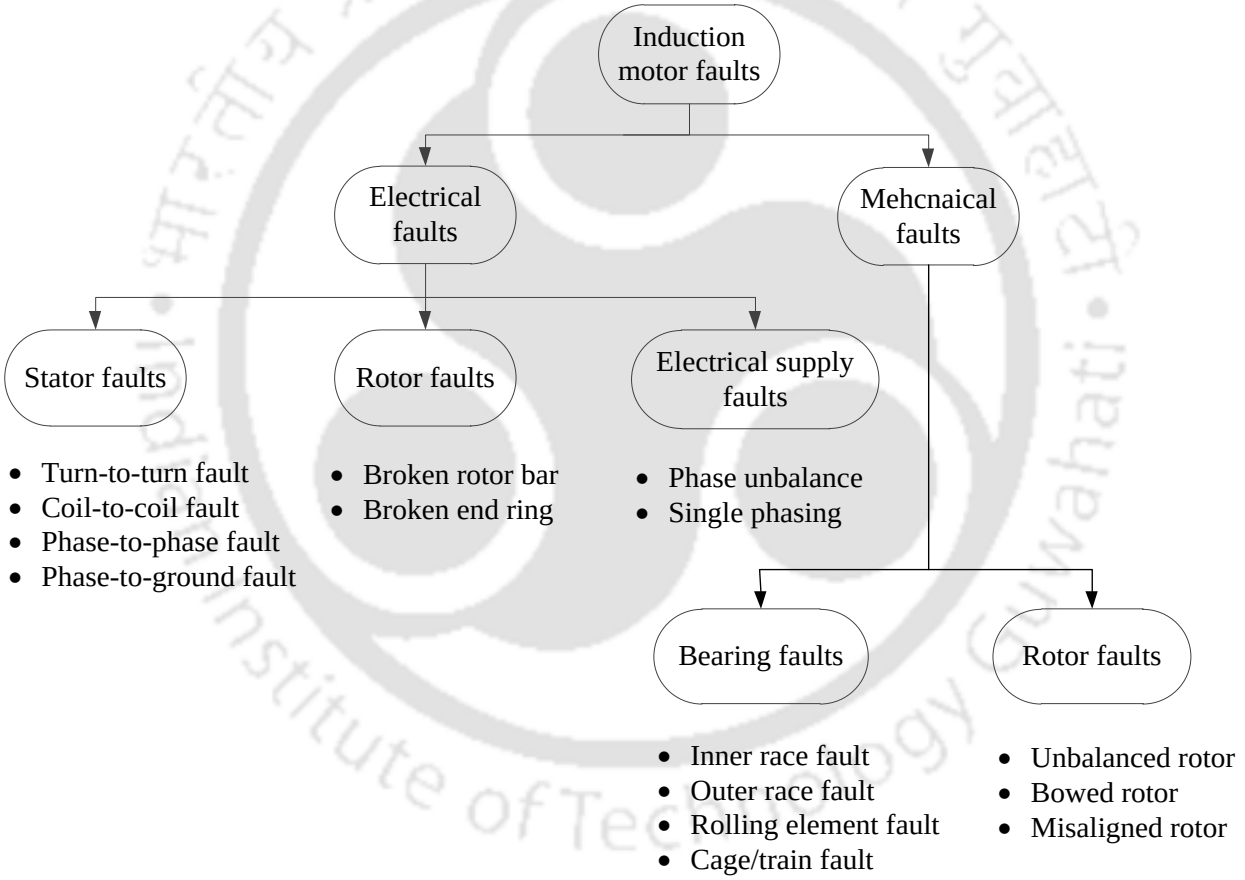

Figure 1.4 Types of common induction motor faults

The mechanical faults include the bearing faults (such as inner race fault, outer race fault, rolling element fault, and cage fault) and the rotor faults (such as unbalanced rotor, misaligned rotor,

bowed rotor, and etc.). The electrical faults include the stator winding fault (such as turn-to-turn fault, coil-to-coil fault, phase-to-phase fault, phase-to-ground fault, and etc.), the rotor related faults (such as broken rotor bar, broken end ring, and etc.) and the electrical supply related faults (such as phase or voltage unbalance, single phasing, and etc.). Different mechanical and electrical faults of IM are discussed here.

1.4.1.1 Mechanical Faults in Induction Motors

About 45-55% of IM failures occur due to mechanical faults. Now, various mechanical faults are described below:

A. Bearing fault*:* The most IM use either the ball or roller bearing, which consists of the inner race, outer race, rolling element and train (or cage) as shown in Figure 1.5. The bearing fault (BF) occurs due to damage in the outer race, inner race, rolling element and train. The main causes of the bearing failure are: high vibration of the rotor due to large output load torque that ultimately leads to high fatigue stress, improper installation of bearing, deterioration of lubrication due to shaft voltage directing to high current in bearing, due to heat conducted through the shaft, and ultimately friction and contamination. The consequence of bearing fault is the motor rotor becomes eccentric in the stator bore, causing unbalanced magnetic pull (UMP), and placing more load on bearings. The bearing fault is one of the reasons of excessive vibration in the motor as the shaft dynamics are affected by the altered air-gap between the rotor and stator, and the bearing stiffness. The ultimate effects of bearing faults are rotor bar failures, which lead to a premature failure of IMs.

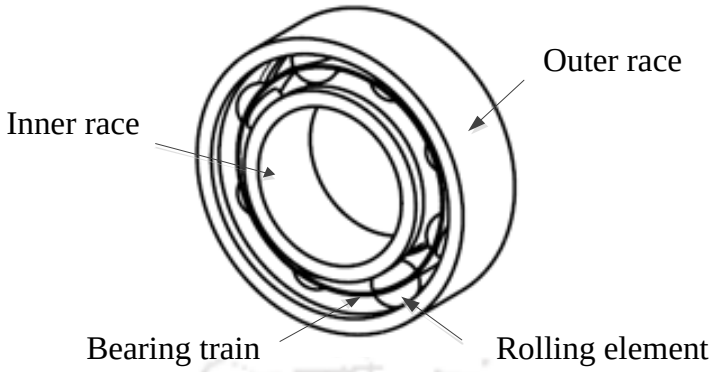

Figure 1.5 A typical ball bearing of an IM

B. Rotor related fault: In a healthy motor, the rotor is centrally aligned with the stator and the axis of rotation of the rotor, and is the same as the geometrical axis of the stator. This results in identical air gap between the outer surface of the rotor and the inner surface of the stator. However, if the rotor is not centrally aligned or its axis of rotation is not the same as the geometrical axis of the stator, then the air-gap will not be identical and the situation is referred as the air-gap eccentricity. In fact, the air-gap eccentricity is a common rotor fault in an IM. Eccentricities can be divided into two types, i.e. the static and the dynamic, as shown in Figure 1.6. In the static eccentricity the position of the minimal radial air-gap length is fixed in space, while in the dynamic eccentricity the position of minimal air-gap rotates with the rotor. When eccentricity becomes large, resulting unbalanced radial forces can cause the stator to rotor rub, and this can result in damage of the stator and the rotor. The eccentricity may be caused by a relative misalignment of rotor and stator in the commissioning stage, wrong placement of bearing, misalignment of load axis and rotor shaft, unbalanced load, bearing wear, and mechanical resonance at the critical speed.

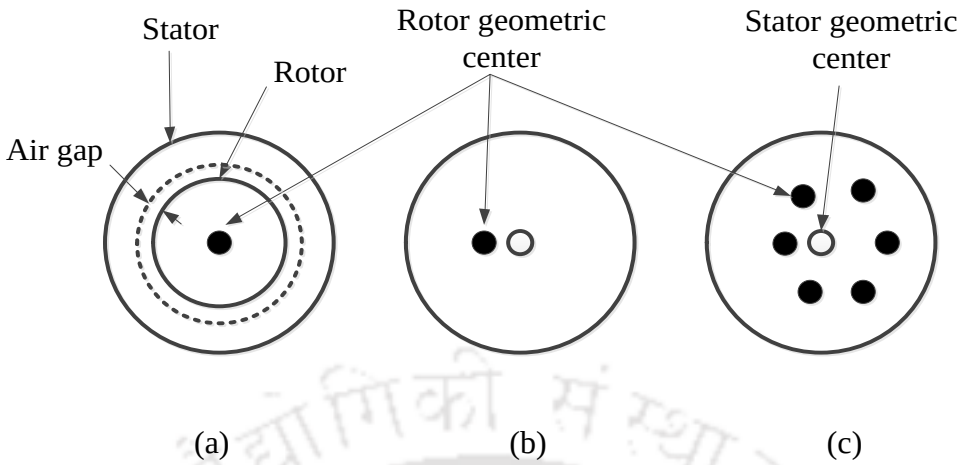

Figure 1.6 The air-gap eccentricity in the IM (a) normal motor (b) motor with static eccentricity (c) motor with dynamic eccentricity

***(i) Rotor Misalignment*:** The rotor misalignment or misaligned rotor (MR) is of two types, i.e. the parallel and angular misalignments. In the parallel misalignment, the minimal air-gap between the rotor and the stator is fixed, and it is due to incorrect positioning of the rotor and the stator core at the commissioning stage. In the angular misalignment, the center of rotor does not coincide with the center of rotation of the rotor, and the minimal air-gap rotates with the rotor; and it is due to several reasons like the bent rotor shaft, unbalance, and bearing wear. Maximum 10 % air-gap eccentricity is permitted in IMs. The MR creates the static air-gap eccentricity. When it crosses a permissible limit, the resulting unbalance force can cause rotor to the stator rubbing, core damage and ultimately the destruction of the IM.

***(ii) Bowed rotor**:* The bowed rotor (BR) and bent rotor are actually same phenomenon, but only difference is that the bowed rotor is measurable inside the machine housing while the bent rotor can be observed outside the machine also. It creates the dynamic air-gap eccentricity. The BR is

caused by local rubbing (resulting in permanent metallurgical changes), local expansion and yielding (resulting in permanent bowing and cracking), weight of the rotor by sitting stationary for a long time, and residual stresses. The ultimate effect of BR is the rotor misalignment, rotor-to-stator rubbing, and ultimately damage of the motors.

***(iii) Unbalanced rotor**:* The unbalanced rotor (UR) can be defined as an uneven distribution of mass on the rotor. This is also a primary cause of vibration in IMs. The UR consists of the static and dynamic unbalances. The static unbalance is due to only unbalanced forces, while the dynamic unbalance is due to the unbalance force as well as the unbalance couple. The UR produces excessive centrifugal forces, vibrations that reduce the life of rotor, bearings, coupling, seals, and gears. The small amount of UR may cause severe problems in high speed induction motors. In actual practice, a rotor can never be perfectly balanced because of the manufacturing defects, non-uniform density of material, and gain or loss of material during operation. The unbalance rotor is caused by mainly broken the rotor bar, resulting total damage of the motor.

1.4.1.2 Electrical Faults in Induction Motors

About 35-40 % of IM failures occur due to the electrical faults. Various electrical faults are described below:

***A. Stator winding fault**:* The stator winding fault (SWF) can occur due to the turn-to-turn, coil-to-coil, phase-to-phase or phase-to-ground fault as shown in Figure 1.7. Most of the winding faults are the consequence of the growth of undetected turn-to-turn faults. The main cause of the turn-to-turn fault is long term thermal aging and ultimately insulation failure. The SWF can occur due

to the excessive heating (thermal stress), the unbalance power supply (electrical stress), the hitting by broken, unbalanced, or misaligned rotor bar (mechanical stress), the vibration, the failure during installation, and the contamination by oil. The SWF may lead to the opening, shorting or grounding of one or more circuit of winding, excessive heating and total damage of machines. These faults produce non-uniform magnetic field in the air-gap of IM that causes unbalanced air-gap voltage and line current, high mechanical vibration and increased torque pulsation.

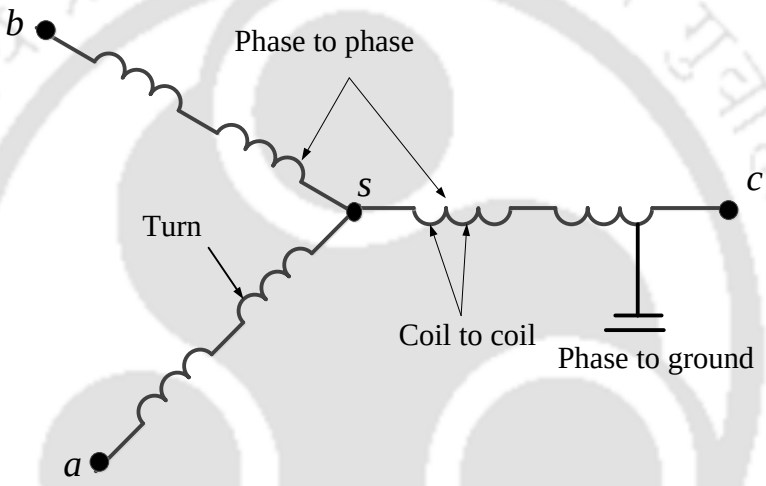

Figure 1.7 Various possible faults in stator winding of an IM

B. Broken rotor bar faults*:* Although the rotor of a squirrel cage induction motor is exceptionally rugged, the broken rotor bar (BRB) occurs due to failure of rotor bars and end rings. The BRB is the main reason of the rotor faults in induction motor, which occurs mainly due to the fluctuation in loading and the direct online starting. The BRB can also occur due to frequent start at rated voltage, thermal unbalance and over-loaded during starting (thermal stress), unbalanced magnetic pull, electromagnetic force and noise (magnetic stress), and fabrication defect (mechanical stress). The main cause of BRB is electrical related, therefore it is characterized in the electrical faults.

These faults produce localized heating or arcing in the rotor, vibration due to expansion of rotor and bowing, stray leakage flux, fluctuation of speed, supply current and torque pulsation. The BRB produces fault frequencies or side-bands in both in the current as well as vibration signals, however, it is more difficult to detect BRB in vibration spectrum than the current spectrum because of its small amplitudes in the former.

C. Phase unbalance and single phasing fault*:* The phase unbalance produced when the voltages are not equal (unbalanced) between three phases. The small amount of voltage variation causes drastically increase of current in the motor winding, if allowed for some time, then the total damage of the motor occurs by overheating. The single phasing produced when the one phase of the IM is suddenly open-circuited during operation. This is caused by loose connections, blown fuse and partial damage of switch gears. The single phasing effect is similar to voltage unbalance and the worst possible case of voltage unbalance is the single phasing. It causes the overheating, shaft vibration noise, ultimately insulation damage and stator winding failures.

1.4.2 Condition Monitoring Techniques of Induction Motors

This section presents the literature survey to shed light on various techniques used and progress made in the condition monitoring and fault diagnosis of IMs. The catastrophic IM failure can occur due to failure of any of its components such as the stator, rotor and bearing. The fault in the different component of IM produces one or more of the symptoms, including (Benbouzid, 2000; Zhongming and Bin, 2002):

- Unbalanced air-gap flux;
- Increased torque and speed variation;
- Decreased average torque;
- Excessive heating;
- Excessive mechanical vibrations;
- Asymmetry and deviation of voltages and currents;
- Increasing losses and decreasing efficiency;

In order to detect these fault symptoms of IMs, a number of condition monitoring techniques have been developed including (Nandi et al. 2005; Alsaedi, 2015):

- Magnetic flux (or axial leakage flux);
- Air gap torque monitoring;
- Acoustic noise measurement;
- Thermal monitoring;
- Partial discharge measurement;
- Chemical analysis (lubricating oil debris; cooling gas);
- Vibration monitoring;
- Current monitoring;

The magnetic flux monitoring can be used to detect the turn-to-turn fault of the stator winding, BRB, and rotor eccentricity by analyzing axial magnetic flux in the shaft using a search coil wound concentrically around the shaft. This method can be used to locate the turn-to-turn fault position

by mounting a minimum of four search coils axis-symmetrically to the motor shaft (Penman et al., 1994). However, this method cannot be used extensively in industry because of installing search coils.

The air-gap torque can be used to monitor the broken rotor bar, stator winding faults and eccentricity related faults. (Salem et al. 2012). The air-gap torque represents the combined effect of all flux linkages and the currents in both stator and rotor of the motor. It is sensitive to any unbalance created by defects as well as by unbalanced voltages (Hsu, 1995; Gyftakis et al., 2013).

The acoustic noise monitoring can be performed by measuring and analyzing the noise spectrum (Akcay and Germen, 2013). The noise is produced due to Maxwell's stresses that act on iron surfaces. The most commonly used noise measurement sensors are microphones, or specialized equipment to measure noise (sound level meter). This monitoring technique can be used for detection of the air-gap eccentricity and stator structure related faults.

The thermal monitoring of IM can be implemented by measuring the local temperature of the motor and model based or parameter based approaches. In order to measure the local temperature, the sensor can be mounted on the winding or embedded in the insulation, which is electronically isolated from its instrumentation. It can be done using thermocouples, embedded temperature detectors, or resistance temperature detector. Temperature signals are usually used to monitor specific areas of the stator core and the bearing. In addition, thermal images are also used to detect the various IM faults, such as the stator winding fault, bearing fault, misalignment and mass-unbalance (Younus and Yang, 2010; Lim et al., 2014).

The partial discharge method can be only used for the insulation related fault. The partial discharge (PD) can be described as a small discharge in a gas filled void or a dielectric surface of a liquid or a solid insulation system. This occurs due to the insulation imperfection. The main factor of partial discharge is the poor manufacturing, delamination within the ground wall insulations or overheating, which results into voids or air pockets in the insulation. A deteriorated winding has a PD activity approximately 30 times higher than a healthy winding (Stone et al., 1996; Tetrault, 1999).

The cooling gas method can be used for the fault detection of insulation and stator winding. The degradation of insulation produces carbon mono-oxide gas, which passes into cooling air circuit and can be detected by an infrared (IR) absorption method (Tavner et al., 1986). The lubricating oil debris method can be used for the bearing damage by analyzing the wear debris particles and impurities in the lubricating oil (Halme, 2002).

The vibration monitoring can detect the mechanical related faults such as bearing faults, and the misaligned, bowed and unbalanced rotors (Iorgulescu and Beloiu, 2008). Moreover, it can be used to identify electrical related faults such as the stator winding fault, phase unbalance and broken rotor bar (Chang and Yacamini, 1996; Maruthi and Vittal, 2005). In order to acquire vibration signal for the vibration monitoring, the sensor like accelerometer can be mounted at the appropriate location on machines. The general principle of using the vibration based monitoring involves those components in mechanical systems that vibrate during operation (Yen and Lin, 2000). When faults develop, some of the system dynamics vary, resulting in significant deviations in vibration

patterns. By employing appropriate data analysis algorithms, it is feasible to detect changes in the vibration signal caused by faulty components and to make decisions about the status of the motor.

The current monitoring or machine current signature analysis (MCSA) is preferred to detect mainly electrical related faults, such as the broken rotor bar, stator winding fault, etc. (Da Silva et al. 2008). In addition to electrical faults, the MCSA can also be used to identify mechanical related faults (Benbouzid et al. 1999; Blodt et al. 2008). In case of MCSA, current signals are measured using sensors, like current probes, by attaching to motor current supply cables. The general principle of using the current based monitoring involves the high variation in current signals caused by faulty components of IMs. Similar to the vibration monitoring, the current variation can be detected by using a suitable data analysis method.

Various condition monitoring techniques have been used to detect different IM faults. However, the most of these techniques are invasive, complex, expensive and not capable of providing rich information about motor operational conditions. In addition, the most of techniques are able to detect a particular fault in IM that means other faults cannot be detected using the same technique. Nowadays, the condition monitoring of IM based on the vibration and current signals are the most preferred monitoring in the industry (Alsaedi, 2015). Kral et al. (2003) suggested that the vibration based CBM technique is a reliable technique for the detection of bearing and other mechanical faults in IMs. Later, many researchers have suggested to use the vibration signal for monitoring of mechanical as well as electrical faults in IMs. In order to acquire current signals for the MCSA, sensors like current probes can be attached to the motor cables. Initially, the current monitoring was used for the stator winding fault, broken rotor bar and rotor eccentricity. Timusk et al. (2008)

compared the vibration monitoring with the MCSA for the detection of IM faults, and finally concluded that the vibration based CBM was most effective technique for the bearing fault detection, while the MCSA was best for the BRB detection. In a study, Thomson and Orpin (2002) presented that an integrated monitoring method based on the vibration and the current can detect the mechanical as well as electrical related faults in IMs effectively.

From the literature, it is found that the vibration and current based monitoring are preferred for IM fault diagnosis because of following reasons:

- These techniques are non-intrusive, reliable and inexpensive.
- Their high accuracy and effectiveness in signal analysis that represents the actual machine condition.
- They are easily measurable or readily available in the motor drive system and for further signal processing.
- Their ability of detecting and distinguishing the most mechanical and electrical faults.
- Motor vibration and current can be measured online, therefore, make online detection possible.

By employing appropriate signal analysis techniques, it is feasible to detect changes in the vibration and current signals caused by faulty components of IMs. To analyze the signals obtained from the condition monitoring of IMs, signal processing techniques has been employed in three domains such as the time domain, frequency domain and time-frequency domain. The choice of these domains depends on the information required for the motor fault diagnosis (Mehrjou et al., 2011). Kral et al. (2004) proposed a time domain based technique for the detection of mechanical

imbalance of the induction machine. In this technique, first the imbalance specific oscillation of the electric power is extracted by a band pass filter. Then the averaged pattern of this component is determined by means of an angular data clustering technique. In this way, the oscillation of the electric power in time domain is mapped into a discrete waveform in an angular domain. The amplitude of the fundamental harmonic of these discrete data served as the imbalance indicator of the proposed scheme.

To improve the current and vibration monitoring of IMs, frequency domain based methods such as fast Fourier transform (FFT), higher order spectrum and Hilbert transform have been applied. Different faults generate a specific vibration and current spectrum, which provide the fault harmonic component related to the particular fault. In a work, Chow and Fei (1995) used the bi-spectrum analysis of vibration signals for the identification of machine faults, such as the asymmetrical fault, mechanical bearing movement, and stator winding fault. They concluded that the bi-spectrum is capable of providing adequate and essential spectral information for the condition monitoring and fault diagnosis, and is advantageous than the power spectrum analysis.

Thomson and Orpin (2002) used the current and vibration spectrums for the identification of various faults in IMs, such as the broken rotor bar, stator winding fault, bearing fault and eccentricity related faults. They concluded that the root cause of the problem can be established using a combination of current and vibration analyses in comparison to only analyzing one signal. However, for complex systems, which involve various components, it is a challenging task to estimate characteristic frequencies of faults, since the vibration and current spectrums can be influenced by several factors such as the electric supply, variable loading, noise and faults

(Benbouzid and Kliman, 2003). Even though characteristic frequencies are available, measured signals from motors are extremely non-stationary and the frequency spectrum analysis may not be suitable for such practices. Didier et al. (2007) used the current spectrum to detect the broken rotor bar by analyzing the phase and concluded that the Fourier transform phase analysis allows to detect one broken rotor bar when motor runs under low load, but the robustness of the method (DFT) decreases for a half broken rotor bar, The Hilbert transform (HT) allows to detect a partially broken rotor bar when the motor operates with the load torque equal or greater than 25% of rated load. In addition, some researchers tried different methods that can eliminate the load effect in the current spectrum. For example, Panadero et al. (2009) used the HT for the identification of the broken rotor bar based on the MCSA, and concluded that this technique can accurately identify broken rotor bar frequencies at a very low slip condition by using only one phase current.

Recently, the time-frequency analysis has been preferred in the condition monitoring and fault diagnosis of IMs. For example, Singh and Ahmed (2004) performed the vibration signal analysis using the wavelet transform (WT) for the identification of electrical faults in IMs. Finally, they concluded that the application of WT for the processing and analysis of the vibration signal in different frequency regions in time domain improves the extraction of the information that can enhance the ability of the system for diagnosis. Awadallah and Morcos (2006) used the WT to process the characteristic waveform of motor signals because of its effectiveness in handling non-stationary signals. Extracted indices could efficiently diagnose and locate the fault by one transform process only. In a study, Gao and Yan (2006) compared several signal processing techniques, such as the STFT, DWT, WPT, and Hilbert-Huang transform in the health monitoring of bearing to handle non-stationary signals. The WPT was able to detect all transient components

embedded in signals and perform better than all other signal processing techniques. Zarei and Poshtan (2007) used the energy of the WPT as a fault index for the detection of incipient bearing fault in IMs using the stator current. Zolfaghari et al. (2014) utilized the root-mean-square (RMS) of wavelet packet coefficients as a fault feature index for the detection of severity levels of the broken rotor bar in IMs.

1.4.3 Artificial Intelligence based Fault Diagnosis of Induction Motors

The condition monitoring and fault diagnosis of rotating machines has moved from traditional techniques to AI techniques in recent years. Various AIs, such as the ANN, fuzzy logic (FL), fuzzy-neural networks, hidden Markov model and SVM have been employed for the fault diagnosis of IMs. For an effective fault diagnosis of the IM based on AI techniques, data preparation is a significant issue, which consists of the feature extraction and its selection. The practical reliability of the diagnostics depends upon the extraction of representative features corresponding to IM health conditions. Various optimization techniques such as principal component analysis (PCA), independent component analysis (ICA), particle swarm optimization (PSO) and genetic algorithm have been used for feature selection (Liu and Bazzi, 2017, Nikranjbar et al., 2009).

In a work, Chow et al. (1991) developed a neural network-based incipient fault detector for small and medium size IM. The neural network-based incipient fault detector avoids the problems associated with traditional incipient fault detection schemes by employing more readily available information such as rotor speed and stator current. Schoen et al. (1995) used combination of FFT and ANN to improve MCSA for detecting various fault condition including BRB. The proposed

methodology does not require any information about the IM or load characteristics. Lasurt et al. (2000) applied the fuzzy logic procedure to develop a method for the condition monitoring and fault diagnosis of IMs. They used higher order statistical (HOS) analysis for preprocessing of vibration signals. Filipetti et al. (2000) performed the IM fault detection based on the neural network and the FL. The amplitudes corresponding to the fault frequency component obtained from FFT were considered as an input vector in AIs. Though, the fault detection is difficult when spectral leakage occurs especially under the low motor slip.

In a study, Haji and Toliyat (2001) developed a pattern recognition method based on Bayes minimum error for BRB fault detection. They used features from Park's transformation of current signal. Ye et al. (2001) used the wavelet packet based features and the ANN for the fault diagnosis of broken rotor bar and air-gap eccentricity in IMs. Kim and Parlos (2002) successfully used a combination of WPT and ANN to develop a model based fault diagnostic system using MCSA, voltage and speed for early detection of various IM faults including BRB. Ye et al. (2003) used MCSA with WPT and ANN for the detection of BRB and air gap eccentricity. This method provides feature representation of multiple frequency resolution for the IM faults.

Tan and Huo (2005) developed a generic neurofuzzy model-based fault detection scheme for detecting BRB in three-phase IM. The fault detector comprises the generic neurofuzzy model and the customized threshold levels. Variable thresholds, selected according to the difference between the output of the generic model and an empirical torque–speed relationship, are then used to account for variations between machines. This approach overcomes a practical limitation of model-based strategies as it reduces the amount of experimental data that are needed to design the

fault detector. Han et al. (2005) used a combination of PCA, GA and ANN for fault detection of IM. In this work, PCA are used to remove the relative features, and extract the principal components (PCs) from the original features. Then the significant features are selected from the extracted features by GA. GA is also used to optimize the ANN parameters.

Ayhan et al. (2006) presented fault-detection performance comparison for BRB between the multiple discriminant analysis (MDA) and the ANN with respect to the two detection scheme i.e., monolith and partition. The monolith scheme is based on a single large-scale MDA or ANN unit representing the complete operating load-torque region of the motor, while the partition scheme consists of many small-scale MDA or ANN units, each unit representing a particular load-torque operating region. Nakamura et al. (2006) presented diagnosis of the electrical and mechanical faults of IM based on the HMM, which is widely used in the field of speech recognition. Siddique et al. (2006) presented a review of recent developments in applications of AI techniques for fault diagnostics in IMs to a specific fault called the stator winding fault. They indicated that till that time the research had been concerned with the development of ANN and fuzzy logic in conjunction with various signal processing techniques, such as the higher order statistics, bi-spectrum, tri-spectrum, cyclo-stationary statistics and wavelets. Moreover, SVM techniques can be explored for the development of IM intelligent diagnostic systems. There is a significant opportunity to add an intelligence diagnostic system to motors itself, providing a level of communications and diagnostic capability. The intelligence can be built into the terminal box of the motor so that the overall package requires no more space.

Ye et al. (2006) used adaptive neuro-fuzzy with wavelet packet decomposition to detect the BRB and air gap eccentricity in variable speed drive system. The system can diagnose these faults even when the precise information regarding motor slip is not available. Ayhan et al. (2006) compared the multiple discriminant analysis and neural-network based detection scheme for BRB using single or multiple signature processing. They have used MCSA for the analysis and showed that multiple signature processing performs better as compared to single signature processing. In addition, the ANN provides higher accuracy performance than the multiple discriminant analysis. Lee et al. (2006) developed an approach based on Fourier and wavelet transforms and ANN using MCSA to detect the various IM faults. Yang and Kim (2006) used vibration and current along with ANN and Dempster-Shafer theory to detect the various IM faults including BF, SWF, BRB, air gap eccentricity and phase unbalance. They showed that the fault classification accuracy increases when the fusion of vibration and current is performed. Bacha et al. (2007) used spectrum analysis and ANN to compare current and flux monitoring for BRB and phase unbalance detections. They showed that the stray flux is more effective than the current to detect these faults using low frequency resolution data especially when there is no load on the motor.

Su and Chong (2007) presented an analytical redundancy method using neural network modeling of the induction motor in vibration spectra for IM fault (air gap eccentricity and BRB) detection. The STFT is used to process the quasi-steady vibration signals to continuous spectra for the neural network model training. Martin et al. (2007) presented a fully automatic on-line diagnosis of three phase IM stator fault using an unsupervised Hebbian-based neural network-based algorithm. The proposed method offers several advantages. First, the absence of previous training, or the incorporation of heuristic knowledge, makes it interesting for industry applications. Second, since

there is no need to perform any FFT computation, it makes it simpler to implement. Third, the method is able to indicate severity of the fault, rather than only detect its presence.

Widodo and Yang (2007) presented the application of nonlinear feature extraction for IM fault diagnosis. In nonlinear feature extraction, they employed the PCA and ICA procedure and adopted the kernel trick to nonlinearly map the data into a feature space. Finally, they compared the classification performance of SVM for linear and nonlinear feature extraction techniques and showed that the non linear feature extraction can improve the performance of the classifier with less number of data. Widodo et al. (2007) presented a combination of the ICA, the PCA and the SVM for the fault diagnosis of IMs based on the vibration and current signatures. The ICA and PCA were used for useful fault feature selection. They showed that the combination of ICA and SVM could serve as an encouraging alternative, and also demonstrated the application of nonlinear feature extraction and SVMs could serve as an alternative. Park et al. (2007) attempted fault diagnosis of IM based on mixed algorithms of PCA and LDA (linear discriminant analysis).

Rodriguez et al. (2008) used fuzzy system with FFT to improve MCSA for the detection of BRB and air-gap eccentricity. Silva et al. (2008) used the Gaussian mixture models and the Bayesian maximum for the detection of BRB and short circuit fault (or stator winding fault). They used envelope analysis of current spectrum for the feature extraction. The proposed method is able to identify the different fault levels of BRB and stator winding fault. Nguyen and Lee (2008) and Nguyen et al. (2008) investigated the mechanical fault diagnosis of IMs based on the vibration using the SVM, decision tree and GA. The study was mainly focused on the selection of useful signal features and SVM parameters. The GA technique was used for selecting fault features as

well as SVM parameters. The feature selection could remove the irrelevant and redundant information by choosing useful features as input of the SVM, while its proper parameters helped to build the SVM model with high performance and accuracy. In other work, Widodo and Yang (2008) utilized the transient current CBM and the wavelet SVM for the fault diagnosis of IMs. The PCA and kernel PCA were performed to reduce the dimension of features and to extract useful features for the classification process that tends to degrade the performance of the classifier. In this work, they built the SVM kernel function using different wavelet functions using the Haar, Daubechies and Symlet wavelets. Introducing nonlinear kernels using wavelets were believed to improve significantly the SVM research fields. Hence, a relatively new intelligent faults detection and classification method called the W-SVM was established.

Kurek and Osowski (2009) presented a fault diagnosis of the broken rotor bars of squirrel-cage IMs based on the SVM. The first detection system discovered only the fact of fault occurrence. The second one (complex diagnosis) was able to find how many bars have been damaged. In this work, they had defined special features relying on the FFT analysis of the registered instantaneous forms of the phase current, voltage and shaft magnetic field in a steady state. As a recognizing and classifying tool, they used the Gaussian kernel support vector machine, which is known for its very good generalization ability. Tran et al. (2009) presented the fault detection of IMs based on the adaptive Neuro-fuzzy inference using the vibration as well as current signals. The classification and regression tree (CART), which is one of the decision tree method was used for the feature selection. Gunal et al. (2009) developed diagnostic system based on Bayesian, Gaussian mixture model, Fisher's linear discriminate analysis using statistical time domain analysis to improve MCSA for the detection of BRB and air gap eccentricity. This system is able to indicate the type

of faults and load levels in multi-dimensional feature representation. Sadeshian et al. (2009) performed the BRB fault diagnosis using MCSA based on WPT and ANN. The proposed diagnostics was shown effective even with reduced load condition. In addition, it does not require any information about motor slip speed.

Morales et al. (2010) introduced the data fusion by using the multi-class SVM to detect mechanical faults in IMs using the vibration and line-current signatures. Zhang et al. (2010) used the WPT and the SVM for the bearing fault diagnosis in IMs. The results were compared with the ANN and found to be better. Garcia et al. (2011) presented the high-resolution spectral analysis for diagnosis of multiple faults in IMs using the multiple signal classification (MUSIC) algorithm based on the vibration and current signatures. Baccarini et al. (2011) presented a practical industrial application of the SVM for the mechanical fault diagnostics of IMs based on frequency-domain vibration signals. From this work, they also determined the best position for signal acquisition, which is very important for the maintenance task. This is valuable information to reduce the number of sensors and to reduce the maintenance costs. Konar and Chattopadhyay (2011) performed the fault diagnosis of bearings in IMs based on the CWT and the SVM. They used a number of wavelet function and finally concluded that the selection of wavelet is crucial for the intelligent fault diagnosis.

Ghate and Dudul (2011) introduced a new approach to intelligent fault detection and classification of three-phase induction motor based on RBF-MLP cascade NN. In this work, they considered stator winding interturn short, rotor eccentricity, and both faults simultaneously for demonstration.

Romero-Troncoso et al. (2011) developed a novel methodology for the identification of multiple combined faults in induction motors through information entropy and fuzzy logic inference. The fusion of these techniques allows satisfactory results for this difficult task in an automatic way by analyzing one phase of the steady-state current signal from the rotating machine. Bacha et al. (2012) and Salem et al. (2012) proposed fault condition monitoring of IM based on Hilbert-Park transform using the SVM. Ergin et al. (2012) presented the fault diagnosis in IMs, i.e. the stator, bearing and rotor using a common vector approach (CVA). In other work, Tran et al. (2013) investigated the transient current CBM based IM fault diagnosis by using the Fourier–Bessel expansion and the simplified fuzzy ARTMAP, a combination of fuzzy logic and neural network architecture based on the adaptive resonance theory (ART). Generalized discrimination analysis (GDA) was used to solve the high dimensionality of feature sets. Soualhi et al. (2013) used artificial ant clustering (ACC) technique for fault diagnosis of IM. In this work, the AAC has been proposed as an unsupervised classification method inspired by the behavior of real ants to optimize the detection and diagnosis of faults. Silva and Pederiva (2013) performed the induction motor fault detection using artificial intelligence techniques, like the SVM, fuzzy logic and ANN, and concluded that the SVM has a good generalization, among others.

In other work, Chattopadhyay and Konar (2014) used features of the continuous and discrete wavelets for the BRB fault diagnosis based on the RBF and multilayer perception (MLP) neural networks, and the SVM. Using the greedy-search feature selection technique (Greedy- CWT) the redundancy was eliminated and found much superior to the widely used DWT technique, even in the presence of high level of noise. To examine the impact of wavelets on the feature extraction, four wavelets from Daubechies family were selected. Finally, they concluded that the db8 gave

the best classification accuracy. Also, they showed that performance of classifiers was promising even in the presence of high noise level and with a lower sampling rate of 5.12 kHz.

Zarei et al. (2014) explored the cascaded NN for fault detection of bearing fault of IM, where first NN are used as a removing non-bearing fault component (RNFC) filter for signal denoising and then the second NN are used this filter output for the fault detection. They showed the proposed approach has better performance ability than the common NN even when dealing with the noisy samples. Seera et al. (2012), and Seera and Lim (2014) developed a hybrid model comprising fuzzy min–max (FMM), the classification and regression tree (CART) and ANN for IM fault detection and diagnosis and showed that this model performs well even in noisy environments when compared with FMM and CART.

Esfahani et al. (2014) used a combination of multiclass linear discriminant analysis (LDA) and quadratic discriminant analysis (QDA) and SVM for eccentricity and bearing fault diagnosis of IM. In this work, the Hilbert–Huang transform (HHT) of vibration data and power spectral density of current and acoustic signals are used as the features in a hierarchical classifier. Finally, multiclass LDA and QDA are used for the primary classification i.e., for classification of fault category, and SVM is used for the secondary classification i.e., for classification of fault sub-category. Seshadrinath et al. (2014) performed interturn fault detection in IM based on dual tree complex wavelet transform (DTCWT) and SVM. They have successfully performed the detection of turn fault (TF) under balanced supply conditions, voltage imbalance and interturn fault with voltage imbalance, both occurring at same time.

Zhou et al. (2014) investigated the fault diagnosis of IMs based on invariant character vectors using a single class-SVM. Das et al. (2014) presented performance of a load-immune classifier for the robust identification of minor faults in the induction motor stator winding. Park's vector modulus (PVM) was obtained through Park's transformation of three-phase stator line currents in all the experiment cases. Several features were extracted through the time domain, frequency domain, and time-frequency domain analyses of the PVM. Support vector machine based Recursive Feature Elimination (SVM-RFE) algorithm was used to select, rank and optimize the number of effective features to be used for the classification.

For the diagnosis of broken rotor bar fault, Keskes et al. (2013) combined the stationary WPT with the one-versus-one (OVO) and one-versus-all (OVA) SVMs. In other work, Keskes and Braham (2014, 2015) used the pitch synchronous wavelet transform (PSWT) and the directed acyclic graph (DAG) SVM. Then, Keskes and Braham (2015) combined the recursive un-decimated wavelet packet transform (RUWPT) and the DAG-SVM, for the BRB detection. In all the studies, they used different wavelet functions, like the Haar, Daubechies, and Symlet for kernel functions of the SVM. The highest classification accuracy was achieved with the Daubechies kernel with the stationary WPT and the OVO-SVM, the Symlet kernel with the PSWT, and the RUWPT with the OVO and the DAG-SVM. Moreover, the RUWPT improved the detection time. Wu et al. (2015) diagnosed bearing faults in IMs based the wavelet packet (i.e., the Daubechies 8) and the ANN with 90 % detection success. Vishwakarma et al. (2015) proposed the bearing fault diagnosis in IMs based on the wavelet packet decomposition and the SVM, and showed that perfect predictions can be achieved using the energy feature of the 3rd level Daubechies mother wavelet. The present

section focused the recent development of condition monitoring and fault diagnosis of IMs. In the next section, the outcomes of the present literature review are summarized.

1.5 Outcome of the Literature Review

Firstly, the literature on the condition monitoring and fault diagnosis of various rotating machines has been reviewed. The CBM program for rotating machines that recommends maintenance actions based on the information collected through condition monitoring have been included. Then the literature which mainly focuses on the condition monitoring and fault diagnosis of IMs has been reviewed. From the literature reviewed in the previous section, following general observation have been made:

- Rotating machines are subjected to various unavoidable stresses such as the mechanical, electrical, thermal and environmental, throughout the operation. The rotating machines encounter several faults, such as the unbalance, misalignment, mechanical looseness, electrical faults, bearing faults, gearbox faults, the hydraulic and aerodynamics forces, rotational disconnections, surge and film whirling motion, etc.
- For early fault detection of machine components that begin to degrade and to avoid the likelihood of catastrophic machine failure, the condition monitoring of rotating machinery is gaining importance in the industry. In order to retain or restore a machine to the specified operable condition or to achieve its maximum useful life, and significantly reduce maintenance cost, the CBM can be applied based on the information collected through the condition monitoring.

- Induction motors are the workhorses and critical machines of any industries as they maintain and accelerate the manufacturing processes. Accordingly, industries are ready to make a great effort for the condition monitoring and early diagnosis of the induced as well as incipient faults in IMs, especially in its critical applications, before it causes the unscheduled maintenance and in most of the cases a complete breakdown of IMs.
- Several types of IM fault such as the bearing faults, stator winding fault, broken rotor faults, rotor related faults, and phase unbalance have been considered in the literature.
- Various techniques for the IM fault diagnosis have been applied by using the MCSA, vibration analysis, electromagnetic torque measurement, acoustic analysis, and thermal analysis. However, most popular techniques are vibration signature analysis and the MCSA because of their easy measurability, high accuracy and reliability.
- Most of the research papers have considered maximum two to three types of faults that are simulated in different IMs, however, it is very important to consider all the possible faults that occur in the mechanical and electrical components of IMs and simultaneously diagnose them so that the chances of further damage or complete motor failure due to occurrence of any specific fault can be reduced.
- In practical applications, the different severity levels of fault may be developed, so it is very important to consider faults under progression to detect the faults at an incipient stage, which is very rare in the literature. A single fault diagnosis system for the simultaneous detection of any possible faults in the mechanical and electrical components, and their severity levels are still uncommon in the literature. This work is of practical significance because if the methodology is robust enough to classify a number of different fault conditions including different severity levels, then it can be easily used to classify any one fault condition and

healthy motor condition. In addition, it is very useful when a number of IM working in the industry are diagnosed simultaneously based on a single developed methodology.

- As the condition monitoring and diagnosis of rotating machines has moved from traditional techniques to AI techniques, so there is much scopes of research in this field. The AI based diagnostic systems still have several challenging tasks to accomplish in regards to its efficiency, reliability, computational time, sufficient database, and robustness.
- Nowadays, the SVM is extensively gaining popularity in machine fault diagnosis owing to their best prediction performance, and less training and testing time. The diagnosis of multi-faults in IMs based on the SVM is still uncommon.
- In all the aforementioned works, a higher sampling frequency has been used to acquire the signals for AI based fault diagnosis, however, it is very significant to choose adjusted sampling frequency and data points (or frequency resolution) that can improve fault diagnostic and detection time, and reduce the cost of implementation.
- The SVM, for the purpose of pattern recognition or fault diagnosis, include a large collection of very different types of mathematical tools, namely, the pre-processing, extraction and selection of suitable statistical features, selection of SVM parameters and final recognition. In many cases, it is difficult to say which features are significant and what kind of tool would be best for a particular problem and machines.
- In order to extract useful fault features, different signal processing approaches have been used, such as the time, frequency, or more advanced time-frequency approach like wavelets. The selection of domain and representative features depends on the type of signals and the needed information from the machine.

- From the available literature, it could be summarized that the wavelets have still an immense prospect and still very few people have tried it for the intelligent fault diagnosis of IMs. Looking into tremendous information comprised in the wavelets, an attempt in conjunction with the SVM particularly for the IM fault diagnosis would be a worth effort, which is lacking in present literatures.
- Based on existing literatures, it could be summarized that several mother wavelet are available that can be used in the intelligent fault diagnostic. In spite of a lot of study on wavelet, the choice of the mother wavelet and their features, which is considerable issue of intelligent fault diagnosis, is still open for discussions.
- The work available up to now in literatures has restricted to diagnose the faults at specific operational condition of IMs and several researchers have shown that it is very difficult to diagnose the IM faults at light loads. The accuracy of fault diagnosis may reduce due to occurrence of fluctuation of rotor speeds during data acquisition under different loadings of IMs. Thus, considering the influence of motor operational conditions on the intelligent fault diagnosis is still an open challenge.
- Usually, AI systems are trained using a symptoms database available by the measurement in the industry. However, it is not always possible to have a database at all IM operational conditions. The intelligent fault diagnosis is difficult when test data do not match the database used for the training. The fault diagnosis of IMs, when the training and testing data available at different operating conditions used for the diagnosis, is not available in the literature.

From the outcome of the literature review the motivation of the present work has been formed. The aims and objectives of the present work are described in the following section.

1.6 Aim and Objective of the Present Work

From the literature review, it could be concluded that among different rotating machineries, the IM is one of the critical machine that need more investigation on the condition monitoring and fault diagnosis. From literature survey, it is evident that the fault diagnosis of IMs based on the SVM is still uncommon and has a lot of potential. Looking at the reported ability of the SVM performing the IM fault diagnosis would be a real beneficial and useful for industries towards automation of condition monitoring and fault diagnosis systems. The main objectives of the present work are as follows:

- To investigate and formulate SVM based machine condition monitoring scheme for the simultaneous detection and diagnosing the most common mechanical faults (bearing fault, unbalanced rotor, bowed rotor and misaligned rotor fault) and electrical faults (stator winding fault, broken rotor bar and phase unbalance fault) in IMs.
- To detect faults under progression (i.e., different severity levels of faults) in IMs based on the proposed SVM based machine condition monitoring scheme.
- To find out which signal(s) (i.e., vibration or/and current) is/are required and sufficient for effective diagnosis of mechanical and/or electrical faults in IMs, the comparative investigation of the vibration and current signals would be performed based on SVM.
- To choose adjusted sampling rate and data points (or frequency resolution) for the fault diagnosis of IMs that can improve the fault diagnosis and detection time, and reduce the cost of implementation.
- To extract and select useful features from IM faults for the effective fault diagnosis, signal processing techniques such as the time, frequency and time-frequency domain (wavelets)

would be considered. In case of the wavelet analysis, different mother wavelets would be used to investigate the impact of them on the performance of present methodology of the IM fault diagnosis.

- To perform the fault diagnosis for the same speed and same load case, when the data or information is available at the required speed and load.
- To perform the fault diagnosis for the intermediate speed and the intermediate load cases, when the data or information is not available at the required speed and load. The aim is to check the performance of the proposed diagnostic when limited information available for the training of the classifier. This is a work of practical significance because often symptoms database may not be available or difficult to obtain at all operating conditions of IMs.
- As the conventional fault diagnosis depends on IM operating conditions and the diagnosis is especially challenging for the light loading and fluctuating speed conditions. Therefore, the fault diagnosis would be performed for a wide range of IM operating conditions (i.e., load and speed) to check the robustness of the present methodology.

.

1.7 Organization of the Thesis

The thesis is organized into nine chapters. The introduction and literature review are presented in Chapter 1. The introduction to support vector machine based fault diagnosis methodology is presented in Chapter 2. In order to generate exhaustive data sets, which are required for the SVM based fault diagnosis; the experimental set-up and experimentation are presented in Chapter 3. In Chapter 4, the multi-fault diagnosis of mechanical and electrical faults in IMs is presented based on a low frequency resolution time domain data. The comparative investigation of the vibration and current signals are performed in order to find out which signal(s) (i.e., vibration or/and current)

is/are required for effective SVM based diagnosis of mechanical and/or electrical faults in IMs. In addition, the fault diagnosis performance is compared in time domain with the low and high sampling rate data. In Chapter 5, the multi-fault diagnosis of IMs is presented based on the high frequency resolution time domain data. In Chapter 6, the multi-fault diagnosis of IM is provided based on frequency domain data. In Chapter 7, the multi-fault diagnosis of IM is provided based on the CWT data. The multi-fault diagnosis of IM is documented based on the WPT data in Chapter 8. In Chapters 5 to Chapter 8, the fault diagnosis has been performed when training and testing is done at same speed and load case. In addition, the diagnosis is further extended to intermediate speed and load cases in all these chapters. The major conclusions and scopes for future works have been added in Chapter 9.

CHAPTER 2

Introduction to Support Vector Machine based Fault Diagnosis Methodology

2.1 Introduction

The fault diagnosis methodology based on support vector machine (SVM) learning algorithms and its procedure will be discussed in this chapter. In this study, the multi-class SVM algorithm has been applied in order to diagnose the multi-fault of IMs. The diagnostic performance of the SVM is dependent on its parameters and fault features, which are used as input to the classifier. Therefore, SVM parameters are optimally selected using the cross-validation method along with grid-search, and fault features are selected based on the wrapper model. These methods will also be briefly discussed in this chapter.

2.2 SVM Classifier

The SVM is a relatively new supervised AI technique based on the statistical learning theory, which analyze data and recognize patterns. It is used for the classification of data and the regression analysis for estimation of system parameters. The basic of SVM algorithms was first introduced by Vladimir Vapnik in 1994. The SVM is based on the principle of structural risk minimization (SRM), which has been proved to be superior to the empirical risk minimization (ERM) that is used by the ANN. The ERM minimizes the error on training sets while the SRM minimizes an upper bound on the expected risk. Therefore, the SVM has the better generalization ability than other AI techniques like ANN, which is the main motive of the machine learning. The SVM was primarily developed for the binary classification, but recently it has been extended to the multiclass classification for handling the real world situation. The SVM has several applications like

handwriting recognition, image recognition and so forth. The SVM is advantageous especially for small sample or database cases for example the machine fault diagnosis cases. The SVM is gaining popularity in the field of machine fault diagnosis from last one decade due to its attractive features and promising empirical performance. The binary as well as multiclass SVMs have been presented in this section briefly.

2.2.1 Binary SVM

The binary SVM deals with a two-class problem and is used to separate two possible classes in a space by a clear gap as wide as possible. When an unseen example is mapped into the same space, then the SVM predicts whether it falls into one category or the other. The basic model of the SVM is a maximal margin classifier, which works only for linearly separable data in the feature space. However, it cannot use for real world problems, but it is a main building block model for a more complex SVM. The SVM constructs a hyper plane or a set of hyperplanes defined by a number of support vectors in a high or infinite dimensional space, which could be used for the further classification (Burgees, 1998).

The basic principle of the SVM is demonstrated in the two-dimensional plane as shown in Figure 2.1 and Figure 2.2. A set of data of two classes represented by a positive sign (class A) and a negative sign (class B) is considered here. The SVM tries to place a linear boundary (or also called the hyperplane) between the two classes in such as a way that the distance between the boundary and the closest data point of each class is maximized. These closest data points define the margin and known as support vectors (SVs). The SVs contain all the necessary information for the

prediction of unseen examples; hence, other data points can be discarded. The margin is chosen as a trade-off between the margin level and the generalization error.

Figure 2.1 depicts a number of hyperplanes; it is called a good separation if the hyper-planes have a largest distance to the closest training data point of any class. Figure 2.2 shows the optimal separating hyperplane that separates two class data, i.e. the positive and the negative. The SVM classification problem is solved by considering an optimization technique for maximizing the margin between two classes. Hence, for a higher margin, the generalization error will be very less. Finally, the SVM algorithm builds a classification model that predicts if the new data falls into the positive class or to the negative class (Vapnik, 1999).

For an optimal separating hyperplane, consider a problem to separate the set of training vectors of two different classes,

$$S = \{(\mathbf{x_i}, y_i), x_i \in R^N, y_i \in \{-1, +1\}, i = 1, \cdots, m\} \tag{2.1}$$

where $\mathbf{x_i}$ is the training sample and denotes the i^{th} vector in a dataset with component x_i, y_i is the label associated with $\mathbf{x_i}$, and m is the number of samples. A separating hyperplane is defined by,

$$(\mathbf{w}, \mathbf{x}) + b = 0; \quad w \in R^N; \quad b \in R \tag{2.2}$$

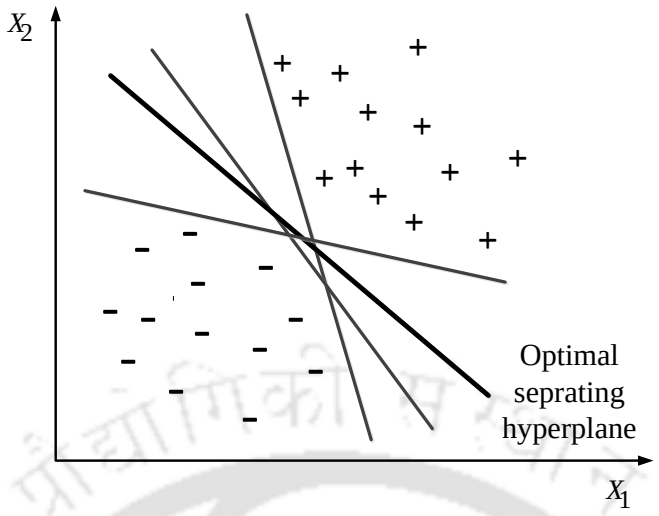

Figure 2.1 Optimal separating hyperplane

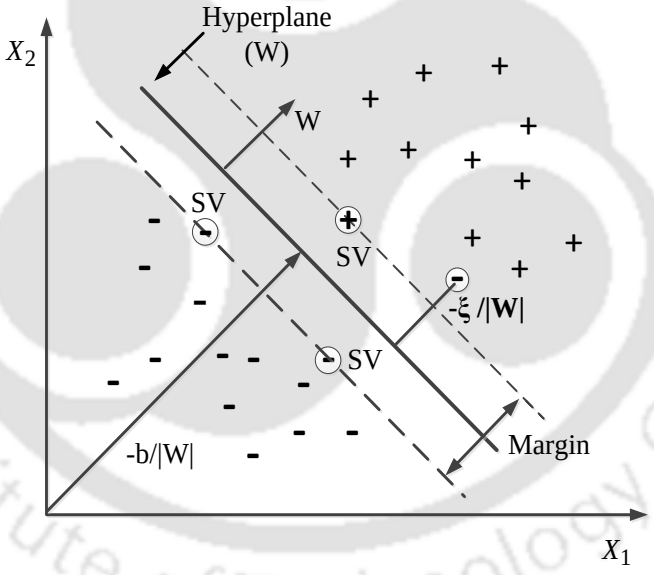

Figure 2.2 Linear separating hyperplane for the non-separable data

where the **w** (a normal vector to the hyperplane) is known as wiegh vector, which defines the boundary, **x** is the input vector of dimension *N*, and *b* is a scalar threshold. If the set of training vector is separated without any error and two adjacent vectors have maximal distance to the

hyperplane, then set of vectors is assumed to be optimally separated by a hyperplane. The following decision function can be used to classify the training data in the positive or negative class.

$$f(\mathbf{x}) = sign(\mathbf{w}.\mathbf{x} + b) \tag{2.3}$$

For a linear separable data, we have

$$y_i(\mathbf{w}.\mathbf{x} + b) > 0 \tag{2.4}$$

Consider a canonical hyperplane, which are defined for the closest point and are called support vectors on either side of the separating hyperplane as described in Equation 2.5 and Equation 2.6, whereas, Equation 2.7 describes the separating hyperplane, as

$$\mathbf{w}.\mathbf{x} + b = +1 \tag{2.5}$$

$$\mathbf{w}.\mathbf{x} + b = -1 \tag{2.6}$$

and

$$\mathbf{w}.\mathbf{x} + b = 0 \tag{2.7}$$

A canonical separating hyperplane must satisfy the following constraint,

$$y_i(\mathbf{w}.\mathbf{x}_i + b) \geq 1; \qquad i = 1, 2, ..., n \tag{2.8}$$

Consider a data point $\mathbf{x_1}$ is a support vector on the positive side of hyperplane (***w***, *b*), then the distance, d, of $\mathbf{x_1}$ from the hyperplane is,

$$d = \frac{(\mathbf{w}.\mathbf{x_1} + b)}{\|\mathbf{w}\|} \tag{2.9}$$

By maximizing the margin, γ, the optimal separating hyperplane could be obtained, hence the margin is,

$$\gamma(\mathbf{w}, b) = \frac{(\mathbf{w}.\mathbf{x_1} + b) - (\mathbf{w}.\mathbf{x_2} + b)}{\|\mathbf{w}\|} \tag{2.10}$$

$$\gamma(\mathbf{w}, b) = \frac{2}{\|\mathbf{w}\|} \tag{2.11}$$

In order to maximize the margin, the following term should be minimized for the optimal hyperplane, then the optimization problem becomes,

$$\min \Phi(\mathbf{w}) = \frac{1}{2}\|\mathbf{w}\|^2 \tag{2.12}$$

$$\text{subject to, } y_i(\mathbf{w}.\mathbf{x_i} + b) \geq 1; \quad i = 1, 2, ..., n \tag{2.13}$$

The optimization problem is solved by the Langrange multipliers, the Langrangian is

$$L = \frac{1}{2}(\mathbf{w}.\mathbf{w}) - \sum_{i=1}^{n} \alpha_i \left\{ y_i (\mathbf{w}.\mathbf{x_i} + b) - 1 \right\} \tag{2.14}$$

Where α_i is the Langrange multiplier. The Langrangian has to be minimized with respect to *b* and **w**, and maximized with respect to $\alpha_i \geq 0$.

$$\frac{\partial L}{\partial b} = 0 \Rightarrow \sum_{i=1}^{n} \alpha_i y_i = 0 \tag{2.15}$$

and

$$\frac{\partial L}{\partial \mathbf{w}} = 0 \Rightarrow \mathbf{w} = \sum_{i=1}^{n} \alpha_i y_i \mathbf{x_i} \tag{2.16}$$

This problem is very difficult to solve directly because the constraints are quite complex. Hence, Lagrangian duality theory is used for simplifying this problem. This approach leads to solving the following dual problem

$$\text{Max}\{D(\alpha)\} = \sum_{k=1}^{m} \alpha_k - \tfrac{1}{2} \sum_{i,j=1}^{m} \{ y_i \alpha_i y_j \alpha_j (\mathbf{x_i}, \mathbf{x_j}) \} \tag{2.17}$$

Constraint, $\sum_{j=1}^{n} y_j \alpha_j = 0$ and $\alpha_i \geq 0, \quad i = 1, 2, \cdots, n$ (2.18)

This dual problem is computationally easier because its constraints are much simpler. After solving the above problem, the optimal separating hyperplane is given by,

$$\mathbf{w}^* = \sum_{i=1}^{n} \alpha_i y_i \mathbf{x_i} \tag{2.19}$$

and

$$b^* = -\frac{1}{2}\left(\mathbf{w}^*, \mathbf{x_p} + \mathbf{x_q}\right) \tag{2.20}$$

where $\mathbf{x_p}$ and $\mathbf{x_q}$ are any SV from each class satisfying,

$$\alpha_p, \alpha_q > 0; \quad y_p = -1; \quad y_q = +1 \tag{2.21}$$

The linear discriminate function can then be written as,

$$f(\mathbf{x}) = \mathbf{w}^*\mathbf{x} + b^* = \sum_{i=1}^{m} \{y_i \alpha_i^* \mathbf{x_i}, \mathbf{x}\} + b^* \tag{2.22}$$

This above optimization problem can solve only the linearly separable case. However, there are the cases where the data are not linearly separable. In that case the margin is "Soft". This means that in-sample classification errors occur and also have to minimize. In order to solve the non-linear separation case, let ξ_i be a slack variables, which allow misclassification for some data in order to decrease the calculation complexity, *C* is a penalty parameter or soft margin classifier, which trade-off between the misclassification and boundary complexity. If $\xi_i = 0,$ that means all

the data points are perfectly classified. The following constrained optimization problem has to solve in order to take care of the non-linear separable case (Gunn, 1998):

$$\min \ \Phi(\mathbf{w}) = \frac{1}{2}\|\mathbf{w}\|^2 + C\sum_{i=1}^{n}\xi_i \tag{2.23}$$

$$\text{subject to} \quad y_i\left(\mathbf{w}.\mathbf{x_i} + b\right) \geq 1 - \xi_i; \qquad i = 1, 2, ..., n \tag{2.24}$$

$$\xi_i \geq 0 \tag{2.25}$$

This formulation is known as the soft-margin SVM. Here, *C* controls the classification ability of the SVM. If *C* is higher, that means the higher weight is given to in-sample misclassifications, consequently it reduces the classification accuracy. The low classification means that the classifier may work well on the training data, but would not perform well on an unseen example. This is called the overfitting. Hence, by choosing a low *C*, the risk of overfitting of an SVM on the training data is reduced. It is noted that the *C* is directly related to the width of the margin. If *C* is smaller, then the margin is wider, the more classification errors are permitted. For the non-linear separation case, a hyperplane can be created by the SVM that allow the linear separation in the higher dimension. In the SVM, it is only possible by the transformation $\phi(\mathbf{x})$ of the data from an *N*-dimensional space to *Q*-dimensional feature space as shown in Figure 2.3.

$$s = \phi(\mathbf{x}); \qquad \text{where,} \qquad \mathbf{x} \in R^N; \qquad s \in R^Q \tag{2.26}$$

The mapping or transformation by the SVM can be achieved by replacing the inner product,

$$(\mathbf{x}, \mathbf{x_i}) \rightarrow \phi(\mathbf{x}).\phi(\mathbf{x_i}) \tag{2.27}$$

A kernel function can be used for the mapping of SVM and the dot product in a single step provided the mapping can be replaced by an equivalent kernel function Boser et al. (1992). It reduces the computational load by retaining the effect of higher-dimensional transformation. The kernel function is given as:

$$k(\mathbf{x}, \mathbf{x_i}) = \phi(\mathbf{x}).\phi(\mathbf{x_i}) \tag{2.28}$$

There are many function kernels available like the Gaussian Radial Basis function (RBF), polynomials, and certain sigmoid function. In this work the RBF kernel is adopted here because it is widely acceptable and famous kernel (Hsu and Lin, 2002). The RBF kernel can be expressed as,

$$k(\mathbf{x}, \mathbf{x_i}) = \exp\left(-\gamma \left\|\mathbf{x} - \mathbf{x_i}\right\|^2\right); \qquad \gamma = \frac{1}{2\sigma_b^{\,2}} > 0 \tag{2.29}$$

where, σ_b is the width of the RBF kernel and γ is the kernel parameter. After solving the optimization problem, the basic form of SVM will be

$$f(\mathbf{x}) = \sum_{i=1}^{m} \{y_i \alpha_i K(\mathbf{x}, \mathbf{x_i})\} + b \tag{2.30}$$

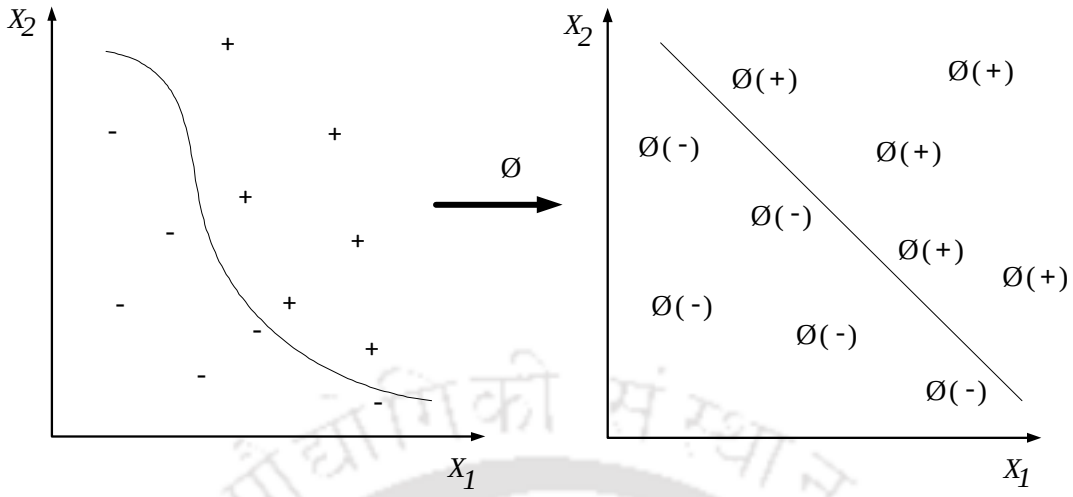

Figure 2.3 Mapping from the input space to the high dimensional space

The above formulation of SVM is based on the binary classification, and it can handle the multiclass case by simply combining the binary case.

2.2.2 Multiclass SVM

The SVM is basically a binary classifier, which deals with only two classes, however, in reality more than two classes can be found. Therefore, a multiclass SVM is required to take care of more than two class problems. In order to solve the multiclass SVM, two types of approaches are available, such as the first method constitutes and combines many binary classifiers; however; the second directly considers all data in a single larger optimization problem. It is computationally less expensive to solve a binary classification problem than a multiclass problem with same numbers of data. Therefore, for handling a multiclass problem, the binary classifier based method is adopted here.

To solve a multiclass SVM using binary classifiers, different coupling strategies, such as one versus one (OVO), one versus all (OVA), and direct acyclic graph (DAG), are developed (Hsu and Lin, 2002). Based on these methods, a multiclass SVM can be achieved by first disintegrating a multiclass problem into number of binary problems. Then training of classifiers is performed to solve the problems allocated to each binary problem. At last the binary SVMs are combined to rebuild the solution of the multiclass problem based on outcomes of different classifiers. For example, the OVO construct $k(k-1)/2$ binary classifiers for *k* class problem, i.e. one classifier for each pair of classes and then voting strategy is applied to get global classification results and finally select the class with maximum votes. The OVA constructs *k* binary SVM classifier, where training of each classifier is performed to separate one class from the rest and then the classifier that shows maximum accuracy is selected. The DAG is the modification of OVO. The training of the DAG is similar to the OVO; however, it employed a rooted binary DAG for testing, which is having $k(k-1)/2$ internal nodes and $(k-1)$ leaves.

Hsu and Lin (2002) presented the comparison between all-together approach and three binary classifiers based approach, like the OVO, the OVA and the DAGS. They experimentally concluded that the OVO is a competitive approach for the practical use because of its advantages over other methods such as the higher generalization accuracy and the lowest training time. Therefore, the OVO method has been adopted in this study. Figure 2.4 demonstrates the OVO method of the SVM. It shows that for a three class problem, the OVO constructs three binary SVMs according to the relation $k(k-1)/2$. Each SVMs are trained for each pair of classes and further solved. Figure 2.4 shows that Class 2 gets maximum votes among three classes. So this class is finally

selected according to the Max Wins strategy. If two classes have identical votes, then it chooses a class with smaller index.

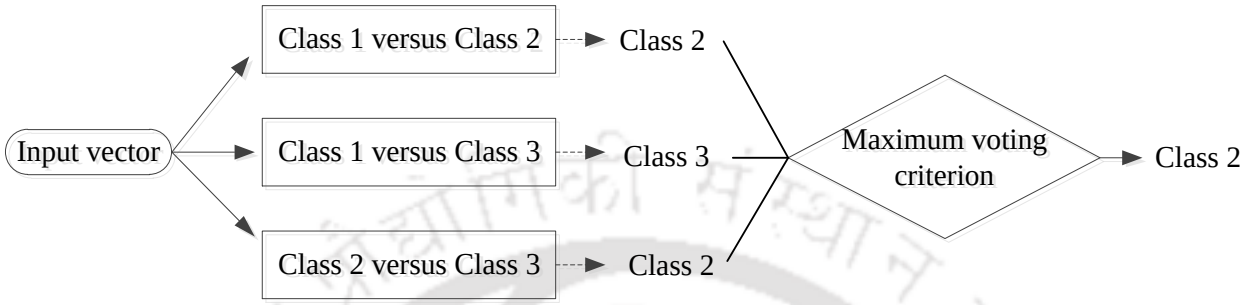

Figure 2.4 One-versus-one multiclass method of the SVM

The following optimization problem of the binary classification can be solved for training example from i^{th} and j^{th} classes

$$\min_{w^{ij},b^{ij},\xi^{ij}} \quad \frac{1}{2}(\mathbf{w^{ij}})^T(\mathbf{w^{ij}}) + C\sum_t \xi_t^{ij}(\mathbf{w^{ij}})^T \tag{2.31}$$

$$(\mathbf{w^{ij}})^T \phi(\mathbf{x_t}) + b^{ij} \geq 1 - \xi_t^{ij}; \qquad \text{if} \quad y_t = i \tag{2.32}$$

$$(\mathbf{w^{ij}})^T \phi(\mathbf{x_t}) + b^{ij} \geq -1 + \xi_t^{ij}; \quad \text{if} \quad y_t = j \tag{2.33}$$

and

$$\xi_t^{ij} \geq 0, \tag{2.34}$$

where, similar to the binary SVM problem, $\phi(\mathbf{x_t})$ is a mapping function, $(\mathbf{x_t}, y_t)$ is the training sample, $\mathbf{w}$ and b are the weighting factors, ξ^{ij} is the slack variable, and C is the penalty parameter. Now, for future testing with unseen examples, a following voting approach is adopted here. The voting strategy is done in every binary classification model for testing on unseen examples, where votes can be casted for each data samples, *x*. If $f(\mathbf{x}) = sign((\mathbf{w^{ij}})^T K(\mathbf{x_n}) + b^{ij})$ decides *x* to be in i^{th} class, then vote for this class is added by one. Otherwise the j^{th} class is increased by one. Then it predicts *x* to be in the class with the maximum votes. This approach is also known as *Max Wins strategy* (Kressel, 1999). If two classes have identical votes, then it chooses a class with a smaller index. For more on the SVM, interested researchers can refer Vapnik (1995).

2.3 Cross-Validation Method Along with Grid Search for SVM Parameters Selection

The performance of SVM is dependent on the selection of SVM parameters. In this study, the multiclass SVM is used with the RBF kernel. There are two parameters while using the RBF kernel, such as the Lagrange penalty parameter or soft margin constant, C, and the inverse-width parameter of RBF kernel, γ. SVM parameters define the decision boundary of the classifier. Therefore, the objective is to choose a pair of (C, γ) which provides the best prediction performance of the SVM. The standard method of choosing the pair of (C, γ) is the cross-validation (CV) method along with grid-search as shown in Figure 2.5 (Hsu et al., 2003). Here 5-fold CV method is used. In 5-fold CV, first the available data are divided into 5 subsets of equal size. At a time, the training folds contain four of the groups (i.e., roughly 4/5 of the data) and the test folds contain the other group (i.e., roughly 1/5 of the data). Each subset at a time takes part as

a testing data and other subset as a training data. Therefore, each instance of the whole training data is predicted once so the CV accuracy is the percentage of data which are correctly validated.

Along with the cross-validation, a grid-search is carried out to choose C and γ by defining a two dimensional grid. Grid points are generally chosen on a logarithmic scale that covers a large range of these parameters for the practical purpose. In this study, C and γ are given in exponentially growing sequence, i.e., $3^{-5}, 3^{-4}, ..., 3^{15}$ and $3^{-15}, 3^{-4}, ..., 3^{3}$, respectively. Now the CV accuracy is estimated for several pairs of (C, γ) first on the coarse grid. After finding the better region on the grid, a finer grid-search on the same region is performed. Finally, the best combination of (C, γ), which gives the highest CV accuracy is retained. After identifying the best (C, γ), the SVM is trained again using the whole training data to generate the final classifier model.

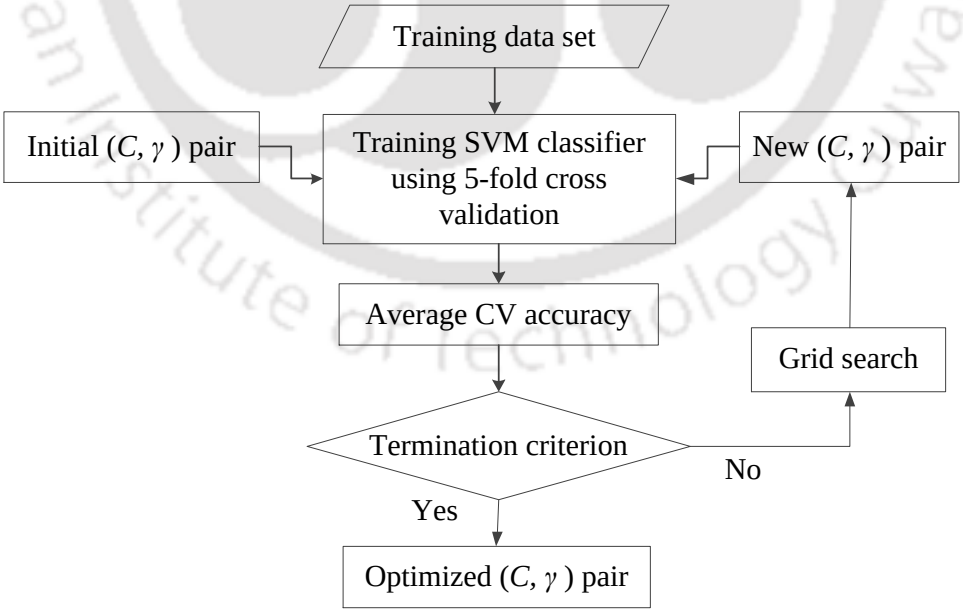

Figure 2.5 The cross validation method along with grid search for SVM parameter selection

The cross-validation can avoid the over-fitting problem (Hsu et al., 2003). To explain this issue, a binary classification problem is used here as shown in Figure 2.6. Hollow circles and rectangles are the training data while filled circles and rectangles are the testing data. Figure 2.6 (a) and (b) show the case of over-fitted classifier. In this case the training accuracy is high, but testing accuracy is low. Figure 2.6 (c) and (d) show the classifiers without any overfitting therefore it gives better CV as well as the testing accuracy.

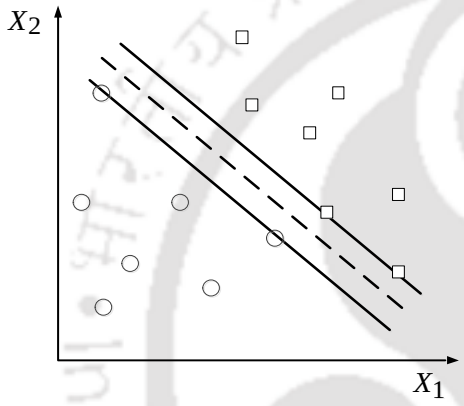

(a) Training data and an overfitting classifier

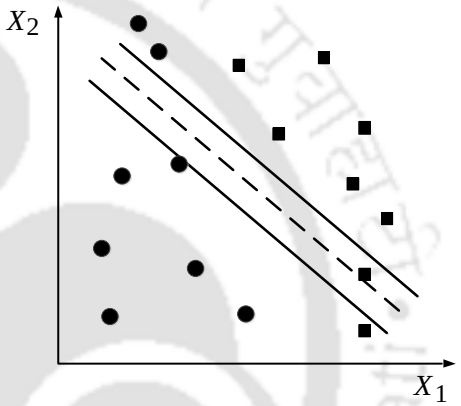

(b) Applying an overfitting classifier on testing data

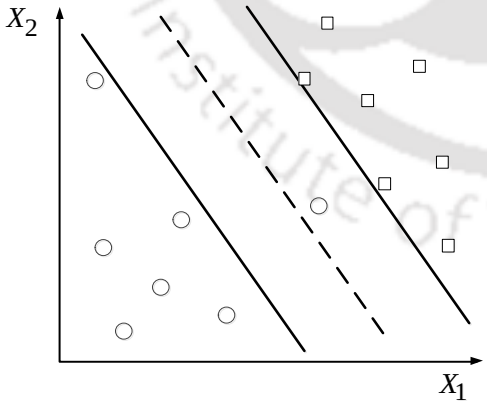

(c) Training data and a better classifier

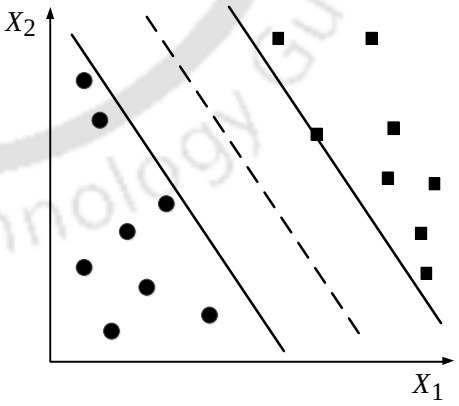

(d) Applying a better classifier on testing data

Figure 2.6 An overfitting classifier and a better classifier

2.4 Wrapper Model for Feature Selection

The feature selection is a dimensionality reduction technique in the machine learning, which aims to choose the most appropriate feature(s) from the original ones. Feature selection leads to better performance of the classifier, i.e. the higher prediction accuracy, better model interpretability and lower computational time by eliminating the irrelevant, redundant or noisy features with a minimum information loss (Sammut and Webb, 2017). An irrelevant feature carries no useful information about fault conditions and does not discriminate samples from different faults. In fact, it may confuse the learning system and cause the memory and computation inefficiency. Redundant features are those which may show good predcition performance independently; however, they do not enhance the performance by adding them with other good performing features. Instead, it adds more memory and computational requirement to learn the classifier, and may create the curse of dimensionality. The feature selection is a real challenge to assess, which features are more sensitive to faults and their severity, especially at an early stage, because many factors affect the effectiveness of features.

The wrapper model is used for the feature selection in the present fault diagnosis. This model is a simple, timesaving and efficient approach of feature selection since it utilizes only the prediction accuracy of a classification tool as a performance measure or evaluation criterion (Kohavi and John, 1997). It is noted that in the AI based fault diagnosis, the main aim of feature selection is to improve the classifier's performance (fault prediction accuracy, in particular). There is no need to go for complex models of features selection for effective fault diagnostics, because of its limitation in the implementation for real time systems. Given a predefined learning algorithm, a general framework of the wrapper model is depicted in Figure 2.7. According to this model, a number of

features are first fed into the classifier. Then it uses predefined learning algorithm to evaluate the performance of each features one by one, which returns the prediction accuracy corresponding to the feature. The feature(s) with the best prediction accuracy is chosen as the most appropriate feature(s). It is noted that for *n* number of features, various feature combinations are possible; however, it is very difficult to consider all the possible combinations for the study, unless *n* is small. So instead of going for an exhaustive search, only the combination of best performing features can be analyzed.

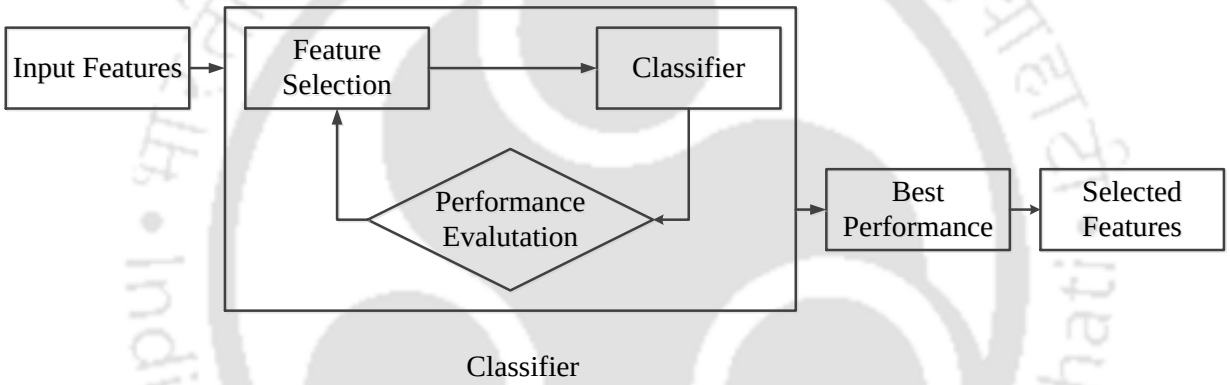

Figure 2.7 The wrapper model for the feature selection

2.5 Fault Diagnosis Procedure through Developed Methodology

In this study, the SVM based methodology is used to diagnose and isolate faults in IMs. The overall execution procedure of the present methodology is shown in Figure 2.8. The methodology consists of four steps: first the data acquisition, second the feature extractions, third the selection of SVM parameters and fault features, and fourth the diagnosis and isolation. In a very first step, the required signals are acquired from the IM. The useful statistical features are then extracted from the raw data of signals for different fault classes of IMs. Different labels are assigned for each IM

fault class. Now the total available feature datasets are divided into the training data and the testing data for the SVM in a proper ratio. In this study, 80% of the total data is used for training and the remaining 20 % is used for the testing. The large data are used for the training as compared to the testing. The reason for this is the training data has a single and essential role that it is used to build the predictive model. Thus more the training data, the more robust the predictive model would be. However, the testing data are used as unseen examples for the final prediction. There is no need to generate large data for testing; the higher prediction is obtained using less number of unseen data (i.e., testing data). Also to focus on the real world problem of fault predictions, the chances of getting more training data are high because this data comes from the vast history available in the industry. However, the testing data comes from current online measurements.

Now the training of the SVM is performed using the training data and the RBF kernel to build a model for further testing or final prediction of faults by selecting optimized SVM parameters. The optimization of SVM parameters is performed based on the cross-validation method along with the grid-search technique. The performance of the classifier also depends on the effectiveness of input features of faults, so the selection of the most effective feature is also a crucial step in the fault diagnosis. The feature selection is performed based on the wrapper model. After selecting the best SVM parameters and fault feature(s), the SVM is again trained using whole training data and then tested with the testing data. The final result of the fault diagnosis is obtained in the form of testing or prediction accuracy, i.e. prediction levels of the testing data as shown in Equation 2.35.

$$\text{Prediction accuracy} = \left(\frac{\text{number of correctly predicted data}}{\text{total number of testing data}} \right) \times 100 \qquad (2.35)$$

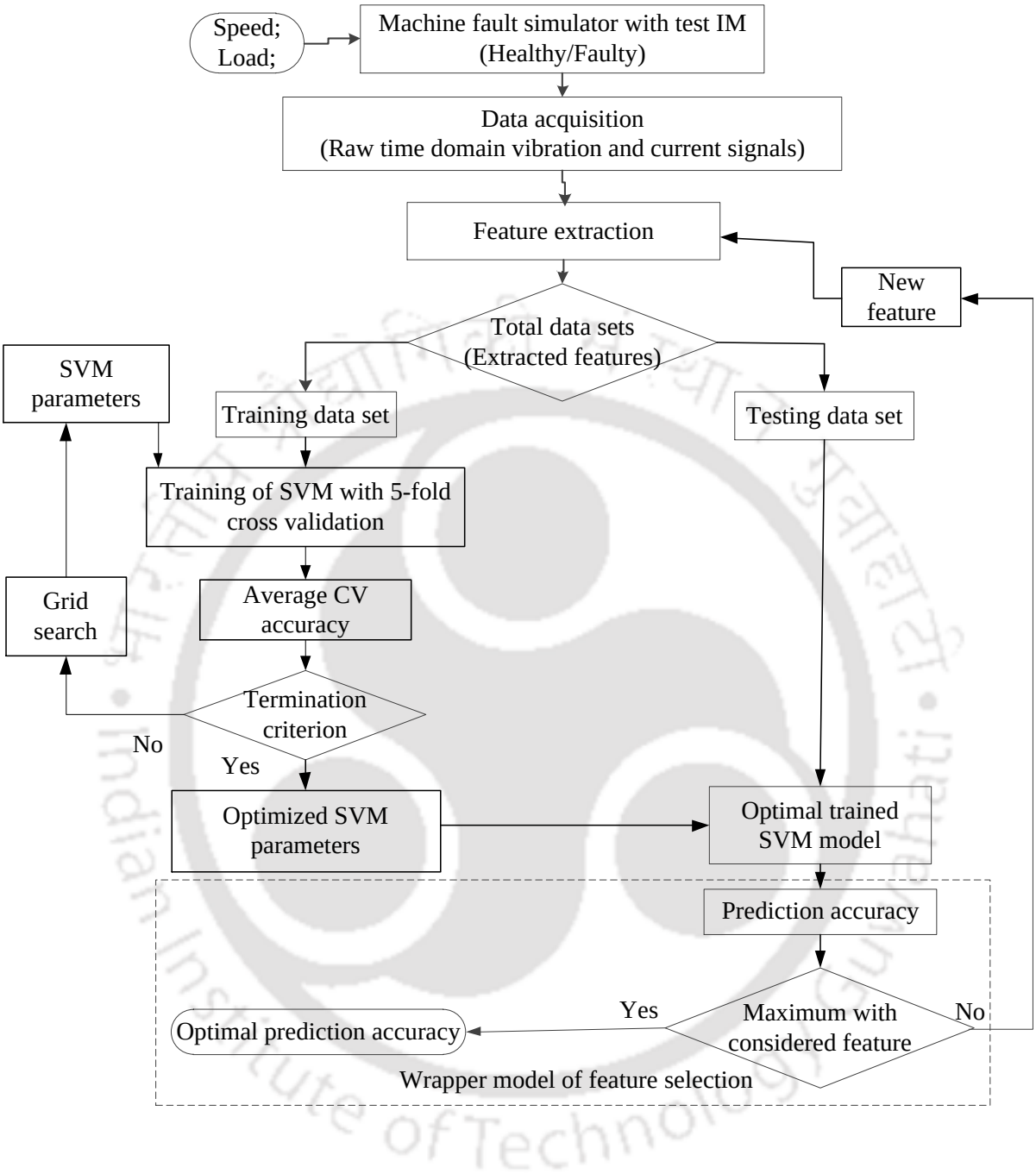

Figure 2.8 The flow chart of proposed fault diagnostics

Two cases of the fault diagnosis are considered here. First when the training of the SVM is performed at particular operating condition (speed and load) of IM followed by the testing of the SVM at the same operating condition as the training. Second, when the training of the SVM is

done at two operating conditions and testing is done at an intermediate operating condition. The second case of fault diagnosis is considered here in order to take care of the situations, where the limited information about IM operating conditions is available. In this study, the LIBSVM toolbox (Chang and Lin, 2011) is used in the MATLAB environment for implementation of the multiclass SVM. The time taken for testing depends upon the specification of the computer. In this work, Intel® Core™ i5-2400 Processor (3.10 GHz) with 3 GB RAM and 32 bit OS is used. The CPU time for training and testing in different cases of fault diagnosis are added in the corresponding chapters.

2.6 Summary

The fault diagnosis methodology based on the SVM has been discussed in this chapter. First the formulation of binary and multiclass SVM are presented in detail. Then the cross validation method along with a grid-search technique and the wrapper model are discussed for the parameter selection of the SVM and the feature selection, respectively. In addition, the procedure for feeding the data to the classifier for the training and the testing is established. In order to apply the SVM based fault diagnosis in IMs, the data from the healthy and faulty motors are needed. In chapter 3, the experimental setup and procedure for the generation of data of different IM faults is discussed.

CHAPTER 3

Experimental Setup and Procedure for Data Generation of IM Faults

3.1 Introduction

This chapter describes the experimental setup followed by the experimental procedure, which are used to acquire the vibration and current signals to perform the IM fault diagnosis. The experimental setup was arranged and experimentation through necessary instruments was performed at the Vibration and Acoustic Laboratory in IIT Guwahati.

3.2 Experimental Setup

Experiments were carried out on a test-rig that consists of a ready-made machine fault simulator (MFS). The test-rig consists of test IMs with different seeded faults, measurement sensors (tri-axial accelerometer and AC current probe), a constant DC power source, and a data acquisition system (DAQ) with a signal monitor. The pictorial view and the schematic diagram of the actual test-rig to perform experiments are as shown in Figure 3.1 and Figure 3.2.

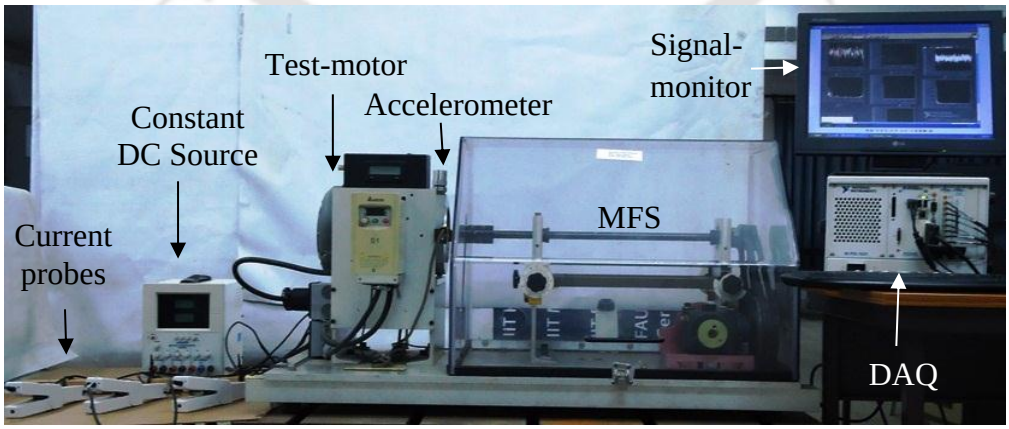

Figure 3.1 A pictorial view of experimental test-rig used in the laborotary

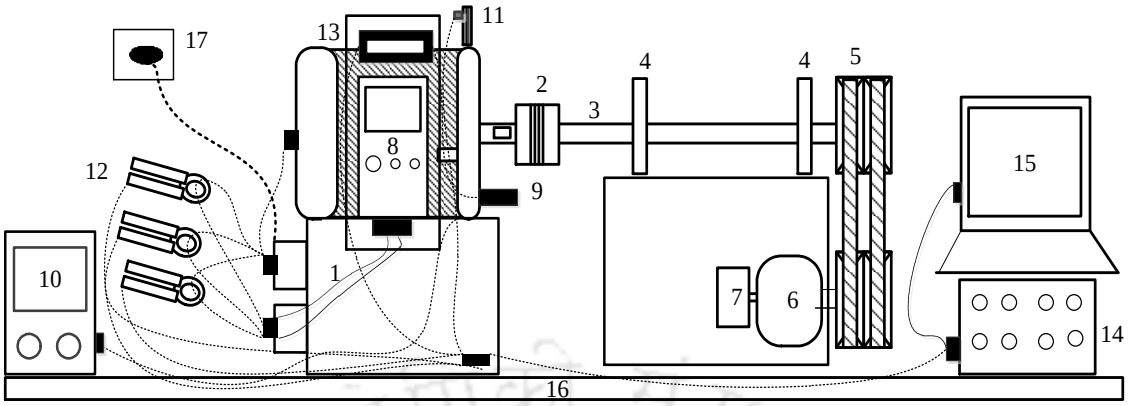

Figure 3.2 A scematic diagram of experimental test-rig with instrumentation

(1-Test IM, 2-Coupling, 3-Shaft, 4-Bearings, 5- Belt-pulley drive, 6-Gear box, 7- Magnetic brake clutch, 8-VFD, 9-Tachometer, 10-DC power source, 11-Accelerometer, 12-Current probes, 13-LCD display for speed, 14-DAQ, 15-Signal monitor, 16-Base-plate, 17-electrical outlet)

3.2.1 Machine Fault Simulator

The MFS (Make Spectra Quest, USA) simulates very closely the faults that come across on a variety of machines like in IM, shaft, bearings, gearbox and pumps. In order to acquire the data for different faulty machines, various transducers could be installed at particular locations in the MFS. The simulator provides a basic setup for performing experiments and learning signatures of different machine faults. The simulator is designed to be both versatile and easy to operate. In this work, the MFS is used to simulate faults in IMs.

The MFS is constructed with an IM (three phase, 0.373 kW (or 0.5 HP), 50 Hz, 2 pole, pre-wired self-aligning mounting system), a split bracket bearing housing, a sliding shaft, rotors with split collar ends, a flexible coupling, pulleys, a multiple belt tensioning, a variable frequency drive (VFD) with multi-featured front panel programmable controller, a magnetic brake attached with a

gear box, and a photovoltaic sensor; all of which are designed to be easily removed and replaced between various experiments. In the basic setup, an IM (test machines in our work) was connected to the shaft through a flexible coupling. The shaft was mounted on the bearings with the split bracket bearing housing. One pulley was attached at the end of the shaft and the other with the gearbox shaft. They were connected using a multiple belt tensioning mechanism. The gearbox mechanism connected the shaft with a magnetic brake. The magnetic clutch was used to apply mechanical load to the IM externally. A variable frequency AC drive was used to control the speed of the motor. A tachometer was mounted near the coupling to measure the mechanical speed of the shaft, which is required a constant DC power supply source to operate. The base plate of the simulator was attached with the vibration isolators and base stiffener. These all mechanisms were installed in such a way so that they could easily shift, removed and replaced for different experiments. The basic MFS setup is shown in Figure 3.3.

In order to acquire vibration and current signal from test IMs, a tri-axial accelerometer was installed on the top of the test motor near the motor shaft end and three AC current probes were clamped with the power leads of the motor which is easily accessible. The sensors were connected to the DAQ thorough proper instrumentation. A signal monitor with NI LabVIEW data acquisition software was used to analyze the data.

The technical specification of a number of components of the test rig is described in the Table 3.1. The basic components of the MFS are described in details in this sections. The experimental procedures are discussed in Section 3.3.

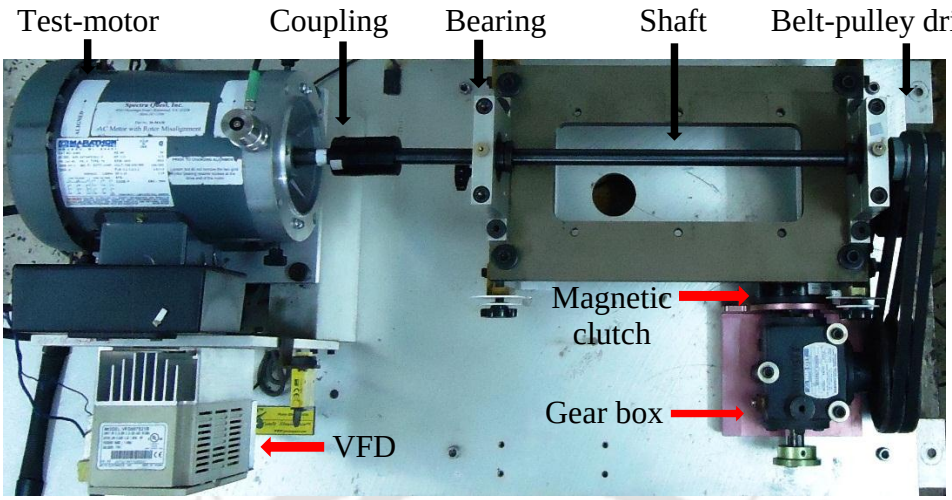

Figure 3.3 The basic machine fault simulator (top view)

Table 3.1 Technical specification of the test rig components

No.	Component name	Technical specification of components
Electrical components:		
1	IMs	Three-phase, 0.372 kW (or 0.5 HP), pre-wired self-aligning mounting system for easy installation and removal, number of rotor bar-34 and number of stator slot-24
2	Speed controller	0.7457 kW (or 1 HP) variable frequency AC drive with multi-featured front panel programmable controller
3	RPM range	0 to 10000 rpm (short duration) variable speed,
4	Voltage	115/230 VAC, single phase, 50 Hz
5	Tachometer	Built-in tachometer with LCD display and one pulse per revolution analog output for DAQ purposes. Requires DC power supply unit (range: ± 30 V/2A)

Table 3.1 Technical specification of the test rig components (continued)

No.	Component name	Technical specification of components
6	Data acquisition system	National instrument make NI PXI-8108 Core 2 Duo 2.53 GHz controller with NI PXI-4472, 8 channels, 24 bits, 102.4 kS/s sampling rate for accelerometer module
7	Current measurement	Power leads accessible for current measurements
Mechanical components:		
1	Shaft diameter	19.05 mm diameter; turned, ground & polished (TGP) steel.
2	Bearings	Two sealed rolling element in aluminum horizontally split bracket housing for easy replacement, tapped for transducer mount. Bearing mounts can be mounted in five different positions for variable rotor span
3	Rotor base	360 mm long, completely movable using jack bolts for easy horizontal misalignments and standard shims for vertical misalignments. Pinned for easy realignment.
4	Belt mechanism	Two double groove "V" belt with one set screw mounting and one bush/key mounting. Positive displacement lever with turnbuckle plus adjustable gearbox platform.
5	Gear box mechanism	Accessible three-way straight cut bevel gearbox with 1.5:1 ratio (number of teeth on pinion-18, number of teeth on gear-27).
6	Torque controller	A manually adjustable permanent magnet clutch, of range 0-0.565 N-m.

Table 3.1 Technical specification of the test rig components (continued)

No.	Component name	Technical specification of components
7	Foundation	12.7 mm die cast aluminum base, base stiffener and eight rubber isolators
Measurement sensors:		
1	Tri-axial accelerometer	Sensitivity: 100.3 mV/g-*x* axis, 100.7 mV/g -*y* axis, 101.4 mV/g -*z* axis,
2	AC-current probe	Frequency range: DC to 100 kHz (-3dB with current de-rating) Current range: 100 mV/A: 100 mA to 10 A peak, 10 mV/A: 1 to 100 A peak.

3.2.1.1 Speed Controller or Variable Frequency Drive

A speed controller or Delta Make variable frequency drive (VFD) is a type of motor controller that drives an IM by varying the frequency and voltage supplied to the IM. It is a power electronic based device which converts a basic fixed frequency, fixed voltage sine wave power (line power) to a variable frequency, variable output voltage used to control speed of IMs. It consists of a rectifier bridge converter, a direct current (DC) link, and an inverter. The VFD can simply turn up or turn down the motor speed as per the application's motor speed requirement change. In this work, a variable frequency AC drive (0.746 kW, Input: 1-phase, 9.2A/3-phase, 5.1A, 200-240V, and 50/60Hz, Output: 3-phase, 4.2A, and 0-240V) was used. In this, the speed can be set with a knob in the range of 0-400 Hz. A VFD, which was used for the experimentation is as shown in Figure 3.4

3.2.1.2 Torque Controller or Magnetic Clutch

A torque controller or Precision Tork™ permanent magnet clutch unit was connected with the gear box mechanism to provide the precise torque adjustment of the IM. This type of controller does not require any external control or power source to operate, therefore their function is independent from power fluctuations. The torque was set with a large knurled adjustment ring. There is infinite adjustability between the minimum and maximum settings. This allows units to be fine-tuned to specific requirement. The torque can be set in the range of 0-0.565 N-m. This unit provides extremely consistent and smooth torque at the low as well as high speeds. Since the torque is transmitted magnetically, there is no friction from which to break away. This means that the static and dynamic torques are almost the same. A torque controller with the gear box mechanism, which was used for the experimentation is shown in Figure 3.5.

Figure 3.4 A variable frequency drive

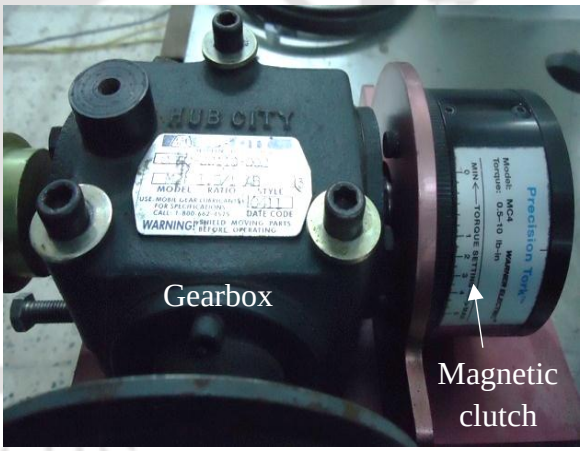

Figure 3.5 A magnetic clutch with a gearbox

3.2.2 Fault Specifications and their Genration Procedure

The main components of an IM are stator, rotor, rotor shaft and bearings (as shown in Figure 1.1). Failure of any of these components can cause damage of other components that leads to complete motor failure. In this study, two types of IM faults are studied: mechanical faults and electrical faults. Mechanical faults include the bearing fault (BF), unbalanced rotor (UR), bowed rotor (BR) and misaligned rotor (MR), whereas electrical faults include the broken rotor bar (BRB), stator winding faults (SWF) and phase unbalance fault (PUF) considered (as shown in Figure 3.6 and illustrated in Table 3.2). In addition, in order to study the fault under progression, two severity levels of stator winding and phase unbalance faults are also considered.

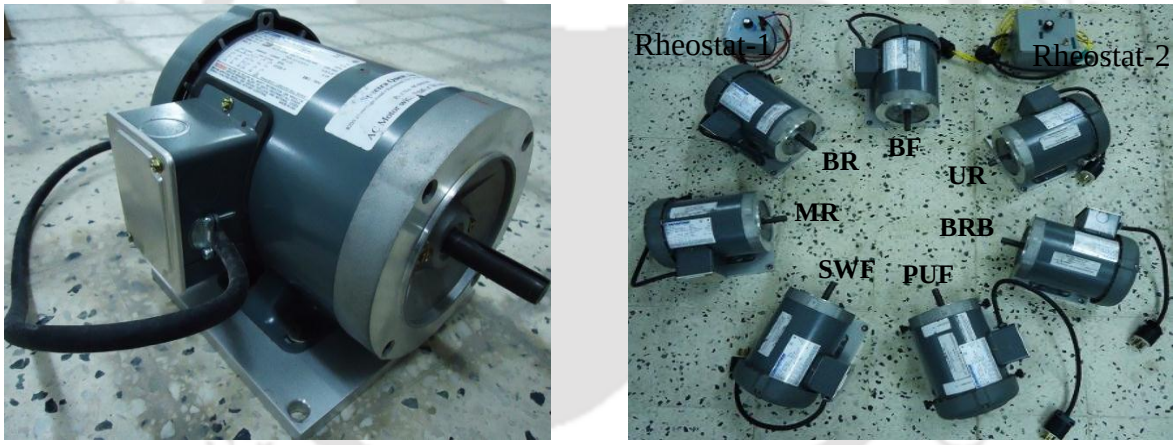

(a) (b)

Figure 3.6 (a) An IM with no defect (b) IMs with various seeded faults

IMs with various seeded faults were available with the ready-made MFS. Five fault conditions (i.e. BRB, BF, UR, BR and MR) were simulated in five different motors; however, four fault conditions (i.e. stator winding fault: level 1 (SWF1) and level 2 (SWF2), and phase unbalance: level 1 (PUF1) and level 2 (PUF2)) were simulated in two motors only. In total, ten different fault conditions of

IMs have been considered in the present study. The procedure of generation of the considered faults in IM is discussed here.

The BRB defects have been manually produced in the workshop by drilling a number of bars in the rotor cage. A solid model of the BRB defect is as shown in Figure 3.7.

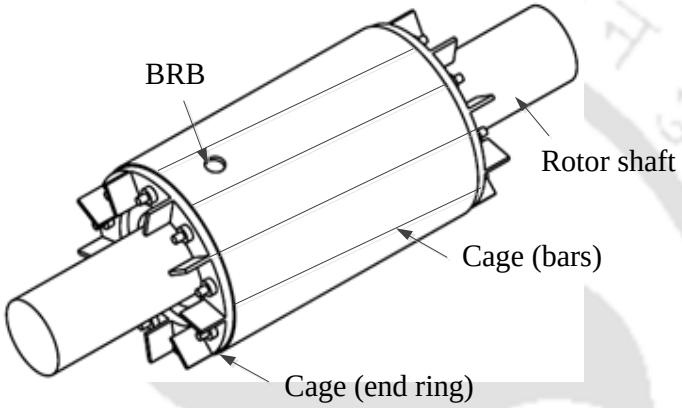

Figure 3.7 A solid model of the broken rotor bar in the IM

The SWF may be due to the turn-to-turn, coil-to-coil, phase-to-phase or phase-to-ground fault as shown in Figure 1.4. Most of the SWF are the consequence of the growth of undetected turn-to-turn faults. Catastrophic failure of IM can be avoided by early diagnosis the turn-to-turn faults within a coil. Therefore, in this study, the turn-to-turn SWF is considered with two severity levels (i.e., SWF1 and SWF2), which was simulated by tapping the stator windings to enable adding an additional load to the winding via an external control box (or rheostats) as shown in Figure 3.8. In this figure, "*a*", "*b*" and "*c*" denote the three phases of IM, I_{as}, I_{bs}, and I_{cs} denote the current in three phases, i_{f1} denotes the current flowing through the short circuit. as_1 denotes the normal turns and as_2 denotes the shorted turns in phase "*a*", and R_f denotes the external resistance.

The variable resistor was used to introduce a varying amount of resistance in the turn-to-turn short between the windings. The control box consists of 0-2 Ω variable resistor. Change of the severity level of the stator inter-turn short fault can be emulated by adjusting the value of this control box, which then be reflected in the variation of the loop current. High resistance simulates a low severe faults and vice versa. The control box also restricts the circulating currents in the shorted portion of the stator winding to a safe level to avoid permanent motor winding damage. However, when the control box is disconnected, the motor becomes a normal. Moreover, other SWF can be simulated using the proposed method. In order to simulate PUF and their severity levels (i.e., PUF1 and PUF2), similar procedure as the generation of SWF was adopted in a separate IM.

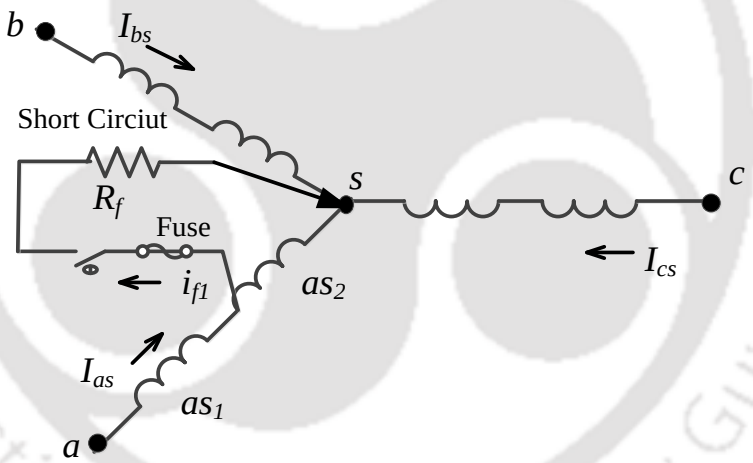

Figure 3.8 Turn fault on a single phase of the IM

The BF may be due to the inner race fault (IRF), outer race fault (ORF), and ball element fault (BEF). In this study, the ORF is considered for the BF, which was artificially developed in the bearing near the shaft end by spalling out or drilling out some material from the outer raceway. A solid model of the ORF in bearing is shown in Figure 3.9.

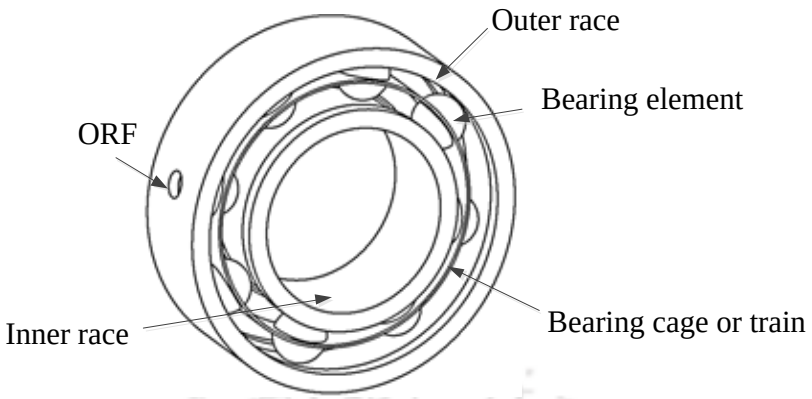

Figure 3.9 A solid model of the bearing fault in the IM

The UR was achieved by taking a balanced rotor from the manufacturer and intentionally removing balance weight and/or adding weight. Here, the balanced weight was attached to small aluminum pins protruding from both ends of the rotor. A solid model of the unbalanced rotor of IM is shown in Figure 3.10.

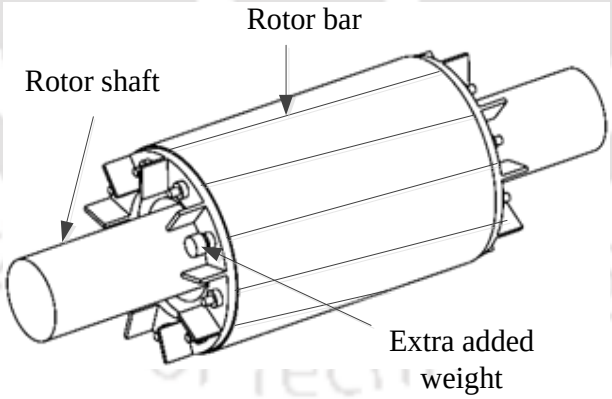

Figure 3.10 A solid model of the unbalanced rotor in the IM

The BR was achieved by carefully bending the rotor at the center, which when produced creates the dynamic air-gap eccentricity. Figure 3.11 shows the centrally bent rotor in the IM.

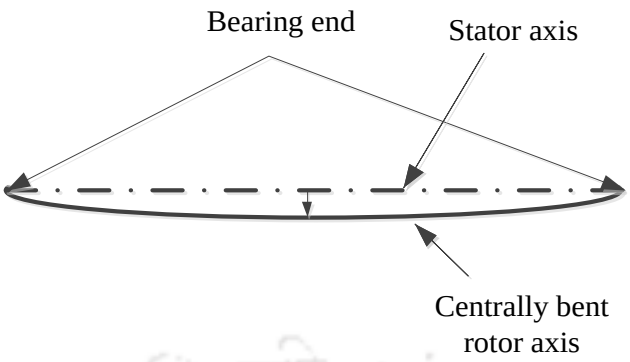

Figure 3.11 The bowed rotor in the IM

The MR can be considered as the parallel misalignment or the angular misalignment as shown in Figure 3.12. The MR creates the static air-gap eccentricity. The parallel misalignment can be achieved by displacing the motor bearing the same amount on each end using four jack bolts attached with the motor. Angular misalignment can be achieved by displacing one end more than the other. In this work, the rotor misalignment is considered as an angular misalignment because the chances of angular misalignment are more than the parallel in IMs.

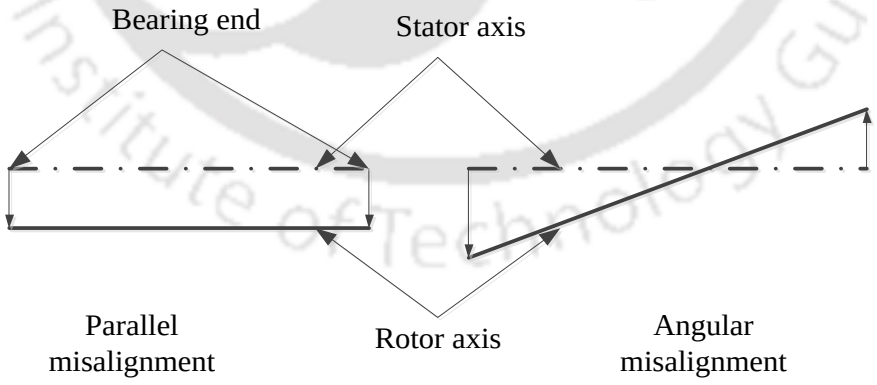

Figure 3.12 The parallel and angular rotor misalignment in the IM

Table 3.2 The discription of motor fault conditions

No.	Motor fault conditions	Fault description	Others
1	No defect condition (ND)	Motor with no defect	Healthy motor
2	Broken-rotor bar (BRB)	12 broken rotor bar out of 34	By drilling bar in the rotor cage
3	Phase unbalance level-1 (PUF1)	Less severe fault	By adding resistance (max)
4	Phase unbalance level-2 (PUF2)	High severe fault	By adding resistance (min)
5	Stator winding fault level-1 (SWF1)	Less severe fault	By adding resistance (max)
6	Stator winding fault level-2 (SWF2)	High severe fault	By adding resistance (min)
7	Bearing fault (BF)	Outer race fault	A spalling on the outer race way
8	Unbalanced rotor (UR)	Motor with unbalanced rotor	By attaching balanced weight
9	Bowed rotor (BR) Or dynamic air gap eccentricity	Motor with centrally bent rotor	Bent the rotor in the center
10	Misaligned Rotor (MR) Or static air gap eccentricity	Angular misalignment	By displacing the motor bearing at one end more than the other.

In total, ten different faulty conditions were artificially created in eight different IMs. It is noted that, in actual case, levels of these faults may be different, but basic features of such faults would remain the same in dynamics and electrodynamics. All the considered faults in this study are common faults of IM failures that occur in the industry. They cover more than 90% of all fault modes occurs in the IM.

3.2.3 Measurement Sensors

3.2.3.1 Tri-axial Accelerometer

A tri-axial accelerometer (Make Meta Mess-und Frequenztechnik, Germany) was temporarily attached to the top of the motor surface with a very strong magnetic base, close to the bearing and at the shaft end, to acquire absolute vibration signals in three orthogonal directions, i.e. the axial, radial and tangential, as shown in Figure 3.13. This accelerometer uses the phenomenon of piezoelectricity. It generates an electric charge signal proportional to vibration acceleration. It has many advantages such as extremely wide dynamic range, low output noise, excellent linearity over their dynamic range, compact yet highly sensitive, no moving parts so no wear, self-generating so no external power required. In this work, vibrations in three orthogonal directions were measured using this tri-axial accelerometer because different faults generate specific signatures in different directions. The accelerometer was connected with the data-acquisition hardware using the BNC cable.

3.2.3.2 AC Current Probes

The three AC current sensors (Keysight 1146B) were clamped to three easily accessible cables of IMs to acquire stator current signals in all three phases as shown in Figure 3.14. This type of

AC/DC current probe provides an accurate display and measurement of currents from 100 mA to 100 A rms, dc to 100 kHz, without breaking the circuit. The sensor uses Hall-effect sensor technology to measure the AC and DC signals. In this work, currents in all three phases were measured because one phase current may not be adequate to precisely recognize IM faults, particularly if the faults is not present in the analyzed phase. These probes were connected with the data-acquisition hardware using BNC cables.

Figure 3.13 Tri-axial accelerometer

Figure 3.14 AC current probes

3.2.3.3 Tachometer or Photovoltaic Sensor with a Constant DC Power Source

The tachometer or photovoltaic sensor was mounted near the coupling in the MFS to measure the angular speed of the shaft as shown in Figure 3.15. The tachometer requires a DC power supply of the range of ±30 V/2A to operate. It was provided through a constant DC power source (Make Scientific MES-Technik PVT. LTD., India). The constant DC power source unit is shown in Figure 3.16. The source converts the AC power from the mains supply to the DC voltage. It protects against the short circuit and the overload, and has a digital display for the current and voltage, and an adjustable current limiter. This source offered the high-resolution, high-power voltage and

current outputs for the same set-up. The tachometer was used to measure the rotor speed, which can be observed in RPM on a LCD display and recorded one pulse per revolution analog output for the DAQ purposes. To measure the rotor speed, tachometer was attached near the shaft end of the motor, which emits laser beam that strikes over the reflecting tap pasted on the motor shaft.

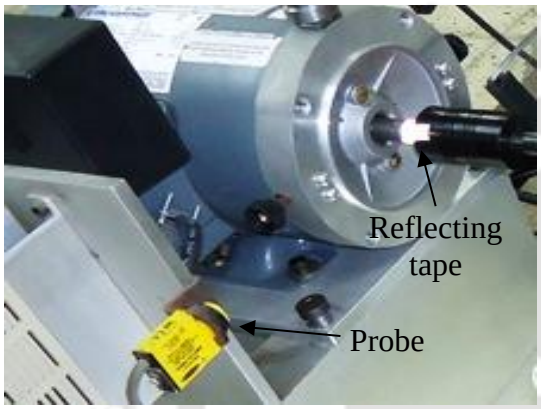

Figure 3.15 The photovoltaic sensor

Figure 3.16 A constant DC power source

3.2.4 Data Acquisition System

A data acquisition system (DAQ) or electronic data collector (Make national instruments, USA) system consists of sensors, a DAQ measurement hardware, and a computer or signal monitor with programmable software as shown in Figure 3.17. The DAQ is an analog-to-digital converter, which converts conditioned sensor signals to digital values. The analog signal output from the sensors is directed to the input channel of the data acquisition system. The analog signal is a continuous varying voltage that is proportional to the vibration and current signals. The DAQ hardware consists of a controller (NI PXI-8108 Core 2 Duo 2.53 GHz) and a dynamic signal analyzer (NI PXI-4472, 8 Ch, 24 bits, sampling rate- 102.4kS/s) mounted on a single PXI chassis. The controller unit runs on the Win XP and consists of input device, like mouse, keyboard, LAN

connector jack, and output device, like the monitor, USB device and hard drive. Among many analyzer (or the signal acquisition module), the time capture module was used to capture signals in the time domain and the frequency capture module was used to capture signals in the frequency domain. The analog or input time domain signal in the analyzer is digitized before performing the FFT so that it is possible to supply continuous data to the algorithm. The sensors (accelerometer, current probes and photoelectric (tacho) probe were connected with the different channel of PXI-4472. The data acquisition software (NI LabVIEW) was preloaded in the system (PXI-8108) and it programmed to collect the real time domain data as well as frequency domain data.

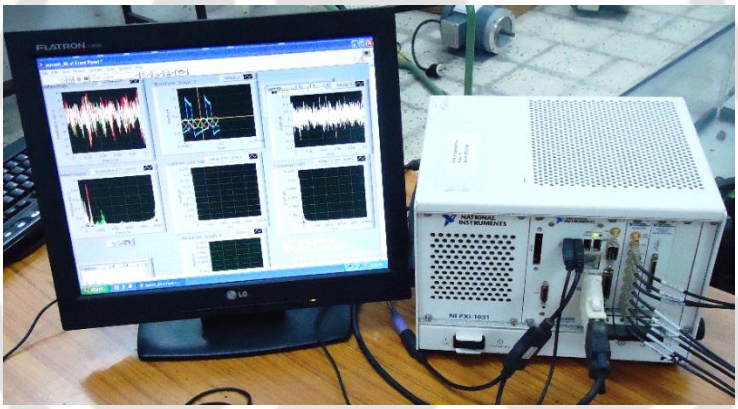

Figure 3.17 A DAQ with a signal monitor

3.3 Experimental Procedure

The LabVIEW^{NI} software was configured to capture the time and frequency domain signals. Data acquisition was carried out for vibration (in three orthogonal directions) and stator current (in three phases) signals, which were acquired using accelerometer and current probes from the test rig. The vibration and current signals were used to measure the physical condition of IMs. The digitized measurement data were collected from each faulty motor and a healthy one, which is a benchmark

for comparison with the faulty one. Measurements were taken at various operating conditions of IMs. The data were collected from each IM fault condition tested under three different loadings such as the no load-0 N-m, i.e. 0% of rated torque (T_1); the light load- 0.113 N-m, i.e. 0.11 % of rated torque (T_2); and the high load- 0.565 N-m, i.e. 0.55 % of rated torque (T_3), and seven different speeds ranging from 10 Hz to 40 Hz in the interval of 5 Hz. It is noted that the conventional fault diagnosis is not always reliable, especially at the light load on the motor, so in order to check the reliability of the present methodology the data were generated at the no and light loads as well as at the high load. Conventional methods are also dependent on motor speeds. Therefore, in order to generate exhaustive data sets, a suitable range of speed that can be easily achieved by machine fault simulator was considered. Ranges of operating conditions were purely based on provisions available and limitations of the experimental setup.

In order to study the effect of the sampling rate and data points (or frequency resolution) on fault diagnostics, two types of experiments were performed. Because, it is very significant to choose the adjusted sampling frequency and data points that can improve the fault diagnostic, detection time, and reduce the cost of implementation. The first experiment (i.e., Experiment-1) was performed with the sampling rate of 20,000 S/s and 2000 sample points so as to capture higher frequencies and to have 10 Hz or lower frequency resolution. The second experiment (i.e., Experiment-2) was performed with the sampling rate of 1000 S/s and 10,000 sample points in order to maintain the higher resolution of data, i.e. 0.1 Hz and capture lower frequencies with more accuracy. In Experiment-1, the data were acquired for 30 second, hence 300 raw datasets (300 datasets$\times$ 2000 sample points) were created in the time domain for a particular fault and an operating condition of IM. Similarly, using the FFT, 1000 samples were collected in the frequency

domain and total of 300 raw datasets (300×1000 sample points) were created. In Experiment-2, the data were acquired for 250 s, hence 25 raw datasets were created in the time domain (25 datasets × 10000 sample points) and the frequency domain (25 datasets× 5000 sample points). Figure 3.18 illustrates the data collection in the time domain and the frequency domain using the LabVIEW for the rotor misalignment fault at 40 Hz speed and T_3 load, obtained from Experiment-2.

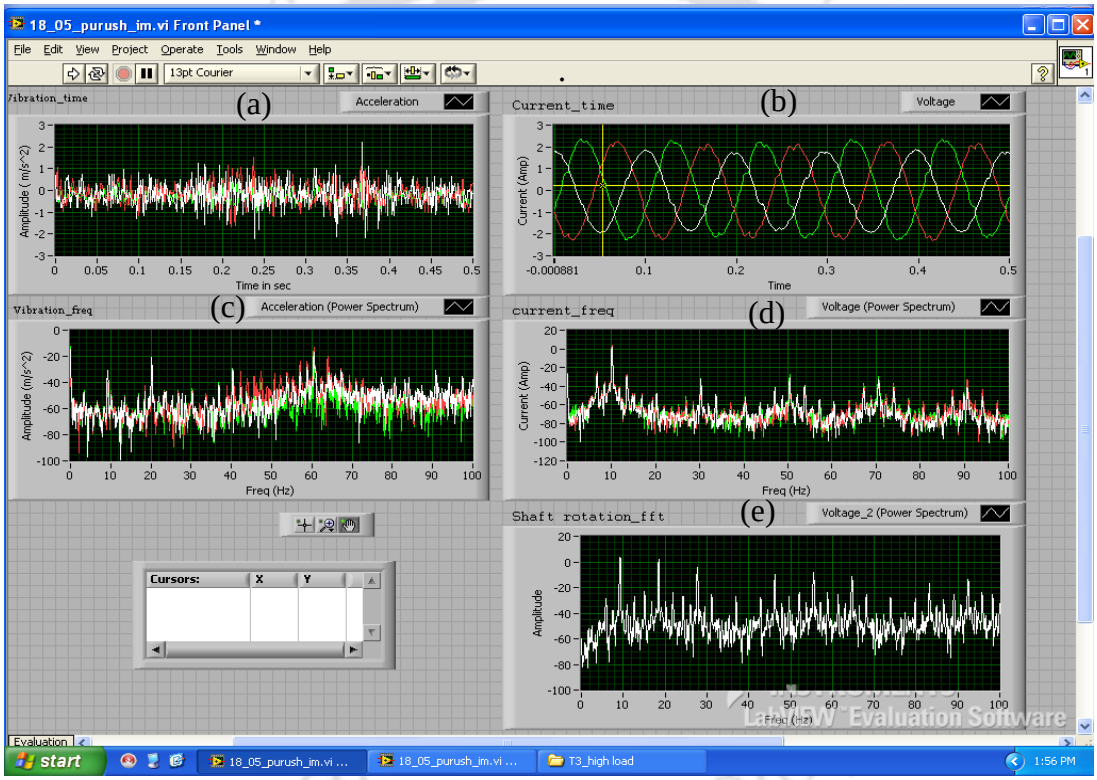

Figure 3.18 Data collection in the time and frequency domains using the LabVIEW

In Figure 3.18, Window (a) and Window (b) show measurement of the time domain vibration in three orthogonal directions showing with three different colors (red- *x* axis, white- *y* axis and green- *z* axis) and current signal in three phases showing with three different colors (red-phase 1, white-

phase 2, and green-phase 3), respectively. Window (c) and Window (d) show the FFT of vibration and current signal, respectively. Window (e) shows the measurement of mechanical speed of the rotor. Finally, raw data sets in the time and frequency domains from both experiments were stored on the hard disk of the system at individual speeds and loads for each IM fault condition, from which can be retrieved for later processing.

3.4 Observations and Discussions

Experiments were performed for a healthy motor and for all the faulty motors under the various operating conditions. The vibration and current measurements were made. Some important observations obtained from experiments are presented in this section.

3.4.1 Time Domain Analysis of IM Faults

When faults occur in different components of IMs, the time-domain vibration and current signals change. Both its amplitude and distribution may be different from those of a time-domain signal under normal conditions. In order to analyze the time domain vibration and current signals from different fault conditions of IMs, the time series plot obtained at 40 Hz speed and T_3 load from Experiment 2, are presented in Figure 3.19. In vibration signals, the difference between the waveform of normal and faulty motors can be seen; however, these cannot be segregated. Moreover, there are many impulses on the waveform of vibration for the bearing fault. For current signals, the variation is not visible among these faults from time domain waveform since the main component is the line frequency; and the fault signal is modulated or riding on the sine wave of the line frequency (50 Hz). However, in the case of phase unbalance and stator winding faults, a high variation of the current magnitude among three phases can be clearly seen. Changes or

variations in both vibration and current signals from different faults cannot be predicted or segregated directly looking into these signals, due to the irrelevant information or high noise and machine unbalances, especially at the early stage of fault. In other word, the variation in raw time domain vibration as well as current signals are too small to be detected, therefore the comparison of raw time domain signals of faulty and healthy IMs is not effective in order to determine whether the component is behaving normally or exhibiting signs of a failure. Thus, in order to reveal the significant information from time domain signals, a signal processing method is needed, which converts raw signals into appropriate condense form. This can be achieved by extracting useful statistical features. Useful features that can be extracted from the vibration and current signals of IMs include the RMS value, standard deviation, skewness, kurtosis, etc.

3.4.2 Frequency Domain Signal Analysis of IM Faults

When faults occur in IMs, the frequency spectrums of vibration and current signals and its distribution changes, which signifies that new frequency components may appear in the spectrum. In order to analyze the frequency domain vibration and current signals from different fault conditions of IMs using two types of experimental data, initially the FFT plots are obtained for the BF at 40 Hz speed and T_3 load. Figure 3.20 and Figure 3.21 show the FFT plot obtained from the data of experiment 1, i.e. data with 10 Hz frequency resolution and experiment 2, i.e. data with 0.1 Hz frequency resolution, respectively. Figure 3.20 shows that in such a low-frequency resolution data the significant peaks and sidebands produced by bearing fault in the vibration and current signals may not be captured correctly, because the low-frequency resolution of 10 Hz may overstep important intermediate peaks and sidebands in vibration as well as current signals at low frequency range.

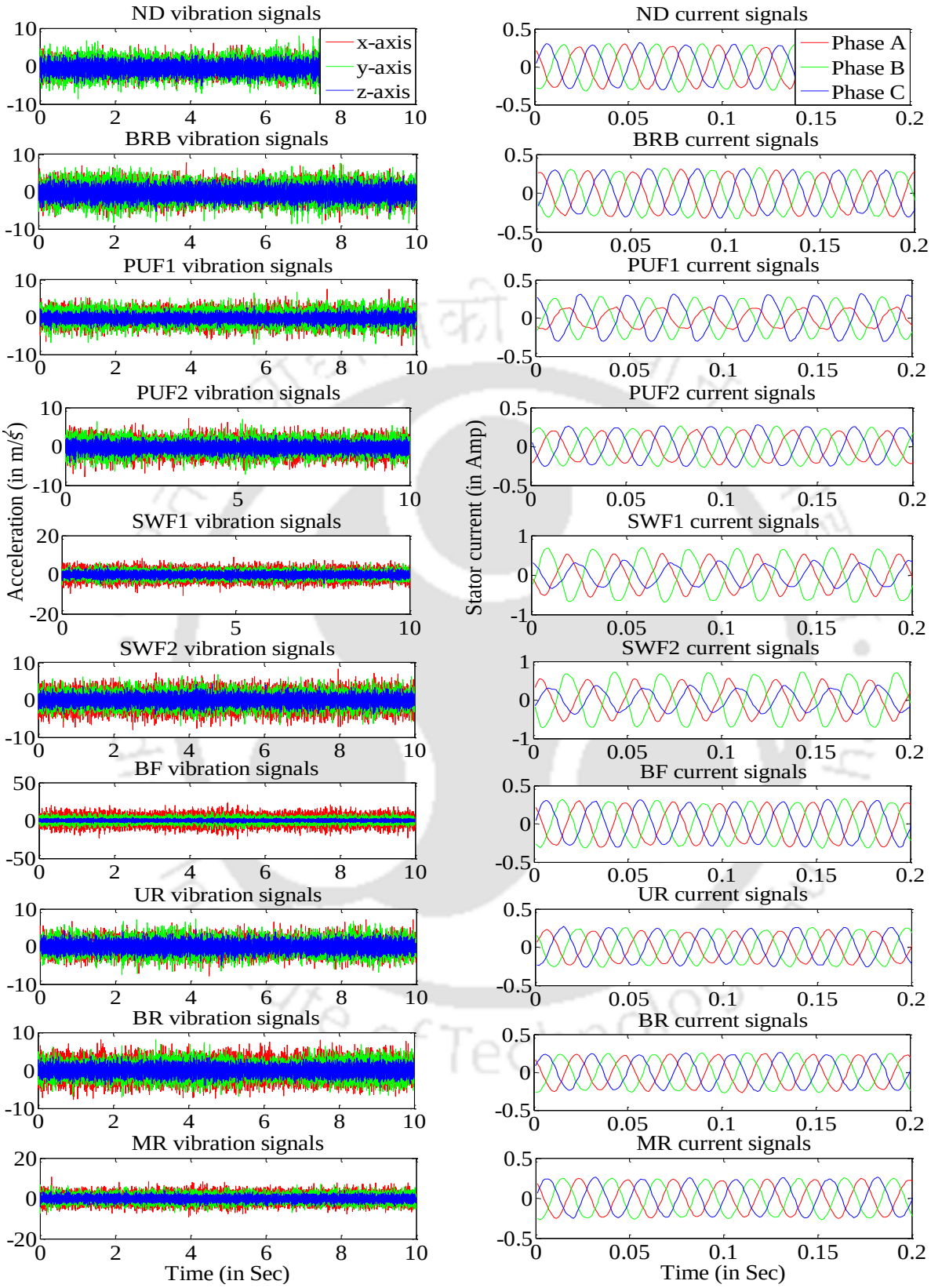

Figure 3.19 The time waveform of vibration and current signals obtained from Experiment-2

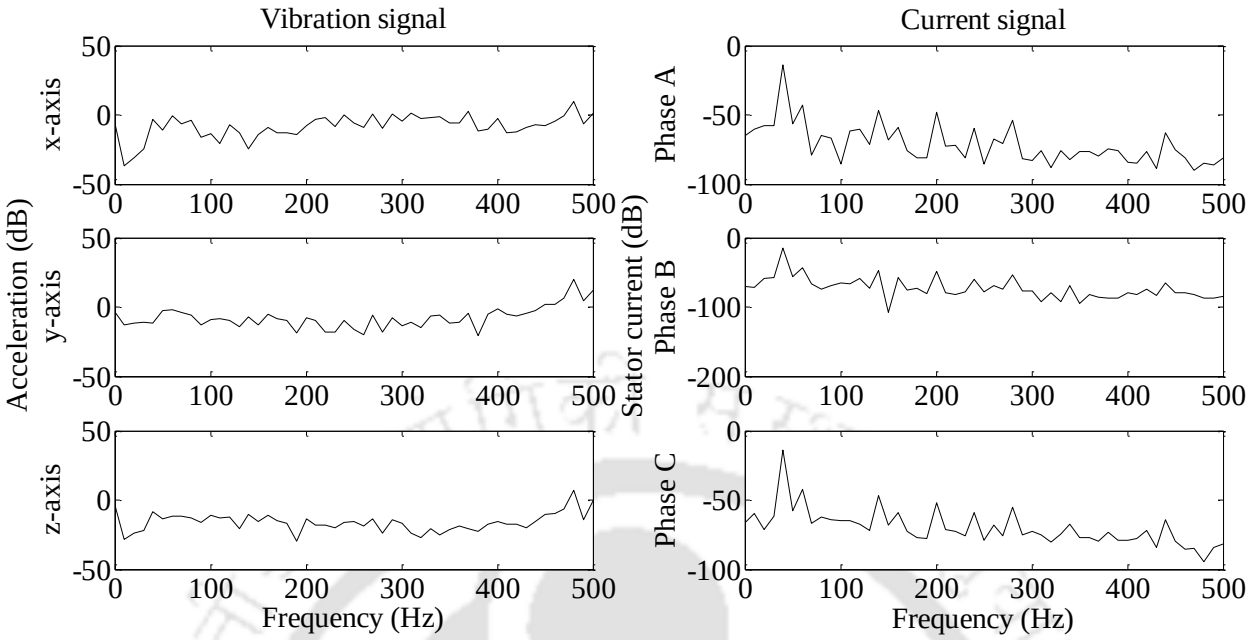

Figure 3.20 Vibration and current spectra of bearing faults obtained at 40 Hz and T_3 using Experiment 1

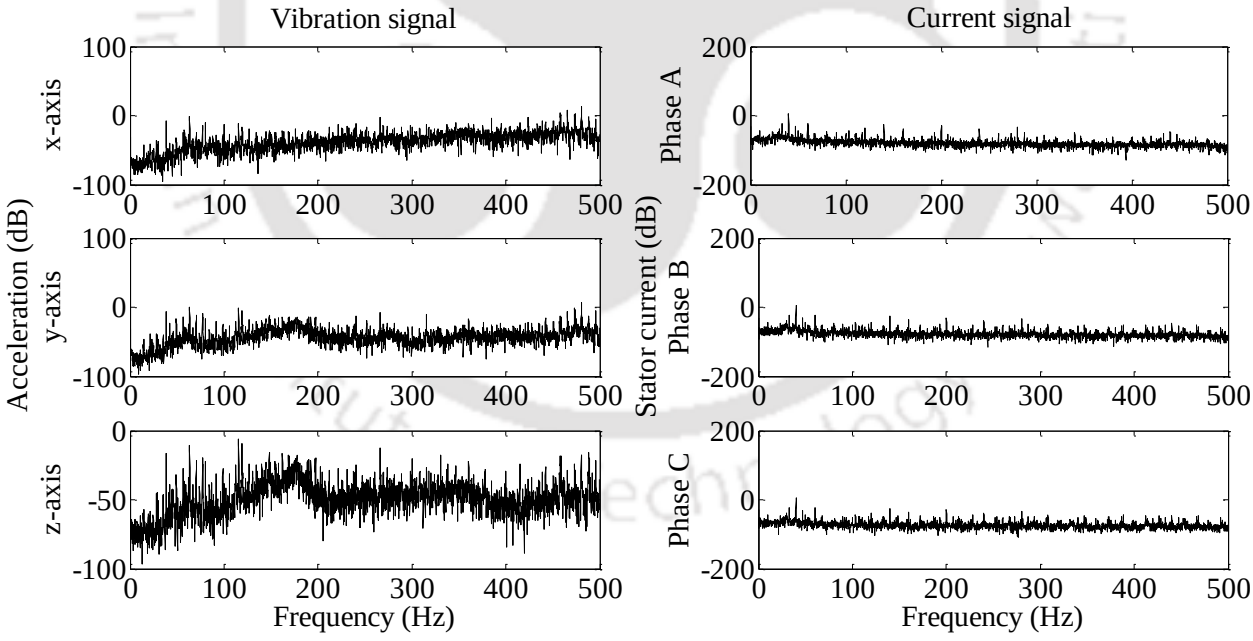

Figure 3.21 The vibration and current spectra of bearing faults obtained at 40 Hz and T_3 using Experiment 2

However, Figure 3.21 shows that the high resolution data of 0.1 Hz are sufficient to capture all the important peaks and sidebands in the vibration and current signals. On taking this perception, the frequency domain analysis is now presented using the high frequency resolution data. The different IM fault conditions are considered one by one for the spectrum analysis.

A. Healthy motor*:* An ideal healthy IM or motor with no defect (ND) has physical constructional symmetry, such as, an equally spaced and constant air-gap length, equal rotor resistances in the rotor and stator windings, and a balanced rotor. However, there are inherent construction asymmetries and imperfections in an actual healthy IM, for example, the air-gap length is not perfectly spaced and as the rotor rotates the air-gap length varies, and the rotor and stator winding resistances for each phase are not the same. These minor physical asymmetries generate unequal magnetic flux and as a result, magnetic force induced vibrations. Hence, a healthy IM is expected to generate some low magnitude vibrations. In addition, due to above problems, some variation can occur in the current signal of healthy motors also.

Figure 3.22 shows the power spectrum of stator current of a healthy motor, when motor was rotating at 40 Hz under the full load condition. In current spectrum of motor with ND, the maximum amplitude comes at 40 Hz; however, the line current frequency is 50 Hz, because the supply frequency applied to the motor is 40 Hz using a VFD. In current signals, sidebands of lower amplitudes around the supply frequency exist even when the machine is healthy, as can be seen in Figure 3.22. This could be due to uneven rotor bar resistance because of the die-casting process, rotor asymmetry, etc. The amplitude and number of sidebands tend to increase if any faults occur and this is an indication of faults.

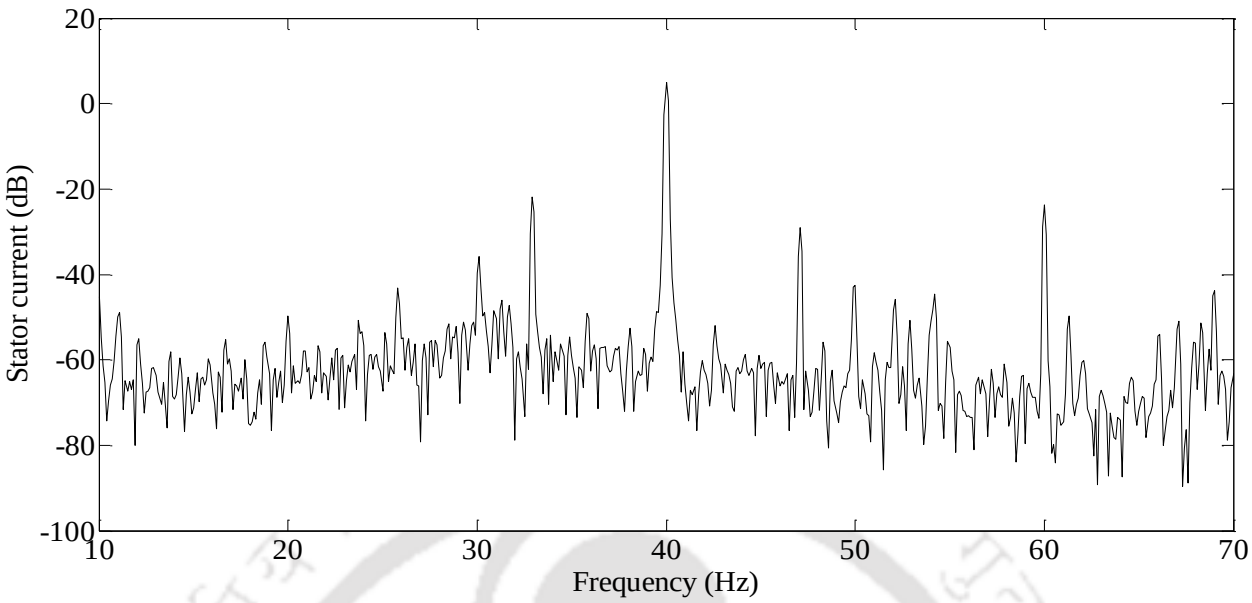

Figure 3.22 Stator current power spectra of a healthy IM at T_3 when VFD is set to 40 Hz

B. ***Broken rotor bars****:* A rotor bar (as shown in Figure 3.7) can be failed due to various stresses such as the thermal, magnetic, mechanical, dynamic, residual, and environmental stresses. When the rotor asymmetry appears due to the broken rotor bar, it creates in addition of a forward rotating field a backward rotating field that turns with the speed of $(-sf_s)$ (where *s* is the operating slip, f_s is the supply frequency). The result of this is an additional frequency component $f_b = (1-2ks) f_s$ in the stator current. This cyclic variation in the current implies a speed oscillation and a torque pulsation at the twice slip frequency $(2sf_s)$. This speed oscillation induces the upper sideband components at $f_b = (1+2ks) f_s$ (where, f_b is the broken rotor bar frequency, and $k = 1, 2, 3, \ldots$). So broken rotor bars tend to induce additional components in the stator current at frequencies given by:

$$f_b = (1 \pm 2ks) f_s \tag{3.1}$$

These sidebands are a function of the slip and supply frequency; therefore, these sidebands are dynamic in nature and vary with the operating condition of IMs.

The BRB also excites the electromagnetic field disturbance and thus intensifies the torque modulations and vibrations of the motor. If a bar is broken in an IM then there will be no flow of current in that bar. Consequently, the field in the rotor around that particular bar will not exist. Thus, the force applied to that side of the rotor would be different from that on the other side of the rotor. It creates an unbalanced magnetic force that rotates at one times rotational speed and modulates at a frequency equal to slip frequency times the number of poles, which is known as pole pass frequency. That means in vibration spectrum increased amplitudes will occur at the rotation frequency f_r and its sidebands (Kanovic et al., 2013)

$$f_{brb} = f_r \pm f_p \tag{3.2}$$

where, f_p is pole pass frequency defined as:

$$f_p = (f_s - f_r).p \tag{3.3}$$

Where p is number of poles and f_s is supply frequency. In addition, the BRB also produces additional sidebands around 1X and higher harmonics $(2f_r,\ 3f_r,....)$ in the vibration spectrum.

In order to study the BRB fault, the stator current power spectra for the BRB when the motor is rotating at 40 Hz under full load is added in Figure 3.23. The sidebands arise around 40 Hz rather than line frequency, i.e. 50 Hz, because the VFD was set to 40 Hz. The slip at this rotating speed and full load is near about 4.29 %, which is found by $s = (N_s - N_r)/N_s$, where N_s is synchronous speed of magnetic field or electrical speed, and N_r is the actual rotor speed or mechanical speed. Fault frequencies or sidebands (as calculated from Equation 3.1) are 37 Hz and 43 Hz when k = 1, 34 Hz and 46 Hz when k = 2, 31 Hz and 49 Hz when k = 3. These sidebands are easily visualized in the current spectrum as shown in Figure 3.23. The rise in sequence of such sidebands as compared to healthy motor spectrum is actually due to broken bars.

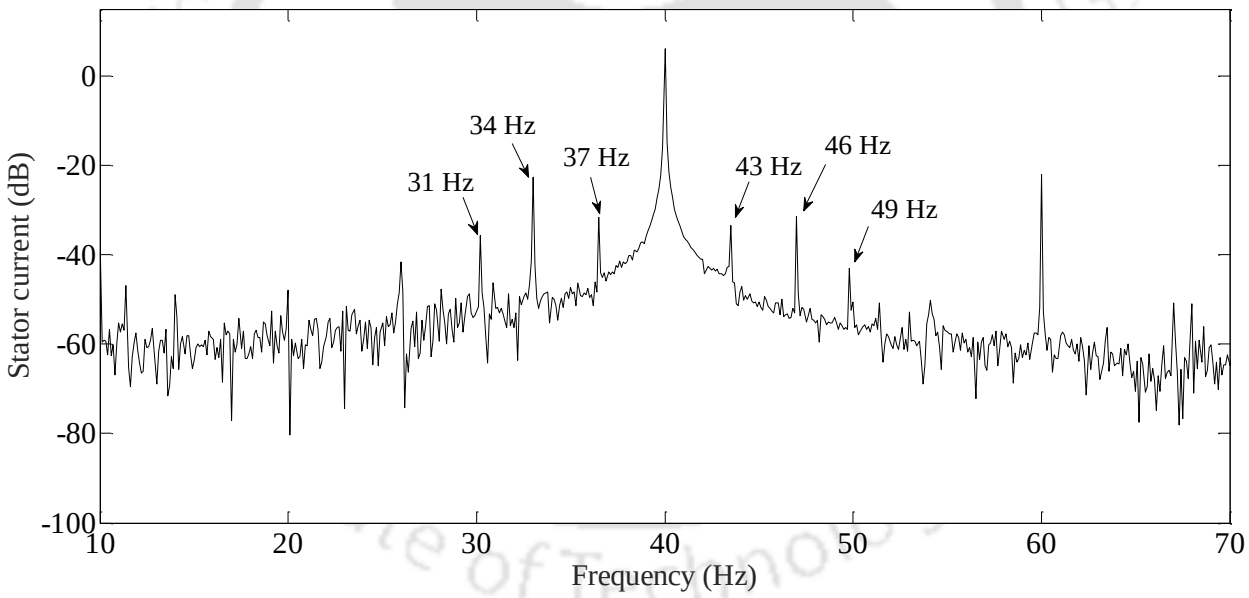

Figure 3.23 Stator current power spectra of IM with the BRB at T_3 when VFD is set to 40 Hz

From Figure 3.23, it can be observed that sidebands for the BRB are visible when the motor is heavily loaded. From Equation 3.1, it is evident that, these sidebands are closely related to motor

slip. If there is no load on the motor, the slip will be almost zero. In that case, the sidebands will be overlapped by the supply frequency and thus make fault diagnosis difficult. Thus, it is necessary to heavily load the motor in order to separate the sidebands (Douglas et al., 2004). Overloading a motor is undesirable since it reduces the motor's operating life and is not generally under control of the operator. Accurate diagnosis of BRB therefore is difficult at light or no load because of low slip operation. In addition, the actual rotor speed is required for calculating slip of the BRB motors, which is not always available.

In order to study the BRB fault, the vibration spectra for the BRB when the motor is rotating at 40 Hz under full load is added in Figure 3.24. Fault frequencies or sidebands (as calculated from Equation 3.2) are 41.72 Hz and 34.84 Hz. In addition, the sidebands occur in higher harmonics of rotational speed are 76.56 Hz and 119.84 Hz. These sidebands can be visualized in the vibration spectrum; however they are of small amplitudes. Similar to current spectrum analysis, low slip due to low load is undesirable in the vibration spectrum analysis is also. The BRB is more difficult to detect in vibration spectrum than the current spectrum because of small amplitudes.

C. Stator winding faults or armature faults: Asymmetrical short circuit in the stator winding are usually related to the insulation damage as shown in Figure 3.8. These faults occur due to hot spots in the stator core, causing the high temperature, electrical discharges, loosening of structural components, moisture, and oil contamination.

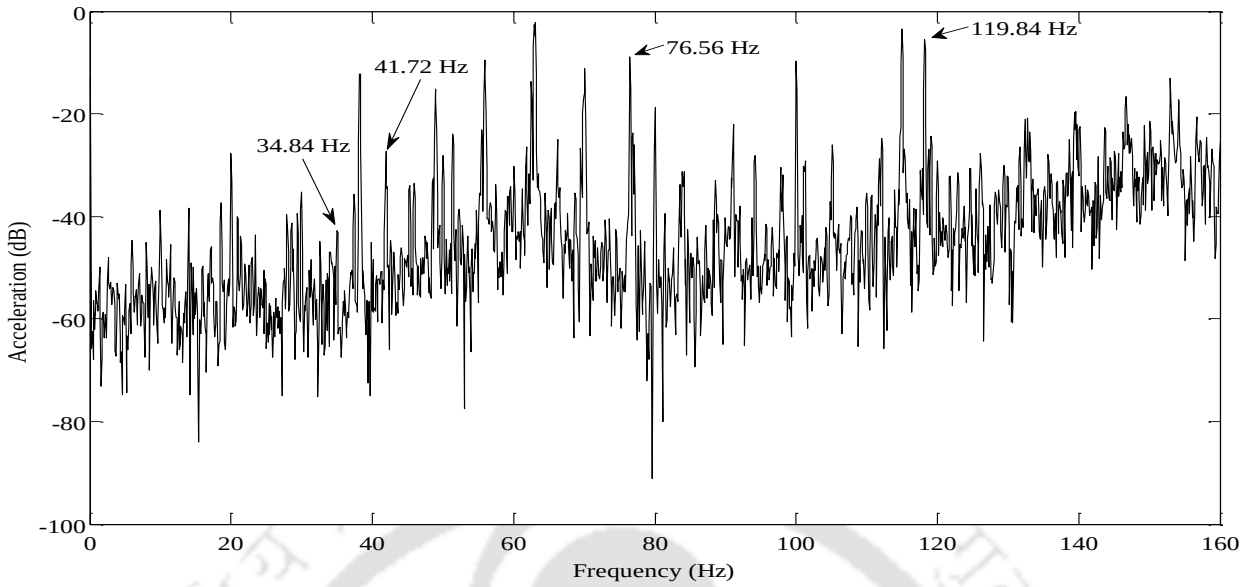

Figure 3.24 Vibration (acceleration) power spectra of IM with the BRB at T_3 when VFD is set to 40 Hz

The additional frequency components appear due to this fault in the current spectrum are given by:

$$f_{st} = \left\{k \pm n\left(1-s\right)/\, p\right\} f_s \tag{3.4}$$

where, f_{st} short turns frequency, f_s is the supply frequency, p is the number of pole pairs, k =1, 3, 5…; n = 1, 2, etc. The stator asymmetry results in the negative sequence components appear in the input current. These faults produce asymmetry in the motor impedance causing the motor to draw an unbalance phase current. This results in induction of negative sequence voltage in the rotor. Since the rotor is short-circuited, this will result in abnormal current flow in the rotor and damage the rotor. In addition, the SWF also produces fault frequencies as (pf_r, $2pf_r$, $4pf_r$,.....) in the vibration spectrum.

In order to study the SWF, the stator current power spectra of an IM with the SWF when the motor is rotating at 40 Hz under full load, is added in Figure 3.25. The slip at this rotating speed and load is near about 4.29 %. The fault frequency (as calculated from Equation 3.4) occurs at 78.5 Hz and 1.5 Hz (when k = 1 and n = 1); 158.5 Hz and 81.5 Hz (when k = 3 and n = 1), 238.5 Hz and 161.5 Hz (when k = 5 and n = 1), 117 Hz (when k = 1 and n = 2), and 155.5 Hz (when k = 1 and n =3). It is observed from Figure 3.25 that fault frequencies are noticeably visible, which indicates the stator winding fault in the IM. However, the supply voltage (or phase) unbalance and load unbalance could also produce the unbalance current and current harmonics at frequencies described by Equation (3.4). This is one of the major problems in the SWF detection based on the current spectrum analysis.

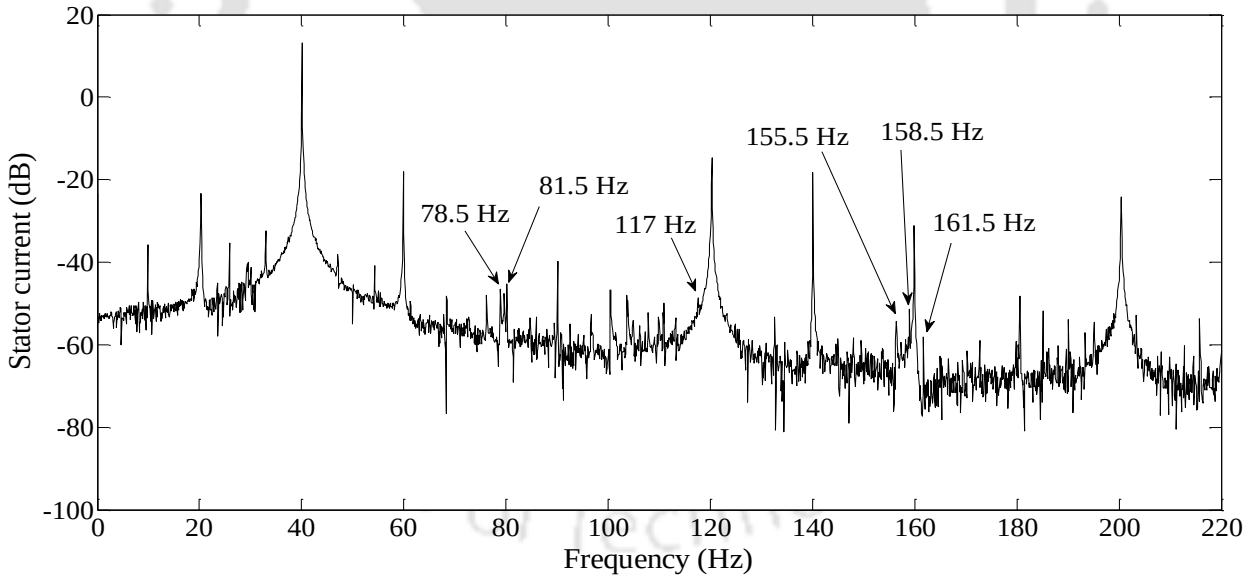

Figure 3.25 Stator current power spectra of IM with the SWF at T_3 when VFD is set to 40 Hz

In order to study the SWF, the vibration spectra of an IM with the SWF when the motor is rotating at 40 Hz under full load, is added in Figure 3.26. The fault frequencies i.e., 76.56 Hz, 153.12 Hz

and 306.24 Hz (as calculated using (pf_r, $2pf_r$, $4pf_r$,.....), can be observed from the vibration spectrum. However these frequencies are not clearly identifiable as there are many other frequencies of higher magnitudes. The SWF cannot be identified by vibration alone, current spectra are also necessary.

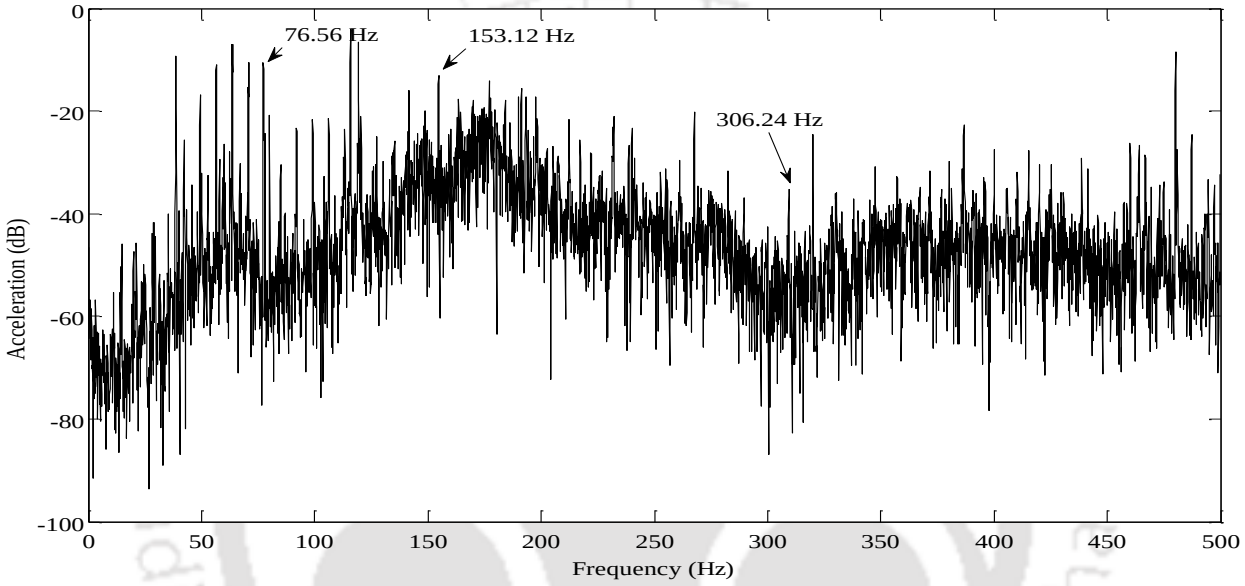

Figure 3.26 Vibration (acceleration) power spectra of IM with the SWF at T_3 when VFD is set to 40 Hz

D. Bearing faults: Bearings are the most affected component of the IM. The bearing faults (BF) are classified as the inner race defect, outer race defect, ball defect and train defect. Defective bearings generate vibrations at the rotational speed of each component. These characteristic frequency components which are related to rolling element and raceways can be calculated from the rotational speed and bearing dimensions. Vibration analysis is commonly used to detect these frequency components. Vibration frequencies associated with different BF are given by:

For inner race defect: $f_i = Zf_r / 2\left(1+\frac{d}{D}\cos\alpha\right)$ (3.5)

For outer race defect: $f_o = Zf_r / 2\left(1-\frac{d}{D}\cos\alpha\right)$ (3.6)

For ball defect: $f_b = Zf_r / \mathrm{d}\left(1-\frac{d^2}{D^2}\cos^2\alpha\right)$ (3.7)

For train defect: $f_t = f_r^{\,2} / 2\left(1-\frac{d}{D}\cos\alpha\right)$ (3.8)

where, Z is the number of rolling elements in the bearing, d is the diameter of rolling element, D is the diameter of pitch circle, α is the contact angle in radians, and f_r is the rotational frequency. These characteristic components can be approximated for most bearings that have 6 to 12 balls by $f_o = 0.4Zf_r$ and $f_i = 0.6Zf_r$. Any BF will generate a radial motion between the rotor and the stator, as the bearing support the rotor. The bearing damages produce mechanical displacement causing variation in the air gap that can be described by a combination of rotating eccentricities moving in clockwise as well as anticlockwise. These variations of the air-gap produce current components at predictable frequencies, f_{bg} related to the vibrational and electrical supply frequencies. Harmonic components introduced by bearing failures in the line current spectrum are given by:

$$f_{bg} = \left| f_s \pm kf_v \right| \quad (3.9)$$

where, k= 1, 2,…, f_v is the one of the characteristic vibration frequencies (for example, f_i is inner race frequency, f_o is outer race frequency, etc.), f_s is the supply frequency.

In order to detect the characteristic frequency in the vibration spectrum, a bearing with outer race fault is considered. The bearing (NSK 6203) with 29 mm pitch diameter and 6.75 mm rolling element diameter, and 8 rolling elements is considered. The characteristic bearing outer race frequency for the bearing (as calculated from Equation 3.6) at 2341 rpm (39.02 Hz) of rotor speed, is $f_o = 119.60$ Hz. Figure 3.27 shows the vibration spectrum for the considered bearing fault conditions. The bearing frequency component may be possible at 119.60 Hz and multiples of it (i.e., 2x: 239.2 Hz, 3x: 358.05 Hz, and 4x: 478.43 Hz) the outer race frequency. These components can be noticeably visualized in vibration spectrum and hence a BF can be detected by the vibration analysis, however, so many peaks can be seen throughout the spectrum. From the vibration analyses of the bearing fault, it can be concluded that for effective detection of fault frequency, the measurement of rotational frequency and accurate dimension of the machine components such as the rolling element diameter, bearing pitch diameter, contact angle, etc. are required. These can cause problems for diagnosing the BF if these parameters are not known (Wang and Chang, 2011).

In order to detect the bearing fault using the current signal, a current spectrum is added in Figure 3.28. The characteristic fault frequency (as calculated by Equation 3.9) is 76.60 Hz, which can be seen in Figure 3.26. Other frequencies of interest in the current spectrum are to be 159.6 Hz (when k = 1), 199.20 Hz and 279.20 Hz (when k = 2), 318.20 Hz and 398.80 Hz (when k = 3). It is observed from Figure 3.28 that the current signature analysis is also capable of detecting BF.

However, similar to vibration spectrum analysis, various factors affect the current harmonics that make the current spectrum analysis difficult for the BF.

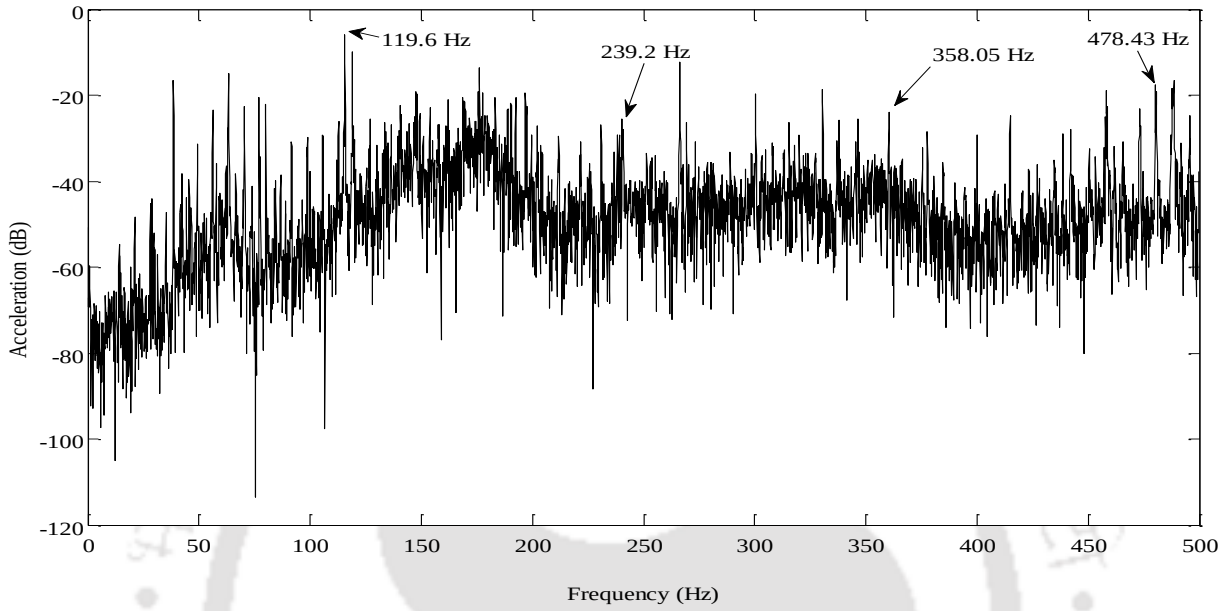

Figure 3.27 Vibration (acceleration) power spectra of IM with the BF at T_3 when VFD is set to 40 Hz

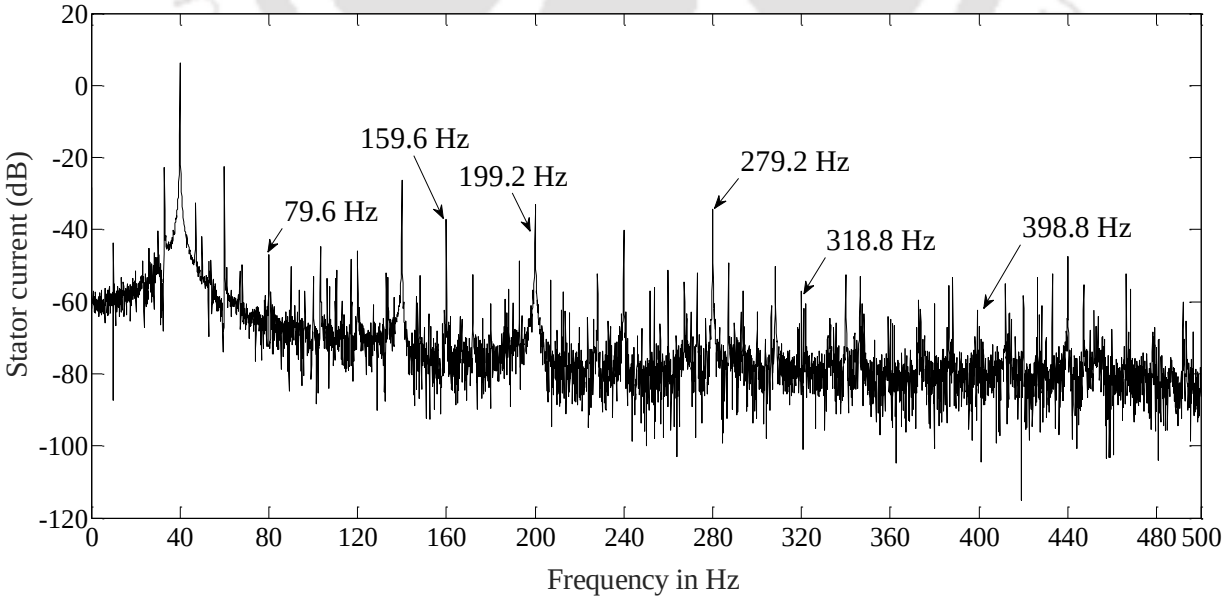

Figure 3.28 Stator current power spectra of IM with the BF at T_3 when VFD is set to 40 Hz

E. Air-gap eccentricity related fault: Uneven air gap that exists between the stator and the rotor is called as the air gap eccentricity as shown in Figure 3.8. The eccentricity causes a force on the rotor that tries to pull the rotor even farther from the stator core center. In the case of static eccentricity, it is a steady pull in one direction. The dynamic eccentricity produces an unbalanced magnetic pull, which acts on the rotor and rotates at the same angular velocity as the rotor. Characteristic frequency components in the current spectrum for the air gap eccentricity are given by:

$$f_{ect} = \left[1 \pm m(1-s)/p\right] f_s \tag{3.10}$$

where f_s is the electrical supply frequency, p is the number of pole pairs and s is the slip. If both the static and dynamic eccentricities exist, a low frequency component near the fundamental can be detected by $F = \left| f_s \pm k f_r \right|$, where f_r is the rotational frequency. In addition, in the vibration spectrum, the UR produces a high amplitude peak at 1X of running speed in radial directions, the BR produces 1X (and often 2X) in the axial direction, the angular misalignment (in case of MR) produces 1X in the axial direction, small 2X and 3X in the axial direction and small 1X in the radial direction.

In order to detect the air gap eccentricity in the IM, a bowed rotor (BR) is considered here. Figure 3.29 shows the plot of the current spectrum for the BR. Characteristic fault frequencies (as calculated from Equation 3.10) are 79.01 Hz (when k = 1), 118.02 Hz (when k = 2), 157.03 Hz (when k = 3) and 196.04 Hz (when k = 4). It is observed from Figure 3.22 that these frequency components can be easily visualized. Hence, the current signature analysis can be used in detecting

the eccentricity related faults in IM. However, it is noted that the SWF can also lead to current harmonics at frequencies described by Equation (3.10), which is one of the major challenges to eccentricity detection.

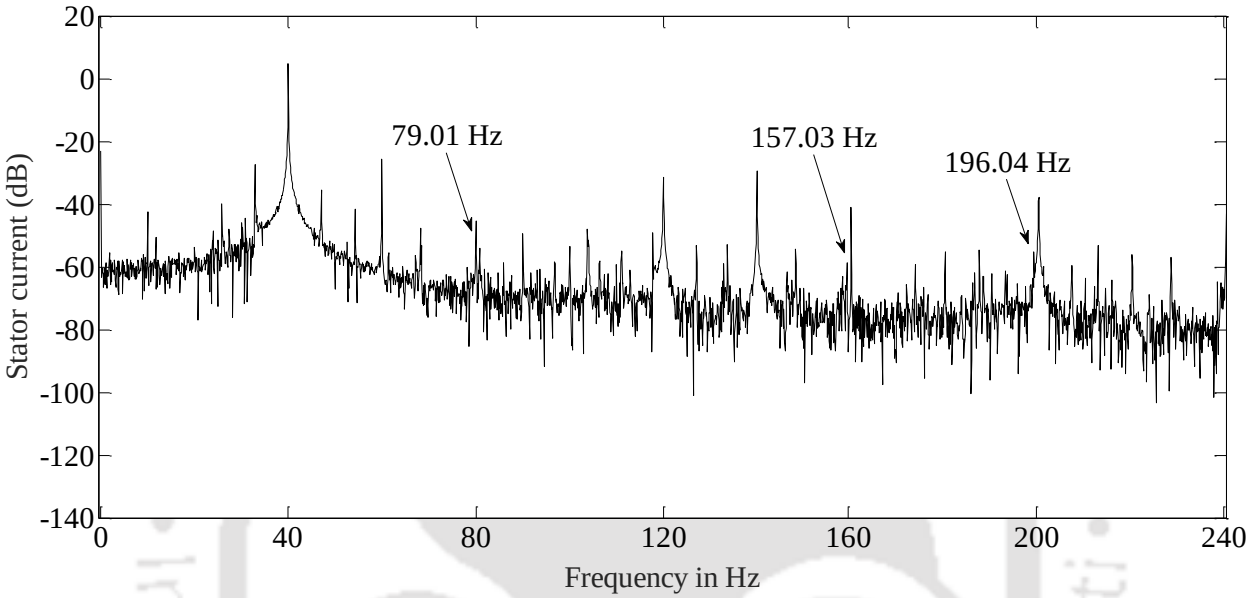

Figure 3.29 Stator current power spectra of IM with the BR at T_3 when VFD is set to 40 Hz

3.4.3 Challenges in the Time and Frequency Analyses of Vibration and Current for IM Faults

Fault diagnosis of IM is not possible by analyzing the time domain vibration and current signals. The reason is, from time domain vibration signals, the difference between the waveform of normal and faulty motors can be seen; however, these cannot be segregated. From time domain current signals, the difference is not visible among these faults from time domain waveform since the main component is the supply frequency and the fault signal is modulated or riding on the sine wave of the supply frequency.

When the speed oscillations are small, the vibration and current spectrum analyses can be implemented in order to detect various faults in IM, provided higher accuracy in the diagnosis is not needed; however, various factors affect the spectrum analysis. Fault signatures sometimes have extremely low signal-to-noise ratio. So in order to capture sufficient harmonic information of individual fault, a suitable high sampling rate is needed and yet at the same time a sufficient frequency resolution is required. When the high frequency resolution is necessary, this posed a constraint that limits the low sampling rate to be used, in order to have a better frequency resolution when using FFT analysis. In addition, different faults generate a specific vibration and current spectrum, which provide the fault harmonic component related to the particular fault. However, for a complex system which involve various components, it is a challenging task to accurately estimate the harmonic component of the fault and locate them in the spectrum.

In the case of current spectrum analysis, various difficulties are associated such as the existence of characteristic harmonics due to the supply voltage distortion, load unbalance, air gap. In addition, harmonics of healthy eccentricity due to both the design and construction of the motor, harmonics caused by variations of the load and the supply frequency, background noise, are also make current analysis difficult for fault diagnosis. In addition, for electrical fault the current spectrum is very sensitive to the accuracy of motor slip and supply frequency measurement, because the fault frequencies or sidebands are function of the motor slip and the line frequency. However, it is not an easy task to estimate these parameters accurately. Even if characteristic frequencies of different faults are available, the measured vibration and current signals from motors are extremely non-stationary and it makes the spectrum diagnosis even more difficult for the fault detection. Moreover, other harmonics from the power electronics equipment, such as the VFD, also make

spectrum analysis of current more difficult. It is noted that, the stator excitation frequency will dynamically change the position of the current harmonics appearing on the stator-current spectrum due to electrical faults is highly dependent on the mechanical motor load and excitation frequency, which affects the slip frequency. As a consequence, the conventional current spectrum analysis must be amended to accommodate the new scenarios (Zhu et al., 2013).

The current and vibration spectrum based methods may be effective for IM fault diagnosis only when the motor is almost fully loaded and running at a constant speed, however there are many applications where these operating conditions are not achieved. In addition, the IM fault diagnosis based on conventional signal processing methods and modern spectrum analysis require practicing engineers to have sufficient knowledge and experience. As the number of IMs is increasing steadily in all types of industries, it is not practical to fulfill the demand of required engineers or experts. Therefore, in order to take care of the limitations of conventional fault diagnosis methods, in recent years the trend of automatic fault diagnosis based on measured symptoms has been increasing by incorporating artificial intelligence (AI) techniques into the online machine condition monitoring. The AI based diagnosis methods are a single reliable procedure for diagnosing any type of mechanical and electrical faults in IMs. These methods reduce the direct human-machine interaction for the diagnosis. Also, these are data based techniques, thus they do not require any detailed knowledge of the IM model and parameters. In addition, AI based methods are powerful and improves the fault diagnosis effectiveness and efficiency in IMs, especially during the predictive maintenance process. Therefore, in this study, the fault diagnosis in IM is considered based on the SVM, an AI.

3.5 Summary

A laboratory test rig for IM was configured to perform experiments to acquire the vibration and current signals. These signals were measured from all IM fault conditions. The data were generated for various operating conditions of motors, i.e. a range of the load torque and the angular speed. In order to investigate the effect of frequency resolution on the fault diagnosis, data were generated by performing two types of experiments, i.e. the first with the sampling rate of 20,000 S/s with 2000 sample points so as to have higher frequencies and a low frequency resolution of 10 Hz, and the second with the sampling rate of 2000 S/s and 10,000 sample points in order to capture low frequencies and maintain the high frequency resolution of 0.1 Hz. The time and frequency domain signals were collected from both experiments through proper experimentation for the future data processing. After collecting the sufficient data, the time and frequency analyses are performed and shown that these conventional signals and FFT based techniques are affected by several factors like machine and environment parameters. Therefore, in order to improve the reliability of the existing diagnosis systems and to automate it, the fault diagnosis is attempted based on the support vector machine (SVM) algorithm in the subsequent chapters. Initially the diagnosis is performed using the time domain data of high sampling rate and results are added in the next chapter.

CHPATER 4

Multi-Fault Diagnosis of IM based on Time Domain Data of High Sampling Rate

4.1 Introduction

In this chapter, multi fault diagnoses are performed in order to present a comparative investigation of the vibration and current signals for the mechanical and/or electrical faults and their severities in IMs. The diagnosis is performed based on the one-versus-one multiclass method of the SVM. Four mechanical fault conditions such as the bearing fault, unbalanced rotor, bowed and misaligned rotor, and five electrical fault conditions such as the broken rotor bar, stator winding fault with two severity levels and phase unbalance fault with two severity levels are considered along with a no defect condition. As signals from the healthy and defective IMs differ in their characteristics in time domain, therefore the fault diagnosis based on statistical features extracted from time domain data is adopted in this chapter. Initially, the data of high sampling rate (i.e., the sampling rate of 20,000 S/s) which is acquired from Experiment 1 (explained in Chapter 3), is used for the fault diagnosis.

The comparative investigation of vibration and current signals are performed in order to find out which signal(s) (i.e., vibration or/and current) is/are required for effective diagnosis of mechanical and/or electrical faults in IM. For this, the useful statistical features, i.e., standard deviation, skewness and kurtosis are extracted from the raw vibration and current signals. The extracted features are further used as the input to the SVM-based classifier. Various cases such as, the mechanical faults with vibration or/and current signals, the electrical fault with vibration or/and

current signals, and the mechanical as well as electrical faults together with vibration or/and current signals, are considered for investigation. In this chapter, SVM parameters are selected by the hit-and-trial method to build an optimal SVM model for the final prediction. The fault diagnosis is performed when training and testing of the SVM done with signals collected at the same speed and load of IM. As the conventional fault diagnosis depends on IM operating conditions, but predictions are especially challenging for the light and no load conditions. Therefore, in order to check the effectiveness of the present method in fault predictions, the fault diagnosis is considered for a wide range of IM operating conditions (i.e. three different loadings with seven speeds of IM). In addition, the fault diagnosis performance is compared for the data of high sampling rate with the data of low sampling rate.

4.2 Fault Feature Extraction

In order to perform an effective fault diagnosis, input features (or vectors) must be selected appropriately. Input features should contain the critical information of each fault condition. The raw data or signal directly from sensors contains high noise and redundant information, and create the problem of dimensionality. The variation in raw signal is too small to be detected, therefore the comparison of raw data of faulty and healthy IMs is not effective in order to determine whether the component is behaving normally or exhibiting signs of a failure. The feature extraction has to be performed to convert a raw signal into compact form that can accentuate the changes and reveal the significant information or certain characteristics of the signal in order to correctly predict the machine's health. Moreover, in order to perform the intelligent fault diagnosis, it is not possible to feed the raw data directly into the classifier for training and testing purpose because the handling

of large data is a challenging task. The feature extraction also provides reduced data sets for an effective application of the intelligent fault diagnosis.

Common statistical features such as standard deviation, skewness, and kurtosis have been used for time domain analysis. Tran et al., 2009 and Nguyen et al. 2008 used the skewness, kurtosis, variance, and crest factor of time domain vibration signals for the mechanical fault detection of IM. Bordoloi and Tiwari (2013) utilized the standard deviation, skewness and kurtosis based on time domain data, for the fault classification of gears and showed that these three features can effectively classify all gear faults. In other study, Gangsar and Tiwari (2014) have also used standard deviation, skewness and kurtosis in order to diagnose faults in the rolling element bearings and showed that the bearing faults can be successfully diagnosed using these features. Therefore, to start with just three most preferred statistical features, i.e. the standard deviation, skewness and kurtosis are chosen to perform the comparative investigation of the vibration and current signals for the diagnosis of IM faults in this chapter. Three statistical parameters are explained as follows:

Standard Deviation **(σ)**: The standard deviation is a dimensional quantity that measure variability of the distribution or fluctuation of signals from the mean. This is a measure of the effective energy or power content of signals. A low standard deviation indicates that the data points tend to be very close to the mean, whereas high standard deviation indicates that the data are spread out over a large range of values. The standard deviation of a data set is the square root of its variance.

The standard deviation is the second standardized moment (or normalized central moment) of the data and is expressed as

$$\sigma = \sqrt{\mu_2} = \sqrt{\frac{1}{N}\sum_{i=1}^{N}(x_i - \mu_1)^2} \tag{4.1}$$

Where, x_i is the amplitude, N is the number of data points in the sample, μ_1 is the first moment or mean and μ_2 is the second moment or variance.

***Skewness* (χ)**: The skewness is a non-dimensional feature that measure the degree of asymmetry of the probability distribution (or shape of the distribution) of a real valued variable around its mean. The skewness value can be positive or negative, or even undefined. Qualitatively, a negative skew indicates that the tail on the left side of the probability density function is longer than the right side and the bulk of the values (including the median) lie to the left of the mean. A positive skewness indicates a distribution with an asymmetric tail extending towards more positive values. A zero value indicates that the values are relatively evenly distributed on both sides of the mean, typically but not necessarily implying a symmetric distribution. The skewness is the third standardized moment of the data and is expressed as

$$\chi = \frac{\mu_3}{\sigma^3} = \frac{\frac{1}{N}\sum_{i=1}^{N}(x_i - \mu_1)^3}{\sigma^3} \tag{4.2}$$

where, μ_3 is the third moment and σ is the standard deviation.

***Kurtosis* (κ)**: The kurtosis is a non-dimensional feature that reflects the flatness or the spikiness of the distribution of signal. It provides a measure of the size of the tails of the distribution and is used as an indicator of major peaks in a set of data. Its value is very high for faulty machines due to the spiky nature of the signals. It is standardized fourth moment of the data and is expressed as:

$$\kappa = \frac{\mu_4}{\sigma^4} = \frac{\frac{1}{N}\sum_{i=1}^{N}(x_i - \mu_1)^4}{\sigma^4} \tag{4.3}$$

where, μ_4 is the fourth moment and σ is the standard deviation..

The features extracted from the time domain vibration and current signals (i.e., *x(t)*) in this chapter are described in Table 4.1. The standard deviation, skewness and kurtosis are calculated from 2000 points available in one data set, which is obtained from Experiment 1. In Experiment 1, 300 raw data sets are collected, so 3×300 feature data sets are extracted for each IM fault and operating condition.

Figure 4.1 and Figure 4.2 show time domain features from the vibration and current signals of BF at 40 Hz and T_3. In addition, the scatter plot or a cluster of three statistical features of the acquired vibration as well as current signals from mechanical and electrical faults (at 40 Hz speed and for the high load) are also added in Figure 4.3 and Figure 4.4, respectively. Figure 4.3 shows that features are well clustered in the case of mechanical faults using vibration signals; however, when these faults are considered with current signals the features are not clustered so well. Figure 4.4 shows that in the case of electrical fault using vibration signals, these features are not clustered

well; however, when these faults are considered with current signals the features are well clustered. It is noted that features, which are produced by current signals, are very difficult to cluster in the case of mechanical faults and features from vibration signals are very difficult to cluster in case of electrical faults. It is evident from scatter plots of the vibration and current features that values of features are linearly inseparable, i.e. apparently it is difficult to find out a straightforward relationship between the features and the corresponding fault type. Therefore, there is a need for fast or automated feature data interpretation techniques, like the artificial intelligence. The SVM is adopted here for automated fault diagnosis of IMs using the vibration and current signals. Now in the next section, a comparative analysis of the vibration and current signals is performed in the mechanical and electrical fault diagnosis based on the SVM.

Table 4.1 The statistical feature parameters in time domain

Signals	Feature parameter for each of the signals (time domain)
Vibration in *x*-axis, Vibration in *y*-axis, Vibration in *z*-axis, Current in Phase A, Current in Phase B, Current in Phase C	Standard deviation (σ), Skewness (χ) and Kurtosis (κ)

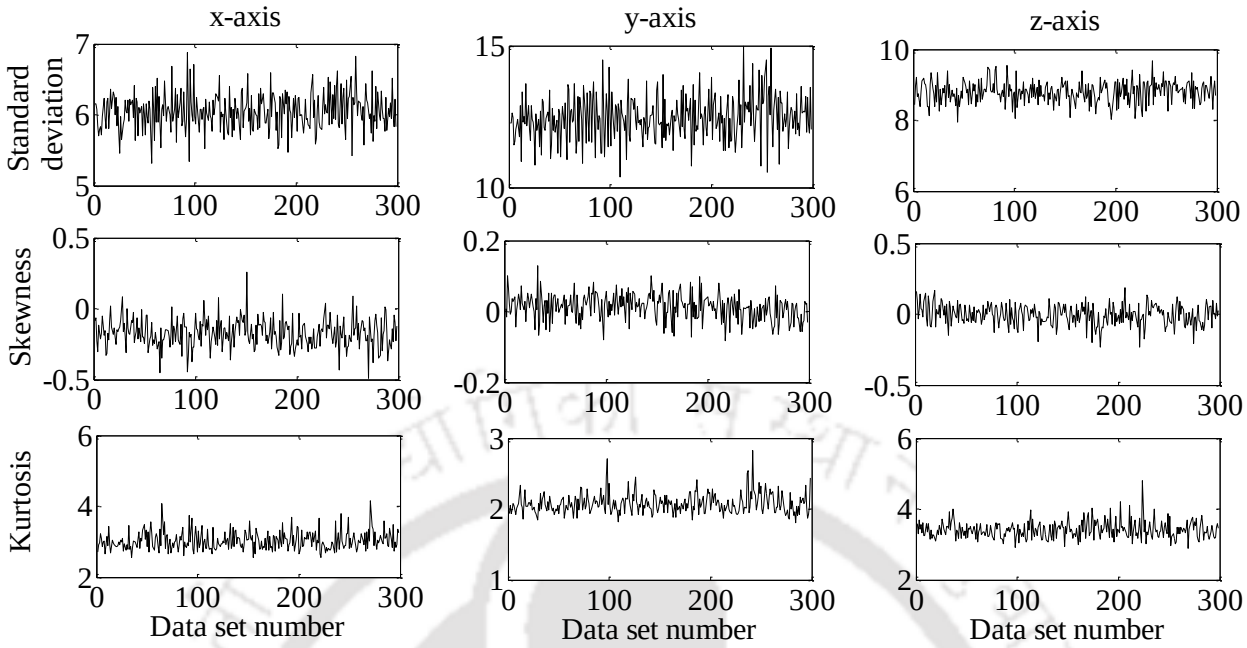

Figure 4.1 Time domain features of acquired vibration signal for BF at 40 Hz and T_3

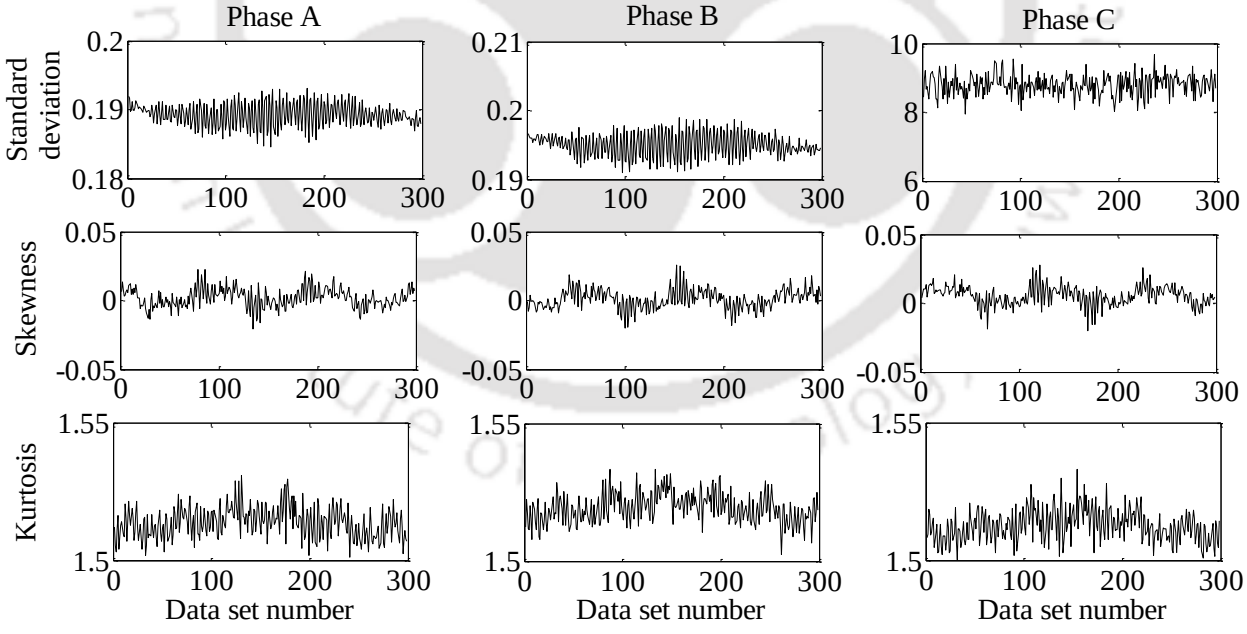

Figure 4.2 Time domain features of acquired current signal for BF at 40 Hz and T_3

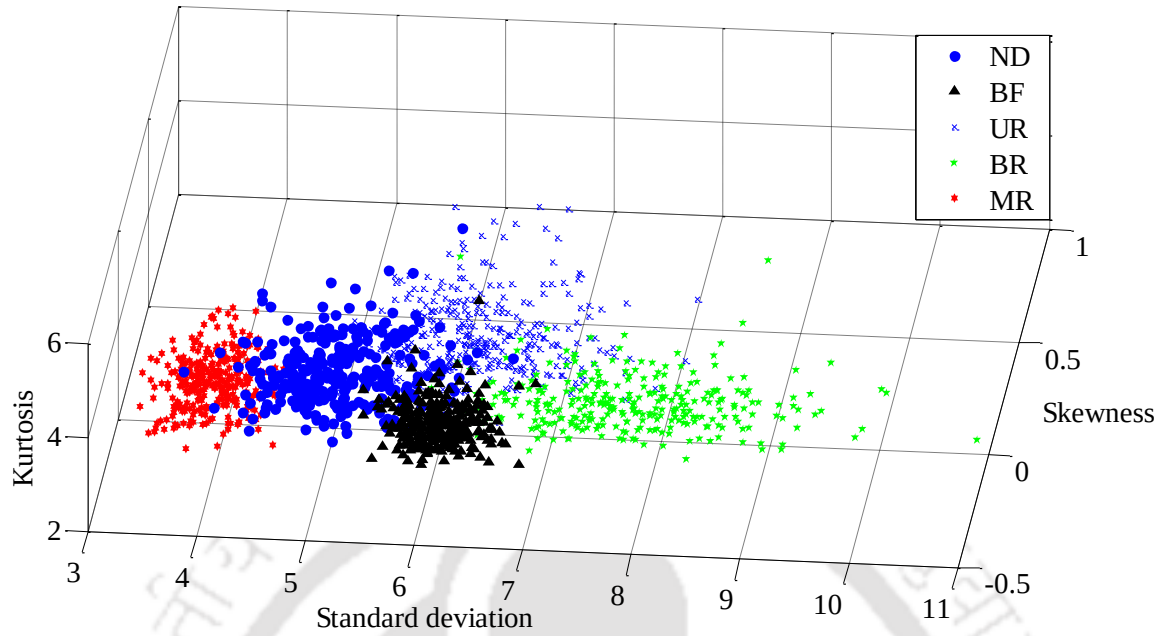

(a) Mechanical fault with vibration signal

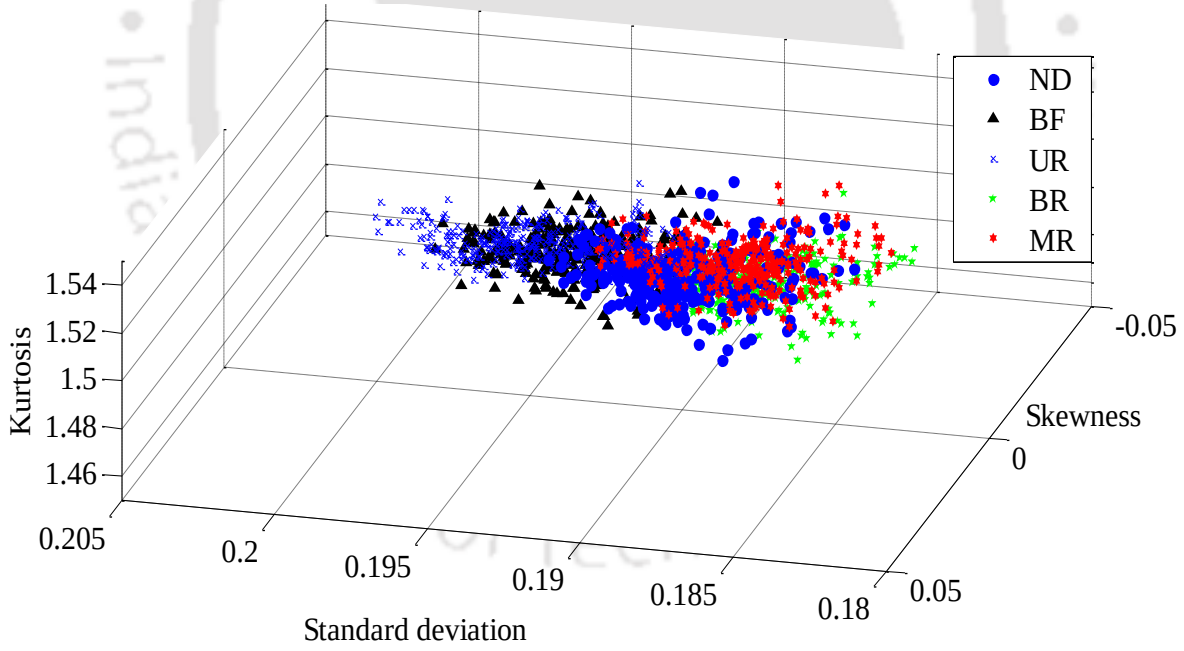

(b) Mechanical fault with current signal

Figure 4.3 Typical scatter plots for mechanical faults using three features ($\sigma, \chi,$ and κ) at 40 Hz for T_3

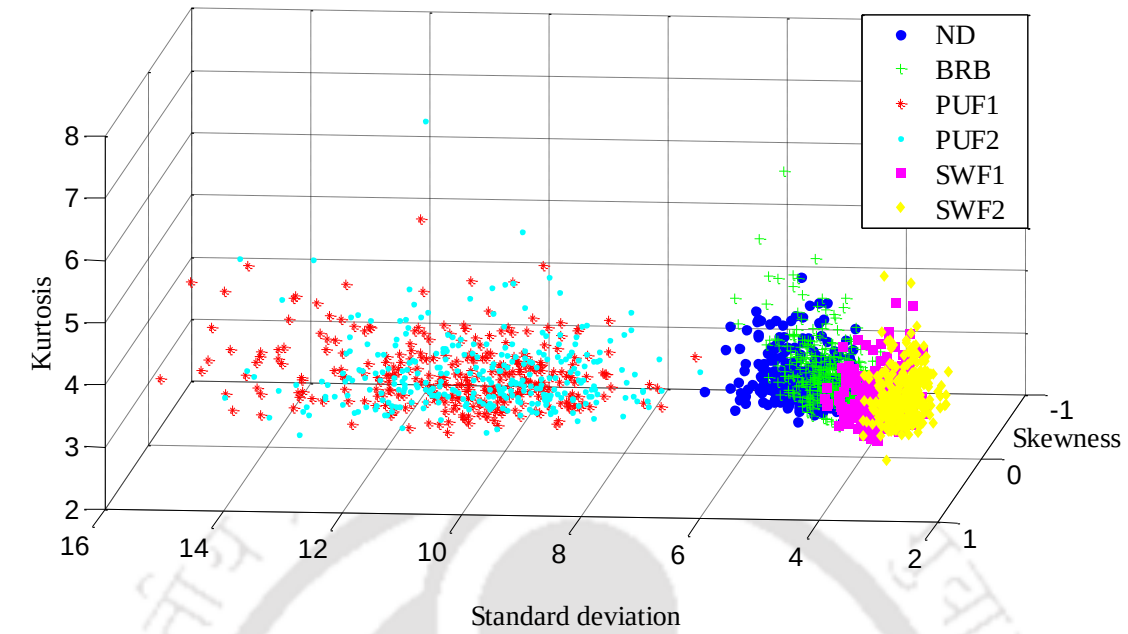

(a) Electrical fault with vibration signal

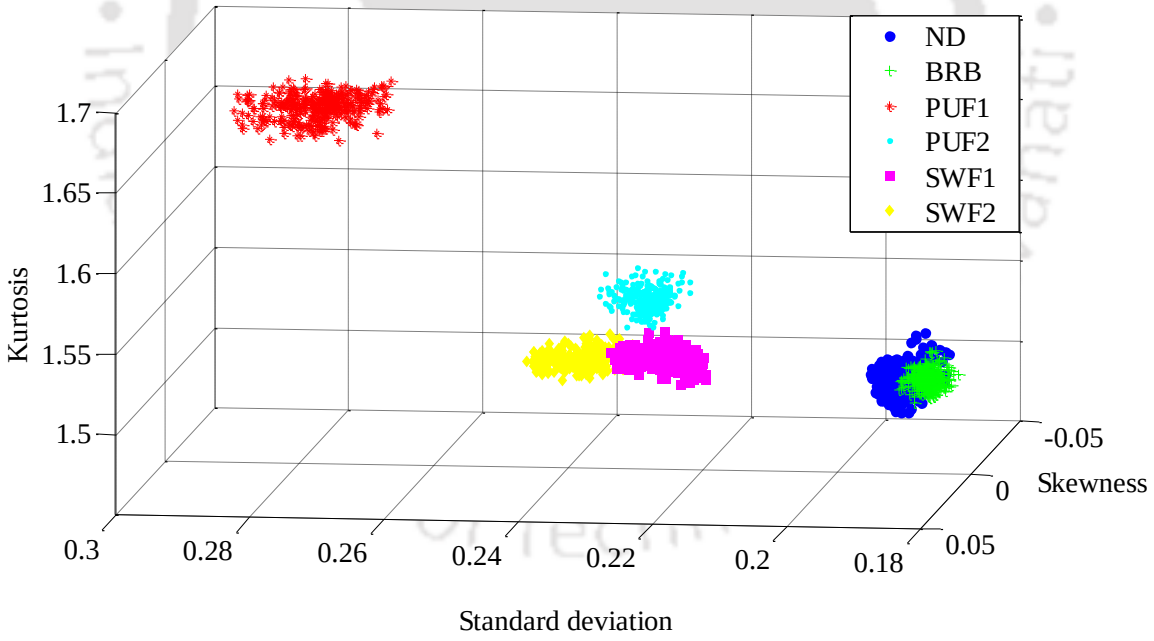

(b) Electrical fault with current signal

Figure 4.4 Typical scatter plots for electrical faults using three features ($\sigma, \chi,$ and κ) at 40 Hz for T_3

4.3 Fault Diagnosis based on SVM

After the feature extraction, the SVM using one-versus-one multi-class method and RBF kernel is applied to perform the multi-fault diagnosis in IM. As all other classifiers to diagnose the fault conditions, first the training of SVM is performed using training data sets to build the SVM model and then final testing is performed using test data sets to predict the unknown data that are not used in the training phase. In order to perform the fault diagnosis, 300 available feature datasets are divided in the proper ratio of 80 % and 20 % for training and testing, respectively. Table 4.2 shows the composition of datasets for the proposed fault diagnosis.

Table 4.2 Composition of the training and testing data sets

Fault condition and their label	Machine operating condition		Training set for each operating condition	Testing set for each operating condition
	Load torque	Speed, Hz		
ND-1	$T_1/T_2/T_3$	10/15/20/25/30/35/40	240	60
BRB-2	$T_1/T_2/T_3$	10/15/20/25/30/35/40	240	60
PUF1-3	$T_1/T_2/T_3$	10/15/20/25/30/35/40	240	60
PUF2-4	$T_1/T_2/T_3$	10/15/20/25/30/35/40	240	60
SWF1-5	$T_1/T_2/T_3$	10/15/20/25/30/35/40	240	60
SWF2-6	$T_1/T_2/T_3$	10/15/20/25/30/35/40	240	60
BF-7	$T_1/T_2/T_3$	10/15/20/25/30/35/40	240	60
UR-8	$T_1/T_2/T_3$	10/15/20/25/30/35/40	240	60
BR-9	$T_1/T_2/T_3$	10/15/20/25/30/35/40	240	60
MR-10	$T_1/T_2/T_3$	10/15/20/25/30/35/40	240	60

In order to classify different IM faults, different label is assigned to each fault such as: ND-1, BRB-2, PUF1-3, PUF2-4, SWF1-5, SWF2-6, BF-7, UR-8, BR-9, and MR-10. The SVM is then trained with the help of 80 % data sets and the radial basis function (RBF) as the kernel. The trained SVM is tested with the 20 % data sets and final results come in the form of testing or prediction accuracy, i.e. the percentage of successfully classified or predicted data. However, for the effective training of the SVM, it is very important to choose the best SVM parameters. The prediction results depend on how well the classifier is trained or built. In order to build a best SVM model, the SVM parameters are chosen by hit-and-trial method, which is discussed in the next section.

4.3.1 SVM Parameter Selection and Training

Training of the SVM is performed with 80 % feature dataset to build a model for further testing or classification of multiple faults. In this work, the Gaussian radial basis function (RBF) kernel is used for the training. The main goal of training is to determine optimal parameters of the SVM so that the best SVM model can be achieved. This SVM model will be further used for the final testing to classify or predict different faults. The SVM with RBF kernel is associated with two parameters, i.e. regularization parameter, C, and the kernel parameter, γ. Inappropriate selection of these parameters may create a problem of over-fitting and hence reduces the prediction performance of the classifier. In this chapter, C and γ, are chosen by the hit-and-trial method. A wide range of C and γ is provided in an exponentially growing sequence, i.e. $3^{-5}, 3^{-4}, ..., 3^{15}$ and $3^{-15}, 3^{-4}, ..., 3^{3}$, respectively. The pair with the best prediction performance is selected. The best γ value obtained from the hit-and-trial method is added in the corresponding case of the fault diagnosis. The best value of C obtained is 1 in all the cases. After selecting the best pair of these parameters, final training is performed to obtain an optimal SVM model. When the final training

step has been done, different data which has not been used in the training process is used to validate the prediction ability of the classifier.

4.3.2 Fault Diagnosis for the Same Speed and Load Case

After building a SVM model by incorporating optimal SVM parameters, now the fault diagnosis is performed. The diagnosis is considered when training and testing of the classifier is done with signals at same speed and same load conditions. For a comparative analysis, the fault diagnosis is performed and discussed for various cases and at diverse operating conditions (i.e., three loads and seven speeds) of IM. The mechanical and electrical fault diagnoses are performed individually and together based on the vibration or/and current signals.

4.3.2.1 Prediction of Mechanical Faults in Induction Motor

Here, following three cases are considered

Case A- Mechanical fault prediction based on vibration signal alone

Case B- Mechanical fault prediction based on current signal alone

Case C- Mechanical fault prediction based on the vibration as well as current signals, concurrently

***Case A. Mechanical fault prediction based on vibration signal alone*:** Figure 4.5 shows the prediction of mechanical faults for various operating conditions of IM using vibration. The prediction performance for BF is 100 % for all considered speeds as well as mechanical loads that means BF is perfectly predicted for any operating conditions of IM. The reason for this is that the generation of intense vibration from the BF due to repetitive impacts of the moving elements on the flaw, and subsequently very different vibration signatures or features than other faults as shown

in Figure 4.3 (a). It is to be noted that the BF is one of the most critical IM fault and share about 40 % of all IM failures. In addition, the SVM could predict the ND, BR, UR and MR successfully (average fault prediction performance is more than 90%) for all considered operating conditions. In overall, mechanical faults are classified successfully using vibration signals. The reason for this is that these faults generate independent and uncorrelated signatures or features ($\sigma, \chi,$ and κ) with each other as shown in Figure 4.3 (a).

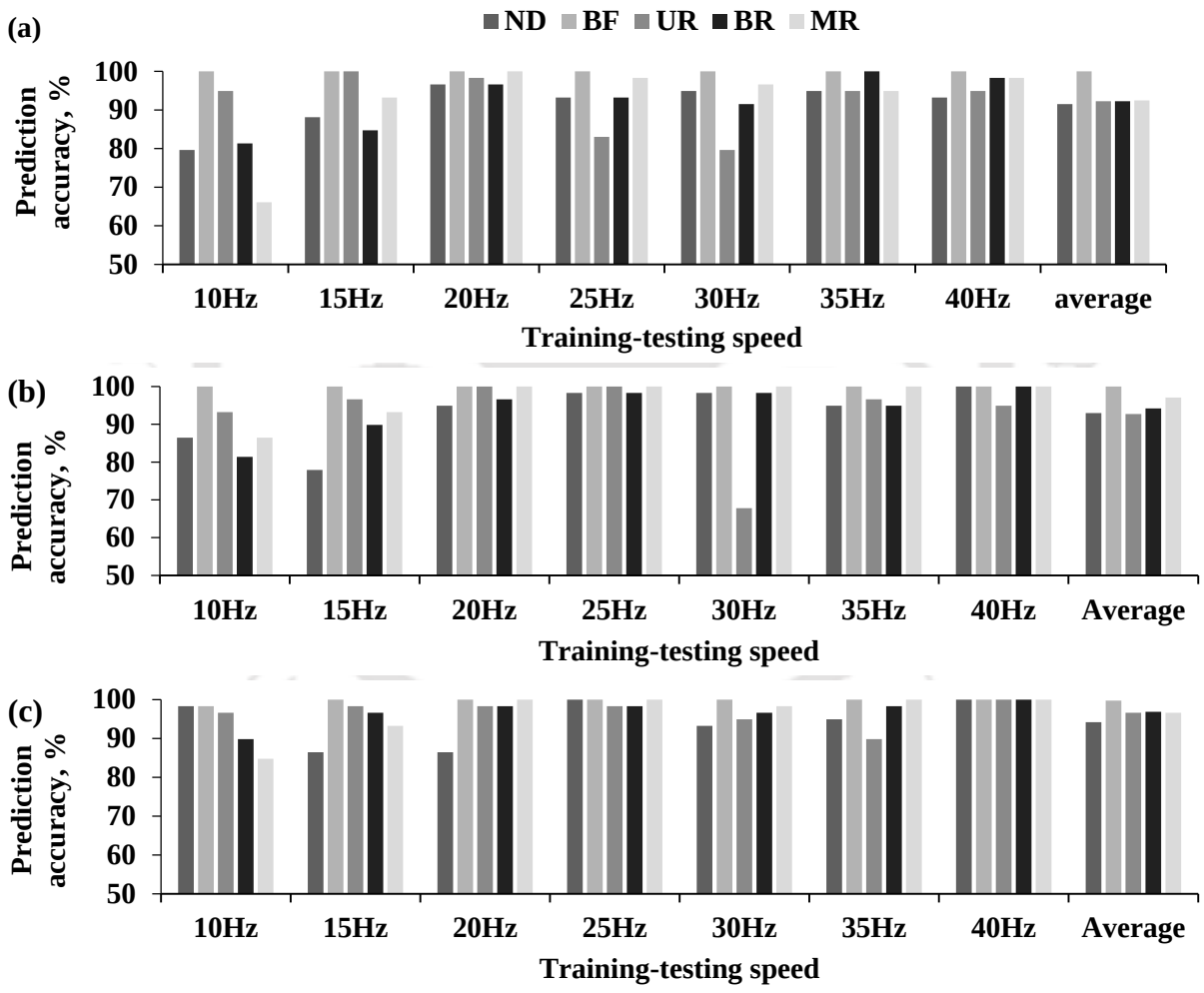

Figure 4.5 Mechanical fault prediction based on vibration signals alone for no load (b) for light load (c) for high load

Table 4.3 shows the maximum, minimum and average values (over the considered speeds) of the overall accuracy. It shows the prediction performance of the SVM improves with the mechanical loading on IM, but does not depend over the speed. It is due to the fact that at higher loads, the signal-to-noise ratio increases due to the amplification of vibration components. That leads to distinct vibration signatures from each faulty condition especially at high loads. Thus, it is beneficial to perform the prediction of the mechanical fault at high mechanical loads using vibration signals. In this case; the optimum value of gamma and computational time are 0.3 and 12 s, respectively.

Table 4.3 Mechanical fault prediction based on vibration signals alone

Fault type	Signals	Load	Overall prediction, %		
			Maximum	Minimum	Average
Mechanical	Vibration	No	98.30 (at 20 Hz)	84.4 (at 10 Hz)	93.69
		Light	99.32 (at 25 Hz)	89.93 (at 10 Hz)	95.44
		High	100 (at 25 Hz)	94.91 (at 10 Hz)	97.48

***Case B. Mechanical fault prediction based on current signal alone*:** Figure 4.6 shows the prediction of mechanical faults for various operating conditions of IMs using the electric current. Table 4.4 illustrates the maximum, minimum and average value (over the considered speeds) of overall accuracy. The prediction performance of SVM reduces (approximately 8 % from the high to no load conditions) with the mechanical loading on IM, unlike for Case A. Thus, the mechanical fault prediction using the current should be performed with no external load on IMs. However, the performance does not depend over the speed, like for Case A. The overall accuracy averages

decreased by 16%, 21%, and 27%, corresponding to the no, light, and high loads, respectively, in comparison to Case A. In overall, mechanical faults are not classified successfully with current signals because there is not much variation in current signals of these faults, due to this, features ($\sigma, \chi,$ and κ) overlap as shown in the scatter plot in Figure 4.3 (b). In this case; the optimum value of gamma and computational time are 300 and 12 s, respectively.

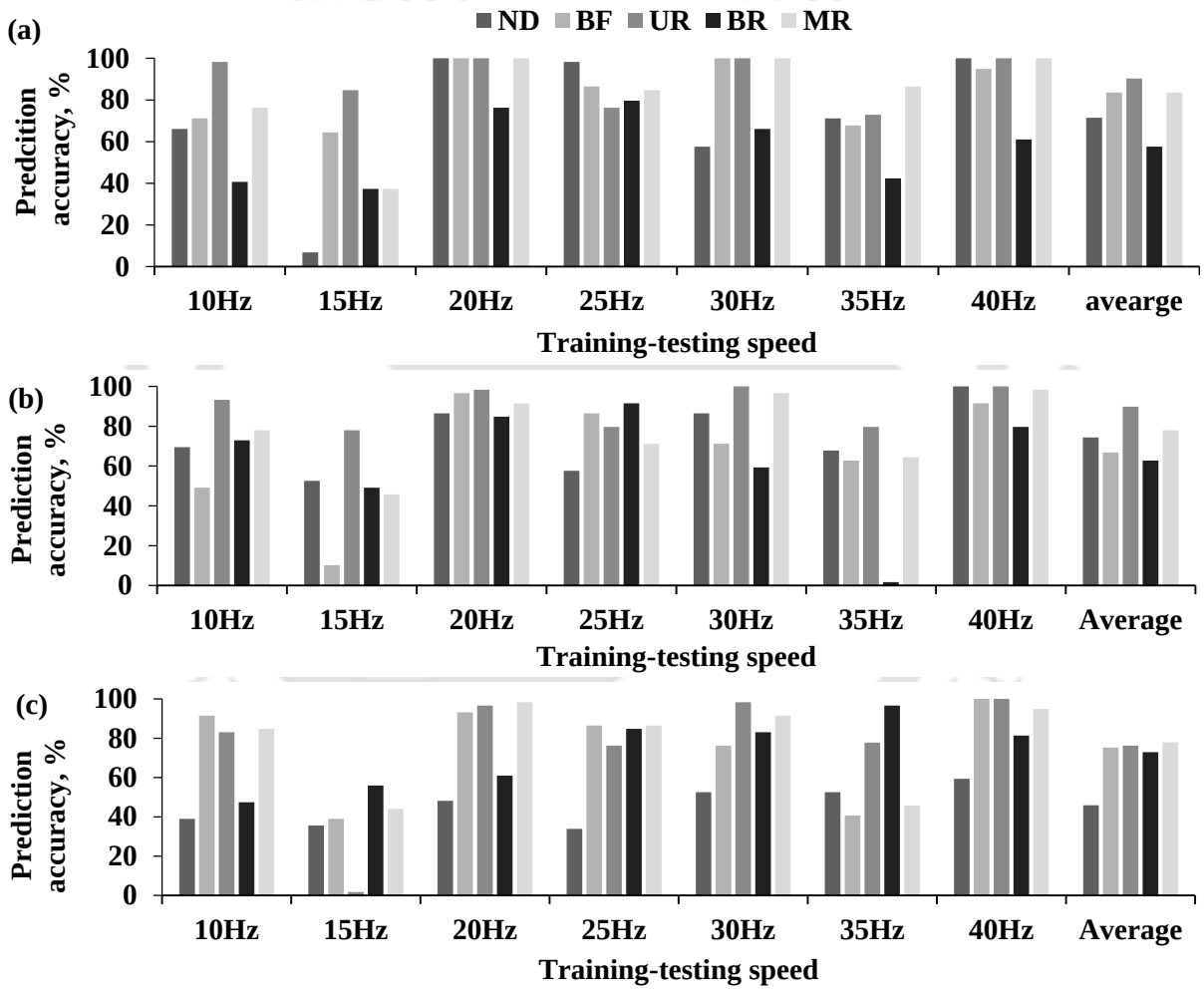

Figure 4.6 Mechanical faults prediction based on current signals alone (a) for no load (b) for light load (c) for high load

Table 4.4 Mechanical faults prediction based on only current signals

Fault type	Signals	Load	Overall prediction, %		
			Maximum	Minimum	Average
Mechanical	Current	No	95.25 (at 20 Hz)	46.1 (at 15 Hz)	77.28
		Light	93.89 (at 40 Hz)	47.11 (at 15 Hz)	74.23
		High	87.11 (at 40 Hz)	35.25 (at 15 Hz)	69.68

***Case C. Mechanical fault prediction based on the vibration as well as current signals concurrently*:** Figure 4.7 shows the prediction of mechanical faults for various operating conditions of IM using both signals. The BF is perfectly predicted (nearly 100 %) for all considered operating conditions of IMs, like for Case A. Other fault conditions like the ND, UR, MR and BR could also be predicted well at all considered operating conditions. Table 4.5 shows the maximum, minimum and average of overall accuracy over the considered speeds. It shows that the prediction performance improves with the mechanical loading on IM and does not depend on speeds, similar to Case A. In this case, the optimum value of gamma and computational time are 0.3 and 16 s, respectively.

***Comparison of the performance of MSVM based on vibration, current or vibration-current signal for mechanical faults*:** Figure 4.8 shows the comparison of investigation of Cases A, B and C. Results show that the maximum of average prediction achieves up to 97.48 % based on the vibration signal alone at the high load condition. Moreover, the SVM with the vibration and vibration-current signals, performs excellent although both of them exhibit nearly similar

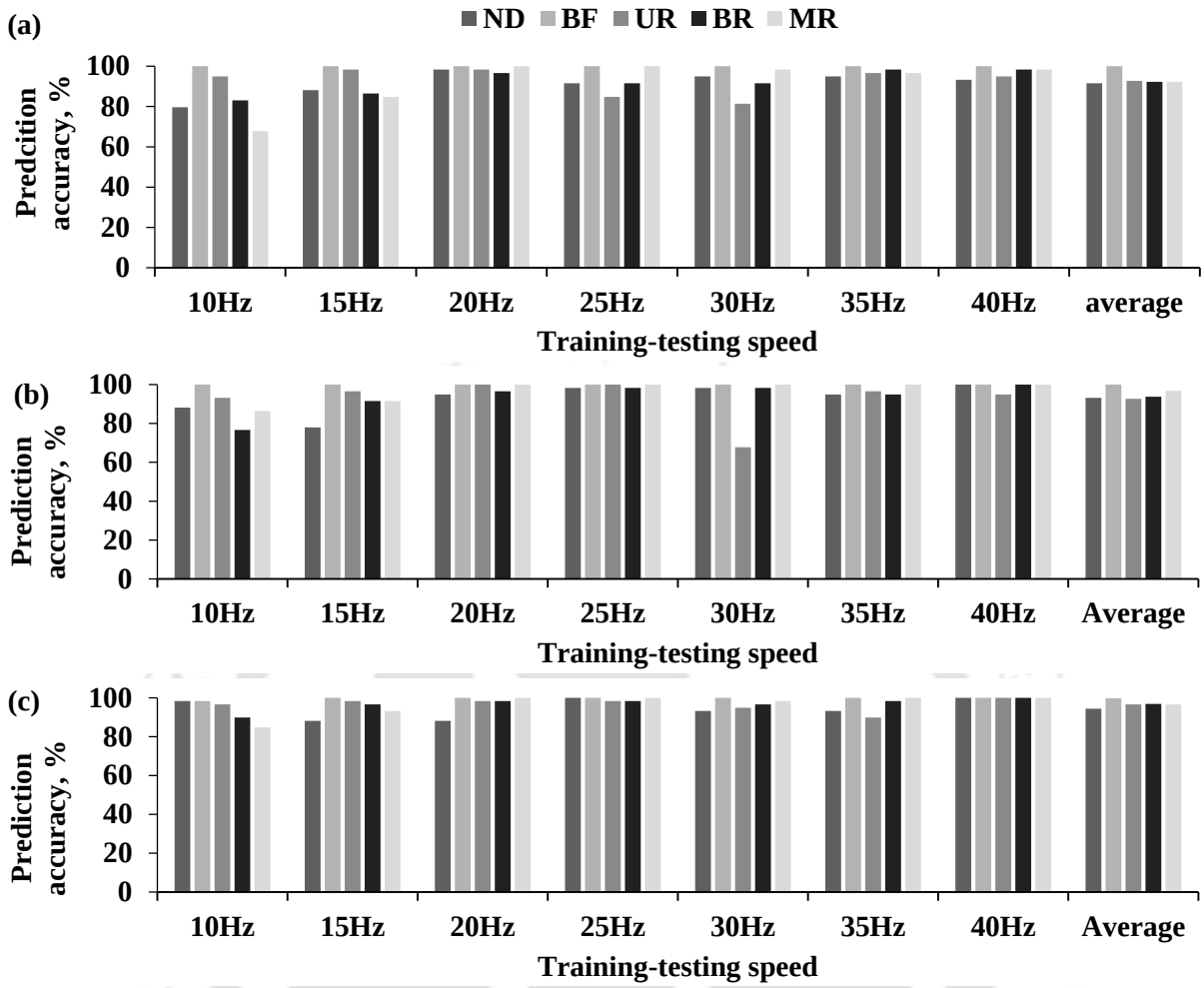

Figure 4.7 Mechanical faults prediction based on vibration as well as current signals concurrently

(a) for no load (b) for light load (c) for high load

Table 4.5 Mechanical fault prediction based on vibration-current signals

Fault type	Signals	Load	Overall prediction, %		
			Maximum	Minimum	Average
Mechanical	Vibration	No	98.64 (at 20 Hz)	85.08 (at 10 Hz)	93.74
	and current	Light	99.32 (at 25 Hz)	89.49 (at 10 Hz)	95.39
		High	100 (at 40 Hz)	93.55 (at 10 Hz)	96.84

prediction performance corresponding to all considered operating conditions. However, the SVM performance, reduces with the current signal alone (i.e., Case B) than the other two cases. Hence, it is not beneficial to perform the SVM prediction for mechanical faults based on only the current signal. In both Case A and Case C, the prediction improves 3-4 % at the higher load with respect to the no load condition. It is due to the higher signal-to-noise ratio occurs in the vibration at the higher load. A high signal-to-noise ratio means the better quality signature and subsequently easy distinction of signatures from different faults. In addition, the prediction performance does not improve much by considering current signals along with vibration signals. The unnecessary computation burden and time of the training and prediction can be reduced by not considering the current signal in conjunction with the vibration.

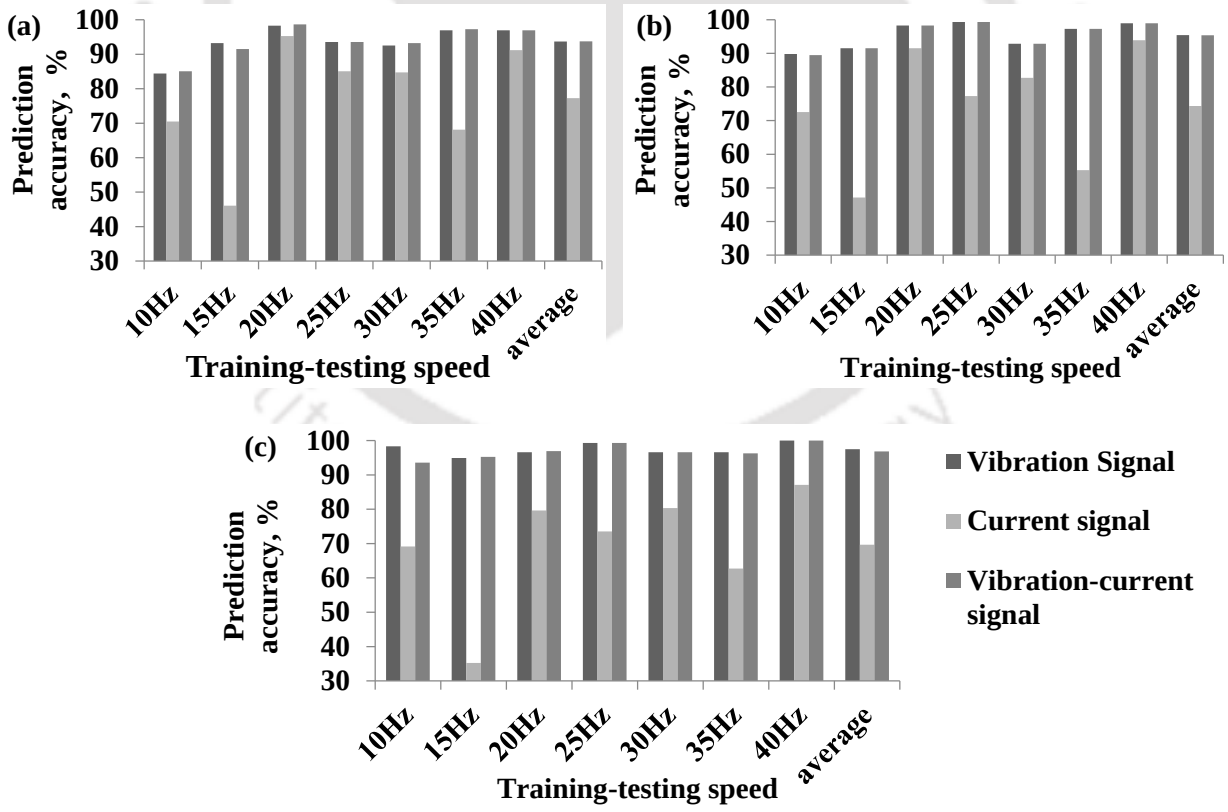

Figure 4.8 Mechanical fault predictions for (a) no load, (b) light and (c) high load

In overall, the mechanical fault can be predicted effectively with vibration signal alone using the SVM. The reason for this is that mechanical faults are physically related with vibration signals and different mechanical faults generate distinct vibration signals and corresponding features (σ, χ and κ) in different directions (axial or two orthogonal directions) as shown in Figure 4.3 (a). On the other hand, there is not much variation occurs in the current signal and corresponding features due to mechanical faults as shown in Figure 4.3 (b).

4.3.2.2 Prediction of Electrical Faults in Induction Motor

Here, following three cases are considered:

Case D- Electrical fault prediction based on vibration signal alone

Case E- Electrical fault prediction based on current signal alone

Case F- Electrical fault prediction based on vibration as well as current signals, concurrently

Case D. Electrical fault prediction based on vibration signal alone: Figure 4.9 shows the prediction of electrical faults for various operating conditions of IMs using vibration signals. The SVM could predict all electrical faults satisfactorily (prediction more than 75 %) at all considered operating conditions, except for the SWF1 and SWF2, at the light and high loads. The reason for the satisfactorily prediction is that these faults generate independent fault vibration signatures and hence features; however, due to some overlapping in the fault information (as shown in Figure 4.4 (a), the performance of SVM reduces. The rotor and stator winding fault generally excite the torsional vibration, but not necessarily the transverse vibration, still these faults could be predicted satisfactorily (prediction more than 80 %) using the axial and transverse vibration signals in this

work. The average predictions for the light and high loads are 74.57 % and 58.35 %, respectively, for the SWF1, and 74.33 % and 69.25 %, respectively, for the SWF2. That means these faults cannot be classified successfully at higher loads using vibration signals due to overlapping of information, and thus current signals is also necessary.

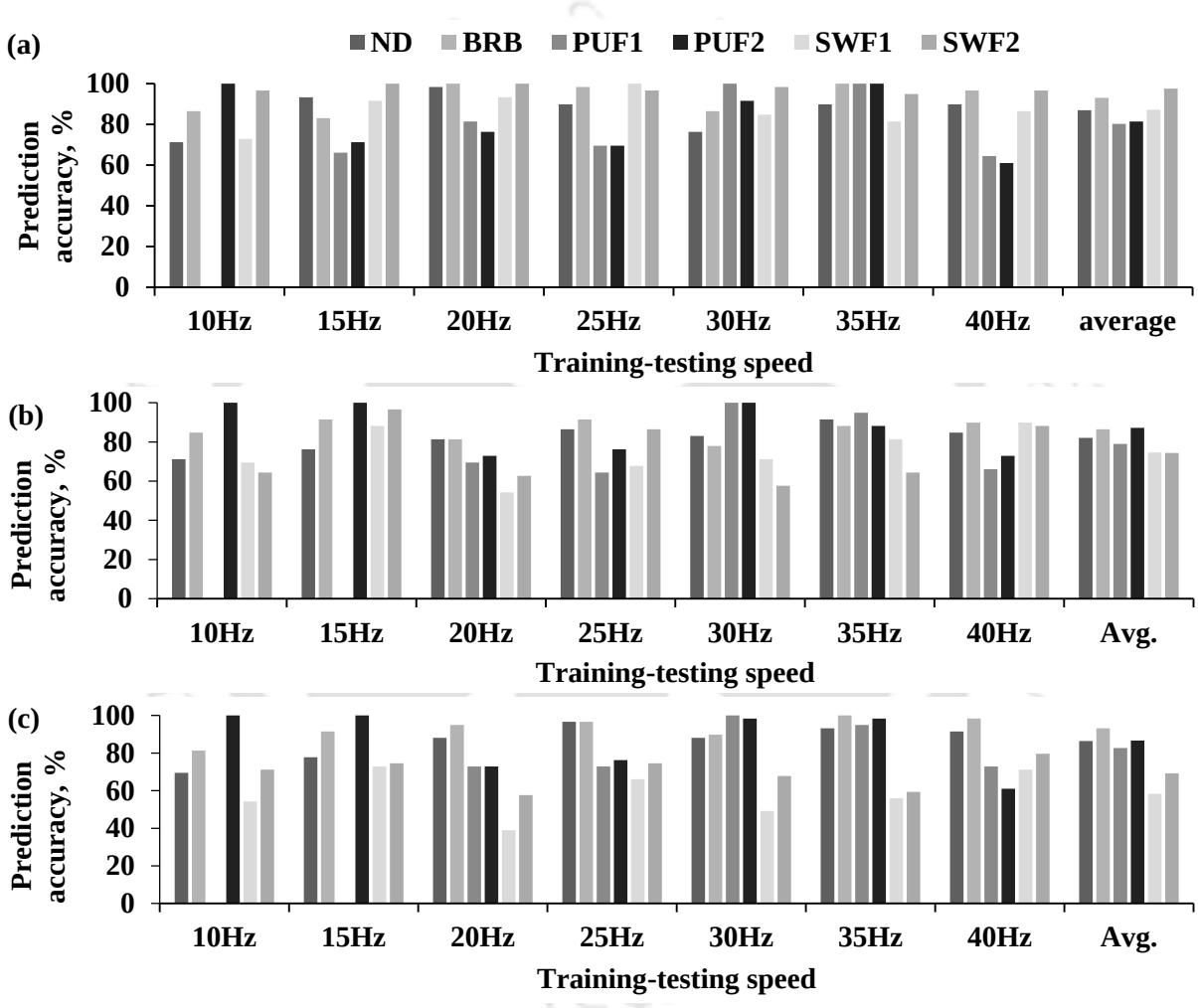

Figure 4.9 Electrical faults prediction based on vibration signals alone for no load (b) for light load (c) for high load

Table 4.6 shows the maximum, minimum and average of overall accuracy for considered speeds. It shows that the prediction performance get reduced with the mechanical loading on IMs. The prediction is independent of the speed. Thus, it is beneficial to perform the electrical fault prediction for this case, when motor is running without any load. In this case, the optimum value of gamma and computational time are 0.3 and 14 s, respectively. Figure 4.9-Figure 4.15 do not display any prediction for the PUF1 for 10 Hz at the no load, for 10 Hz and 15 Hz at light as well as high load, since the IM with the PUF1 could not run at such a low speed, so raw data are not generated.

Table 4.6 Electrical faults prediction based on only vibration signals

Fault type	Signals	Load	Overall prediction, %		
			Maximum	Minimum	Average
Electrical	Vibration	No	94.35 (at 35 Hz)	82.84 (at 40 Hz)	87.82
		Light	90.50 (at 15 Hz)	70.33 (20 Hz)	80.84
		High	83.61 (at 35 Hz)	70.90 (at 20 Hz)	79.29

***Case E. Electrical fault prediction based on current signal alone*:** Figure 4.10 shows the prediction of electrical faults for various operating conditions of IM using current signals. The electrical fault conditions could be predicted successfully (prediction accuracy is more than 90%) for all considered operating conditions except for the ND at some speeds. The overall prediction accuracy for all electrical faults is 100 % for no load at all considered speeds, except for the 10, 15 and 30 Hz. The SVM could be able to predict the PUF1, PUF2, SWF1, and SWF2 perfectly (i.e., with 100 % prediction accuracy) for all considered operating conditions, unlike for Case D.

The reason is that these faults generate very independent and uncorrelated current signals and corresponding features as compared to other faults (as shown in Figure 3.19 and Figure 4.4 (b), respectively). Hence, no overlapping occurs in features information of these faults. Different levels of severity of the stator winding fault, and in the phase unbalance and the single phasing could be predicted perfectly by only current signals. It is noted the stator winding fault and phase unbalance are the most critical electrical faults in IMs and share 30-40 % of all IM failures. The prediction performance for the ND and the BRB reduces at no-load and high load due to some overlapping of features of these fault conditions as shown in Figure 4.4 (b).

Table 4.7 shows the maximum, minimum and average of overall accuracy over the considered speeds. It is noted that the prediction performance is higher at the light and no loads as compared to the full load. Thus, it is possible to perform fault diagnosis at the no and light loads, which is the main challenge of traditional diagnostic method. Stator winding faults generate an unbalance in the current signal similar to the phase unbalance as shown in Figure 3.19, it is very difficult to distinguish these two faults by traditional methods, especially under no load condition. These faults are perfectly predicted here using three features (σ, χ and κ) and the SVM. In addition, detection of the low level severity of stator winding faults under various operating conditions is a major issue. Both low as well as high level severities of stator winding fault is perfectly classified here based on the current signal and the SVM. In this case; the optimum value of gamma and computational time are 300 and 14 s, respectively.

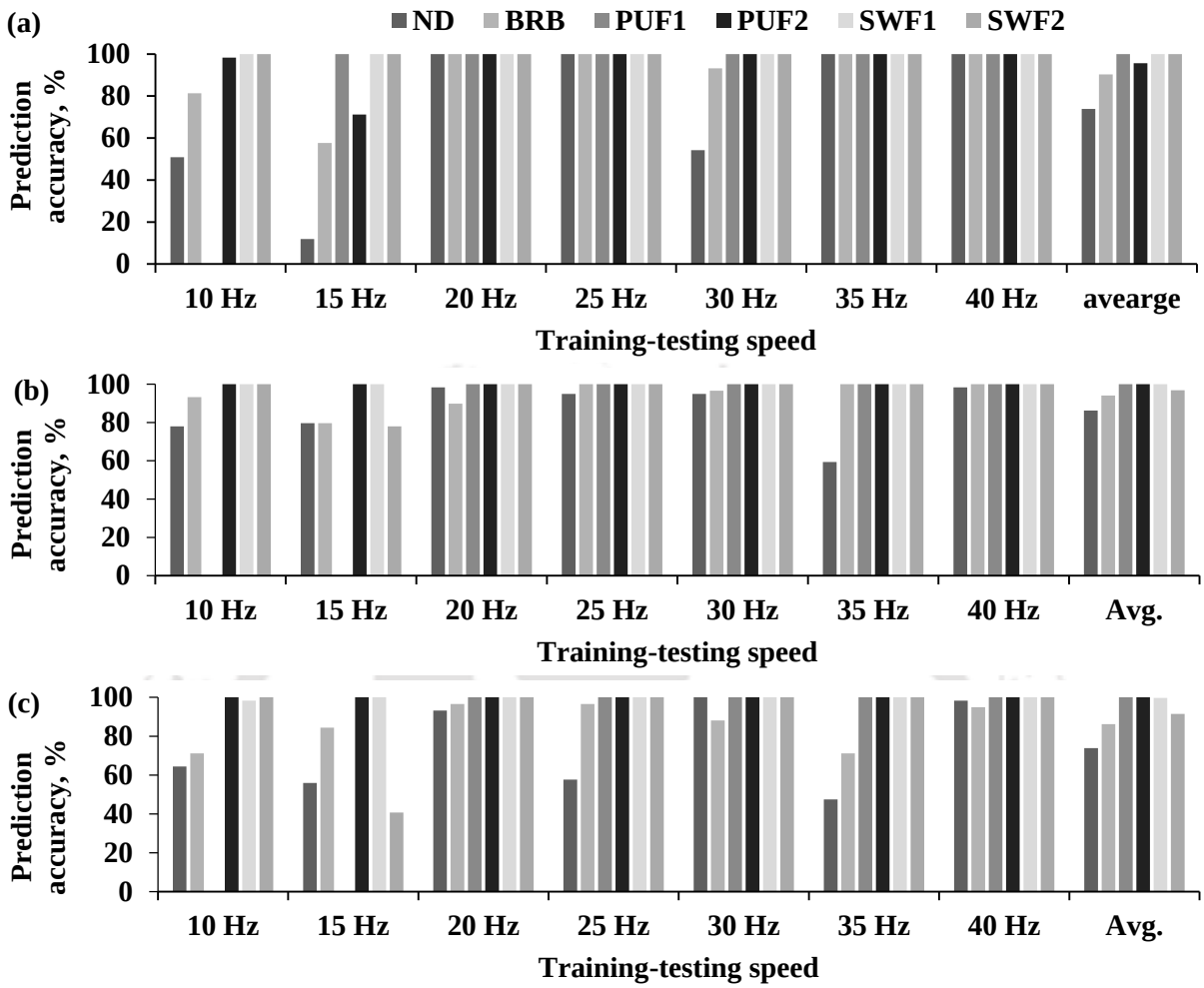

Figure 4.10 Electrical faults prediction based on current signals alone for no load (b) for light load (c) for high load

Table 4.7 Electrical fault prediction based on current only signals

Fault type	Signals	Load	Overall prediction, %		
			Maximum	Minimum	Average
Electrical	Current	No	100 (at 15, 20, 35, and 40 Hz)	73.44 (at 15 Hz)	92.96
		Light	99.71 (at 40 Hz)	87.45 (at 15 Hz)	95.76
		High	98.87 (at 40 Hz)	76.61 (at 15 Hz)	91.05

***Case F. Electrical fault prediction based on the vibration as well as current signals concurrently*:** Figure 4.11 shows the prediction of electrical faults for various operating conditions of IMs for this case. The SVM could be able to predict all considered electrical faults successfully (the prediction accuracy is more than 90%) at no load, and satisfactory (the prediction accuracy is more than 80 %) at the light and high load conditions, except for PUF2 at the 10 and 15 Hz. Also for different level of severity in the stator winding fault, and in the phase unbalance and the single phasing could be predicted perfectly as like in of Case E.

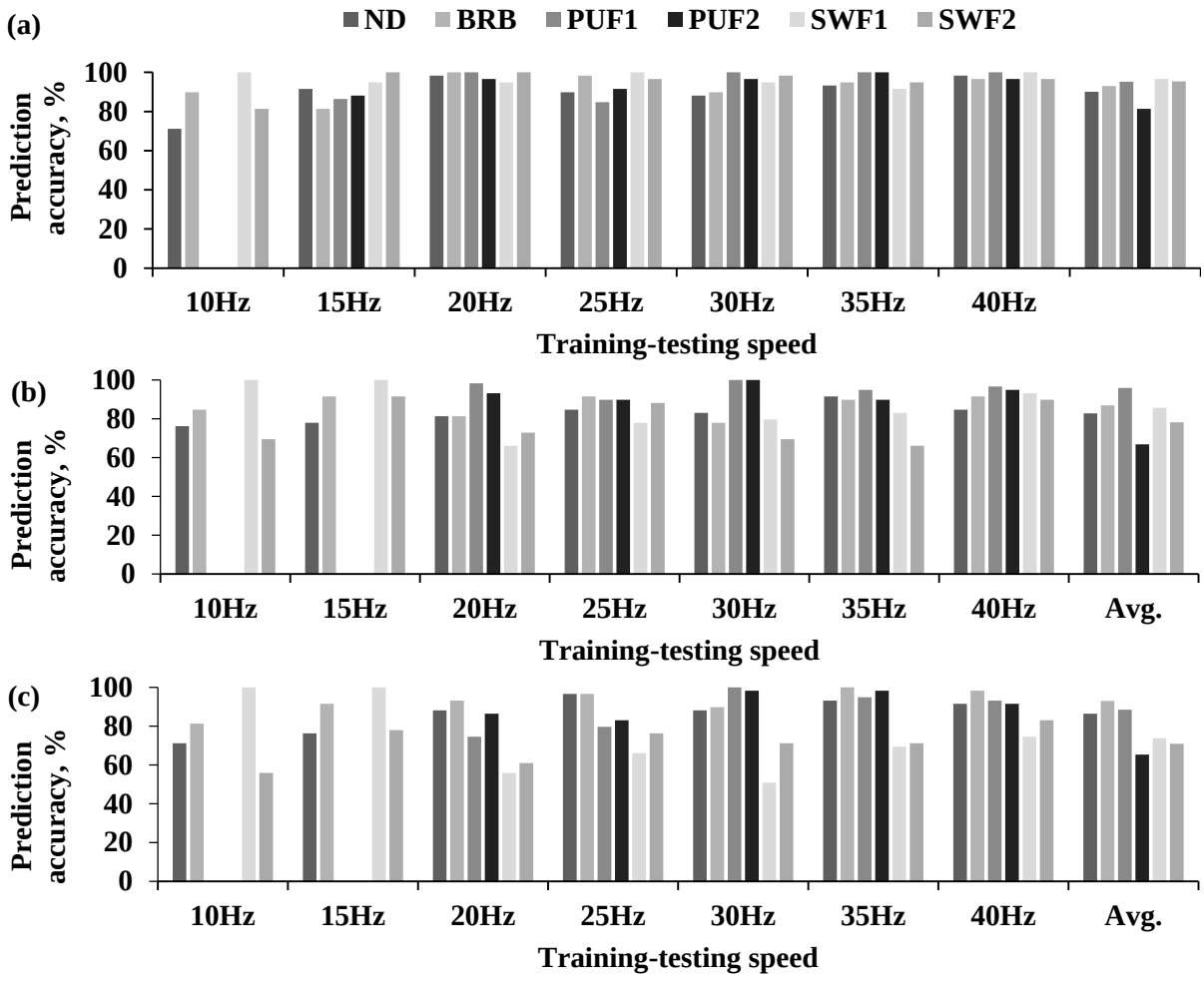

Figure 4.11 Electrical faults prediction based on vibration as well as current signals concurrently for no load (b) for light load (c) for high load

Table 4.8 shows the maximum, minimum and average of overall accuracies over the considered speeds. The prediction performance of SVM gets reduced with the mechanical loading on IMs, like for Case B and Case D, and does not depend over speeds like any other previous cases. The percentage improvement is 8-12% at no load in comparison to the light load and high loads. Thus, for this case, the fault prediction should be performed when there is no external load on IM. In this case, the optimum value of gamma and computational time are 0.3 and 18 s, respectively.

Table 4.8 Electrical fault prediction based on vibration-current signals

Fault type	Signals	Load	Overall prediction, %		
			Maximum	Minimum	Average
Electrical	Vibration and current	No	98.30 (at 20 Hz)	87.79 (10 Hz)	94.05
		Light	91.86 (at 15 Hz)	79.66 (10 Hz)	86.2
		High	88.70 (at 40 Hz)	76.55 (at 20 Hz)	82.83

***Comparison of the performance of MSVM based on the vibration, current and vibration-current signals for electrical faults*:** Figure 4.12 illustrates the comparison of investigation of three cases (i.e., Cases D, E and F) for the no, light and high load conditions. Results show that the maximum of average prediction accuracy of 95.76 % is achieved using the SVM with the only current signals (i.e., Case D) at the light load condition. For no load condition, the MSVM performs the best based on the vibration in conjunction with the current signals (Case F) than two other cases (Cases D and E), but the performance of this is nearly similar to the analysis based on only current signals (i.e., Case D). For the light and high load conditions, the SVM performs the best based on only current signals (Cases E) than two other cases (Cases D and F). The SVM performance, reduces based on

only vibration signals (Case D) than the other two cases (Cases E and F). Also with vibration signals, much difference in performance occurs corresponding to different loads, unlike in the case of current signals. Thus, it is not beneficial to perform the SVM prediction based on only vibration signals for electrical faults. Hence, it is possible to use vibration-current signals as a reliable information to predict electrical faults, only in specific operating condition, i.e. no load. On the other hand, current signals are the best indicator of electrical faults for all considered operating conditions. The reason for this is that the high variation in current signals and corresponding features (as shown in Figure 3.19 and Figure 4.4 (b)) is occurred depending on the type of electrical faults. For the electrical fault prediction, there is no need to train and test the SVM with only vibration signals or in conjunction with current signals. More signals (i.e., vibration and current) mean more feature data sets; hence this can be an unnecessary burden on the SVM. As the average accuracy with vibration signals are 80 to 87 %, so if the current signals are not available, still the electrical fault diagnosis can be performed successfully with vibration signals.

4.3.2.3 Prediction of Mechanical as well as Electrical Faults of Induction Motor together

Here, following three cases are considered

Case G- Mechanical as well as electrical fault prediction based on vibration signal alone

Case H- Mechanical as well as electrical fault prediction based on current signal alone

Case I- Mechanical as well as electrical fault prediction based on vibration as well as current signals concurrently

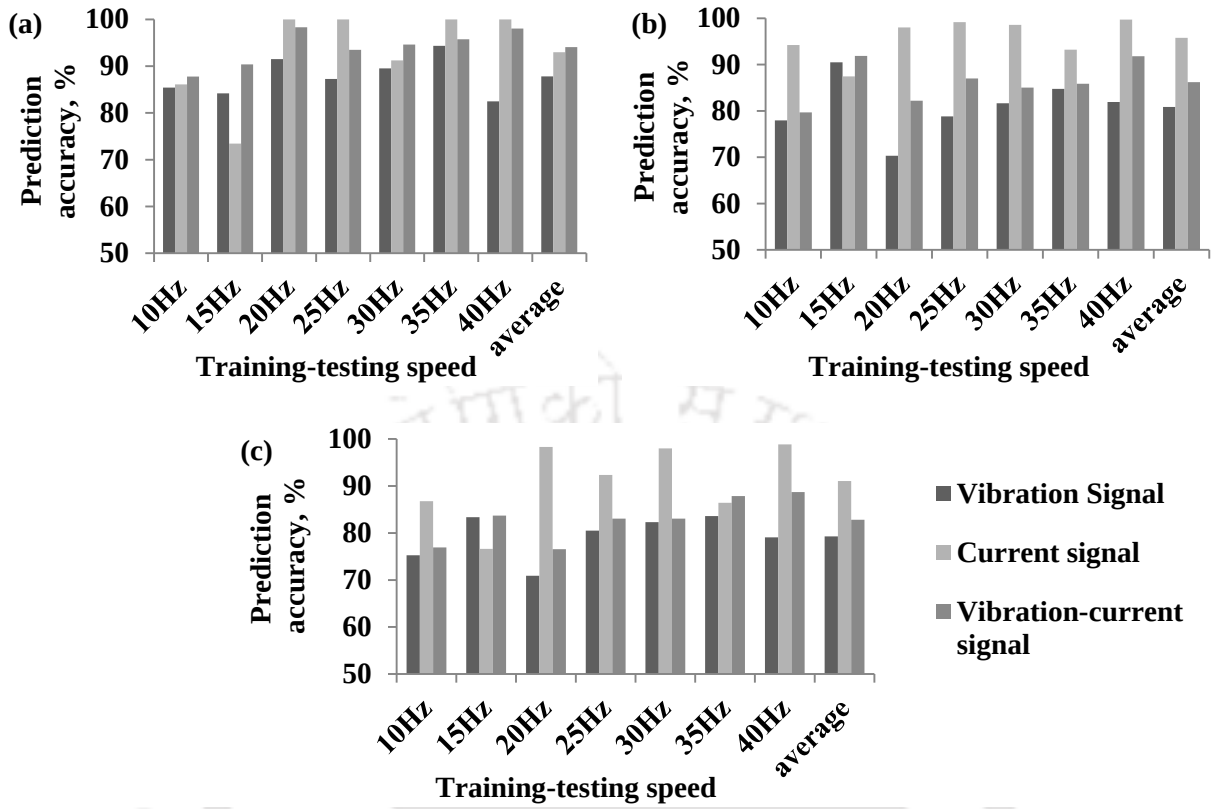

Figure 4.12 Electrical faults prediction for (a) no load, (b) light load and (c) high load

***Case G. Mechanical as well as electrical fault prediction together based on vibration signal alone*:** Figure 4.13 shows the prediction of all considered faults together for various operating conditions of IMs based on only vibration signals. The SVM could predict the BRB up to 93.22 % at no load and high load, that means the BRB also generate significant vibration signatures. The individual prediction performance of BF is nearly 100 % for various speeds as well as mechanical loadings. That means the BF is perfectly predicting for all considered operating conditions of IMs even when all faults are considered simultaneously. The SVM could predict the ND, BRB and all considered mechanical faults successfully (prediction is more than 90 %) at all considered speeds and loads. The SVM could predict the PUF1, PUF2, SWF1 and SWF2 satisfactorily (the prediction

is near about 80 %) for the no load. That means fault severity of the stator winding fault, and the phase unbalance could be predicted at the no load. However, for the light and high load conditions the SVM performance for the PUF2, SWF1, and SWF2 reduces. The reason may be the stator fault generally excite torsional vibration, but not necessary the transverse vibrations.

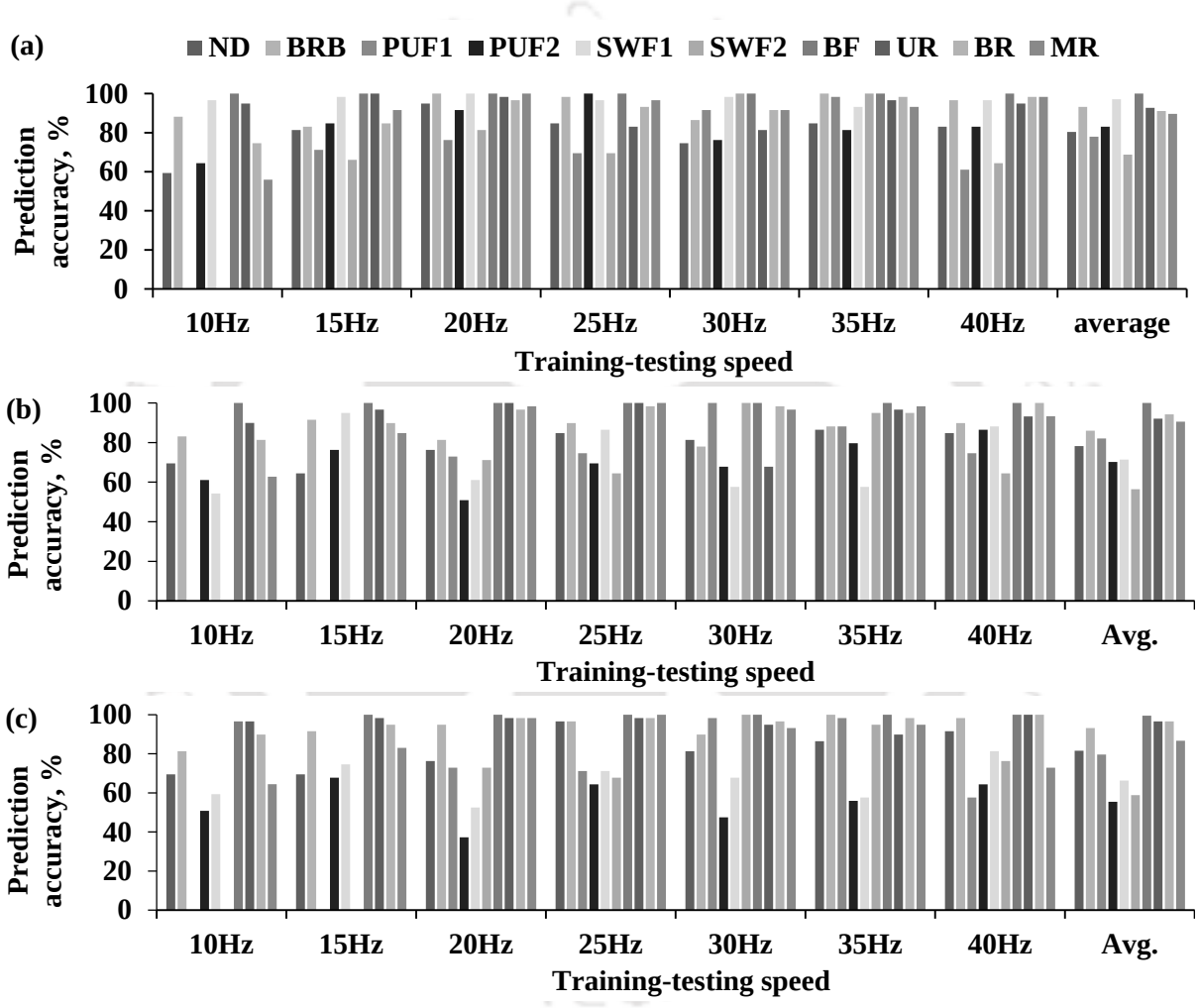

Figure 4.13 Prediction of all fault together based on vibration signal alone for no load (b) for light load (c) for high load

Table 4.9 shows the maximum, minimum and average of overall accuracy over considered speeds. It is noted that the prediction performance of MSVM reduces with the mechanical loading on IMs, like Cases B, D and F and does not depend over speed, like any other case. In this case, the optimum value of gamma and computational time are 0.3 and 20 s, respectively.

Table 4.9 Prediction of all fault together based on vibration signal alone

Fault type	Signals	Load	Overall prediction, %		
			Maximum	Minimum	Average
All Faults	Vibration	No	94.57 (at 35 Hz)	81.54 (10 Hz)	88.86
		Light	88.70 (at 15 Hz)	77.96 (at 10 Hz)	84.99
		High	87.62 (at 35 Hz)	78.71 (at 10 Hz)	84.38

***Case H. Mechanical as well as electrical fault predictions all together based on current signal alone*:** Figure 4.14 shows the prediction of all faults together for various operating conditions of IM based on only current signals. The SVM could predict the stator winding fault, the phase unbalance with the different severity levels perfectly (or nearly 100 %) for all considered operating conditions of IM (i.e., speed and torque). That means different levels of severity in the stator winding fault, and in the phase unbalance could be predicted perfectly at various loads or speeds of the IM. Also the SVM could predict the BRB satisfactorily at the high load (average performance is up to 67.31 % at the higher load). The SVM could predict all considered electrical faults except the ND, BRB and BR successfully (prediction is more than 90 %) at all considered speeds and loads; however, in some cases the ND also could be classified successfully. The average individual prediction performance of the BR is nearly 40-50 % at any operating conditions

that means the SVM based on only current signals could not able to predict BR well, when all faults are considered together unlike for Case G, where it could classify successfully (or more than 90 %). Other faulty conditions, like the UR and MR, could be predicted satisfactorily (prediction is more than 75 %) at each operating condition. The reason for reducing the prediction performance of these mechanical faults (BR, UR and MR) is that these faults do not generate very distinct current signals, so chances of fault feature overlapping is more (as shown in Figure 4.3 (b)). The individual performance for the BF is nearly 75% for the no and high mechanical load conditions, that means the BF is predicted satisfactorily based on only current signals even when all faults are considered simultaneously, unlike for Case A, Case C and Case G, where the BF could be classified perfectly (or 100%) at all considered operational conditions.

Table 4.10 shows the maximum, minimum and average of overall accuracy over the considered speed range. It shows that the prediction performance of SVM is independent of mechanical loadings on IMs (like for Case E) and does not depend on the speed, like any other cases. Also the overall performance, reduces as compared to the previous case, i.e. Case G. In this case, the optimum value of gamma and computational time are 300 and 20 s, respectively.

***Case I. Mechanical as well as electrical fault prediction all together based on vibration as well as current signals concurrently*:** Figure 4.15 shows the prediction of all faults together for various operating conditions of IMs based on the vibration as well as current signals, concurrently. The individual prediction performance of BF is nearly 100 % for each considered speeds as well as loadings that means the BF is perfectly predicted even when all faults are considered, simultaneously.

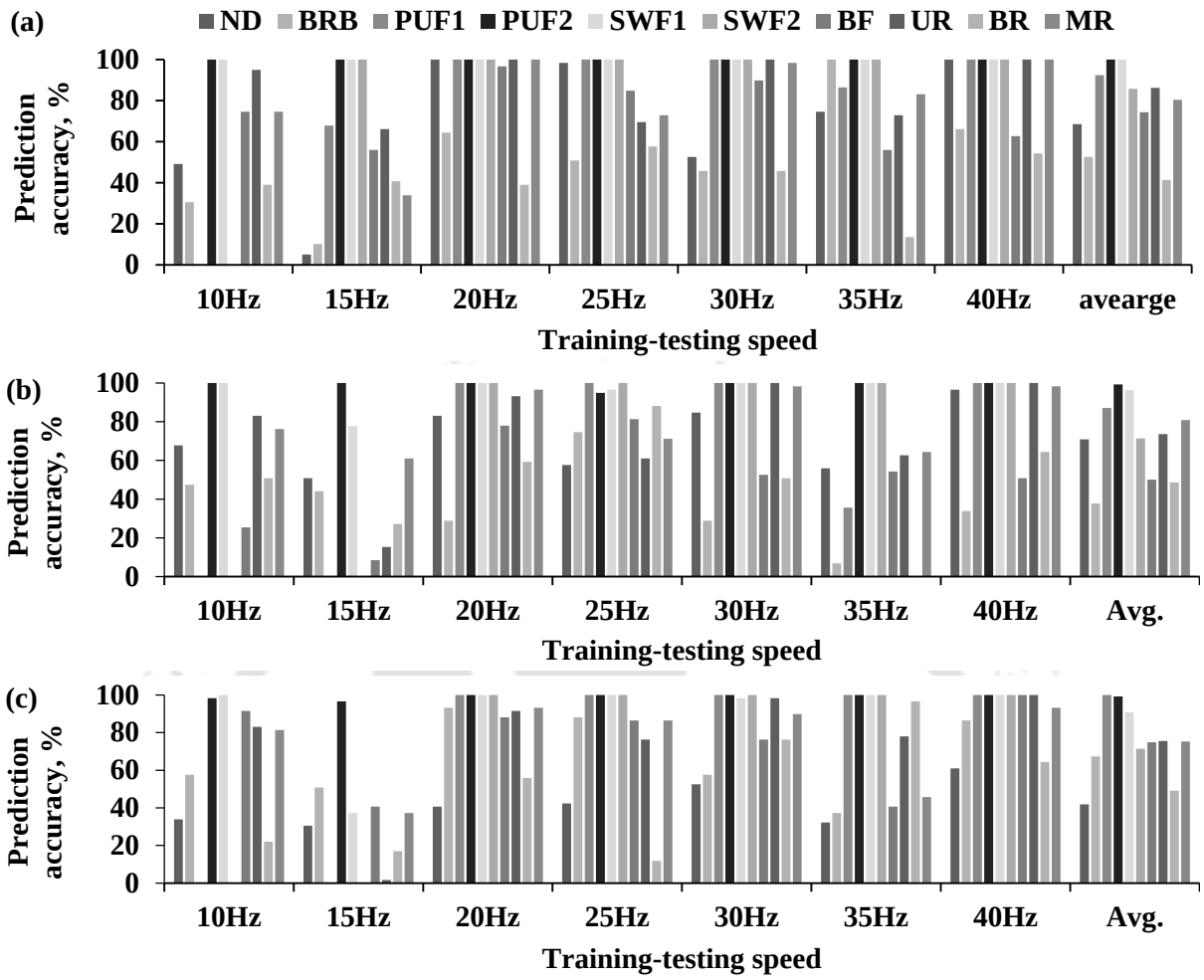

Figure 4.14 Prediction of all fault together based on current signal alone for no load (b) for light load (c) for high load

Table 4.10 Prediction of all fault together based on current signal alone

Fault type	Signals	Load	Overall prediction, %		
			Maximum	Minimum	Average
All Faults	Current	No	90 (at 20 Hz)	57.96 (at 15 Hz)	79.27
		Light	84.40 (at 15 Hz)	53.86 (at 40 Hz)	73.78
		High	90.5 (at 40 Hz)	45.57 (at 15 Hz)	76.23

The prediction of phase unbalance is better than stator winding faults at most of considered operating conditions. Also the SVM could be able to predict the BRB well at various loads (average performance up to 92.98 % at the light and high loads) unlike for Case H. The reason is that faults generate distinct vibration as well as current signals. That is why when the vibration and current both signals are used, then the prediction increases for these faults.

The average individual prediction performance of the BR increases up to 96.61 % at the high load, unlike for Case H (prediction was 40-50 % at each operating conditions based on only current signals). The reason may be that vibration signals are considered with current signals in this case and this fault generates distinct vibration signatures only. Hence, for the ND, BRB and BR the prediction of all faults together, it is necessary to train the SVM with vibration signals in conjunction with current signals. Other faulty conditions, like the ND, UR and MR, could be predicted successfully (prediction is more than 90 %) at each of operating conditions. Table 4.11 shows the max, min and average of overall accuracy over considered speeds. Hence, the prediction performance of SVM reduces with the mechanical loading on IMs like for the Case B, Case D, Case E and Case G. In this case, optimum value of gamma and time are 0.3 and 25 s, respectively.

***Comparison of the performance of MSVM based on the vibration, current or vibration-current signals for all faults*:** Figure 4.16 illustrates the comparison of Case G, Case H and Case I for the no, light and high load conditions, respectively. Results show that, for this case, the maximum of average prediction accuracy achieves up to 93.28 % at the no load using vibration-current signals (Case I). The SVM performs the best based on vibration signals in conjunction with current signals, i.e. Case I, at each considered operating conditions of IMs.

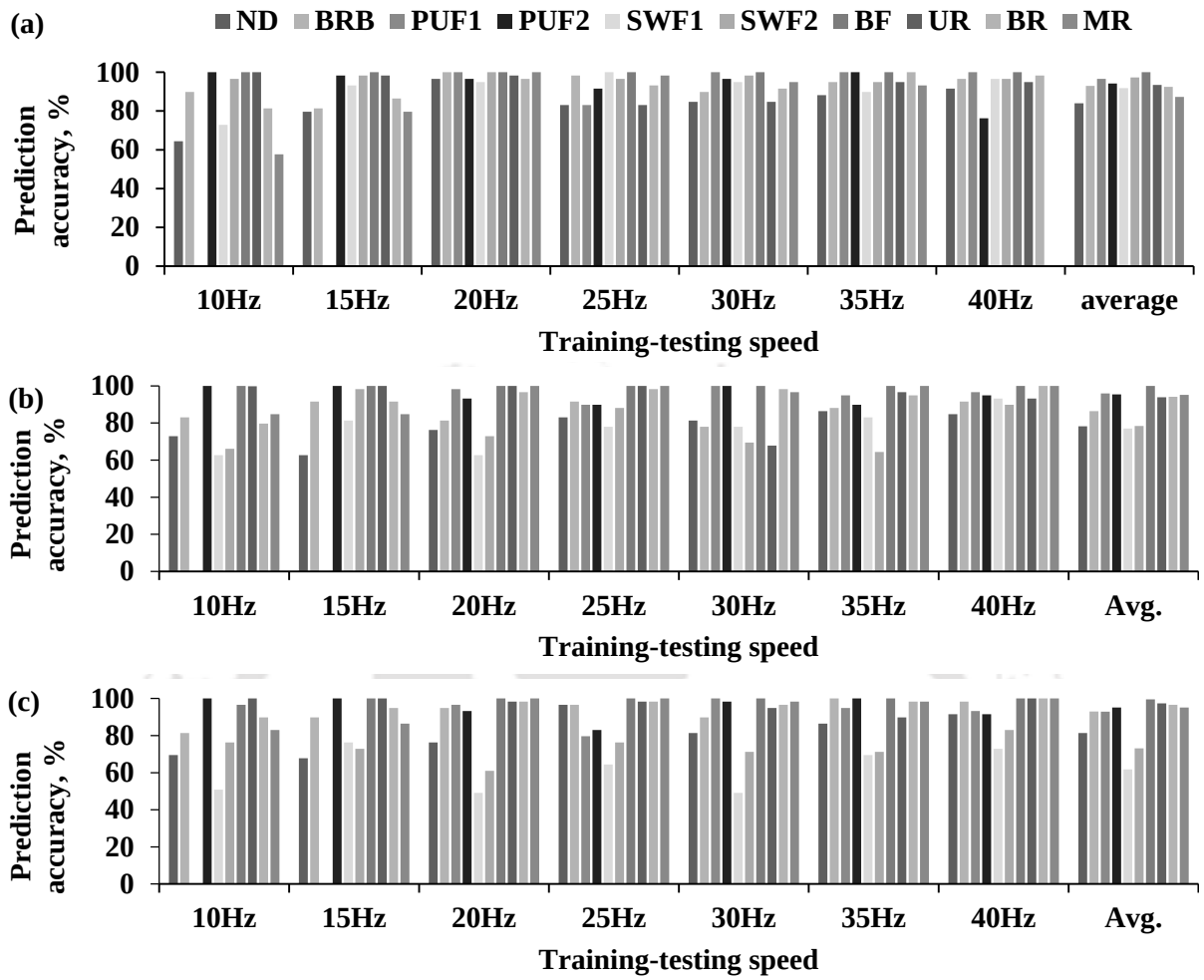

Figure 4.15 Prediction of all fault together based on vibration as well as current signals concurrently (a) for no load (b) for light load (c) for high load

Table 4.11 Prediction of all fault together based on vibration-current signals

Fault type	Signals	Load	Overall prediction, %		
			Maximum	Minimum	Average
All Faults	Vibration and current	No	98.3 (at 20 Hz)	84.18 (at 10 Hz)	93.28
		Light	94.4 (at 35 Hz)	82.10 (at 10 Hz)	88.95
		High	93.05 (at 40 Hz)	82.67 (at 10 Hz)	88.28

The SVM also performs better for the fault prediction based on only vibration signals (Case G), but the performance, reduces much for the prediction based on only current signals (Case H). Thus, it is not beneficial to perform the prediction of all faults together using the SVM based on only current signals (Cases H). Hence, it is effective to predict all faults together using the SVM with vibration signals in conjunction with current signals. The reason is all the mechanical faults generate distinct vibration signal in three orthogonal directions to each other and electrical faults, create high variation in three phases of current with each other. In addition, the electrical faults also generate some unique vibration signatures. So it is effective to collect the vibration as well as current signals when both types of faults are considered for the fault prediction.

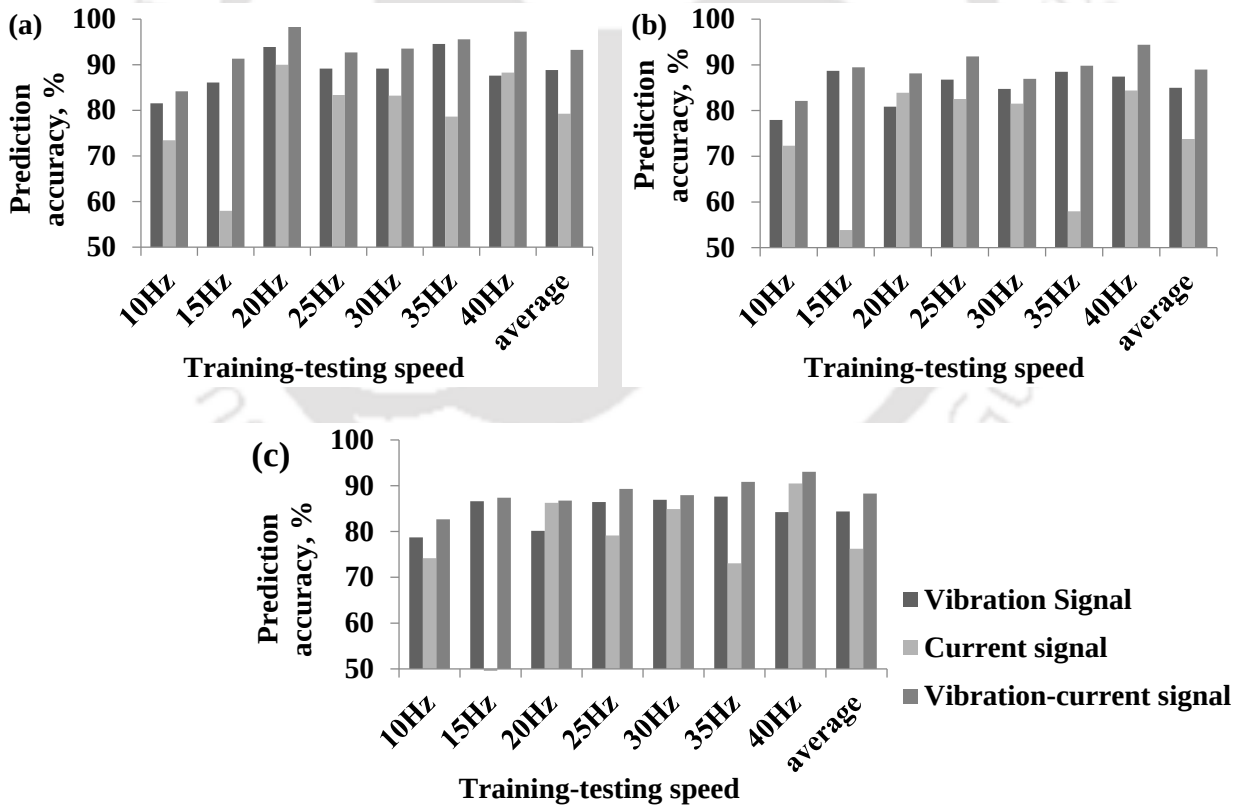

Figure 4.16 Prediction of all fault together for (a) no load, (b) light load and (c) high load

4.4 Comparison of Fault Diagnosis based on Data of Experiment 1 and Experiment 2

In order to study the effect of sampling rate and data points (or frequency resolution) on the fault diagnosis of IMs based on the SVM, the high resolution time domain data is now used. It is very significant to choose adjusted sampling rate and data points (or frequency resolution) that can improve fault diagnostic, detection time, and reduce the cost of implementation. Therefore, the fault diagnosis is now performed based on the low sampling time domain data obtained from Experiment 2 (i.e., the sampling rate of 1,000 S/s with 10,000 sampling points, 0.1 Hz frequency resolution). Then the results of the fault diagnosis are compared with the former case of high sampling time domain data (Experiment 1, i.e., i.e., the sampling rate of 20,000 S/s and 2,000 sampling points, 10 Hz frequency resolution). Here, the fault diagnosis performance is compared to the case when all the ten IM faults are considered with vibration and current signals. The diagnosis based on the vibration and current signals is considered here, because in previous section, it was shown that when the mechanical and electrical faults are considered simultaneously, the vibration as well current signals should be adopted for the effective SVM fault diagnosis. In both cases, the diagnosis is performed using three statistical features, i.e. the standard deviation, skewness and kurtosis, and the SVM classifier is tested at the same speed and load as for the training.

Figure 4.17 shows the comparison of overall prediction performances. It shows that, average fault prediction accuracies are 97.60 % and 99.71 % at the no load, 96.74 % and 98.3 % at the light load, 97.96 % and 99.71 % at the high load for the Experiment 1 and Experiment 2, respectively. That means the fault prediction is slightly higher (around 2 % at all load) with Experiment 2 data as compared with Experiment 1 data, at all operating conditions.

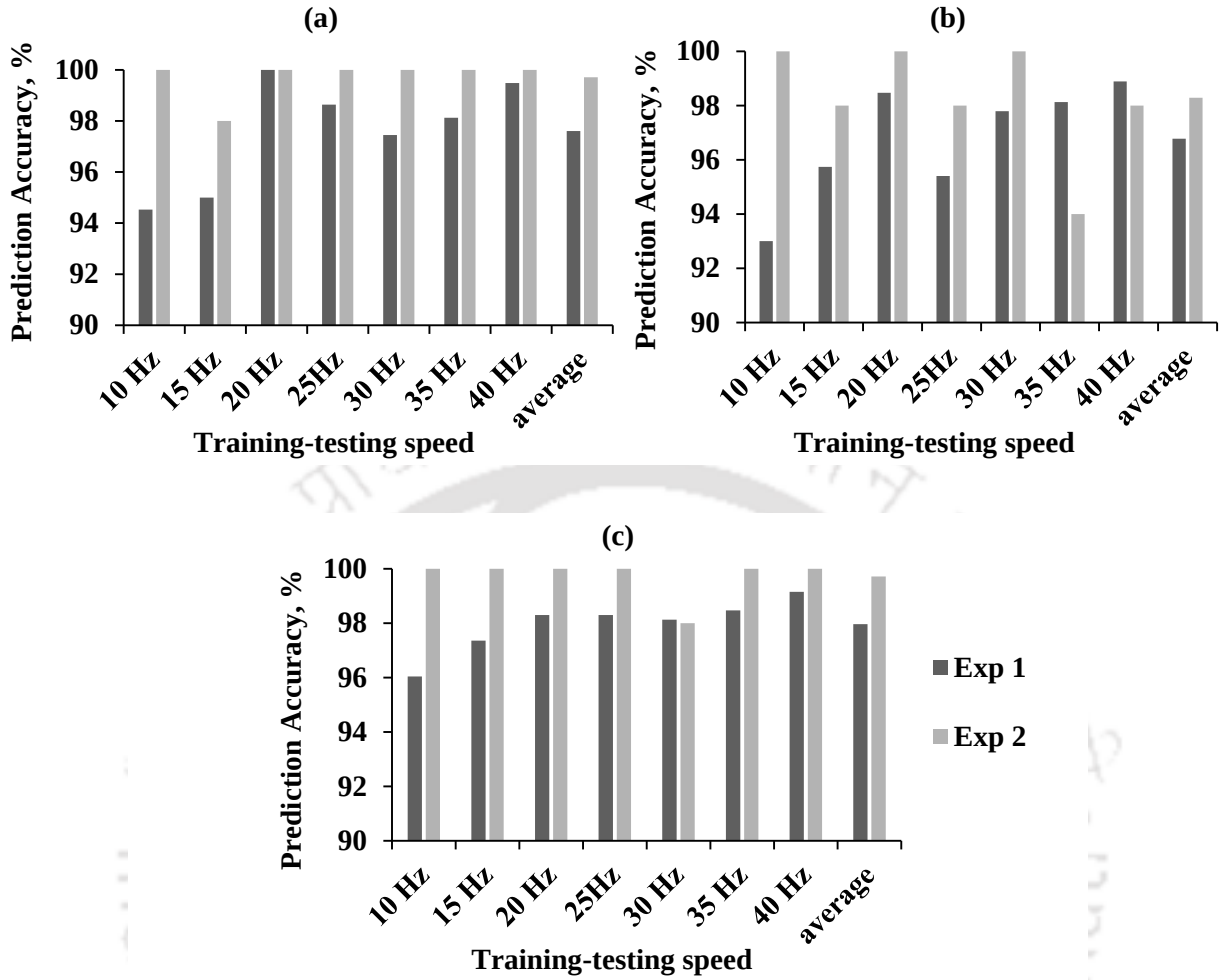

Figure 4.17 Comparison of prediction accuracy based on Experiment 1 and Experiment 2 (a) no load (b) light load (c) high load

The reason of high prediction accuracy with the low sampling rate data may be that, almost all the considered IM faults produce the fault frequencies, sidebands and fault signatures at lower frequencies, and low sampling rate data can capture the low frequencies with more precession. In addition, chosen frequency resolution for first experiment is very low, i.e., 10 Hz. In such a low-frequency resolution data the significant peaks and sidebands produced by different IM faults may not be captured correctly, because the low-frequency resolution of 10 Hz may overstep some of

intermediate. Due to this, the features extracted from the high sampling data are not so effective. The features extracted from the two experimental time domain data are added in feature clusters, and found that the more overleaping of features occur in the feature space for data of Experiment-1 as compared to data of Experiment-2, as shown in Figure 4.18 and Figure 4.19. Therefore, when the features of data of Experiment-1 are used for the fault diagnosis, the prediction performance, reduces significantly. It is noted that, the fault diagnosis with Experiment 2 data does not only perform better at all motor operating conditions, but also reduces the cost of implementation, which are the vital requirement of an intelligent fault diagnosis. Therefore, only the low sampling data will be adopted for further fault diagnosis of IMs in subsequent chapters. It is noted that, it might have possible to get better results with Experiment 1 data also if more sample points were acquired. However, it is a big computational burden in acquiring more sample points (i.e., 2, 00,000 samples) in order to get high frequency resolution (i.e., 0.1 Hz) with a high sampling rate of 20 kHz. In addition, it increases the cost of implementation, which is highly undesirable in the fault diagnosis.

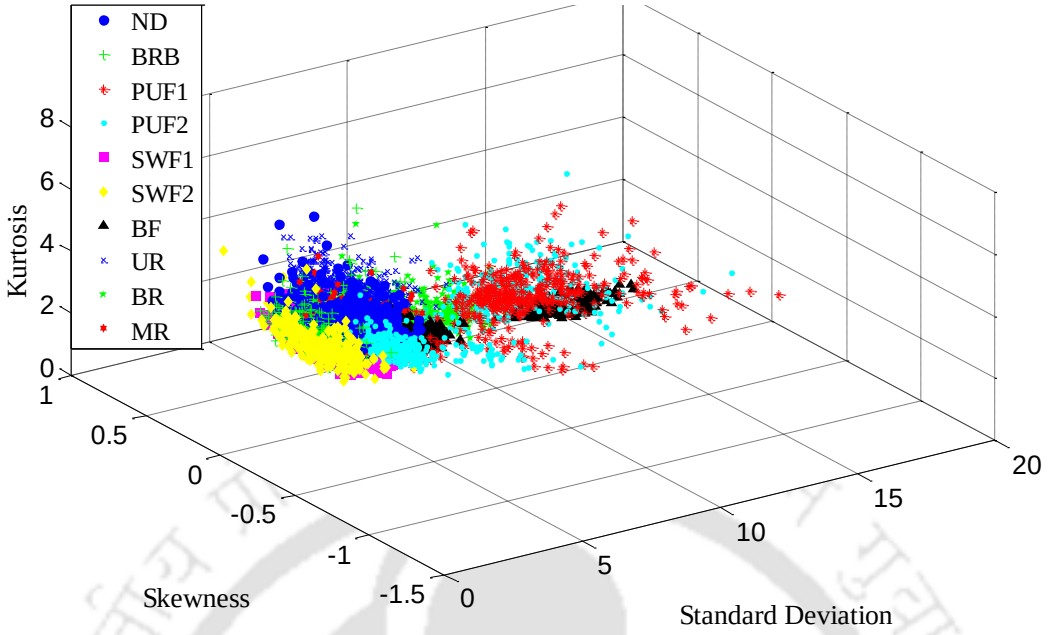

Figure 4.18 Typical scatter plots for all faults using three features ($\sigma, \chi,$ and κ) of vibration and current obtained from experiment-1 at 40 Hz for T_3

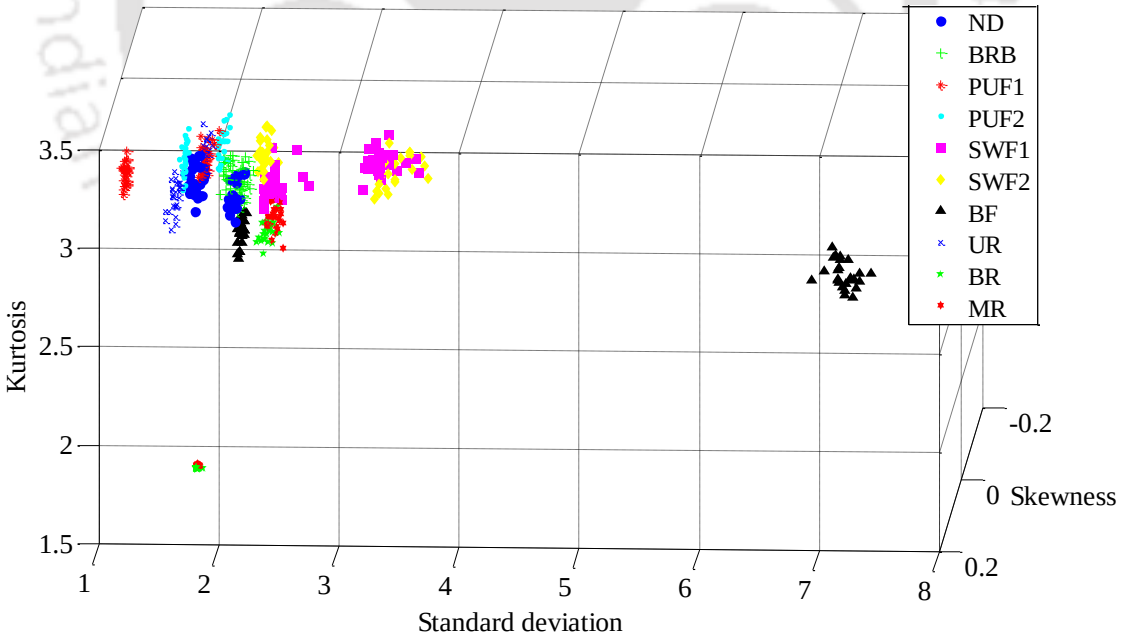

Figure 4.19 Typical scatter plots for all faults using three features ($\sigma, \chi,$ and κ) of vibration and current obtained from experiment-2 at 40 Hz for T_3

4.5 Summary

A comparative investigation of the vibration and current signals has been done for the fault diagnosis of mechanical and electrical faults in IM. Three statistical features (i.e., $\sigma, \chi,$ and κ) extracted from high sampling rate-time domain data are used for the investigation. The investigation concludes that the SVM could predict all mechanical faults effectively based on vibration signal. However, when the mechanical fault diagnosis is considered with the current signal, the prediction performance reduces significantly. When both the vibration and current signals are considered for the diagnosis of mechanical faults, the prediction performance is similar to the case when the only vibration signal is used. Therefore, to diagnose mechanical faults, the vibration signal is better and sufficient. The electrical fault diagnosis can be performed successfully with vibration signals, however, the prediction performance increases significantly when these faults are diagnosed with current signals. When the electrical fault diagnosis is performed using vibration signal in conjunction with the current signal, the performance reduces at most of operating conditions as compared to the case when only current signals are used. Therefore, to diagnose electrical faults, the current signal is good and sufficient, however, when the current signal is not available, the diagnosis can be performed successfully with the vibration signal.

When the mechanical as well as electrical faults are considered for the simultaneous diagnosis using vibration signals, the diagnosis is performed successfully. When these faults are diagnosed using current signals, the performance reduces significantly. However, when vibration signals are used in conjunction with current signals to diagnose the mechanical and electrical faults simultaneously, the prediction performances improve significantly as compared to the case when

the vibration or current signal is used. Therefore, for further study (i.e., with high resolution time domain data, frequency domain data, and time-frequency domain data), the vibration signal in conjunction with the current signal are used to diagnose the mechanical as well as electrical faults, simultaneously. In addition, in this chapter, the fault prediction performance of data of the high sampling rate is compared with the data of low sampling rate. It is found that the fault prediction and detection time is slightly improved with the data of low sampling rate obtained from Experiment 2. Therefore, this data will be further adopted for the study in subsequent chapters. The fault diagnosis using time domain data of low sampling rate is further extended in the following chapter.

CHAPTER 5

Multi-Fault Diagnosis of IMs based on Time Domain Data of Low Sampling Rate

5.1 Introduction

In this chapter, the multi-fault diagnosis of the combined mechanical and electrical faults and their severities in IMs is performed based on the multiclass SVM using the time domain data of low sampling rate. In the previous chapter, it was shown that, the fault diagnosis is slightly increased with the low sampling rate data that is why this data is adopted in this chapter. In addition, it was also shown that when all the mechanical and electrical faults are considered simultaneously for the fault diagnosis, then it is beneficial to consider the vibration as well as current signals for the same. Therefore, in this chapter, the vibration as well as current signals are considered for the fault diagnosis.

In the previous chapter only three statistical features were used for the fault diagnosis, however, the diagnostics performance highly depends on the choice of the features. Therefore, a number of statistical features are considered here that are extracted from time domain data, and further used as input to the SVM based classifier to perform fault diagnosis. SVM parameters are selected based on the cross-validation method along with the grid-search technique to build an optimal SVM model by avoiding the over-fitting problem. In order to remove the inappropriate features or to select the suitable one that can efficiently represent the fault, the wrapper model has been used. Finally, the fault diagnosis of IMs is performed based on an integrated SVM method that combines the wrapper model and cross-validation with grid-search methods. The fault diagnosis is presented

when training and testing of the SVM is done at the same speed and load. To check the robustness of the present fault diagnosis methodology, the diagnosis is implemented for a wide range of IM speeds and loads. In addition to this, in this chapter, the work is extended to perform the diagnosis at different speeds and loadings as the training of the classifier. The aim of this is to check the prediction capability of the proposed diagnostics for limited information for trainings.

5.2 Fault Feature Extraction

In the previous chapter, only three standard statistical features based on previous literatures, i.e. the standard deviation, skewness and kurtosis were extracted from time domain data. This is because in preliminary analysis the main aim was to perform the comparative investigation of vibration and current signals in fault diagnosis of the mechanical and electrical faults of IM based on the SVM. In this chapter, a fairly wide set of statistical features from the raw time domain data are selected for the basis of the study because the best feature(s) selection is one of the main aim here so that effective fault diagnosis of IM can be achieved.

In order to perform fault diagnosis of different machines, the mean, root mean square (RMS), standard deviation, skewness, kurtosis, crest factor, entropy error, etc., are often used statistical features in time domain. In a study, time domain features such as probability density and kurtosis were utilized in order to detect the bearing defect (Dyer and Stewart, 1978). Some other features such as RMS and Crest Factor have also used to detect localized defects (Tandon and Choudhury, 1999). Jack and Nandi (2002) used a number of different statistical features based on moments and cumulants of the vibration signal in order to perform the bearing fault diagnosis. Samanta (2004) has also used moments from the time domain vibration signal for the fault diagnosis of

gears and found promising results. Widodo and Yang (2007) have used a number of features such as the mean, RMS, shape factor, crest factor, skewness, kurtosis and entropy from the vibration and current signals for the fault diagnosis of IMs.

Various factors affect the effectiveness of the feature; thus it is a big challenge to estimate which feature(s) is/are more sensitive to the particular machine faults. Therefore, in this chapter, fourteen features are extracted from the time domain data, in order to select the most efficient features that can effectively characterize the signal of healthy and defective IM. Eight features are calculated based on statistical moments, and another six features are calculated using statistical parameters, such as the peak-to-peak ratio, crest factor, mean-to-standard-deviation ratio, standard deviation, skewness and kurtosis. These features are very sensitive to incipient or already induced faults or any changes in machine faults. The statistical moments offer a compact way to characterize time-series data. Statistical moments are single number indices or descriptors, similar to the time waveform indices except they are based on the probability density function (PDF). Or in other word, the statistical moments can be obtained by decomposing a probability distribution function (PDF). Any changes in the fault condition cause change in the PDF of the signals, then the moments may also change, and therefore these can provide diagnostic information.

For the probability density function, $p(x)$, of the time waveform data, the moment provides an indication of general features of the distribution of data variables, x. A number of significant statistical features which describe the behavior of the data, are constructed by the first few moments. The k^{th} moment about the mean of the discrete data x, can be calculated using following equation [26, 27]

$$\mu_k = \frac{1}{N}\sum_{i=1}^{N}(x_i - \mu_1)^k \tag{5.1}$$

With

$$\mu_1 = \bar{x} = \frac{1}{N}\sum_{i=1}^{N}x_i^k \tag{5.2}$$

Where, N is the number of points in the sample, k = 1, 2,..., N and μ_1 is the mean, which is the first moment of the signal. Moments are generally defined about the mean so as to obtain the statistical central moment. The second central moment is called variance σ^2 (where σ is the standard deviation). When the third moment is normalized by the standard deviation to the third power, the skewness is obtained; and when the fourth moment is normalized standard deviation to the fourth power, the kurtosis is obtained. The fifth and sixth moments are also called hyper-skewness and hyper-flatness, respectively. The odd moments reflect the peak position of PDF relative to the mean and even moments are proportional to the spread of the distribution. In case of a Gaussian process (i.e., a stationary signal with a Gaussian PDF), the first and second order statistics completely describe the signal. In particular, a Gaussian process has null skewness, while its kurtosis value is 3. It may be concluded that if a signal is non-Gaussian, then higher-order moments are needed to completely describe its properties.

Higher statistical moments up to k = 8 have been considered as statistical features for the present study. The other statistical features used in this study are the peak-to-peak ratio, crest factor, mean-to-standard-deviation, standard deviation, skewness and kurtosis. These features are often used to quantify the time signal. The standard deviation, skewness and kurtosis were explained in the previous chapter. The definition of other considered features is described as follows:

Peak-to-peak (R_{pp}): The peak-to-peak is a non-dimensional statistical parameter and defined as

$$R_{pp} = \frac{x_{p\max}}{x_{p\min}} \tag{5.3}$$

where, $x_{p\max}$ is peak value and $x_{p\min}$ is the RMS value.

Crest factor (CF): The crest factor is defined as the ratio of the peak value to the RMS of the signal. It is a non-dimensional feature that measure the spikiness of the signals. Also, it reflects the impulse in the signal corresponding to continuous signal of lower level. The crest factor increases, if any peaks appear in the time domain signal. This can be written as

$$CF = \frac{x_p}{x_{rms}} \tag{5.4}$$

where, x_p is peak value and x_{rms} is the RMS value.

Mean to standard deviation ratio (R_{msd}): It is defined as the ratio of the mean value to the standard deviation of the signal. It is reciprocal of the coefficient of variation. A coefficient of variation is a statistical measure of the dispersion of data points in data series around the mean value. It is a useful statistic for comparing the degree of variation from one data series to another, even if the means are drastically different from one another.

The mean-to-standard-deviation ratio is calculated as follows:

$$R_{msd} = \frac{\mu_1}{\sigma} \tag{5.5}$$

where, μ_1 is the first moment or mean and σ is the standard deviation.

Fourteen statistical features are extracted from the time domain vibration and current signals (see Appendix. A, Figure A.1 and Figure A.2). The features are calculated from 10,000 points available in one dataset obtained from Experiment 2. Since 25 raw data sets are available, so 14×25 feature data sets are obtained. Figure A.1 and Figure A.2 illustrate the statistical features extracted from time domain vibration (in three orthogonal directions) and current signals (in three phases) for BF at 40 Hz speed and for T3 load. However, on observing extracted features, it is impossible to distinguish various faults of IMs, because these features show a high variance and may contain superfluous or imprecise information. Further, these feature data sets would be used in the fault diagnosis.

Table 5.1 The statistical feature parameters calculated from time domain data

Signal	Feature parameter (time domain)
Vibration in *x*-axis, vibration in *y*-axis and vibration in *z*-axis Current in Phase A, current in Phase B and current in Phase C	Initial eight statistical moments (μ_1 to μ_8), peak to peak (R_{pp}), crest factor (CF), mean to standard deviation (R_{msd}), standard deviation (σ), skewness (χ) and kurtosis (κ)

5.3 Fault Diagnosis based on SVM

After collecting the sufficient datasets of useful fault features from time domain data, the multi-fault diagnosis in IM is performed using one-versus-one multi-class method of SVM classifier. In order to perform the fault diagnosis, first total 25 feature data sets are divided into training and testing data in a proper ratio, i.e. 80 % and 20 % (similar to Chapter 4), respectively. The composition of training and testing data sets for each operating condition is added in Table 5.2

Table 5.2 The composition of training and testing data sets

Fault condition and their label	Machine operating condition		Training set for each operating condition	Testing set for each operating condition
	Load torque	Speed, Hz		
ND-1	$T_1/T_2/T_3$	10/15/20/25/30/35/40	20	5
BRB-2	$T_1/T_2/T_3$	10/15/20/25/30/35/40	20	5
PUF1-3	$T_1/T_2/T_3$	10/15/20/25/30/35/40	20	5
PUF2-4	$T_1/T_2/T_3$	10/15/20/25/30/35/40	20	5
SWF1-5	$T_1/T_2/T_3$	10/15/20/25/30/35/40	20	5
SWF2-6	$T_1/T_2/T_3$	10/15/20/25/30/35/40	20	5
BF-7	$T_1/T_2/T_3$	10/15/20/25/30/35/40	20	5
UR-8	$T_1/T_2/T_3$	10/15/20/25/30/35/40	20	5
BR-9	$T_1/T_2/T_3$	10/15/20/25/30/35/40	20	5
MR-10	$T_1/T_2/T_3$	10/15/20/25/30/35/40	20	5

As prediction results depend on how well the classifier is trained, therefore, here the optimization of SVM parameters is performed. The cross-validation method along with the grid search

technique is used for this. In addition, the performance of the classifier also depends on effectiveness of input features, so the selection of the most effective feature(s) is performed based on the wrapper model. The fault diagnosis is considered for three cases, i.e. the same speed and same load case, the intermediate speed case, and the intermediate load case.

5.3.1 SVM Parameter Selection and Training

In total, 10×21 data sets (where, 10 is the fault conditions) are used for the parameter selection and training. All fourteen features are used for the training one by one and performed the cross-validation at each operating condition of IMs. Finally, the result comes in the form of training accuracy, which shows how well the model is learned for the particular SVM parameters. The CV accuracy in the grid-search technique for a typical case of 40 Hz and T_3 load, when the training is performed with all the features individually or in sets are shown in Figure 5.1 and Figure 5.2. In these, contour lines are plotted and the best training accuracy is marked. Figure 5.1 (a) is added for the case when the cross-validation is performed with μ_1 only, at 40 Hz and T_3 load. It shows that the maximum CV or training accuracy is achieved up to 99.5 %. That means the SVM model is well learnt for this case. However, the CV accuracy decreases with higher moments as shown in Figure 5.1 (b)-(h). The minimum CV accuracy (69.5 %) comes in the case when the model is trained with the crest factor (CF) as shown in Figure 5.2 (b). That means the SVM model is not trained successfully with this feature. The maximum accuracy (100 %) comes with the standard deviation used individually, and in combination with the skewness and the kurtosis as shown in Figure 5.2 (d) and Figure 5.2 (g), respectively. That means the SVM model is well trained using these features. Now corresponding to the maximum CV accuracy the optimal pair of (C, γ) is achieved for each feature and IM operating condition.

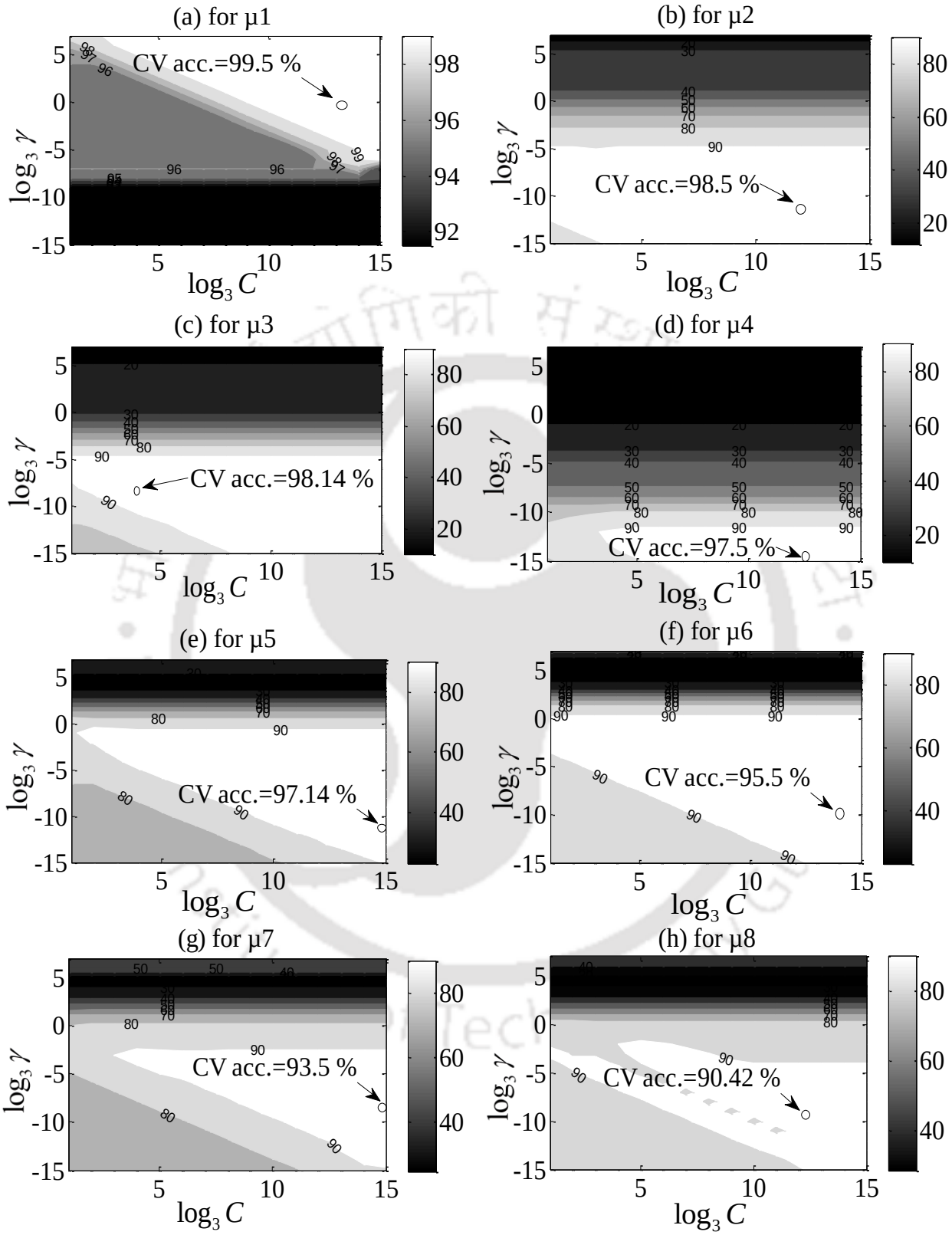

Figure 5.1 Cross validation accuracy at 40 Hz and T_3

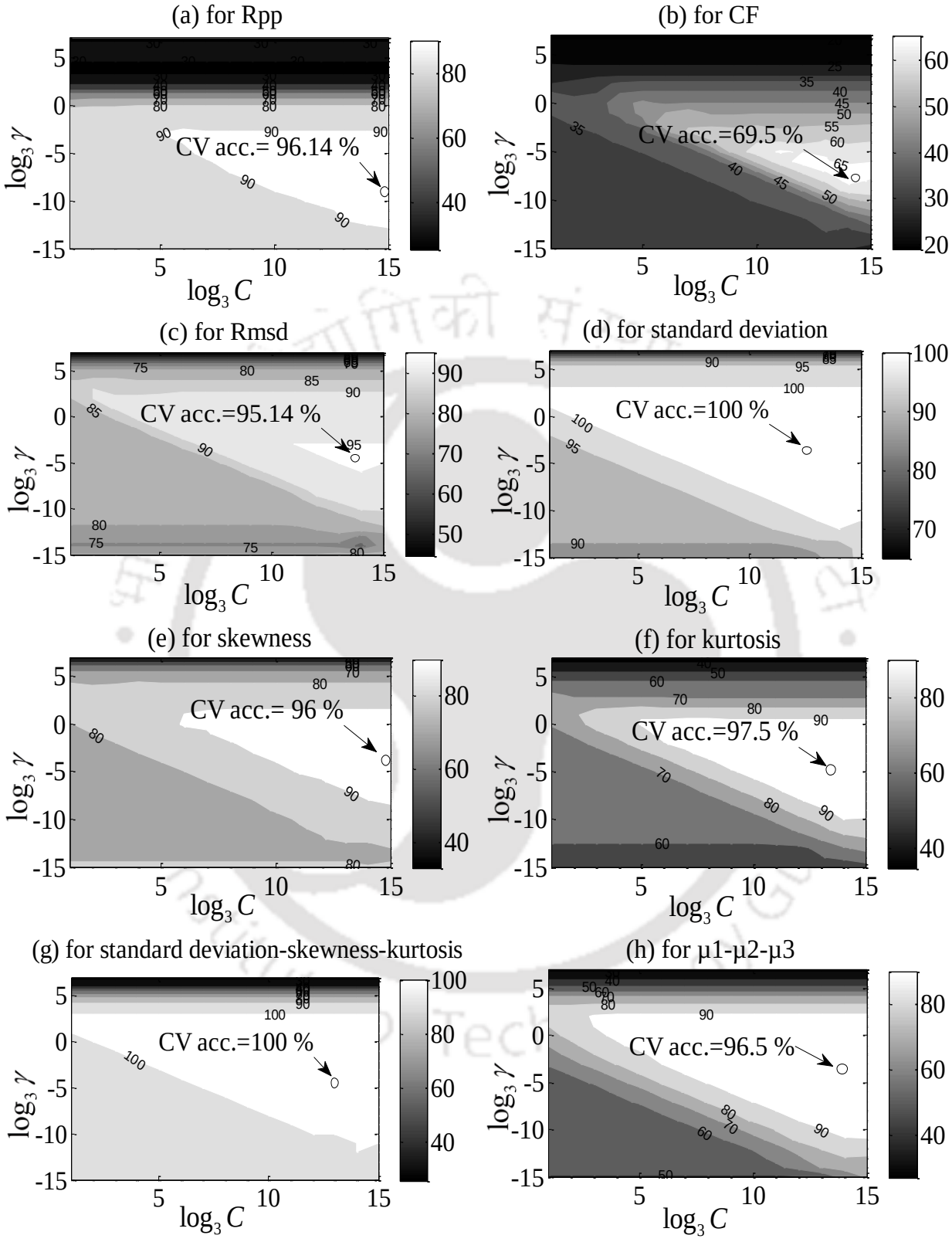

Figure 5.2 Cross validation accuracy at 40 Hz and T_3

Ultimately, using the optimal pair of these parameters, a best model of the SVM is trained for each feature or feature set and operating conditions. Now it will be used for the final testing or fault classifications. It is noted that the testing or final prediction accuracy depends on how well the classifier is trained after inputting the optimal SVM parameters (i.e., avoiding over-fitting).

5.3.2 Fault Feature Selection

In previous sections, initially fourteen features were extracted from the vibration and current signals that represent IM fault conditions. Then optimal SVM parameters are selected to build an optimal SVM model. However, the classifier's accuracy depends on the SVM parameter as well as the features. Therefore, silent feature providing IM fault related information must be selected from the feature set. Therefore, feature selection is now performed in this section.

For the selection of most representative features from fourteen features, a wrapper model of feature selection is used in this work. Initially, all fourteen features individually are tried with the SVM classifier as input vectors. The training and testing of SVM are done at each considered speed of the high load and final result comes in the form of prediction accuracy at each speed. The overall accuracy is calculated by averaging the accuracies at each speed only for the high load and results are added in Table 5.3. Now, according to the wrapper model, the feature or set of features with highest overall prediction accuracy, are selected as the optimal one. The result shows that all considered features perform the IM fault diagnosis successfully with more than 90% accuracy except eighth moment (88.8 %) and *CF* (68 %). Prediction accuracy decreases significantly with these two features. That means these features do not represent the IM fault condition efficiently. Two sets of features, i.e. μ_1, μ_2 and μ_3, and $\sigma, \chi,$ and κ from the most effective six features are

then used for the fault diagnosis. The results show that the set of $\sigma, \chi,$ and κ gives the highest prediction accuracy as compared to other feature set as well as other features individually. That means the set of $\sigma, \chi,$ and κ represents the IM fault condition more efficiently. Now, this set of feature is selected as an optimal feature set from time domain vibration and current signals for the fault diagnosis of IM for various cases.

Table 5.3 Statistical features selection by wrapper model and SVM at high load

Statistical features	Average prediction accuracy, %	Statistical features	Average prediction accuracy, %
μ_1	98	R_{pp}	93.71
μ_2	97.8	CF	68
μ_3	97.5	R_{msd}	93.14
μ_4	96.85	σ	99.14
μ_5	97	χ	97.28
μ_6	94	κ	97.87
μ_7	91.42	μ_1 to μ_2	97.71
μ_8	88.8	σ- χ- κ	99.71

5.3.3 Fault Diagnosis for the Same Speed and Load Case

After selecting optimal SVM parameters and optimal feature set, now the fault diagnosis is performed when training and testing of the classifier done at the same speed and load. In order to check the robustness of the methodology, the fault diagnosis is performed for various operating

conditions (i.e., three loads and seven speeds) of IM. In total twenty-one different operating conditions are considered for the diagnosis as shown in Table 5.4.

Table 5.4 Various conditions of the same speed and load case of the fault diagnosis

Training torque	Testing torque	Training speed (Hz)	Testing speed (Hz)
		10	10
		15	15
T_1	T_1	20	20
T_2	T_2	25	25
T_3	T_3	30	30
		35	35
		40	40

Fault prediction: The results of the fault diagnosis are shown in Table 5.5. It shows the overall as well as individual prediction accuracies. At the no load condition, overall accuracies are 100 % at all the speeds except at 15 Hz where the accuracy is 98 %. At 15 Hz speed, the individual accuracy is 80 % for SWF2 (i.e. second severity levels of stator winding fault). That means for this particular operating condition the SWF2 is not predicted successfully; however, other fault conditions of the motor are predicted perfectly, i.e. with 100 % accuracy. Table 5.6 shows the confusion matrix of fault diagnosis, which show how much data of one fault is misclassified with others. The matrix shows that for T_1 load and 15 Hz, 20 % of the SWF2 data is misclassified with the SWF1 data. As these are only two severity levels of stator winding faults, therefore some chances are always there that the features from SWF2 are misclassified with SWF1. The reason is that the SWF2 may

generate similar current signature as the SWF1 (as shown in Figure 3.19) until there is large severity gap between them. Therefore, features obtained from the signals of these faults may overlap. Due to this, these faults can be misclassified with each other.

At the light load, the highest and lowest overall prediction accuracies are 100 % (at 10, 20 and 30 Hz) and 94 % (at 35 Hz). At 15 Hz speed, the individual accuracy for PUF2 is 80 %. The confusion matrix shows that 20 % of the PUF2 data is misclassified with the PUF1 data. This is because PUF1 and PUF2 are two severity levels of the same faults, they may generate similar current signatures, and therefore the feature obtained from these signatures may overlap. At 35 Hz speed, 60 % of SWF2 data is misclassified with SWF1. That means at this speed, the SWF2 data are not classified in the appropriate class (but indicating the same fault). At 40 Hz, 20 % of the UR data is misclassified with the BR. The reason is that the UR and the BR generate approximately similar vibration signatures (as shown in Figure 3.19) and hence the same features (approximately). For the high motor load condition, overall accuracies are 100 % at all speeds except one speed condition of 30 Hz (98%). For this load also, at 30 Hz speed, some features of SWF2 are misclassified with SWF1 as shown in Table 5.5.

From Table 5.5, it is noted that the average performances over considered angular speeds are 99.71, 98.3, and 99.71 for the no load, light load and high load conditions, respectively. This shows that the proposed methodology is able to predict (or classify) all mechanical as well as electrical faults at all operating conditions of IM, even when all ten faults conditions are considered, simultaneously. In addition, the two severity levels of the phase unbalance as well as stator winding faults are also classified successfully at the most of operating conditions.

Table 5.5 Fault diagnosis for various operating conditions of IM for the same speed and load case

Train speed (Hz)	Test speed (Hz)	Prediction accuracy, %										
		ND	BRB	PUF1	PUF2	SWF1	SWF2	BF	UR	BR	RM	Over.
For no load, T_1												
10	10	100	100	100	100	100	100	100	100	100	100	100
15	15	100	100	100	100	100	80	100	100	100	100	98
20	20	100	100	100	100	100	100	100	100	100	100	100
25	25	100	100	100	100	100	100	100	100	100	100	100
30	30	100	100	100	100	100	100	100	100	100	100	100
35	35	100	100	100	100	100	100	100	100	100	100	100
40	40	100	100	100	100	100	100	100	100	100	100	100
	Avg.	100	100	100	100	100	97.14	100	100	100	100	99.71
For light load, T_2												
10	10	100	100	100	100	100	100	100	100	100	100	100
15	15	100	100	100	80	100	100	100	100	100	100	98
20	20	100	100	100	100	100	100	100	100	100	100	100
25	25	100	80	100	100	100	100	100	100	100	100	98
30	30	100	100	100	100	100	100	100	100	100	100	100
35	35	100	100	100	100	100	40	100	100	100	100	94
40	40	100	100	100	100	100	100	100	100	80	100	98
	Avg.	100	97	100	97	100	91.4	100	100	97	100	98.3
For high load, T_3												
10	10	100	100	100	100	100	100	100	100	100	100	100
15	15	100	100	100	100	100	100	100	100	100	100	100
20	20	100	100	100	100	100	100	100	100	100	100	100
25	25	100	100	100	100	100	100	100	100	100	100	100
30	30	100	100	100	100	100	80	100	100	100	100	98
35	35	100	100	100	100	100	100	100	100	100	100	100
40	40	100	100	100	100	100	100	100	100	100	100	100
	Avg.	100	100	100	100	100	97.14	100	100	100	100	99.71

The prediction performance of the proposed methodology does not depend on motor operating conditions, i.e. loads and speeds. The high prediction performance of the classifier may be attributed to the capability of the selected features (σ, χ and κ) to form distinctive clusters of various faults in the feature space as shown in Figure 5.3 and Figure 5.4. Features of vibration signals are completely separable for all ten IM faults. Though, little overleaping occurred between features of current signals of some faults, this does not affect the fault prediction by the SVM. The average training and testing time for the fault diagnosis are very less i.e., 3 s and 0.6 s (approximately), respectively.

Table 5.6 Confusion matrix of fault diagnosis of the same speed and load case

Operating conditions	Miscla-sified fault	Classification percentage									
		ND	BRB	PUF1	PUF2	SWF1	SWF2	BF	UR	BR	MR
T_1, 15 Hz	SWF2	0	0	0	0	20	80	0	0	0	0
T_2, 15 Hz	PUF2	0	0	20	80	0	0	0	0	0	0
T_2, 25 Hz	BRB	20	80	0	0	0	0	0	0	0	0
T_2, 35 Hz	SWF2	0	0	0	0	60	40	0	0	0	0
T_2, 40 Hz	BR	0	0	0	0	0	0	20	80	0	0
T_3, 30 Hz	SWF2	0	0	0	0	20	80	0	0	0	0

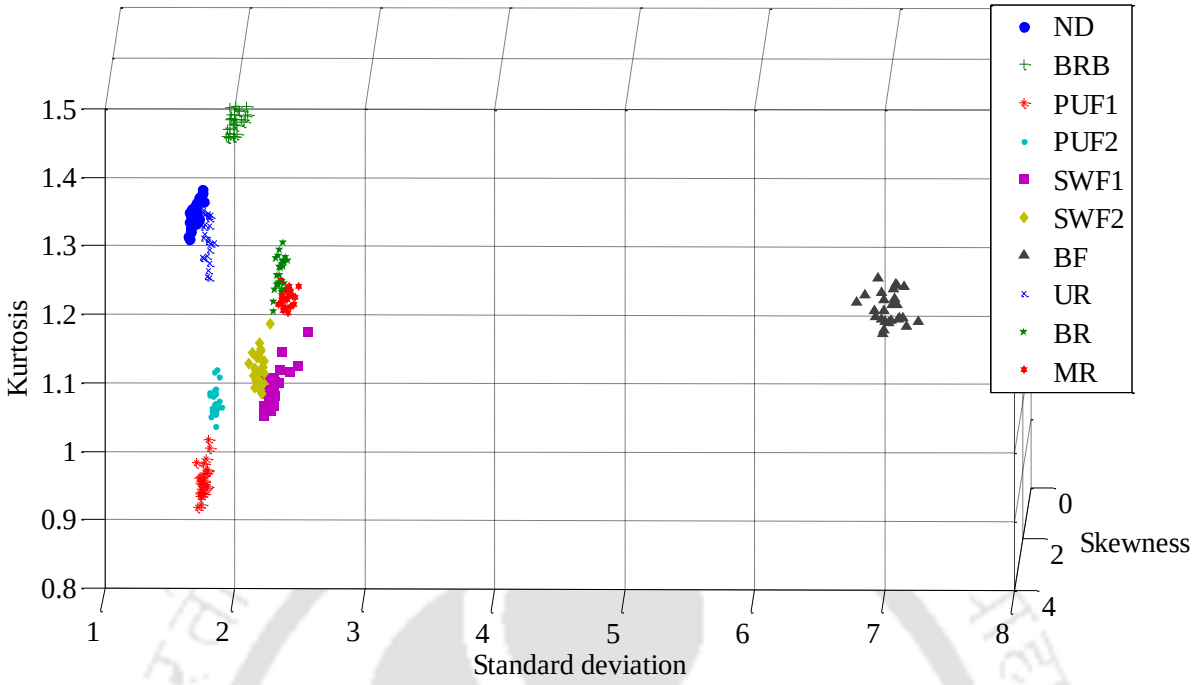

Figure 5.3 Feature distribution of vibration for all IM faults at 40 Hz and T_3

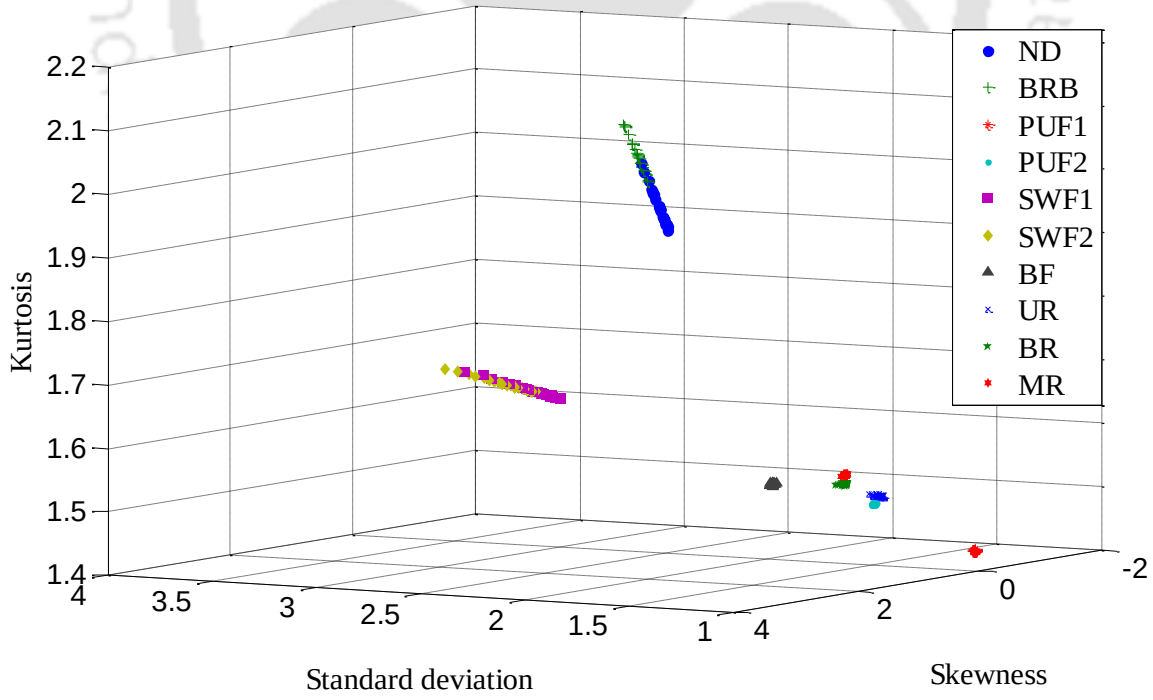

Figure 5.4 Feature distribution of current for all IM faults at 40 Hz and T_3

5.3.4 Fault Diagnosis for the Intermediate Speed case

The fault diagnosis is performed when the training of SVM done at two speeds and testing done at an intermediate speed; however, for all condition the training and the testing is done at the same load. Five conditions of intermediate speed are considered for no, light and high load as shown in Table 5.7. Here, speed range of 10 Hz is considered for training the classifier.

Table 5.7 Various conditions of the intermediate speed case of the fault diagnosis

Training load	Testing load	Training speeds (Hz)	Testing speed (Hz)	Training speed range (Hz)
		10, 20	15	10
T_1	T_1	15, 25	20	10
T_2	T_2 ➡	20, 30	25	10
T_3	T_3	25, 35	30	10
		30, 40	35	10

Fault prediction: The results of fault diagnosis for the case of intermediate speed are shown in Table 5.8. For the no load condition, the lowest overall prediction accuracy is 84 % at 35 Hz and it increases up to 100 % at 25 Hz intermediate speed condition. The lowest average of Individual accuracies over a considered speeds is 66.67 % for SWF2 fault because this fault is not predicted at 10 Hz (13.33 %) and 35 Hz (20 %) testing speeds. However, at other speeds SWF2 is predicted perfectly. Moreover, other fault conditions are successfully predicted at approximately all considered speeds except for some cases such as PUF1 (40 %) at 30 Hz, and MR (26.7 %) at 35 Hz testing speed. For the light load, the lowest overall prediction accuracy is 80 % at 30 Hz and

the highest accuracy is 98 % at 25 Hz testing speed. The lowest average of individual accuracies is 60.7 % for the BR because this fault condition is not predicted at most of the speeds. In addition, for the UR also, the average of individual accuracies is lower, i.e. 76 %, because this fault is also not classified at 30 Hz (40 %) and 35 Hz (23.3 %) testing speed. Besides, other fault conditions are predicted successfully at most of the speeds except SWF 2 (33.33 %) at 15 Hz and BRB (40 %) at 30 Hz. For the high load of the IM, the lowest and highest overall prediction accuracies are 77.47 % at 35 Hz and 98 % at 25 Hz. The lowest avareage of individual accuracies is 68.07 % for the SWF2 similar to no load case. In this case, misclassifications are more as compared to the no load and the light load, such as the SWF2 at 15 Hz (43.66 %) and 35 Hz (16.67 %), BRB at 30 Hz (60 %), SWF1 at 30 Hz (40 %), UR at 30 Hz (21.8 %) and 35 Hz (56.7 %), and MR at 35 Hz (21.3 %). From tabulated results, it is noted that for the intermediate speed case, the fault prediction is better at the lower testing speed for all load conditions.

Avearges prediciton accuracies are 93.20 %, 88.73 % and 88 % for the no, light and high loads, respectively. The reason for good accuracy in this case is that for all three different speeds the selected features (σ, χ and κ) are able to club the distinct faults separable, as shown in Figure 5.5 to Figure 5.8. However, for this case some fault features of vibration and current are overlapped that is why the prediction reduces to 7-12 %. From Table 5.8, it is noted that the overall prediction is better at no load as compared to other loads, however, the prediction was independent of loading for the same speed and load cases. The reason for the reduction of prediction performance under loading conditions is due to the fact that the fluctuation of rotor speed (about 2-3 rpm) cannot be avoided under loading conditions. Therefore, under load the features extracted are pertaining to fault signatures at fluctuating speeds, so chances of the feature overlapping is more. This can be

seen in the cluster of selected features (σ, χ and κ) of the vibration and current signals in Figure 5.5 to Figure 5.8.

The overall fault prediction is not perfect (varying from 77.47 % to 100 %), still there is a reasonable prediction of faults at intermediate speeds. That means the proposed methodology allows detecting each fault condition with different speed data as training. The fault prediction is 6-11% less in comparison to the same speed and the same load case. At the first glance it may seem that performance in this case is inferior than the same speed and same load case. However, it is to be noted that this case is considered with the testing performed at different (or intermediate) speed as training, while former case is presented with the testing performed at the same speed and same load as the training. In this case features from three different speeds are used for the training and the testing, hence the chances of feature overlap are more as shown in Figure 5.5 to Figure 5.8. However, in the same speed case, features obtained at a single speed is used so the chances of feature overlap are less as shown in Figure 5.3 and Figure 5.4. Thus prediction performances in this case seems to reduce as compared to the same speed and same load case. The fault prediction can be further improved if the narrow range of the training speeds or more numbers of speeds are considered in the intermediate speed case.

Table 5.8 Fault diagnosis for various operating conditions of IM for the intermediate speed case

Train speed (Hz)	Test speed (Hz)	Prediction accuracy, %										
		ND	BRB	PUF1	PUF2	SWF1	SWF2	BF	UR	BR	RM	Over.
For no load, T_1												
10,20	15	100	100	100	100	100	20	100	100	100	100	92
15,25	20	100	80	100	100	100	100	100	100	100	100	98
20,30	25	100	100	100	100	100	100	100	100	100	100	100
25,35	30	100	100	40	80	100	100	100	100	100	100	92
30,40	35	100	100	100	100	100	13.3	100	100	100	26.7	84
	Avg.	100	96	88	96	100	66.7	100	100	100	85.3	93.2
For light load, T_2												
10,20	15	100	100	100	80	100	33.3	100	100	100	100	91.3
15,25	20	100	80	100	100	100	100	100	100	40	100	92
20,30	25	100	80	100	100	100	100	100	100	100	100	98
25,35	30	100	40	100	100	100	100	100	20	40	100	80
30,40	35	100	100	100	100	100	100	100	60	23.3	40	82.3
	Avg.	100	80	100	96	100	86.7	100	76	60.7	88	88.7
For high load, T_3												
10,20	15	100	100	100	80	100	43.7	100	100	100	100	92.4
15,25	20	100	80	100	100	100	80	100	100	80	80	92
20,30	25	100	100	100	100	100	100	100	100	100	80	98
25,35	30	100	60	100	100	40	100	100	21.8	80	100	80.2
30,40	35	100	100	100	100	100	16.7	100	56.7	80	21.3	77.5
	Avg.	100	88	100	96	88	68.1	100	75.7	88	76.3	88

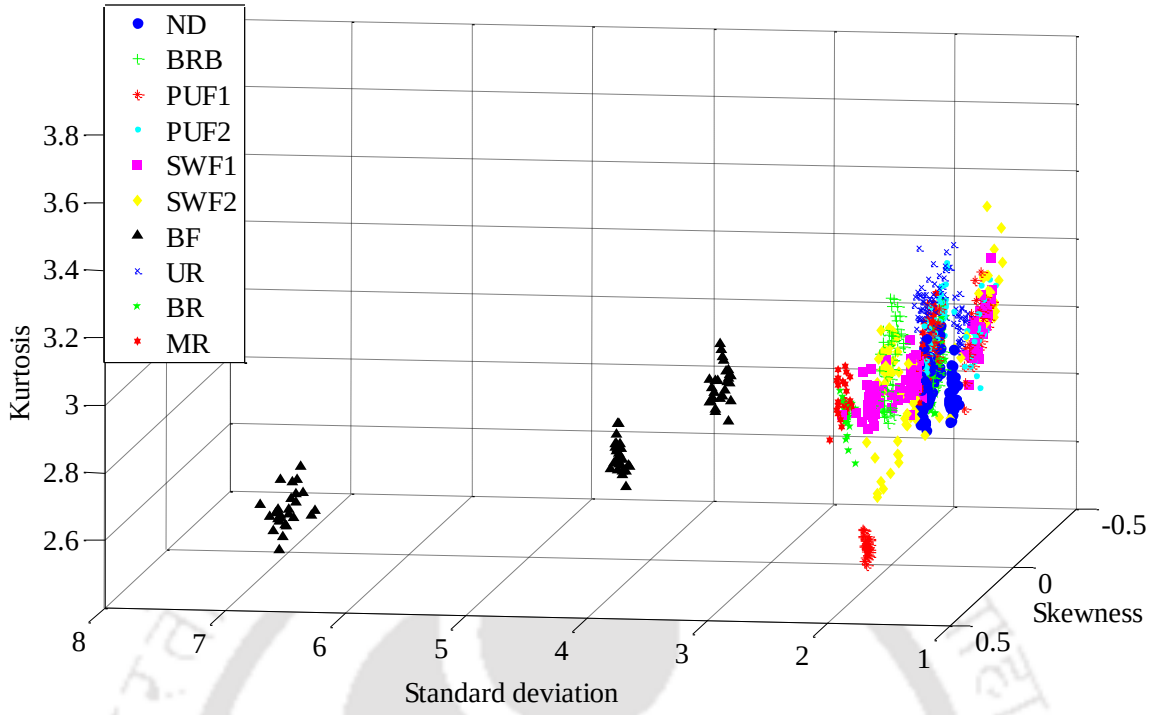

Figure 5.5 Feature distribution of vibration for all IM faults at 30, 35 and 40 Hz, and T_1

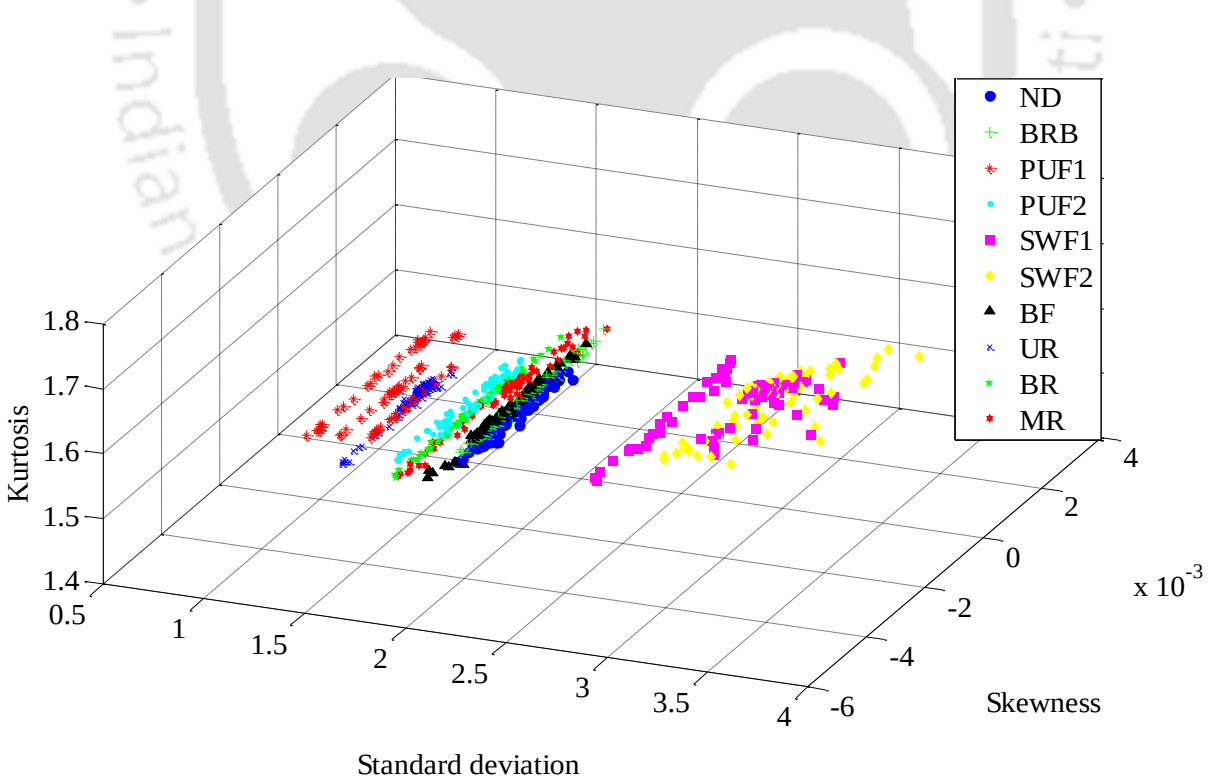

Figure 5.6 Feature distribution of current for all IM faults at 30, 35 and 40 Hz, and T_1

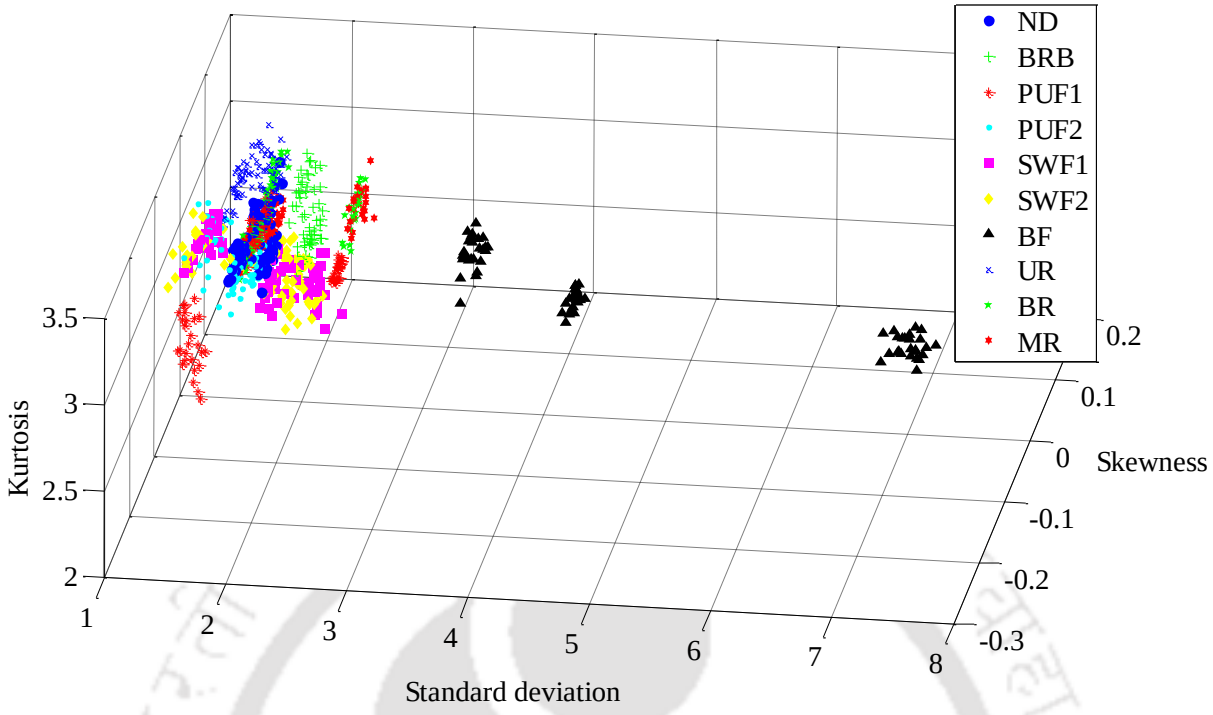

Figure 5.7 Feature distribution of vibration for all IM faults at 30, 35 and 40 Hz, and T_3

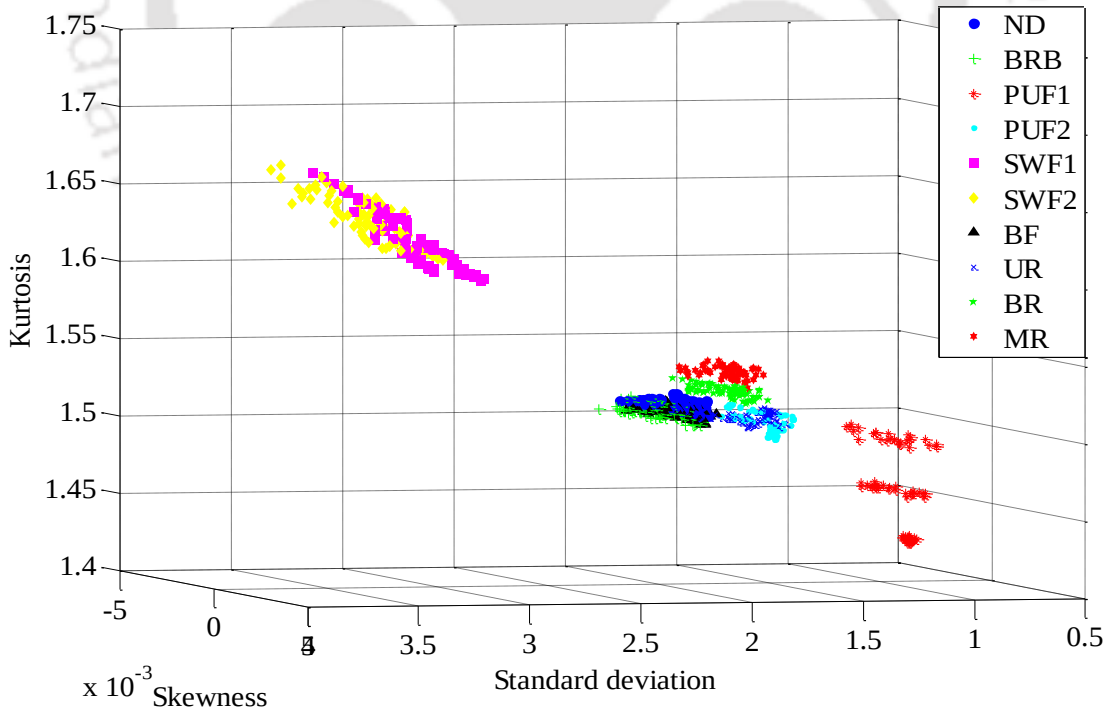

Figure 5.8 Feature distribution of current for all IM faults at 30, 35 and 40 Hz, and T_3

5.3.5 Fault Diagnosis for the Intermediate Load Case

The fault diagnosis is performed when the training of SVM is performed at two load levels and testing is done at an intermediate load; however, for all cases the training and the testing are done at same speeds. In total, one case of interpolation of load with seven speeds is considered for fault diagnosis, as shown in Table 5.9. Here, features obtained from the high resolution data are used.

Table 5.9 Various conditions of the intermediate load case of the fault diagnosis

Training torque	Testing torque	Training speed (Hz)	Testing speed (Hz)
T_1, T_3	T_2 →	10	10
		15	15
		20	20
		25	25
		30	30
		35	35
		40	40

Fault prediction: Table 5.10 shows the fault prediction for the interpolation of load at T_2. It is observed that the average of overall prediction accuracy is 96.59 %, which is quite good. The lowest average of individual prediction accuracy is 82.8 % and 85.9 % for BR and SWF2, respectively. The BR and SWF2 are not predicted at 10 Hz (40 %) and 30 Hz (21.33 %), respectively. Besides these cases, all other motor faults are predicted successfully at all considered speeds. In addition, severity levels of the phase unbalance and the stator winding fault is also perfectly classified at the most of speeds. In total, prediction results show that the SVM could

classify all IM faults and their severities successfully for a wide range of speeds in the interpolation load case also. The reason for this is that though the fault manifestation changed in vibration and current signals with the variation of load (T_1, T_2 and T_3), the selected features (σ, χ and κ) are able to club the distinct faults separable. This can be seen in feature clusters of vibration and current in Figure 5.9 and Figure 5.10, respectively. From cluster plots, it is noted that a particular IM fault generates approximately similar features (σ, χ and κ) at different load torque. Thus justifying the successful fault prediction even in the intermediate load case. In this case also, the fault diagnosis does not depend over the speed of IMs. In addition, the overall prediction accuracy is higher by 3-8 % as compared to the intermediate speed case; however, it is nearly 3-4 % less as compared to the same speed and load case.

Table 5.10 Fault diagnosis for various operating conditions of IM for the intermediate load case

Train speed (Hz)	Test speed (Hz)	Prediction accuracy, %										
		ND	BRB	PUF1	PUF2	SWF1	SWF2	BF	UR	BR	RM	Overall
Training at T_1 and T_3, Testing T_2												
10	10	100	100	100	100	100	100	100	80	40	100	92
15	15	100	100	100	100	100	100	100	100	100	100	100
20	20	100	100	100	100	100	100	100	100	80	100	98
25	25	100	100	100	100	100	100	100	100	80	100	98
30	30	100	100	100	100	100	21.33	100	100	80	100	90.13
35	35	100	100	100	100	100	100	100	100	100	100	100
40	40	100	100	100	100	100	80	100	100	100	100	98
	Avg.	100	100	100	100	100	85.9	100	97.1	82.8	100	96.59

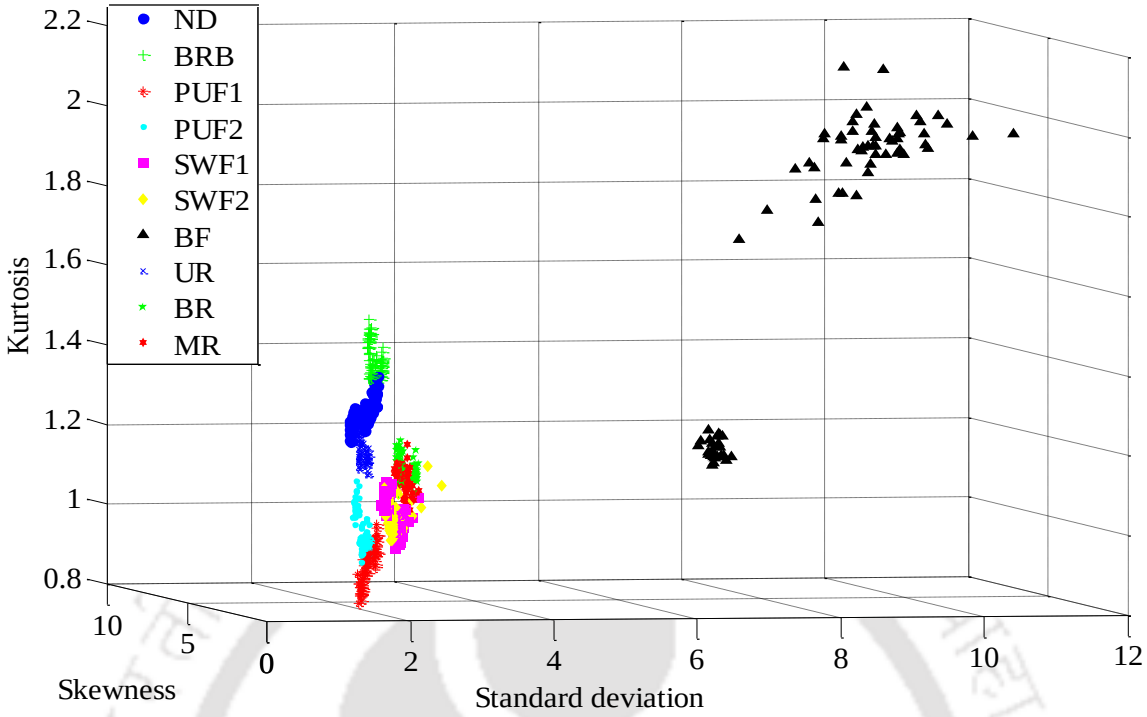

Figure 5.9 Feature distribution of vibration for all IM faults at 40 Hz, and T_1, T_2 and T_3

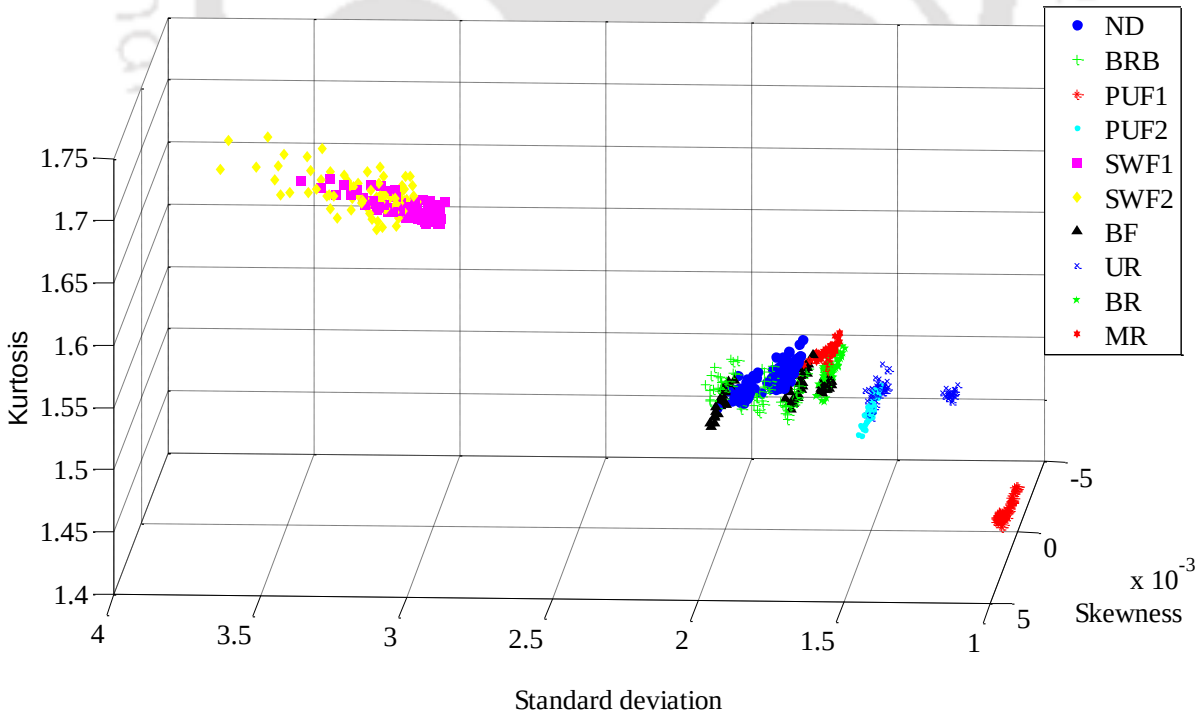

Figure 5.10 Feature distribution of current for all IM faults at 40 Hz, and T_1, T_2 and T_3

5.4 Summary

To perform the fault diagnosis of induction motors, initially fourteen features are extracted from low sampling rate data in time domain. The cross-validation along with the grid-search methodology is performed to select optimal SVM parameters, which is required to build an optimal SVM model. The wrapper model is used to select the most suitable features for the present fault diagnosis. It is found that most of the considered features performed fault diagnosis successfully; however, when the set of three features $\sigma, \chi,$ and κ are used for the IM fault diagnoses, the highest prediction accuracy is achieved. Therefore, this set of features is selected for the final fault diagnosis. After the selection of the most effective features, initially the fault diagnosis is performed for the same speed and same load case for various operating conditions of IMs using the one-versus-one MSVM. The result shows that the proposed methodology is able to predict all considered mechanical as well as electrical faults at all operating conditions of IMs, even when all ten fault conditions are considered, simultaneously. In addition, two severity levels of the phase unbalance a well as stator winding faults are also classified successfully at the most of operating conditions.

In this chapter, the fault diagnosis is also performed when testing is done at the intermediate speed, but at the same load, and the prediction is found to be still reasonable. At last the diagnosis is performed for the intermediate load, but at the same speed, results show that the fault prediction is encouraging. The prediction performances for intermediate speed and load cases show the efficiency of the proposed fault diagnostics even with the limited information about operating conditions. In the following chapter, the multi-fault diagnosis is performed using the features based on the frequency domain data. The frequency domain analysis is another description of a signal,

which can reveal spectral information that cannot be found in the time domain (Han et al., 2006). Therefore, frequency domain features is used for the fault diagnosis in the next chapter.

CHAPTER 6

Multi-Fault Diagnosis of IM based on Frequency Domain Data

6.1 Introduction

In this chapter, the multi-fault diagnosis of the IM is performed by using the multiclass SVM based on frequency domain features of the vibration and current signals. The statistical features in the time and frequency domain have different representation capabilities for fault patterns. The reason is that the frequency domain analysis shows how the energy of signal is distributed over a range of frequencies, while the time domain analysis shows how a signal changes over time. Moreover, fault features are sometimes very sensitive in the frequency domain as compared to time domain (Li et al., 2016). Therefore, the fault prediction ability of the SVM classifier using frequency domain feature is now discussed in this chapter.

Similar to Chapter 5, a number of statistical features are extracted from the frequency domain data. Frequency domain features are calculated on the basis of FFT from time domain vibration and current signals, these features involve statistical results of frequency. Similar to the previous chapter, first the selection of SVM parameters as well as fault features are done. After that, the fault diagnosis is performed when testing of the SVM is done at the same speed and the same load as that of training. To check the robustness of the present fault diagnosis methodology, the diagnosis is performed for a wide range of IM operating conditions. In addition to this, in this chapter also, the work is extended to perform the testing or prediction at different speeds and loads as the training of the classifier, i.e. for intermediate speed and load cases.

6.2 Fault Feature Extraction

Statistical features such as standard deviation, skewness, kurtosis, RMS, frequency center, etc., from frequency domain are often used in the fault diagnosis of the mechanical system (Lei et al., 2008, Widodo and Yang, 2008, Tran et al., 2009, Bordoloi and Tiwari (2013)). The spectral kurtosis is one of the most popular and effective fault features in the frequency domain (Randall and Antoni, 2011). Signal analysis in the frequency domain such as statistical spectral moments is taken to employ simple feature extraction method based on data reduction procedure in order to obtain scalar features (Worden et al., 2011). The statistical features in frequency domain show the vibration energy in the frequency domain, the convergence of the spectrum power, variation in the position of main frequencies, etc.

Therefore, all the fourteen features (i.e., eight statistical moments, peak-to-peak, crest factor, mean-to-standard deviation, standard deviation, skewness and kurtosis) that were extracted from the time domain signals in the previous chapter, are now extracted from frequency domain signals (as described in Table 6.1). For this, all of the vibration and current signals is processed together to calculate the features from their FFT spectrum, (i.e., S_i). The features extracted from the FFT spectrum are described in Table 6.1. The features are calculated from 5000 sample points available in one data set of the frequency domain. Since 25 data sets are available, so 14×25 feature data sets are collected for each IM fault condition and operating condition. In Appendix. A, Figure A.3 and Figure A.4 illustrate frequency domain features of vibration signals (in three orthogonal directions) and current signals (in three phases) for the BF at 40 Hz speed and T_3 load. Now, these features would be used in the fault diagnosis in the next section.

Table 6.1 The statistical feature parameters in frequency domain

S.N.	Features	Mathematical formula	Description
1.	First moment (Mean)	$\mu_1 = \bar{x} = \frac{1}{N}\sum_{i=1}^{N} S_i$	where, S_i is a spectrum for i=1,2,…,N, number of spectrum lines;
2.	Second moment about mean (Variance)	$\mu_2 = \sigma^2 = \frac{1}{N}\sum_{i=1}^{N}(S_i - \mu_1)^2$	where, σ is standard deviation
3.	Third to eight higher statistical moments about mean	$\mu_k = \frac{1}{N}\sum_{i=1}^{N}(S_i - \mu_1)^k$	where, k = 3, 4, 5, …, 8 is for 3rd to 8th moments
	Standard deviation	$\sigma = \sqrt{\mu_2} = \sqrt{\frac{1}{N}\sum_{i=1}^{N}(S_i - \mu_1)^2}$	where, μ_2 is second moment
4.	Skewness	$\chi = \frac{\mu_3}{\sigma^3} = \frac{\frac{1}{N}\sum_{i=1}^{N}(S_i - \mu_1)^3}{\sigma^3}$	where, μ_3 is third moment
5.	Spectral Kurtosis	$\kappa = \frac{\mu_4}{\sigma^4} = \frac{\frac{1}{N}\sum_{i=1}^{N}(S_i - \mu_1)^4}{\sigma^4}$	where, μ_4 is fourth moment
6.	Peak to peak	$R_{pp} = \frac{S_{p\max}}{S_{p\min}}$	where, $S_{p\max}$ is maximum peak and $S_{p\min}$ is minimum peak value
7.	Peak to RMS (Crest factor)	$CF = \frac{S_{p\max}}{S_{rms}}$	where, $S_{p\max}$ is peak value and S_{rms} is the RMS value
8.	Mean to standard deviation	$R_{msd} = \frac{\mu_1}{\sigma}$	where, μ_1 is the first moment

6.3 Fault Diagnosis based on the SVM

After the useful feature extraction from the raw frequency domain data for all considered IM faults and operating conditions, now the diagnosis is performed based on one-versus-one multiclass method of the SVM. The procedure to perform the fault diagnosis has been discussed in Chapter 5 in detail. In order to select the optimized SVM parameters, the SVM training based on the cross-validation along with the grid search technique is performed, and to select the most efficient fault feature(s), the wrapper model of the feature selection with the SVM is used, results are added in subsequent subsections.

6.3.1 SVM Parameter Selection and Training

Training of the SVM is performed to build an optimized SVM model. SVM parameters are optimally chosen by applying the cross-validation with grid-search techniques. The procedure is explained in detail in Chapter 5. The CV or training accuracy in the grid-search technique for a typical case of 40 Hz and T_3 load, when the training is performed with all the features individually and in sets are shown in Figure 6.1 and Figure 6.2. Figure 6.1(a) is added for the case when cross-validation is performed with μ_1 only at 40 Hz and T_3 load. It shows that the maximum CV accuracy is achieved up to 98.5 %. The maximum CV accuracy for μ_2 and μ_3 are also very promising; however, from the fourth moment, the accuracy goes down to 81.14 % for μ_8. That means the classifier is well trained only for the first three spectral moments out of eight moments. Now when the cross-validation is performed using in peak-to-peak, R_{pp}, the accuracy reduces to 47.28 %. The worst CV accuracy is found for the *CF*, which is 32 %. That means these two features are not able to represent the IM faults. When R_{msd}, σ, χ, and κ are used for the training, then classifier is successfully trained with all these features as shown in Figure 6.2 (c, d e and f).

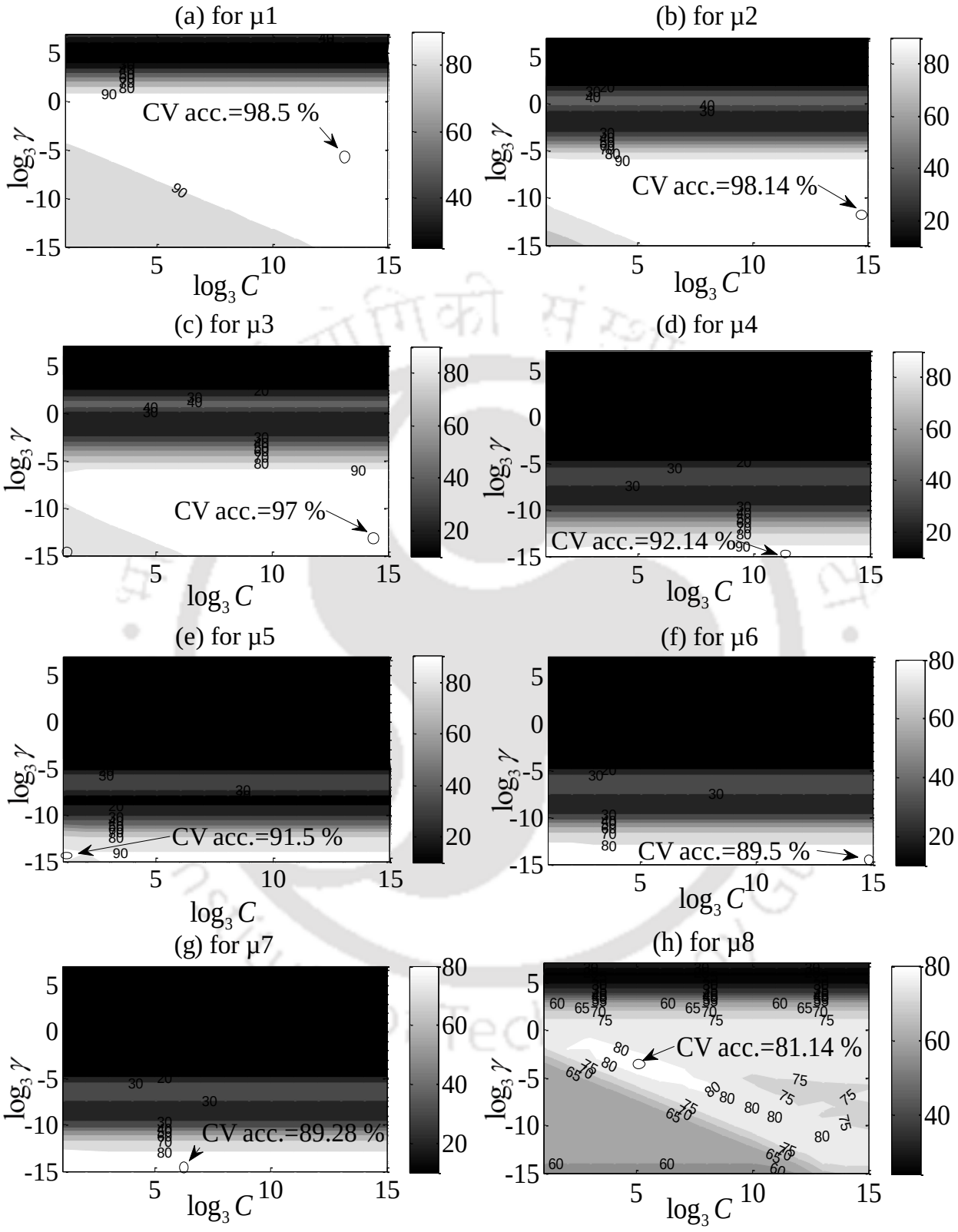

Figure 6.1 Cross validation accuracy at 40 Hz and T_3

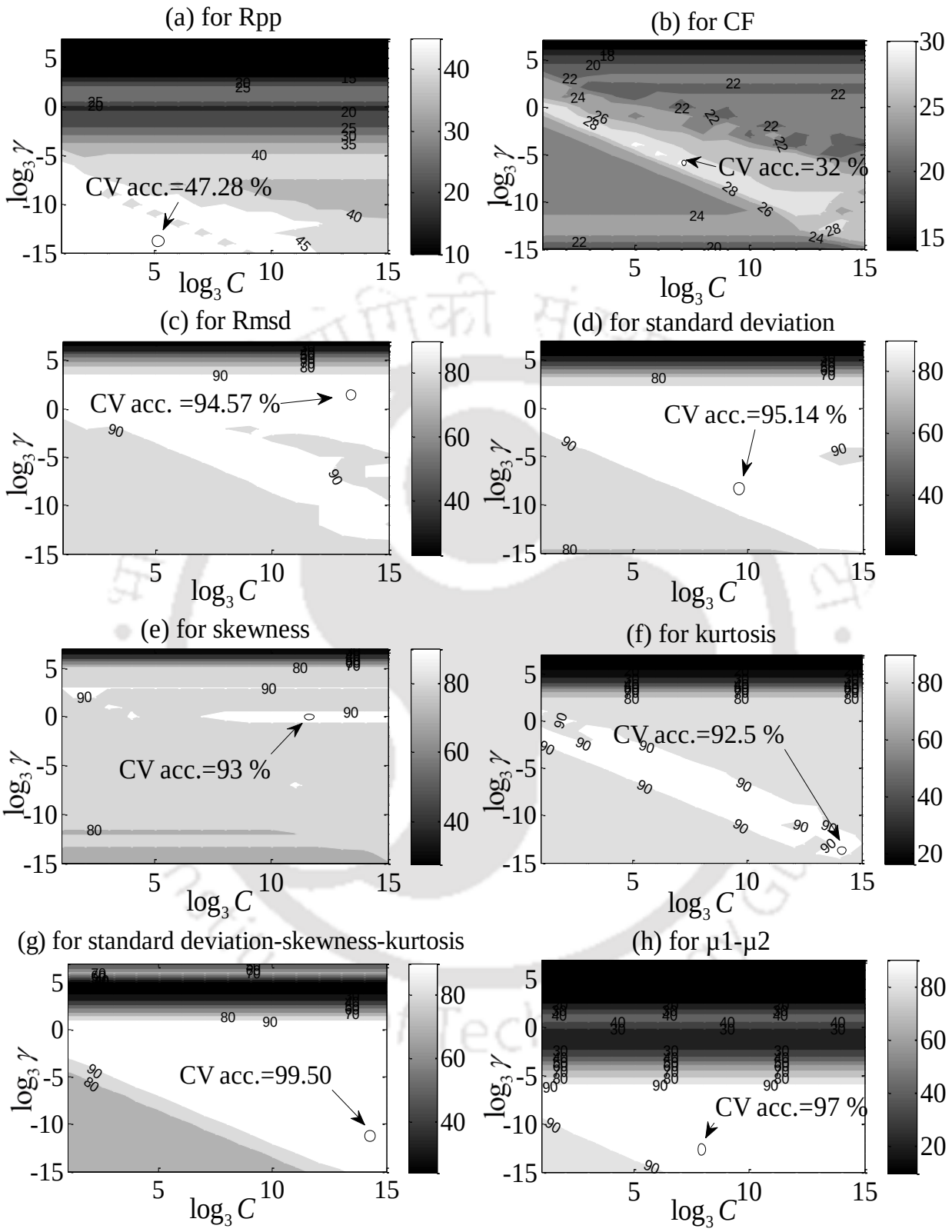

Figure 6.2 Cross validation accuracy at 40 Hz and T_3

Now the classifier is trained with sets of good features, i.e. (σ, χ, κ) and (μ_1, μ_2) then accuracies are found to be 99.50 % and 97%, respectively. From Figure 6.1 and Figure 6.2, it is noted that the highest CV accuracy (i.e., 99.50%) is achieved when the combination of σ, χ, and κ is used for the training. Now, optimal SVM parameters are selected for each feature corresponding to the maximum CV accuracy. Then these parameters are used as input to the classifier for final training of the classifier so that an optimal classifier model can be built. Now, this model is used for the final fault prediction using unseen data or testing data.

6.3.2 Fault Feature Selection

The feature selection is performed based on the wrapper model along with the SVM classifier, similar to Chapter 5. According to the wrapper model, the feature or set of features with the highest overall prediction accuracy is selected as optimal one. Initially, all fourteen features are used with the SVM classifier as input vectors one by one. The training and the testing of the SVM are done at each considered speed for the high load, and results of the fault diagnosis corresponding to different features are tabulated in Table 6.2. The table shows the overall accuracy of the fault diagnosis. It shows that initial five moments (i.e., μ_1 to μ_5), R_{ms}, σ, χ, and κ, perform the fault diagnosis successfully, i.e. with more than 90% prediction accuracy, and among these three statistical moments individually provides the accuracy of more than 95 %. However, other features, like last three higher moments (i.e., μ_5 to μ_8), R_{pp}, and *CF* do not perform well for the present fault diagnosis, among these, the eighth moment, R_{pp} and *CF* could not perform the fault diagnosis. Hence, it can be concluded that these features in frequency domain do not represent the IM fault effectively. Now the combinations of some good features are tried and results are compared with each other and individual features as shown in Table 6.2. The results show that the

best prediction accuracy of 98% is achieved with the feature combination of $\sigma, \chi,$ and κ. It is noted that although the SVM performance of fault diagnosis corresponding to $\sigma, \chi,$ and κ individually is lower than corresponding to three initial moments individually, the set of $\sigma, \chi,$ and κ provides higher accuracy than the set of three moments (i.e., μ_1, μ_2 and μ_3). Moreover, this feature set also provides the highest accuracy than any other feature individually and in a set. So according to the wrapper model of the feature selection, the set of $\sigma, \chi,$ and κ is found to be an optimal feature set from frequency domain data for the present fault diagnosis.

Table 6.2 Statistical features selection by wrapper model and SVM at high load

Statistical features	Average prediction accuracy, %	Statistical features	Average prediction accuracy, %
μ_1	97.43	R_{msd}	91.71
μ_2	97.43	σ	92.57
μ_3	95.71	χ	91.14
μ_4	92.29	κ	90.86
μ_5	92.86	μ_1- μ_2	97.71
μ_6	88	μ_1 to μ_3	96.57
μ_7	85.71	μ_1 to μ_4	95.33
μ_8	71.71	μ_1 to μ_6	90
R_{pp}	41.57	μ_1 to μ_8	70
CF	32.57	$\sigma, \chi,$ and κ	98

6.3.3 Fault Diagnosis for the Same Speed and Load Case

After selecting optimal SVM parameters, i.e. (C, γ) and feature set, i.e. ($\sigma, \chi,$ and κ), the fault diagnosis is performed when testing of the SVM are done at same load as well as speed as the training. The fault diagnosis is performed for various operating conditions (i.e., three loads and seven speeds) of IMs as shown in Table 5.4.

Fault predictions: The fault diagnosis results are shown in Table 6.3. It shows the overall as well as the individual prediction accuracies. When the fault diagnosis is performed at no load condition, it is observed that, the overall prediction accuracy is 100% at higher speeds, i.e. above 25 Hz; 94% at 25 Hz; 96 % at 10 Hz and 15 Hz. That means the SVM could classify the faults perfectly at higher speeds; however, at lower speeds, i.e. below 25 Hz, the SVM performance reduces by nearly 5%. In addition, the individual prediction accuracy is 100% at all considered speeds for the BRB, PUF1, PUF2, BF and MR. Also for the ND, SWF1, SWF2, UR and BR, the accuracies are 100% at all considered speeds except for the ND at 15 Hz, SWF1 at 20 Hz, SWF2 at 10 Hz, UR and BR at 20 Hz. When the fault diagnosis is performed at the light load, the overall prediction accuracy is 100% at speeds above 30 Hz, and 98% at 20 Hz, 96% at 15 and 20 Hz, and 94% at 10 Hz. The individual prediction accuracy is 100% for the ND, BRB, PUF2, BF and MR. Also, individual accuracies for other faults are 100% at all speeds except for PUF1 at 25 Hz, and UR and BR at 10 Hz. It is noted that, unlike the fault diagnosis at no load, the misclassification for SWF1 and SWF2 are more, i.e. 6 % and 9 %, respectively. When the fault diagnosis at the high load is done, the overall prediction accuracy is 100% at higher speeds, i.e. above 25 Hz (same as no load case), 98% at 20 Hz and 10 Hz, and 90% at 15 Hz. In addition, the individual prediction accuracy is 100% at all the speeds for the HM, BRB, PUF1, PUF2, BF and MR. Also for other faults like the SWF1,

SWF2, UR and BR accuracies is 100% at all speeds except for some operating conditions such as the SWF1 at 20 Hz, SWF2 at 15 Hz, UR at 20 Hz, and BR at 10 and 15 Hz.

From Table 6.3, it is noted that averages of overall prediction accuracy over the entire range of speeds are 98%, 97.71% and 98% corresponding to the no load, light load and full load, respectively. That means for this case, the SVM performs excellent and nearly same at all IM load conditions. In other words, the present fault diagnosis of IMs using the SVM is nearly independent of IM load and can be performed at any load conditions for which the data are available in the industry. In addition, the results show that the performance of SVM is good at all the considered motor speeds but slightly reduces from 2 to 10 % at lower speeds for all the considered load conditions. It is noted that SWF1, SWF2, UR and BR could not successfully classify at lower speeds. In order to show the data misclassification, a confusion matrix is added in Table 6.4. It shows that in the most of cases, feature points of SWF1 are misclassified with SWF2, and UR with the BR. The reason behind it is that the SWF1 and SWF2 generate approximately similar current signatures, the UR and the BR generate approximately similar vibration signals, especially at lower speeds. So the features calculated from the signals of these faults, overlap and consequently reduces the prediction accuracy. From the Table 6.3, it is noted that the SVM could perfectly classify the BF, PUF, and SWF (except at some speeds). These faults contribute 85-90% of all IM failures. Furthermore, it can be observed that two different levels of the PUF, as well as SWF could also be successfully classified nearly for all considered operating conditions. That means, it is also possible to diagnose different levels of IM faults with good prediction accuracy using the SVM.

In overall, the SVM can be used for the IM fault diagnosis at any speeds and loads. The present fault diagnosis does not depend on the IM load but it depends on speeds (with higher accuracy at high speeds), however, the diagnosis in time domain were independent of speeds as well as loads. The reason may be due to low signal to noise ratio in frequency domain to at low speeds. In overall, ten different faults (mechanical and electrical) conditions can be classified simultaneously, using feature combination of σ, χ and κ of frequency domain vibration and current signals, based on SVM. This may be attributed to the capability of the selected frequency domain based features (σ, χ and κ) to characterize various IM faults effectively in the feature space as shown in Figure 6.3 and Figure 6.4. The average CPU time for training and testing are 2 sec and 0.6 sec (approximately), respectively.

6.3.4 Fault Diagnosis for the Intermediate Speed Case

In order to perform fault diagnosis for the intermediate case, following two different situations of training of the classifier is considered for the study.

6.3.4.1 Training with the data of two different speeds

The fault diagnosis is performed, when the training of SVM is done at two-speed levels and further testing is done at an intermediate speed. However, for all cases, the training and the testing are done at same loading. For the no, light and high loads, five cases of intermediate speeds with 10 Hz speed range are considered for the intermediate speed (Case-1) for the fault diagnosis as shown in Figure 5.7.

Table 6.3 Fault diagnosis for various operating conditions of IM for the same speed and load case

Train speed (Hz)	Test speed (Hz)	Prediction accuracy, %										
		ND	BRB	PUF1	PUF2	SWF1	SWF2	BF	UR	BR	MR	Over all
For no load, T_1												
10	10	100	100	100	100	100	60	100	100	100	100	96
15	15	60	100	100	100	100	100	100	100	100	100	96
20	20	100	100	100	100	80	100	100	80	80	100	94
25	25	100	100	100	100	100	100	100	100	100	100	100
30	30	100	100	100	100	100	100	100	100	100	100	100
35	35	100	100	100	100	100	100	100	100	100	100	100
40	40	100	100	100	100	100	100	100	100	100	100	100
	Avg	94.3	100	100	100	97.1	94.3	100	97.1	97.14	100	98
For light load, T_2												
10	10	100	100	100	100	100	80	100	80	80	100	94
15	15	100	100	100	100	80	80	100	100	100	100	96
20	20	100	100	100	100	100	80	100	100	100	100	98
25	25	100	100	80	100	80	100	100	100	100	100	96
30	30	100	100	100	100	100	100	100	100	100	100	100
35	35	100	100	100	100	100	100	100	100	100	100	100
40	40	100	100	100	100	100	100	100	100	100	100	100
	Avg	100	100	97.1	100	94.3	91.4	100	97.1	97.1	100	97.7
For high load, T_3												
10	10	100	100	100	100	100	100	100	100	80	100	98
15	15	100	100	100	100	100	40	100	80	80	100	90
20	20	100	100	100	100	80	100	100	100	100	100	98
25	25	100	100	100	100	100	100	100	100	100	100	100
30	30	100	100	100	100	100	100	100	100	100	100	100
35	35	100	100	100	100	100	100	100	100	100	100	100
40	40	100	100	100	100	100	100	100	100	100	100	100
	Avg	100	100	100	100	97.1	91.4	100	97.1	94.3	100	98

Table 6.4 Confusion matrix of fault diagnosis for the same speed and load case

Operating conditions	Miscla-sified fault	Misclassified data, %									
		ND	BRB	PUF1	PUF2	SWF1	SWF2	BF	UR	BR	MR
T_1, 10 Hz	SWF2	0	0	0	0	20	60	0	0	20	0
T_1, 15 Hz	ND	60	40	0	0	0	0	0	0	0	0
T_1, 20 Hz	SWF1	0	0	0	0	80	0	0	0	20	0
T_1, 20 Hz	UR	0	0	0	20	0	0	0	80	0	0
T_1, 20 Hz	BR	0	0	0	0	0	0	0	20	80	0
T_2, 10 Hz	SWF2	0	0	0	0	20	80	0	0	0	0
T_2, 10 Hz	UR	0	0	0	0	0	0	0	80	20	0
T_2, 10 Hz	BR	0	0	0	0	0	0	0	20	80	0
T_2, 15 Hz	SWF1	0	0	0	0	80	20	0	0	0	0
T_2, 15 Hz	SWF2	0	0	0	0	20	80	0	0	0	0
T_2, 20 Hz	SWF2	0	0	0	0	20	80	0	0	0	0
T_2, 25 Hz	PUF1	0	0	80	20	0	0	0	0	0	0
T_2, 25 Hz	SWF1	0	10	0	0	80	10	0	0	0	0
T_3, 10 Hz	BR	0	0	0	0	0	0	0	0	80	20
T_3, 15 Hz	SWF2	0	0	0	0	60	40	0	0	0	0
T_3, 15 Hz	UR	0	0	0	0	0	0	0	80	0	20
T_3, 15 Hz	BR	0	0	0	0	0	10	0	10	80	0
T_3, 20 Hz	SWF1	0	0	0	0	80	20	0	0	0	0

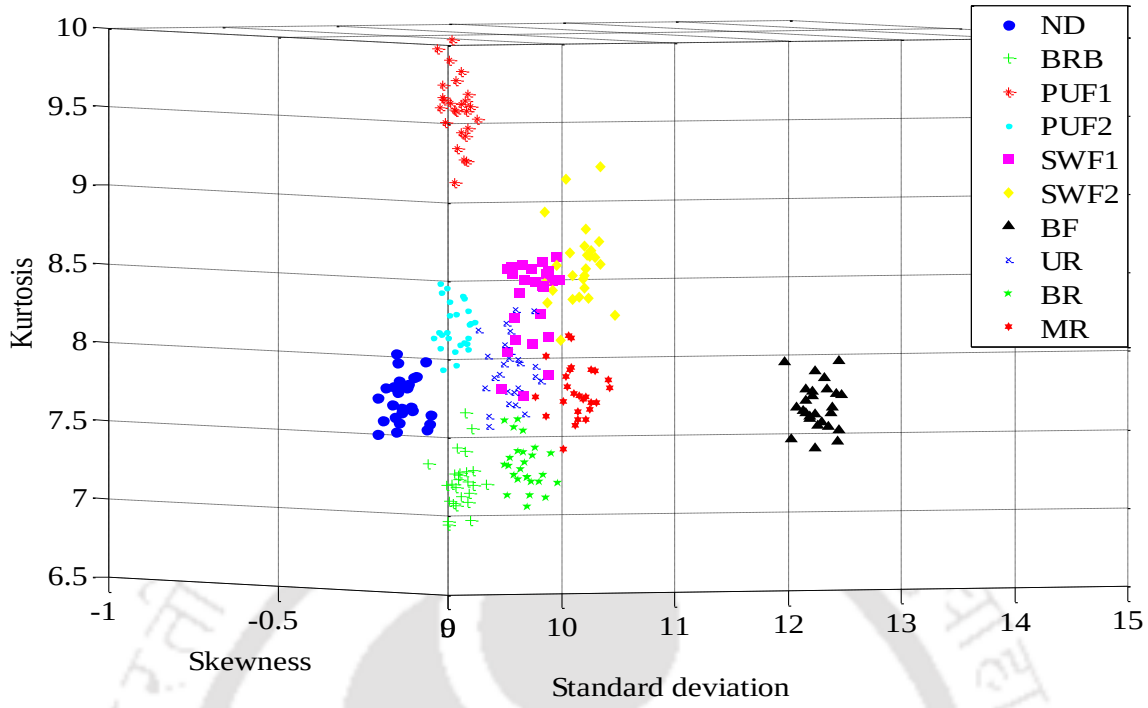

Figure 6.3 Feature distribution of vibration for all IM faults at 40 Hz and T_3

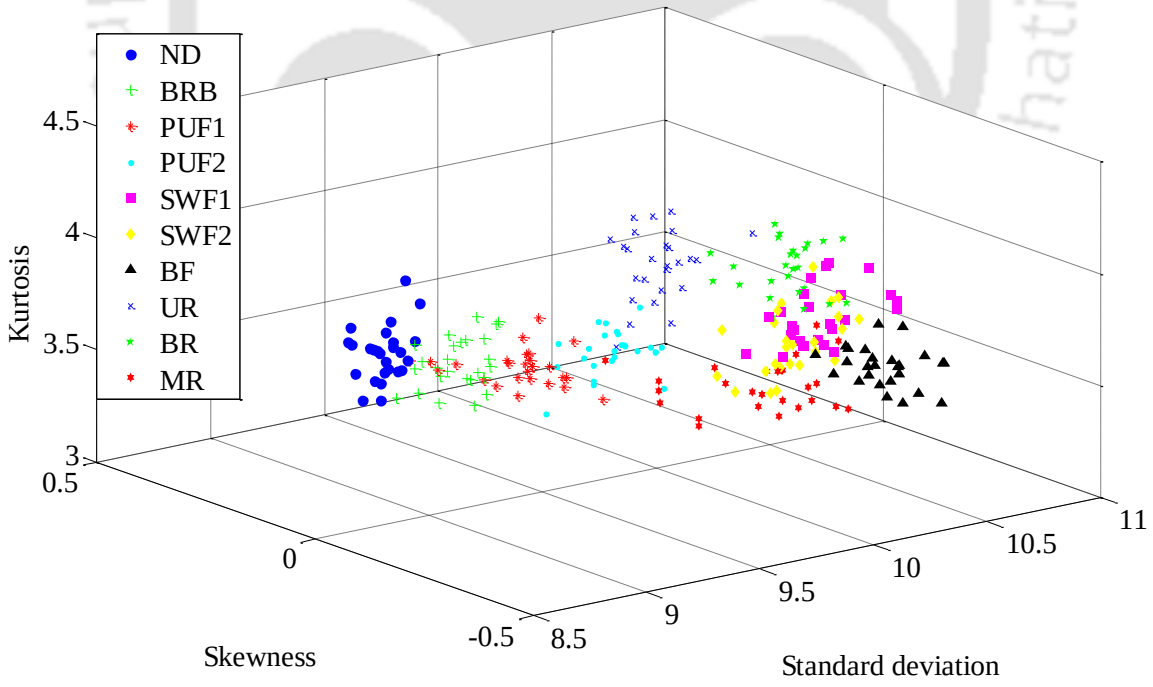

Figure 6.4 Feature distribution of current for all IM faults at 40 Hz and T_3

Fault prediction: The result of fault diagnosis for the present intermediate speed case is shown in Table 6.5. When the fault diagnosis at no load is performed, the lowest overall prediction accuracy is 82 % at 25 Hz and it increases up to 92 % at the 15 Hz and 35 Hz intermediate speeds. In addition, the lowest average individual prediction over considered speed is 76 % for ND and SWF1. Because, the ND and SWF1 are not predicated at 30 Hz (0 %) and 25 Hz (20 %), respectively. However, at other speeds, these two faults are predicted successfully and sometimes perfectly. Moreover, other faults are predicted successfully at approximately all the speeds excepts for some cases like the BRB at 20 Hz (0 %), PUF2 at 25 Hz (25 %), UR at 25 Hz (60 %) and 35 Hz (40 %), and MR at 15 Hz (40 %). When the fault diagnosis is considered for the light load on IM, the lowest and highest overall predictions are achieved 82 % at 15 Hz, and 92 % at 30 and 35 Hz, respectively. The lowest average of individual accuracies over speeds is 48 % for the SWF2 because this fault is not predicted at the most of the considered speeds except 15 Hz (100 %). In addition, other IM faults are predicted at the most of the speeds successfully, except for few cases such as the ND at 35 Hz (40 %), PUF1 at 25 Hz (40 %), PUF2 at 25 Hz (60 %), UR at 15 Hz (40 %) and MR at 15 Hz (0 %). For the high load condition, the overall prediction accuracy is varied from 80 % (at 25 Hz) to 96 % (at 30 Hz). The lowest average of individual accuracy is 60% for SWF1 faults, because this fault condition is not predicted successfully specially at lower speeds, i.e. below 25 Hz. Similar to the no and light load conditions, other faults conditions are predicted successfully at most of the speeds except for few conditions such as the BRB at 20 Hz (0 %), SWF2 at 25 Hz (40 %), UR at 25 Hz (20 %) and MR at 15 Hz (60 %).

From Table 6.5, it is found that the average of overall accuracies for the no, light and high loads are 88.8 %, 88 % and 87.6 %, respectively. That means the fault diagnosis of IMs for this case

does not depend on the IM loads unlike in time domain, where the diagnosis was better at the no load. In comparison to the same case in the time domain, the overall accuracy is nearly same for the light and high loads; however, it is decreased by 5 % (approximately) at the no load condition. In addition, from tabulated results (Table 6.7), it is found that the prediction is not dependent on the running speed of the IM. However, for the same case in the time domain, the prediction was better at lower speeds for all load conditions. Though the overall prediction performance for this case varied from 80% to 96% and decreased about 10 % at all load conditions as compared to the same speed and same load case, still the fault prediction is reasonable. The reduced prediction accuracy, in this case, is attributed to the overlapping of selected features (σ, χ and κ) of some fault conditions in the feature space, as shown in Figure 6.5 and Figure 6.6. The overlapping of features occurs because three different speeds are used for the training and the testing. So selected features are not capable of completely distinguishing different faulty conditions of IM, at three different speeds. The prediction may be further increased if the narrow range of speeds is considered for this case. The average training and testing time are 6 s and 1.2 s, respectively. In this case, at some operating conditions the individual prediction accuracy is found to be zero for some fault conditions. Therefore, a second case on the intermediate speed is considered, where the training is done with more than two speeds or multiple speeds, unlike this case.

6.3.4.2 Training with the data of multiple speeds

Now, the fault diagnosis is performed, when the training of SVM is performed at multiple speed levels and further testing is done at an intermediate speed. However, for all cases, the training and the testing are done at the same loading. For the no, light and high loads, five conditions of intermediate speeds are considered for the intermediate speed (Case-2) for the fault diagnosis as shown in Table 6.6.

Table 6.5 Fault diagnosis for various operating conditions of IM for intermediate speed (Case 1)

Train Speed (Hz)	Test speed (Hz)	Prediction accuracy, %										
		ND	BRB	PUF1	PUF2	SWF1	SWF2	BF	UR	BR	MR	Overall
For no load, T_1												
10,20	15	100	100	100	80	100	100	100	100	100	40	92
15,25	20	100	0	100	100	80	100	100	100	100	100	88
20,30	25	100	100	100	60	20	100	100	60	100	80	82
25,35	30	0	100	100	100	100	100	100	100	100	100	90
30,40	35	80	100	100	100	80	100	100	40	100	100	92
	Avg.	76	80	100	88	76	100	100	80	100	84	88.8
For light load, T_2												
10,20	15	80	100	100	100	80	100	100	40	100	0	82
15,25	20	100	100	100	100	80	20	100	100	100	100	90
20,30	25	100	100	40	60	100	40	100	100	100	100	84
25,35	30	100	100	100	100	100	20	100	100	100	100	92
30,40	35	40	100	100	100	100	60	100	100	100	100	92
	Avg.	84	100	88	92	92	48	100	88	100	80	88
For high load, T_3												
10,20	15	100	100	100	100	60	80	100	80	80	60	86
15,25	20	100	0	100	100	20	80	100	100	100	100	80
20,30	25	100	100	100	100	60	40	100	20	100	100	82
25,35	30	100	100	100	100	80	80	100	100	100	100	96
30,40	35	100	100	100	100	80	80	100	100	80	100	94
	Avg.	100	80	100	100	60	72	100	80	92	92	87.6

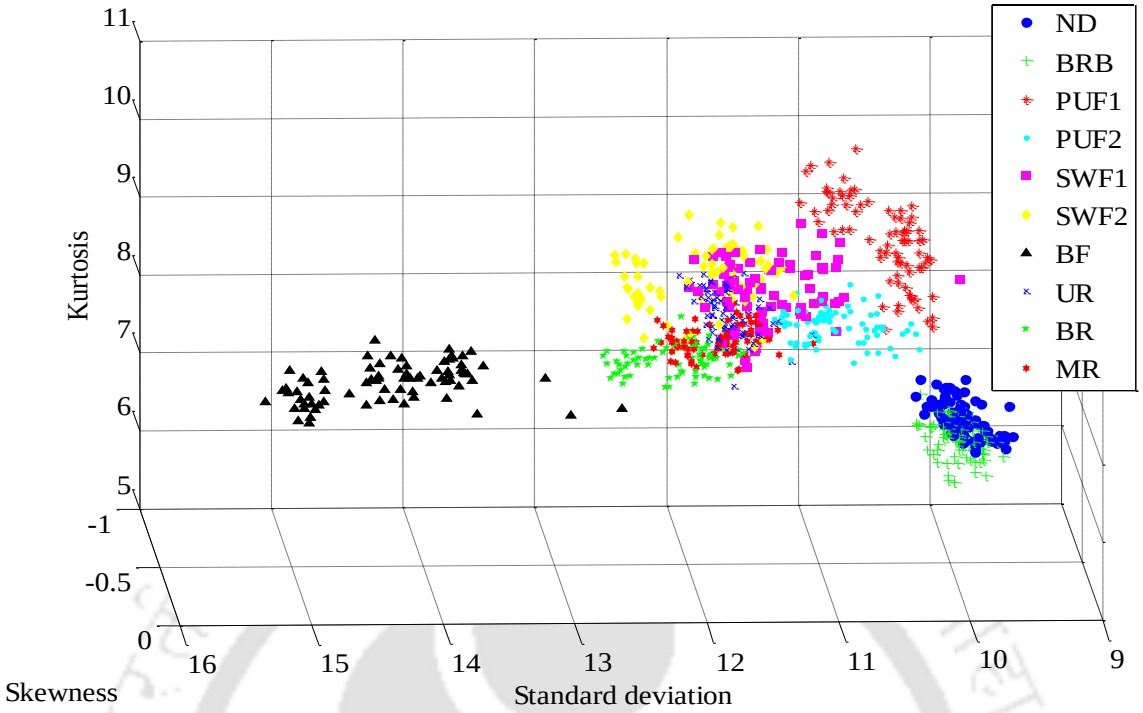

Figure 6.5 Feature distribution of vibration for all IM faults at 30, 35 and 40 Hz, and T_1

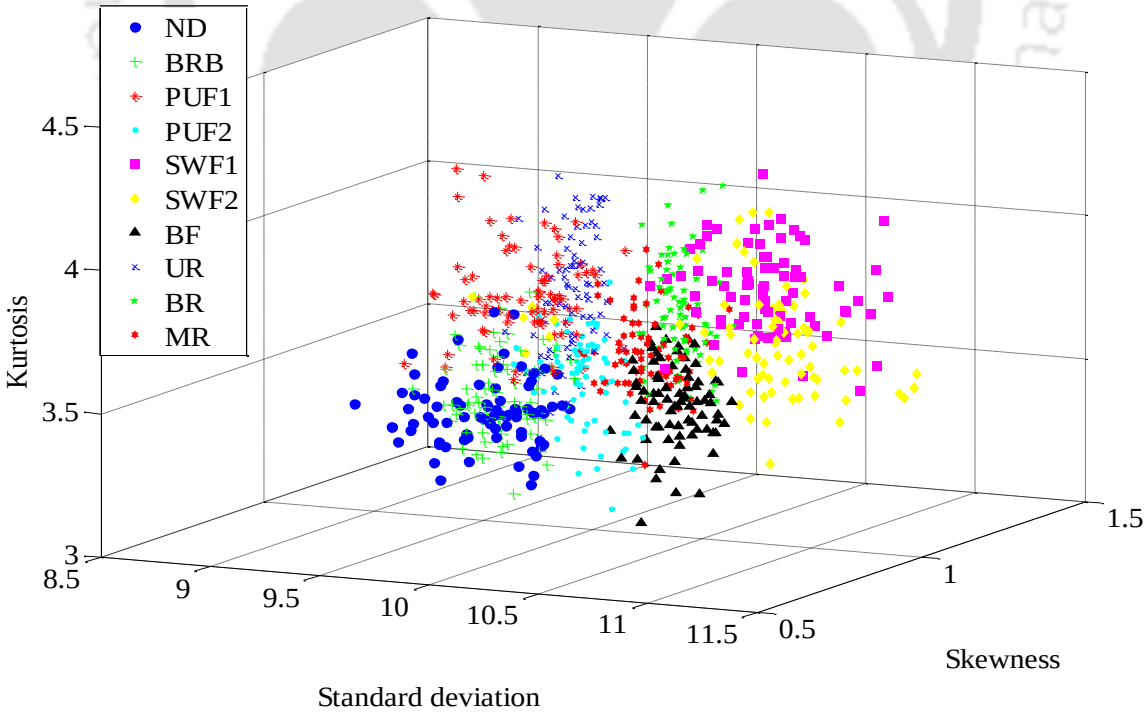

Figure 6.6 Feature distribution of current for all IM faults at 30, 35 and 40 Hz, and T_1

Table 6.6 Various conditions of the intermediate speed (case-2) of the fault diagnosis

Training load	Testing load	Training speeds (Hz)	Testing speed (Hz)	Minimum range of Training speed (Hz)
		10, 20, 25, 30	15	10
T_1	T_1	10, 15, 25, 30	20	10
T_2	T_2 ➡	10, 15, 20, 30	25	10
T_3	T_3	15, 20, 25, 35	30	10
		20, 25, 30, 40	35	10

***Fault prediction*:** The result of fault diagnosis for the present intermediate speed case is shown in Table 6.7. When the fault diagnosis is performed at no load condition, the overall prediction accuracy varies from 86 % at 30 Hz to 98 % at the 15 Hz and 35 Hz intermediate speeds. In addition, the lowest average individual prediction over considered speed is 84 % for PUF1 and MR. Because, the PUF1 and the MR are not predicated at 35 Hz (20%) and 15 Hz (60%), respectively. However, at other speeds, these two faults are predicted successfully. Moreover, other faults are predicted successfully at approximately all speeds except one case, i.e. the SWF1 at 35 Hz (60 %). For the light load condition, the lowest and highest overall prediction accuracies are 88 % (15 Hz) and 98 % (at 30 Hz), respectively. The lowest average individual accuracy is 76 % for the SWF1. This is because the fault condition is not classified at 25 Hz (40 %). Other faults are successfully predicted at all speeds except some cases, i.e. the ND at 35 Hz (40 %), SWF2 at 20 Hz (60 %), UR (60 %) and BR (60 %) at 10 Hz. Now the fault diagnosis is performed when the high load is applied to the IM, the overall prediction accuracy varies from 84 % (15 and 25 Hz) to

100 % at higher speeds. The lowest individual accuracy is 56.66 % for the SWF1. This is because this fault is not classified at lower speeds. Other faults conditions are classified successfully at all IM speeds, except the SWF2 (60 %) and the BR (40 %) at 25 Hz.

From Table 6.7, it is noted that averages of overall prediction accuracies over the entire range of the intermediate speeds are 93.2 % at the no load, 91.6 % at the light as well as high load. That means the fault diagnosis of IM can be performed successfully at all considered loads and speeds successfully. Though, in feature space the overlapping of selected features is more in this case (as shown in Figure 6.7 and Figure 6.8), the overall accuracy increases by 4-5 % in comparison with Case 1 of the intermediate speed. The reason is that the classifier learned the training data very well because for this case the classifier is given the more data (data of multiple speeds) of a particular fault for training. That means if the SVM is trained with more than two speeds rather than with two speeds only, and further tested at the intermediate speed, the prediction performance is expected to be improved. However, in this case, the average training and testing time are 20 s and 2 s, which are significantly increased as compared to Case 1 of the intermediate speed. The SVM could predict IM faults successfully, even when data are not available at the required speed, by considering the intermediate speed case. However, for better fault predictions, it is advisable to perform the diagnosis with training performed at more than two speeds or multiple speeds.

6.3.5 Fault Diagnosis for the Intermediate Load Case

The fault diagnosis is now performed when the training of SVM is done at two load levels and testing is done at an intermediate load (torque); however, for all cases, the training and the testing

are done at the same speed. Various conditions of the intermediate load case are considered for the fault diagnosis, as shown in Table 5.9.

Table 6.7 Fault diagnosis for various operating conditions of IM for the intermediate speed (Case 2)

Train Speed (Hz)	Test speed (Hz)	Prediction accuracy, %										
		ND	BRB	PUF1	PUF2	SWF1	SWF2	BF	UR	BR	MR	Overall
For no load, T_1												
10,20,25,30	15	80	100	100	80	80	100	100	80	100	60	88
10,15,25,30	20	100	100	100	100	100	100	100	80	100	100	98
10,15,20,30	25	100	100	100	80	100	100	100	100	100	80	96
15,20,25,35	30	100	100	100	100	100	100	100	100	100	80	98
20,25,30,40	35	100	100	20	100	60	100	100	80	100	100	86
	Avg.	96	100	84	92	88	100	100	88	100	84	93.2
For light load, T_2												
10,20,25,30	15	80	100	100	100	80	100	100	60	100	60	88
10,15,25,30	20	100	80	100	100	80	60	100	100	100	100	92
10,15,20,30	25	80	100	80	100	40	100	100	100	100	100	90
15,20,25,35	30	100	100	100	100	100	80	100	100	100	100	98
20,25,30,40	35	40	100	100	100	80	100	100	80	100	100	90
	Avg.	80	96	96	100	76	76	100	88	100	92	91.6
For high load, T_3												
10,20,25,30	15	100	100	100	100	40	80	100	80	60	80	84
10,15,25,30	20	100	80	100	100	60	100	100	80	80	100	90
10,15,20,30	25	100	100	100	100	40	60	100	100	40	100	84
15,20,25,35	30	100	100	100	100	100	100	100	100	100	100	100
20,25,30,40	35	100	100	100	100	100	100	100	100	100	100	100
	Avg.	100	96	100	100	56.6	88	100	92	76	96	91.6

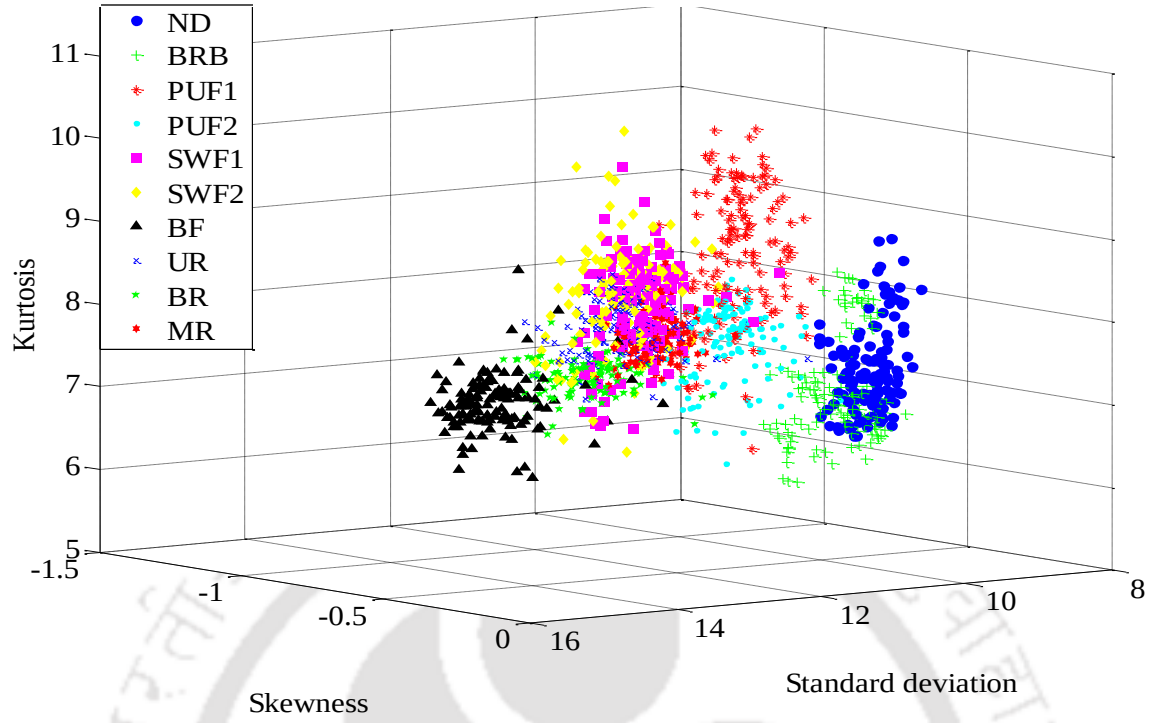

Figure 6.7 Feature distribution of vibration for all IM faults at 20, 25, 30, 35 and 40 Hz, and T_1

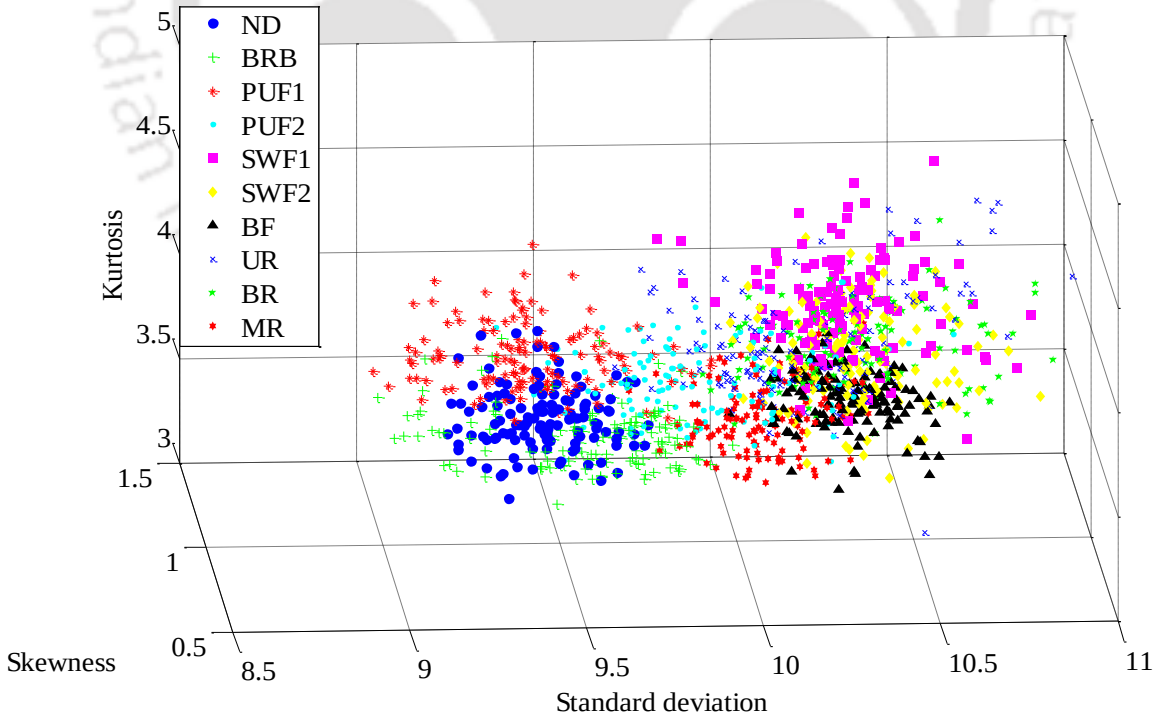

Figure 6.8 Feature distribution of current for all IM faults at 20, 25, 30, 35 and 40 Hz, and T_1

Fault prediction: The results of the fault diagnosis for the intermediate load case is shown in Table 6.8. It is observed the overall accuracy varies from 82 % (at 15 Hz) to 94 % (at 30 and 40 Hz). The lowest average of individual accuracy is 62.9 % for the SWF2. It is because this fault is not classified at the most of the considered speeds. In addition, individual prediction accuracies are 100% for the BF, MR, ND (except at 35 Hz), PUF2 (except at 25 Hz), PUF1 (except at 15 and 25 Hz) and BR (except at 10 and 25 Hz). However, the SVM could not classify the BRB at 15 Hz (20 %), SWF1 at 20 Hz (60 %) and 25 Hz (60 %), SWF2 (except at 10 and 25 Hz), UR at 35 Hz (60 Hz) and BR at 10 Hz (40 Hz). In overall, except SWF at some operating conditions, all other fault conditions are successfully classified at almost all the speeds. It is also noted that the average prediction accuracy over considered speeds is achieved 90.3%. That means the fault diagnosis of IMs can be performed under any operating conditions of IMs even for the intermediate load case. The fault diagnosis does not depend on speeds for the present case unlike the same speed and load case. The reason for the successful fault prediction is, the capability of selected frequency domain features (σ, χ and κ) of vibration and current signals to cluster different IM faults distinctively (Figure 6.9 and Figure 6.10). Selected features make only one cluster of a particular fault even at three different loads on the IM. This makes a classifier to perform successfully even when three different loads (T_1, T_2 and T_3) are used for the training and the testing. The performance, in this case, is reduced by nearly 8% as compared to the same speed and load case, 1-3 % as compared to the Case 2 of intermediate speed; however, it is increased by nearly 2 % as compared to the intermediate speed of Case 1. For the same case, the performance is reduced by 6-7 % in comparison to the time domain analysis.

Table 6.8 Fault diagnosis for various operating conditions of IM for the intermediate load case

Train speed (Hz)	Test speed (Hz)	Prediction accuracy, %										
		ND	BRB	PUF1	PUF2	SWF1	SWF2	BF	UR	BR	MR	Over.
Training at T_1 and T_3, Testing at T_2												
10	10	100	100	100	100	100	100	100	80	40	100	92
15	15	100	20	100	100	100	20	100	80	100	100	82
20	20	100	100	100	100	60	60	100	100	100	100	92
25	25	100	80	80	100	60	100	100	100	80	100	90
30	30	100	100	100	80	100	60	100	100	100	100	94
35	35	80	100	100	100	80	60	100	60	100	100	88
40	40	100	100	100	100	100	40	100	100	100	100	94
	Avg.	97.1	85.7	97.1	97.1	85.7	62.9	100	88.6	88.6	100	90.3

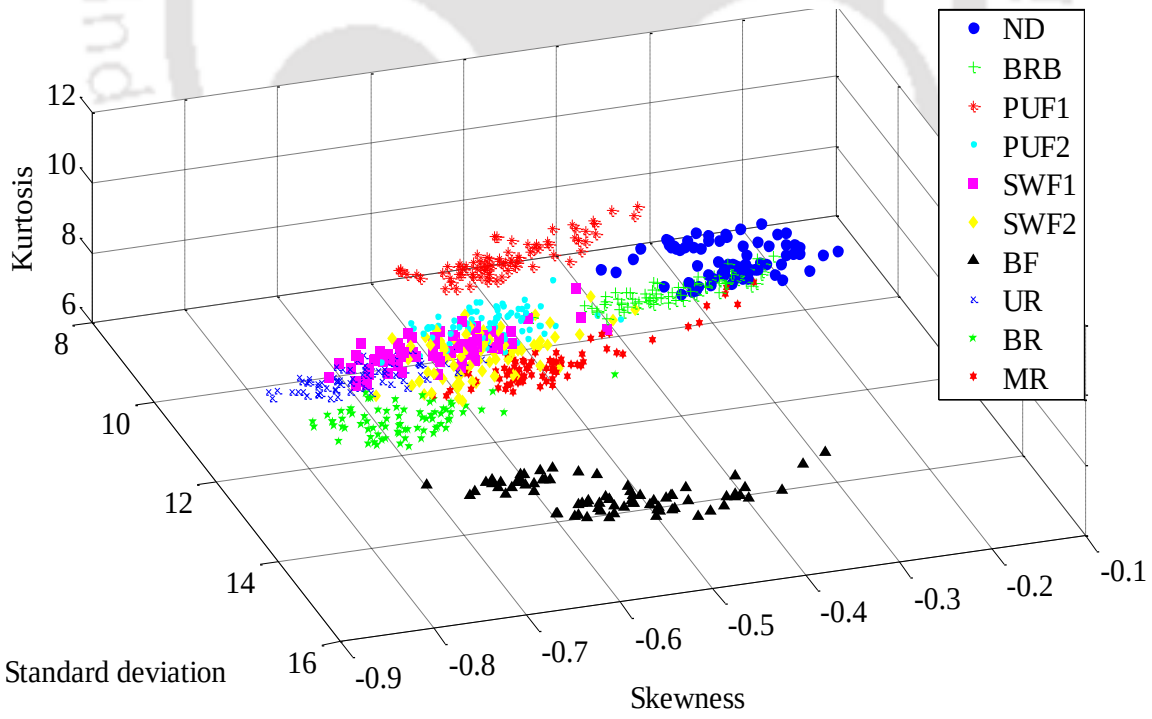

Figure 6.9 Feature distribution of vibration for all IM faults at 40 Hz, and T_1, T_2 and T_3

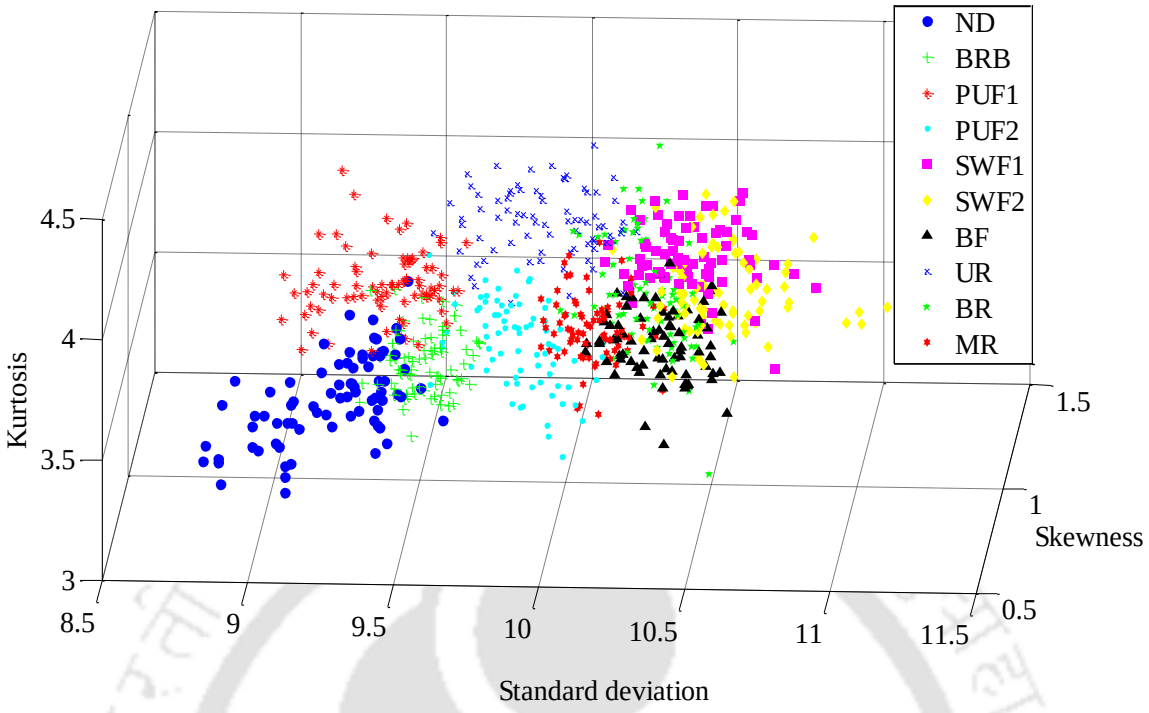

Figure 6.10 Feature distribution of current for all IM faults at 40 Hz, and T_1, T_2 and T_3

6.4 Summary

The fault diagnosis of IM is performed based on the SVM using frequency domain features of vibration and current. In order to select optimized SVM parameters and effective fault features, the cross-validation along with grid-search and the wrapper model are used, respectively, in the present chapter. It is found that the combination of three features $\sigma, \chi,$ and κ is the most effective feature set for the fault diagnosis among the considered features and feature sets, similar to the time domain analysis. After selecting effective features, the fault diagnosis is performed for the same operating condition case. In order to check the fault diagnosis performance of the SVM over a wide range of IM operating conditions, three different loadings with seven speeds of IMs are considered. Results show that the proposed method is able to diagnose IM faults effectively at any considered load and speed, even with the consideration of ten different mechanical and electrical

faults, simultaneously. The fault diagnosis is found to be independent of the IM load; however, it depends on speeds (i.e., a higher accuracy is achieved at higher speeds) unlike time domain analysis, where the diagnosis was not dependent on loads as well as speeds. Critical faults like BF, PUF and SWF, which contribute 85-90% of all IM failures, could be classified perfectly at all considered IM operating conditions. In addition, different levels of severity of the PUF and the SWF could also be successfully classified. From the industrial perspective, the proposed fault diagnosis in this work is extended at intermediate loads as well as speeds cases in order to perform the diagnosis when the data base is not available at all IM operating conditions. The performance of fault diagnosis for these cases also are found to be reasonable.

In comparison to time domain analysis, the overall accuracy is reduced by 1-2 % at the same speed and load case, 1-5 % at the intermediate speed case, and about 6 % at the intermediate load case. In Chapter 5 and Chapter 6, the time and frequency domain based features were used for the fault diagnosis, respectively. It is noted that the time and frequency domain assume the system linearity and signal stationarity (i.e., the idealization and simplification of signals); however, the IM works under nonstationary conditions when its normal duty cycle consists of continuous and random load fluctuations and/or changes in supply conditions due to various faults. Electrical vehicle, wind generation, or any other industrial processes including variable frequency drive (VFD), are examples of actual applications in which IMs work under non-stationary conditions (Henao *et al.*, 2014). To take care of the complex and non-stationary signals a time-frequency domain (or the continuous wavelet transform (CWT)) based feature extraction method will be considered for fault diagnosis in the following chapter.

CHAPTER 7

Multi-Fault Diagnosis of IM based on Continuous Wavelet Transform Data

7.1 Introduction

In this chapter, the multiple fault diagnosis of mechanical and electrical faults and their severity, in IMs is performed by using the multiclass SVM based on one variant of the wavelet transform (WT), i.e. the continuous wavelet transform (CWT). The wavelet, a time-frequency analysis has been developed to handle nonstationary (or transient) and complex signals with high noise. Due to these properties, the wavelet is finding application in the condition monitoring and fault diagnosis (Peng and Chu, 2004). The wavelet transform split up a signal into the scaled and shifted versions of the mother wavelet, like Fourier transform, in which a raw signal divides into sine waves of several frequencies with different phases. This makes wavelet capable of revealing local as well as global information from a signal. It has the ability of extracting significant characteristics, like the breakdown points, trends, higher derivative's discontinuities, and self-resemblance, which describe a signal (Konar and Chattopadhyay, 2011).

Therefore, the one variation of WT, i.e. the CWT is adopted in this chapter. Acquired signals in the time domain are transform to time-frequency domain based on the CWT. The choice of mother wavelet has no fixed guideline; instead it is purely dependent on the nature of the problem. Therefore, ten different base wavelets are used to investigate the impact of different wavelet functions on the IM fault diagnosis. Initially, signals are partitioned into sub signals and then CWT coefficients are thus obtained corresponding to all scales. To eliminate redundant information, the Relative Wavelet Energy (RWE) criterion is used to determine the most appropriate scales and

corresponding coefficients. In the next step, a number of statistical features are extracted from the CWT coefficient corresponding to the best scale. Appropriate feature(s) are selected based on the wrapper model and then fed to the SVM to detect whether a defect has occurred. If a defect exists at any stage, the SVM identifies it, then isolates and finds its severity. The fault diagnosis is performed using different wavelets for various IM operational conditions to check the robustness of the present methodology. The fault diagnosis is performed for three cases when the testing is done, first at the same speed and the same load, then at the intermediate speed, and finally at the intermediate load as training.

7.2 Fault Feature Extraction

To obtain effective features, the continuous wavelet transform (CWT) based feature extraction method is adopted in this chapter. It is a crucial method that shows both time and frequency components of the signal. The CWT converts time domain signal into the time-frequency domain. The basic CWT theory and its application in fault diagnosis have been discussed in several literatures (Peng and Chu, 2004, Yan et al., 2014). For a signal, $x(t)$, the CWT is achieved through a convolution operation between the signal and complex conjugate of a family of wavelet, which is defined as

$$\omega(s,\tau) = \int_{-\infty}^{+\infty} x(t)\psi^*(t)dt \tag{1.1}$$

with

$$\psi^*(t) = \frac{1}{\sqrt{s}}\psi\left(\frac{t-\tau}{s}\right) \tag{1.2}$$

where, $\psi^*(t)$ denotes the window function and is known as the mother wavelet, *s* is a scale, which is related to the frequency information that either compresses or dilates the signal. The high scale denotes to the low frequency of a signal and vice versa. The term τ is a translation parameter, which is related to the time information that decides position or location of windows, as the window shift through the signal, and thus defines which part of the signal $x(t)$ is being analyzed. The wavelet transform uses the mother wavelet function, and perform the decomposition of the signal $x(t)$ into weighted set of scale wavelet function, $\psi^*(t)$. The wavelet is analogous to the Fourier transform but the wavelet family substituted the sine and cosine functions by an infinite set of possible basis functions. The wavelet comprises of two parameters, i.e. the scale and the translation, so it transforms the signal into a two-dimensional space of time and scale, unlike the Fourier transform where the signal is in one dimension. For the wavelet transform, as opposed to the Fourier transform, the choice of the wavelet base is flexible and may differ for different applications. It is possible that different results will appear when the same signal is analyzed using different wavelet bases. Sometimes an unsuitable choice of the wavelet base will lead to no solution for the targeted problem. Therefore, it is not easy to select the wavelet base for different applications of the wavelet transform.

At present, this choice mainly depends on the experience (Zhitong et al., 2001). The different wavelet families make different tradeoffs between how compactly the basis functions are localized in space and how smooth they are. Among the available mother wavelets, the Haar wavelet is one of the oldest and simplest wavelet. It is discontinuous and resembles a step function. It represents the same wavelet as Daubechies db1. Daubechies wavelets are the most popular wavelets. They represent the foundations of the wavelet signal processing and are used in numerous applications.

The Symlet wavelet is nearly symmetrical wavelet and a modified version of the Daubechies family. The Haar, Daubechies, Symlets and Coiflets are compactly supported orthogonal wavelets. These wavelets along with the Meyer wavelets are capable of a perfect reconstruction. The Meyer, Morlet and Mexican Hat wavelets are symmetric in shape. The wavelets are chosen based on their shape and their ability to analyze the signal in a particular application (Rafiee et al., 2009).

Rafiee et al. (2009) presented the application of CWT in the machine fault diagnosis by considering several different mother wavelet candidates, finally showed that the Daubechies44 wavelet is most appropriate wavelet for the gear fault diagnosis. In addition, the Morlet wavelet is also a proper function in this field. In other work, Rafiee et al. (2010) showed that db44 has the most similar shape across the gear and bearing vibration signals. The variance, standard deviation, and fourth central moment of continuous wavelet are proper features for the automatic gear and bearing fault diagnoses; however, the kurtosis is only useful in the case of gears. Kankar et al. (2011) used six different wavelets based on CWT and AIs, for the fault identification in ball bearings. Finally, they concluded that Meyer and the complex Meyer wavelets with the SVM gives the best performance. Konar and Chattopadhyay (2011) performed the fault diagnosis of bearings in IMs based on the CWT and the SVM, and concluded that the selection of wavelets is a crucial for the intelligent fault diagnosis. In other work, Chattopadhyay and Konar (2014) used features of the continuous and discrete wavelet for the BRB fault diagnosis in IMs based on the RBF and multilayer perception (MLP) neural networks, and the SVM. To examine the impact of wavelets on the feature extraction, four wavelets from the Daubechies family are selected. Finally, they concluded that the db8 showed the best classification accuracy. Also showed that the performance of the diagnostics is promising even in the presence of high level noise. Bordoloi and Tiwari (2014) used

features obtained from the Mexican Hat and Meyer wavelets for the gear fault diagnosis and showed that the considered wavelets performed excellently.

From the aforementioned work, it is noticed that the performance of AI based fault diagnostics depends upon the different wavelet function and their features. Therefore, in this work, in order to investigate the impact of wavelet functions and their feature on the fault diagnostics, ten different mother wavelets are considered for the present fault diagnosis as presented in Table 7.1. Figure 7.1 and Figure 7.2 show the representation of the real and complex valued wavelet functions that are considered in this study, respectively. However, it is very difficult to find out which wavelet or shape can represent the signals from IM faults, effectively. Therefore, the CWT using all ten different mother wavelets are applied to the time domain vibration and current signals. These signals are decomposed into 2^7 sub-signals, i.e. 128 scales in the 7^{th} level of decomposition. It returns wavelet coefficients corresponding to all scales. Each data point (i.e., 10 000 points of one data set) consists of the wavelet coefficient for each scale. That means for a particular data set a matrix of 128×10000 coefficients is obtained. Figure 7.3 shows the plot of wavelet coefficient (absolute value) corresponding to 128 scales of the Haar, Coiflet and Shanon wavelets of the vibration and current signals. Calculation of wavelet coefficients at each scale involves a lot of space and time (huge amount of data). Moreover, if scales are selected randomly (or not properly) the subsequent scale may emphasize one original aspect of the waveform; however, other aspects can be inevitably missed. A relative wavelet energy (RWE) based scale selection criterion is used in this work. According to the RWE criterion, an appropriate wavelet scale is one, which is having maximum relative energy. The RWE is considered as the time-scale density that can be used to

detect a specific phenomenon in the time-frequency domain. The RWE is the probability distribution of energy and described by

$$p_m = \frac{E(m)}{E_{overall}} \tag{1.3}$$

where $\sum_m p_m = 1$, Now the overall energy is given by

$$E_{overall} = \sum_m \sum_i \left| C_{m,j} \right|^2 = \sum_n E(m) \tag{1.4}$$

where $C_{n,j}$ denotes j^{th} wavelet coefficients of n^{th} scale, m denotes number of wavelet coefficients, where $m = 1, \ldots, n,$. The energy at each resolution level is the total energy of detail signal and is given by

$$E(m) = \sum_{j=1}^{n} \left| C_{m,j} \right|^2 \tag{1.5}$$

Now the energy is determined for all the scales. Then, the RWE is calculated for each scale by using Equation (7.3). Figure 7.4 shows the RWE plot of the scale selection at 40 Hz speed and T_3 load for the BF. The scale having maximum RWE is selected for each wavelet. Now corresponding to the best scale, the continuous wavelet coefficient (CWC) are obtained for all data sets. Figure 7.5 shows wavelet coefficients obtained corresponding to the best scale for the vibration and current signals of the BF at 40 Hz speed and T_3 load.

Now features of the CWC related to the best scale are extracted. A feature extraction procedure is used for the data preparation to be given as an input to the fault classifier. This procedure can reduce the computation time and the actual amount of data needed for the fault diagnosis. However, there is no prior knowledge in regards to which wavelet features would be more appropriate for the present application. Therefore, a number of statistical features such as higher statistical moments upto eight moments ($\mu_1 - \mu_8$), peak-to-peak (R_{pp}), crest factor, (CF), mean-to-standard-deviation (R_{msd}), standard deviation (σ), skewness (χ), kurtosis (κ), are considered in this chapter. The procedure for feature extraction based on the CWT is shown in Figure 7.4.

Table 7.1 Wavelet families and their order considered in this work

S. No.	Wavelet family (short name)	Real/complex valued	Considered order
1	Haar (haar or db1)	real	db1
2	Daubechies (db)	real	db44
3	Meyer (meyr)	real	meyr
4	Mexican Hat (mexh)	real	mexh
5	Coiflet (coif)	real	coif 5
6	Symlet (sym)	real	sym 15
7	Gaussian (gaus)	real	gaus 7
8	Shannon (shan Fb-Fc)[1]	complex	shan 1-0.1
9	Complex Morlet (cmor Fb-Fc)[1]	complex	cmor 1-0.1
10	Complex Gaussian (cgau)	complex	cgau8

[1]Fb- bandwidth parameter, Fc- wavelet center frequency

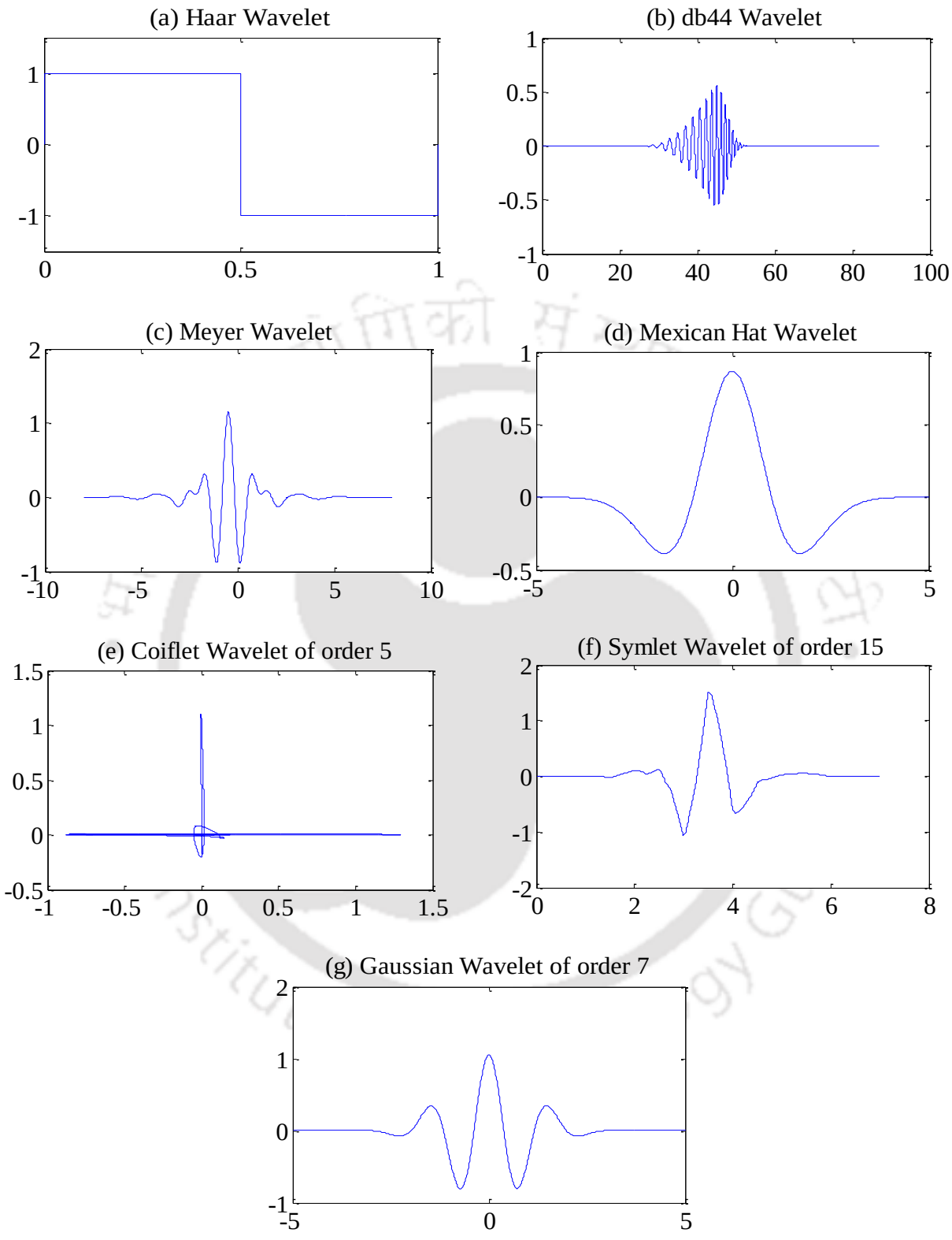

Figure 7.1 Different real wavelet functions considered in the study

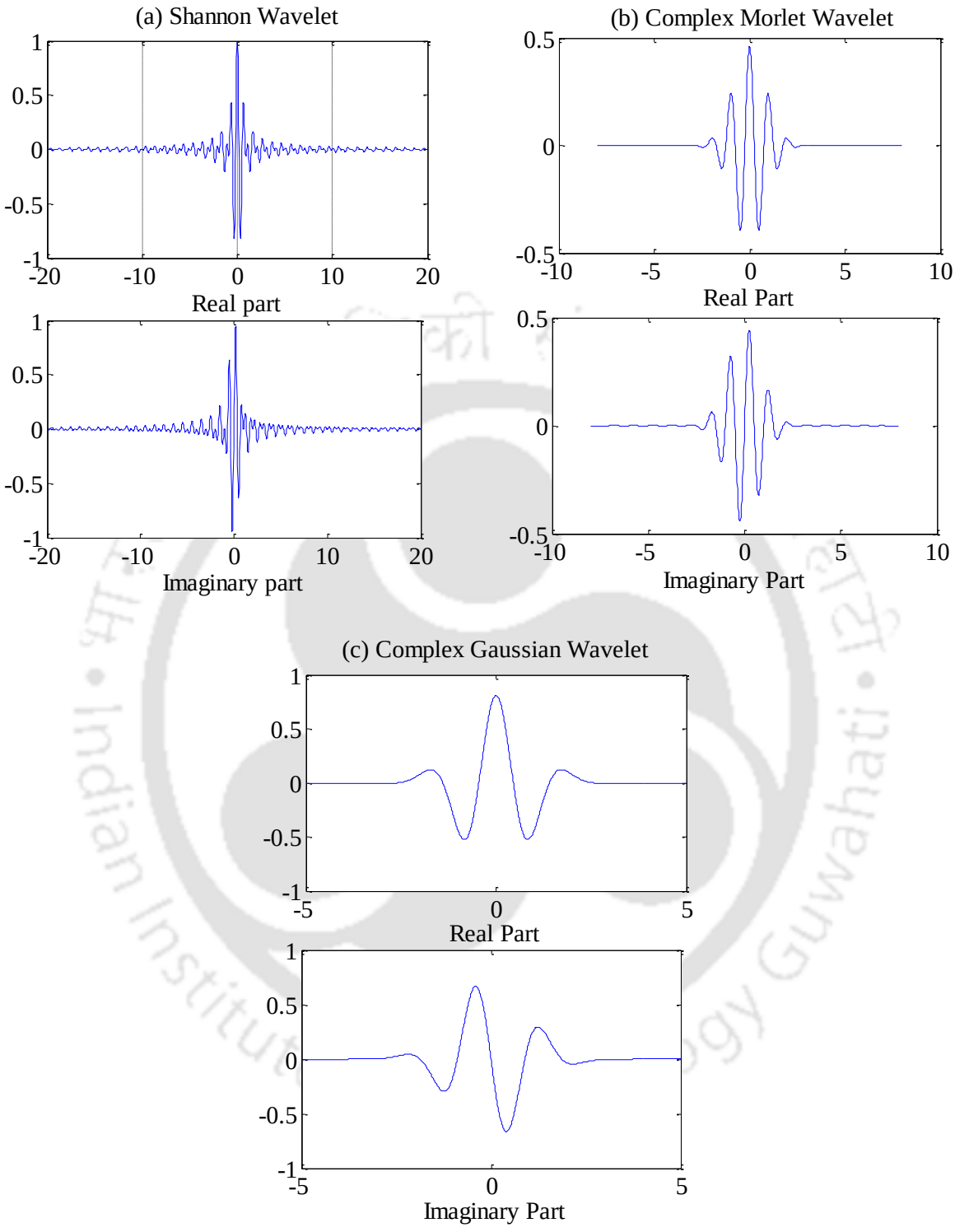

Figure 7.2 Different complex wavelet functions considered in the study

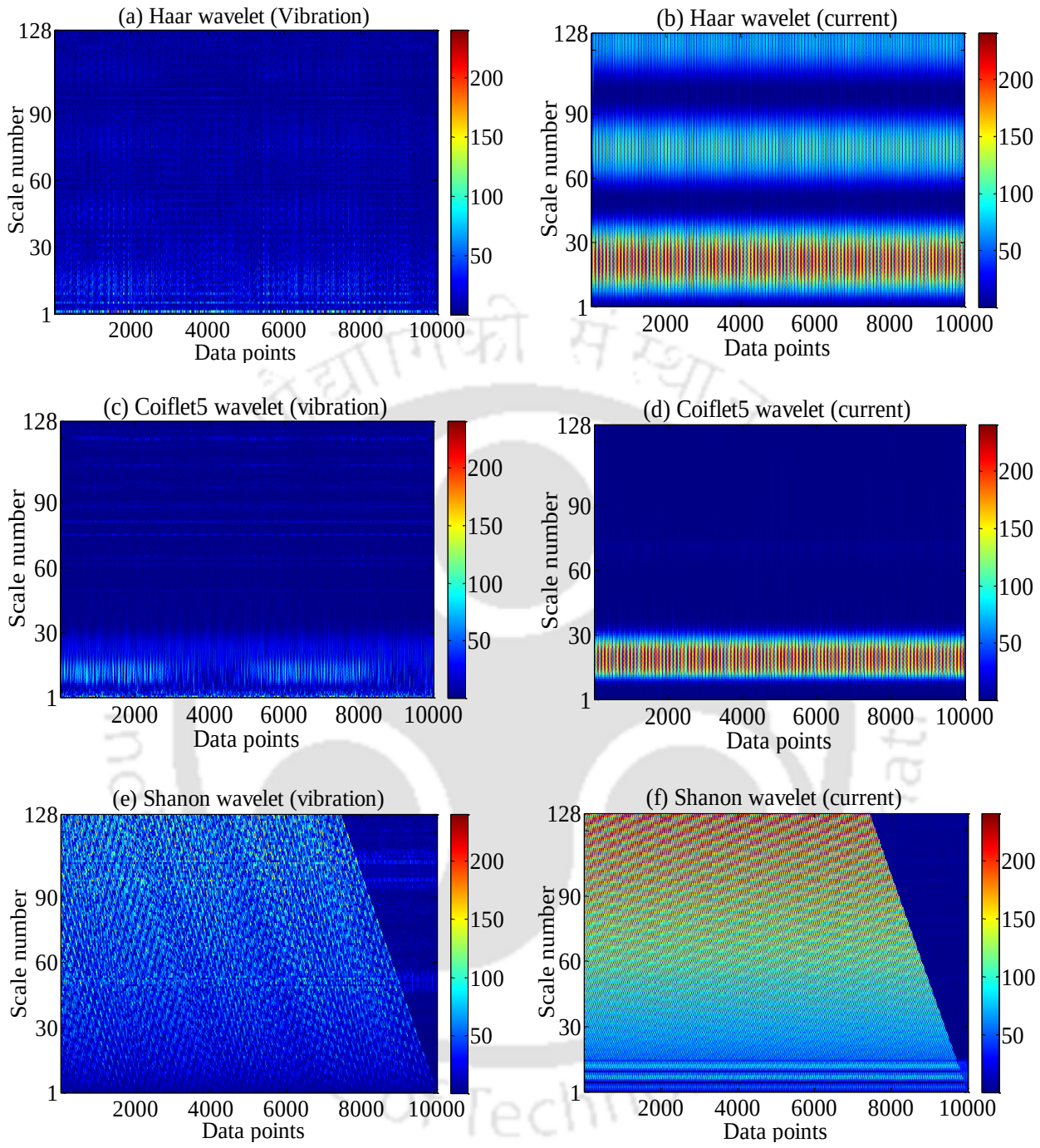

Figure 7.3 Wavelet coefficient (absolute value) plots of vibration (x-axis) and current (phase A) of BF at 40 Hz and T_3

In total 25 sets of wavelet coefficients are obtained corresponding to 25 time domain datasets. Now 14×25 feature datasets are extracted for each motor fault and operation conditions. The variation of statistical features of all data sets for Haar wavelet coefficients of the vibration and current signals, for BF at 40 Hz speed and T_3 load, (See Appendix. A, Figure A.5 and Figure .6, respectively). However, on observing extracted wavelet features, it is impossible to distinguish various faults of IMs. Therefore, to diagnose multiple faults in IMs, the SVM classifier is used. Now, these fourteen features serve as an input vector to the SVM for the feature selection and further fault diagnosis.

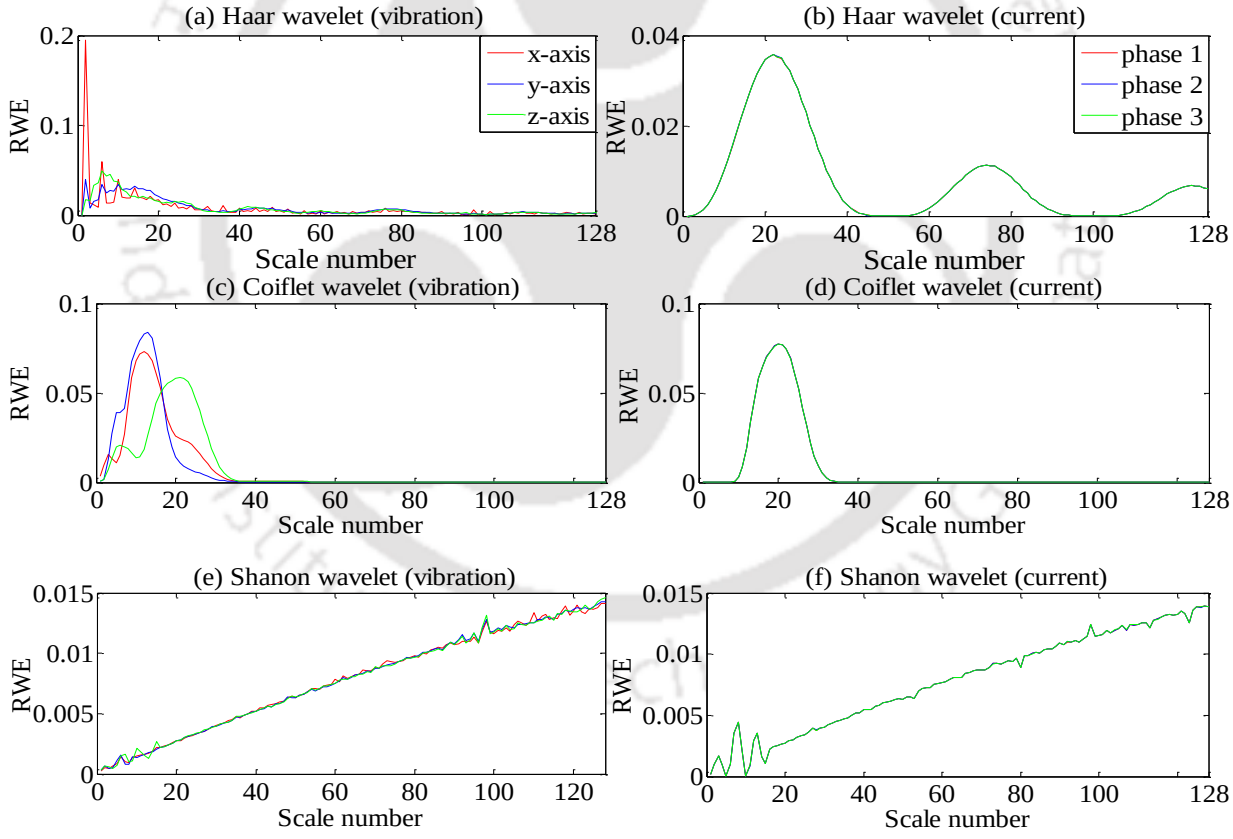

Figure 7.4 Relative wavelet energy (RWE) plot of scale selection for (absolute value) from vibration and current of BF at 40 Hz and T_3

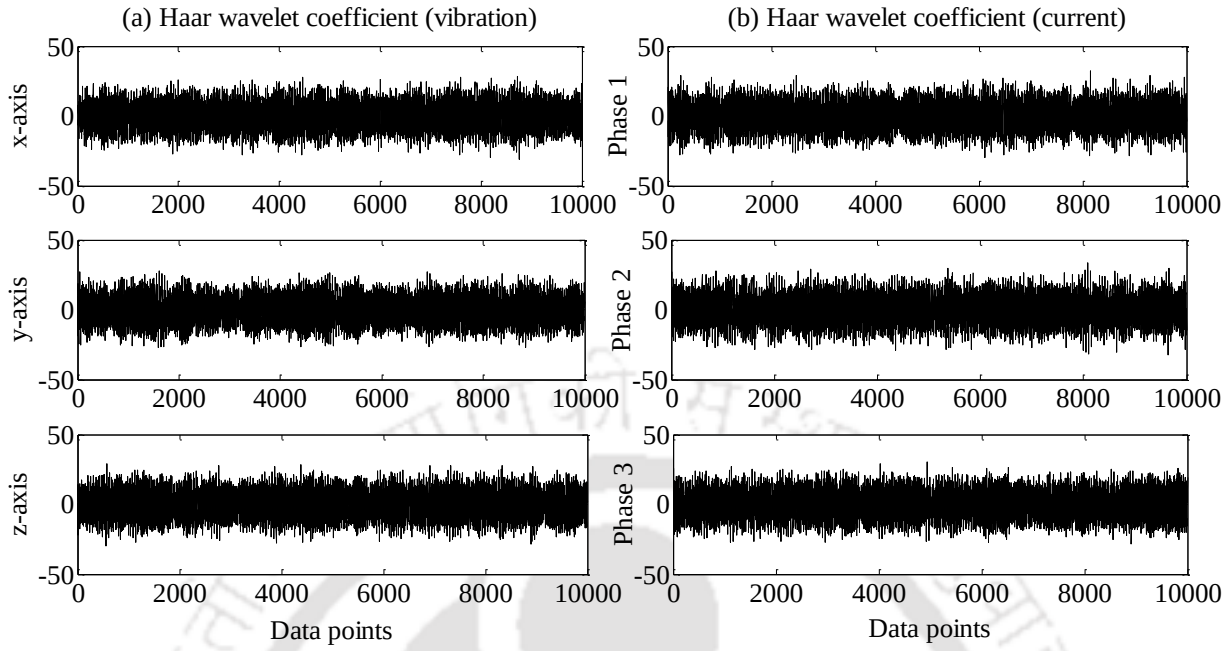

Figure 7.5 Variation in wavelet coefficients of Haar wavelet corresponding to a best scale of the vibration and current signals of BF at 40 Hz speed and T_3

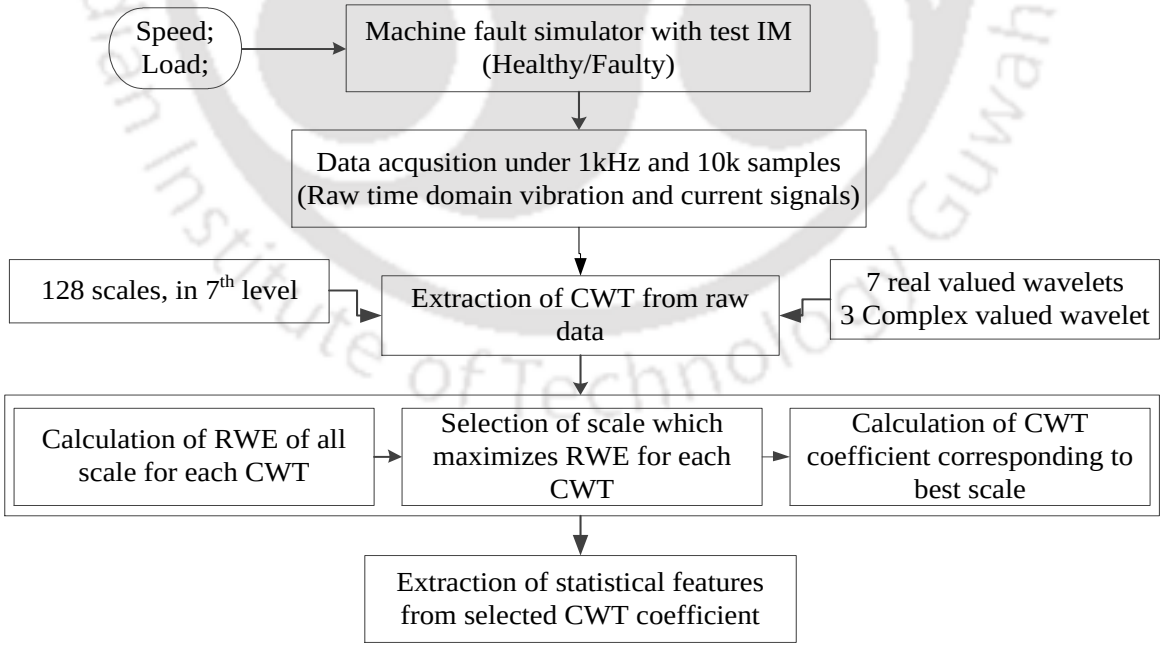

Figure 7.6 The procedure of feature extraction based on CWT

7.3 Fault Diagnosis based on SVM

After collecting feature datasets using the continuous wavelet transform, the one-versus-one multiclass methodology of the SVM is used in order to classify ten different IM faults. The fault diagnosis is considered for three cases, i.e. the same speed and same load case, the intermediate speed case, and the intermediate load case.

7.3.1 SVM Parameter Selection and Training

Training of the SVM is performed for each feature of all the wavelet functions at all the considered operating conditions of IM. The CV accuracy in the grid-search technique for a typical case of 40 Hz and T_3 load, when the training is performed with all the features from the Haar wavelet individually are shown in Figure 7.7 and Figure 7.8. Figure 7.7 (a) is added for the case when the cross-validation is performed with μ_1 only, at 40 Hz and T_3 load. It shows that the maximum CV accuracy is achieved up to 41.5 %. That means the SVM model is not well trained for this case. The accuracy of 100 % and 98.92 % are achieved for the second and fourth moments, respectively. However, the accuracy decreases with other higher moments, like the frequency domain analysis, as shown in Figure 7.7 (b)-(h). The minimum CV accuracy (29.21 %) comes in the case when model is trained with the eighth moment (μ_8) as shown in Figure 7.7 (h). That means the SVM model is not trained at all with these features. The maximum accuracy (100 %) comes with the μ_2 and σ features individually, as shown in Figure 7.7 (b) and Figure 7.8 (d). When these features are used in combination, the accuracy is achieved up to 99.47 %. That means the SVM model is perfectly trained using these features individually and in combination. Now corresponding to the maximum CV accuracy the optimal pair of (C, γ) is achieved for each feature and IM operating conditions, and the best SVM model is built by using the optimal pair of (C, γ).

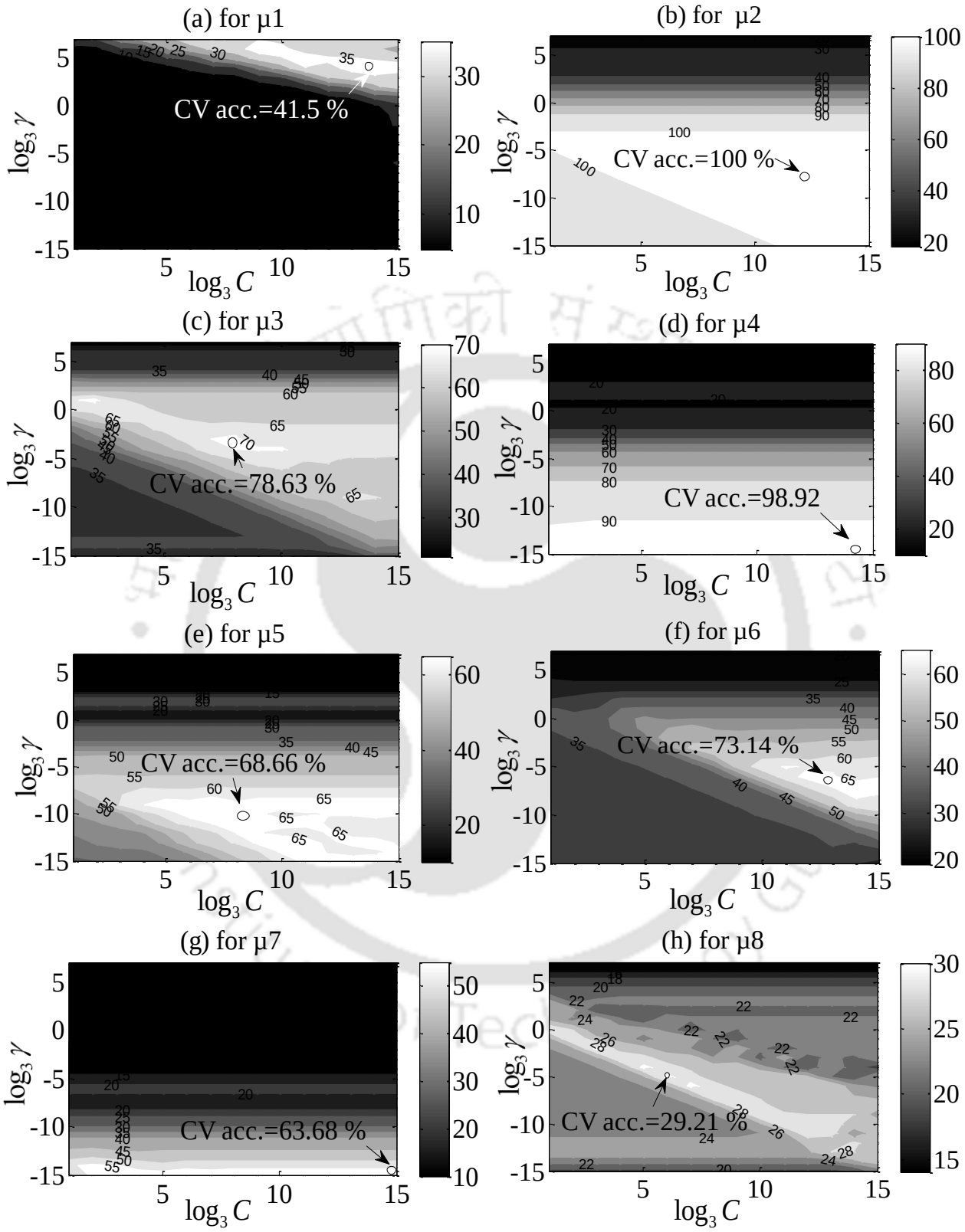

Figure 7.7 Cross-validation accuracy for the Haar wavelet at 40 Hz and T_3

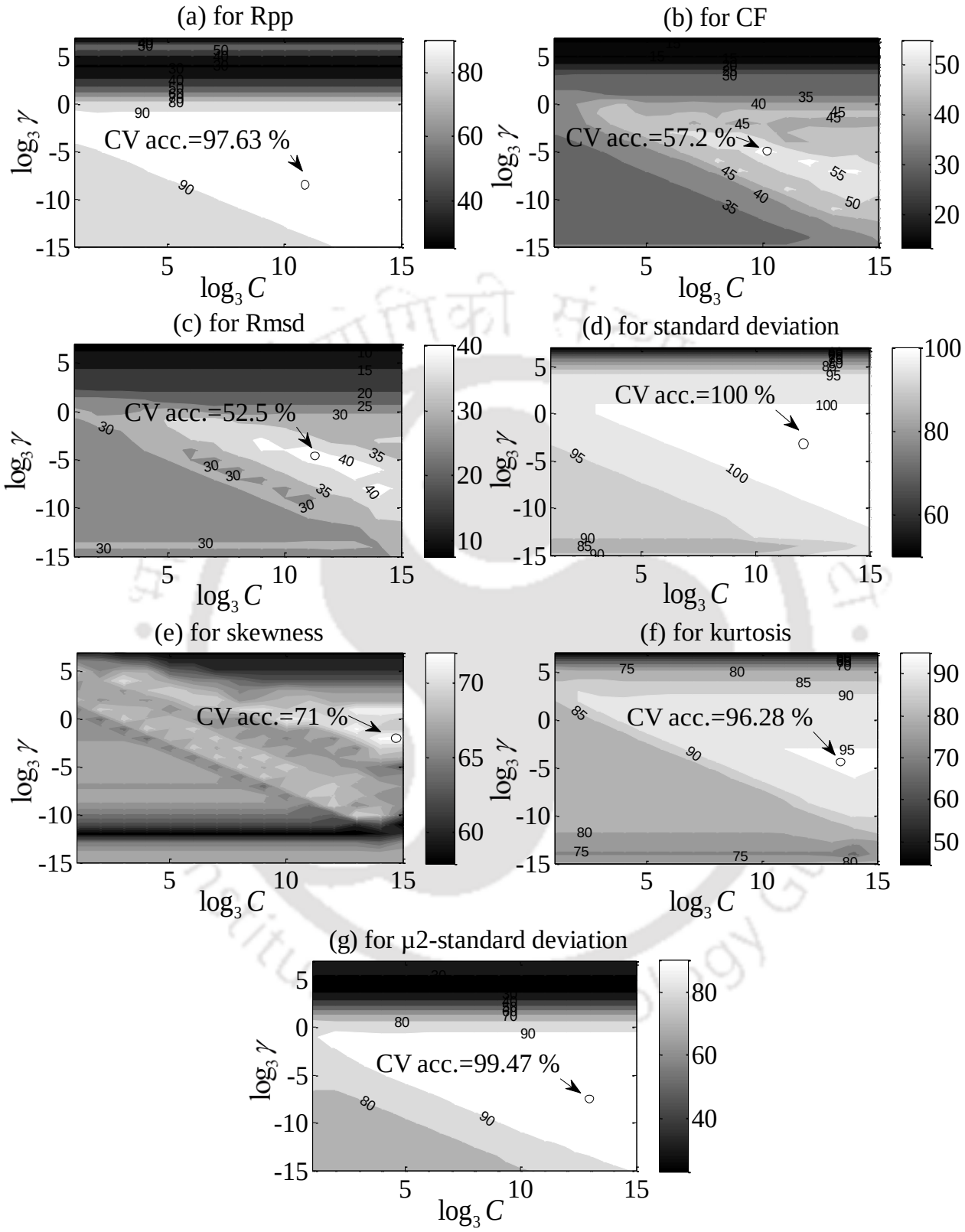

Figure 7.8 Cross-validation accuracy for the Haar wavelet at 40 Hz and T_3

The same procedure is applied to other wavelet functions that are considered in the study. After building an optimal model for each feature or feature set for each wavelet function one by one and for each operating condition, the final testing or classification will be done to predict the unknown data that are not used in the training phase. It is noted that the final prediction or classification accuracy depends on how well the classifier is trained.

7.3.2 Fault Feature Selection

In order to choose effective features, initially fourteen features from each wavelets are considered, one at a time, which constitutes the input vector of the classifier. The wrapper model is used to select useful features. The overall prediction performance for the feature selection at 40 Hz and T_3, using all considered wavelet functions is shown in Table 7.2. It shows that the overall performance of the SVM corresponding to the μ_2 and σ features of all considered wavelet is 100 %, except for one case, i.e. the Mexican hat wavelet with σ (98 %). But for other considered features, the prediction accuracy has gone below 75 %, except μ_4 (96.2%), which are unacceptable in intelligent fault diagnostics. The fourth central moment, i.e. μ_4, also shows good performance for all the considered wavelet functions with average accuracy of 96.20%, however the performance is about 4 % less than the μ_2 and σ. From the results, it can be concluded that the μ_2 and σ features of wavelets present better characteristic of all IM faults than other considered wavelet features. Therefore, these two wavelet features are selected as the most effective features from the time domain vibration and current signals for the IM fault diagnostic application. Now this feature subset will be used for the fault diagnosis at various operating conditions.

Table 7.2 Statistical features selection by the wrapper model, at 40 Hz and T_3

CWT	Overall prediction accuracy (in %)													
	μ_1	μ_2	μ_3	μ_4	μ_5	μ_6	μ_7	μ_8	R_{pp}	CF	R_{msd}	σ	χ	κ
haar	64	100	80	100	70	76	66	10	96	54	56	100	62	95
db44	40	100	56	94	46	56	38	10	92	42	54	100	42	84
meyr	48	100	54	94	36	60	34	10	98	50	44	100	38	56
mexh	66	100	80	92	72	90	38	58	86	68	68	98	54	50
coif5	74	100	62	94	52	78	42	10	94	68	56	100	42	66
sym15	60	100	62	94	70	68	36	10	90	48	68	100	54	78
gaus7	32	100	72	100	70	84	68	84	88	30	50	100	62	56
shan1-0.1	80	100	84	94	92	44	10	10	54	42	72.5	100	68	76
cmor1-0.1	80	100	96	100	94	68	58	10	56	54	82	100	80	83
cgau8	60	100	56	100	66	96	52	86	24	56	58	100	86	36
Avg.	60.4	100	70	96.2	66.8	72	44.2	29.8	77	51	60.8	99.8	58.8	68

7.3.3 Fault Diagnosis for Same Speed and Same Load case

After selecting the optimal SVM parameter and effective features for different wavelet functions, the fault diagnosis is performed when the testing of SVM is done at the same speed and load as the training. Various conditions are considered for the fault diagnosis as shown in Table 5.4. Here, ten mother wavelets are considered to study the impact of different wavelet on the IM fault diagnosis. For any fault diagnosis, it is also very important to select the most suitable wavelet that can extract the relevant information of all fault conditions from considered signals. A suitable wavelet is chosen as the base wavelet that shows the highest prediction accuracy because the main objective of fault diagnosis is to achieve a maximum prediction. To study the effect of wavelets

on the prediction accuracy, two effective features, i.e. σ and μ_2 of the wavelet function as selected from the previous section, are considered first individually then in combination for the fault diagnosis. In order to effectively select the wavelet function, the fault diagnosis is performed at three different speeds. The experimental prediction results of the SVM for all the considered wavelet functions at three selected speeds and a load of T_3 are shown in Table 7.3.

Experimental results show that all the considered wavelet functions with the σ and μ_2 features give more than 93 % prediction accuracy. Therefore, it can conclude that all the considered mother wavelets successfully classified IM fault conditions. However, the goal of fault diagnosis is to achieve a perfect prediction. For this, a comparison of the prediction performance of all the wavelets is added in Table 7.3, it shows the average performance of the Haar, Daubechies, Meyer, Coiflet, Symlet and complex Morlet wavelets is lower than the Mexican-hat, Gaussian, Shannon and complex Gaussian wavelets. The complex Morlet with σ-μ_2 shows the lowest accuracy, i.e. 93.33 %, among other wavelets; however, the accuracy improves by 4-5 % when only σ is considered. That means, μ_2 of the complex Morlet does not represent all the faults correctly. The Meyer and Coiflet wavelets show the lowest prediction performance with 4-6 % misclassification. The Symlet wavelet also shows less accuracy, i.e. 94.67 % with σ; however, its accuracy improves by 4-5 % when μ_2 is considered alone or in combination with σ. The Daubechies wavelet shows 98 % accuracy with σ; however, by considering μ_2 only or with σ, the accuracy reduced by 1.5 %. The Haar wavelet shows the average prediction up to 98 % with σ, and also with μ_2 and their combination. That means these two features of the Haar wavelet shows almost the same performance and any of them can be used for the fault diagnosis; however, still 1.5 to 2 %

misclassification occurs. The Mexican-hat and complex Gaussian wavelets with σ and μ_2, the Gaussian and the Shannon wavelets with σ shows nearly 99 % of the prediction accuracy. That means σ of these four wavelet functions represent all IM faults with good accuracy; however, some misclassification are there. In addition, μ_2 of the Mexican-hat, complex Gaussian, and Gaussian wavelets also show 99 %, 99% and 98 % of prediction accuracies, respectively; however, the accuracy reduces by 1 to 3 % when the combination of μ_2 and σ are considered.

Fault prediction results show that the Shannon wavelet with σ gives 100% performance. That means it provides a perfect fault prediction for considered operating conditions, i.e. three speeds and a load. Whereas for the same wavelet, by considering μ_2 only or in combination with σ, the prediction performance has decreased by 2-4 % especially at low speeds. Comparing the performance of ten mother wavelet with selected feature(s), the Shannon wavelet with σ is found to be stable and consistent at selected operational conditions (i.e., three speeds and a load) of IM. This wavelet feature combination is found to capture all ten fault conditions the most effectively. From the investigation, it can be concluded that the Shannon wavelet with σ has emerged as the most suitable wavelet-feature combination for the present application. However, it is very important to check the robustness of this wavelet feature with different operational condition of IMs.

Therefore, fault diagnostics are now performed based on σ of the Shannon wavelet for a wide range of operational condition of IMs, i.e. motor speeds from 10 Hz to 40 Hz with 5 Hz of interval and three external loadings from no load to full load. Fault diagnostic results are shown in Table 7.4. The outcome illustrated that the SVM has predicted all electrical and mechanical faults perfectly,

i.e. with 100 % accuracy, at all considered operational conditions of IMs. In addition, two different severity levels of the phase unbalance and stator winding faults are also perfectly classified, i.e. without any misclassification even at all the operating conditions as shown in Table 7.4.

Table 7.3 Mother wavelet selection for same speed and same load case, at three speeds and T_3

CWT	Overall prediction accuracy (in %)											
	σ				μ_2				σ- μ_2			
	10Hz	25Hz	40Hz	Avg.	10Hz	25Hz	40Hz	Avg.	10Hz	25Hz	40Hz	Avg.
haar	100	96	100	98.67	98	96	100	98.00	98	96	100	98.00
db44	98	96	100	98.00	98	92	100	96.67	98	92	100	96.67
meyr	96	86	100	94	98	92	100	96.67	98	92	100	96.67
mexh	100	100	98	99.33	100	100	98	99.33	100	96	98	98
coif5	98	88	100	95.33	96	92	100	96	98	92	100	96.67
sym15	98	86	100	94.67	98	96	100	98	98	96	100	98
gaus7	98	100	100	99.33	98	96	100	98	98	94	10	97.33
shan1-0.1	100	100	100	100	94	100	100	98	94	96	100	96.67
cmor1-0.1	94	100	100	98	92	90	100	94	92	88	100	93.33
cgau8	98	100	100	99.33	100	98	100	99.33	98	92	100	96.67

The perfect prediction of IM faults and its severity levels is obtained at all chosen speeds and loads, because there is no overlap of feature (i.e., σ) distribution of the vibration as well as the current signal. This can be observed in clusters of selected feature of vibration and current signals at 40 Hz and T_3 load in Figure 7.9 and Figure 7.10. Figures show that the selected wavelet and its feature is capable of clustering different IM faults. Additionally, the selected wavelet feature combination is capable of clustering different levels of severity of the faults. Finally, it can be concluded that the fault diagnostics with the Shannon wavelet and the σ has yielded the perfect prediction, not

only for different IM faults, but also for their severity at all the speeds and different levels of the load torques considered. The prediction of IM faults based on the present methodology does not depend on IM operational conditions similar to the time domain. The diagnosis based on CWT is better as compared to time and frequency domain based features, this may be due to the ability of joint time and frequency representation of the CWT. The average training and testing time are 3.8 s and 0.87 s, respectively.

7.3.4 Fault Diagnosis for the Intermediate Speed case

After performing the fault diagnosis for the same speed condition, now it is extended to the intermediate speed condition. In order to implement diagnosis for the intermediate speed case, the SVM classifier has to be built by training at two considered motor speeds and tested at an intermediate speed from which the SVM is not trained as shown in Table 5.7. However, the SVM is trained and tested at the same motor load. Similar to the same speed case of the fault diagnosis, first, the selection of the effective feature is performed.

It is known that the type of feature(s) appropriate for one case can vary for the other. The selection of appropriate feature(s) for a specific case can be considered as a combination of hit-and-trial and application of experience. Hence, fourteen features from the Shannon wavelet are used for the feature selection, as shown in Table 7.5. The diagnosis is performed at 35 Hz intermediate speed and T_3 load. It shows that at the very first instant, i.e. μ_1 and σ of the Shannon wavelet give a good fault prediction performance, i.e. 94 % and 89.23 %, respectively. Other features are not able to predict IM faults effectively in this case. Therefore, μ_1 is chosen for the fault diagnosis for the intermediate speed case for all other load conditions.

Table 7.4 Fault diagnosis for various operating conditions of IM for the same speed and load case

Train speed (Hz)	Test speed (Hz)	Prediction accuracy (in %)										
		ND	BRB	PUF1	PUF2	SWF1	SWF2	BF	UR	BR	MR	Over.
For no load, T_1												
10	10	100	100	100	100	100	100	100	100	100	100	100
15	15	100	100	100	100	100	100	100	100	100	100	100
20	20	100	100	100	100	100	100	100	100	100	100	100
25	25	100	100	100	100	100	100	100	100	100	100	100
30	30	100	100	100	100	100	100	100	100	100	100	100
35	35	100	100	100	100	100	100	100	100	100	100	100
40	40	100	100	100	100	100	100	100	100	100	100	100
	Avg.	100	100	100	100	100	100	100	100	100	100	100
For light load, T_2												
10	10	100	100	100	100	100	100	100	100	100	100	100
15	15	100	100	100	100	100	100	100	100	100	100	100
20	20	100	100	100	100	100	100	100	100	100	100	100
25	25	100	100	100	100	100	100	100	100	100	100	100
30	30	100	100	100	100	100	100	100	100	100	100	100
35	35	100	100	100	100	100	100	100	100	100	100	100
40	40	100	100	100	100	100	100	100	100	100	100	100
	Avg.	100	100	100	100	100	100	100	100	100	100	100
For high load, T_3												
10	10	100	100	100	100	100	100	100	100	100	100	100
15	15	100	100	100	100	100	100	100	100	100	100	100
20	20	100	100	100	100	100	100	100	100	100	100	100
25	25	100	100	100	100	100	100	100	100	100	100	100
30	30	100	100	100	100	100	100	100	100	100	100	100
35	35	100	100	100	100	100	100	100	100	100	100	100
40	40	100	100	100	100	100	100	100	100	100	100	100
	Avg.	100	100	100	100	100	100	100	100	100	100	100

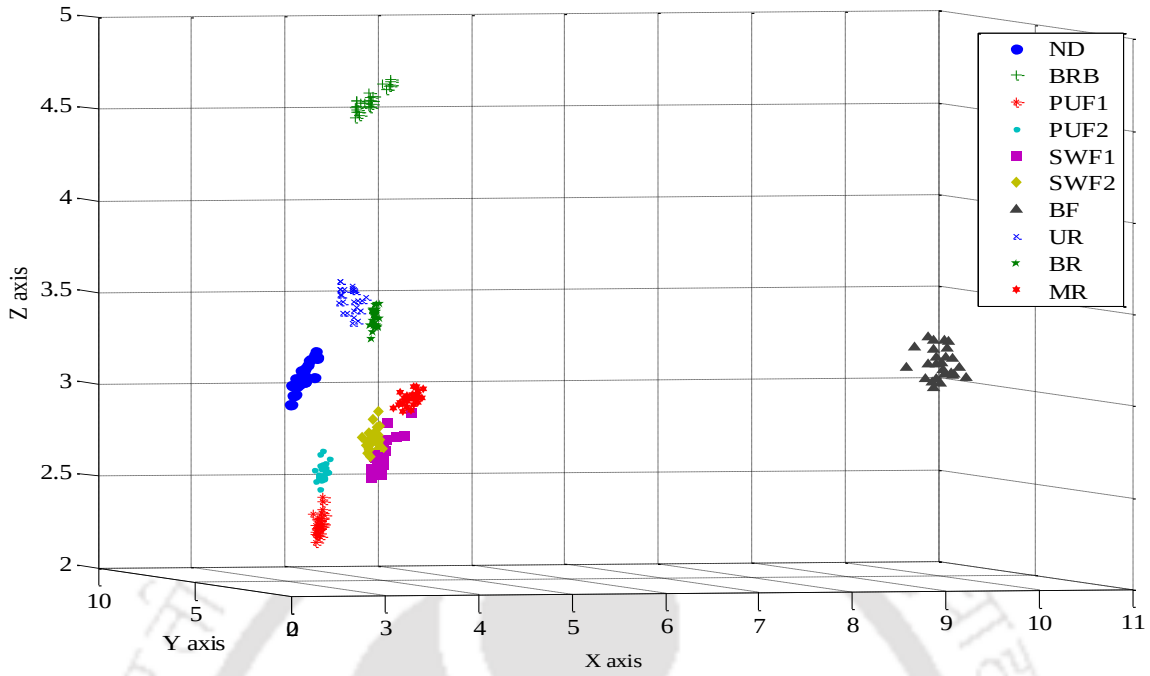

Figure 7.9 Feature distribution (σ) of Shannon wavelet coefficient of vibration for all IM faults at 40 Hz and T_3

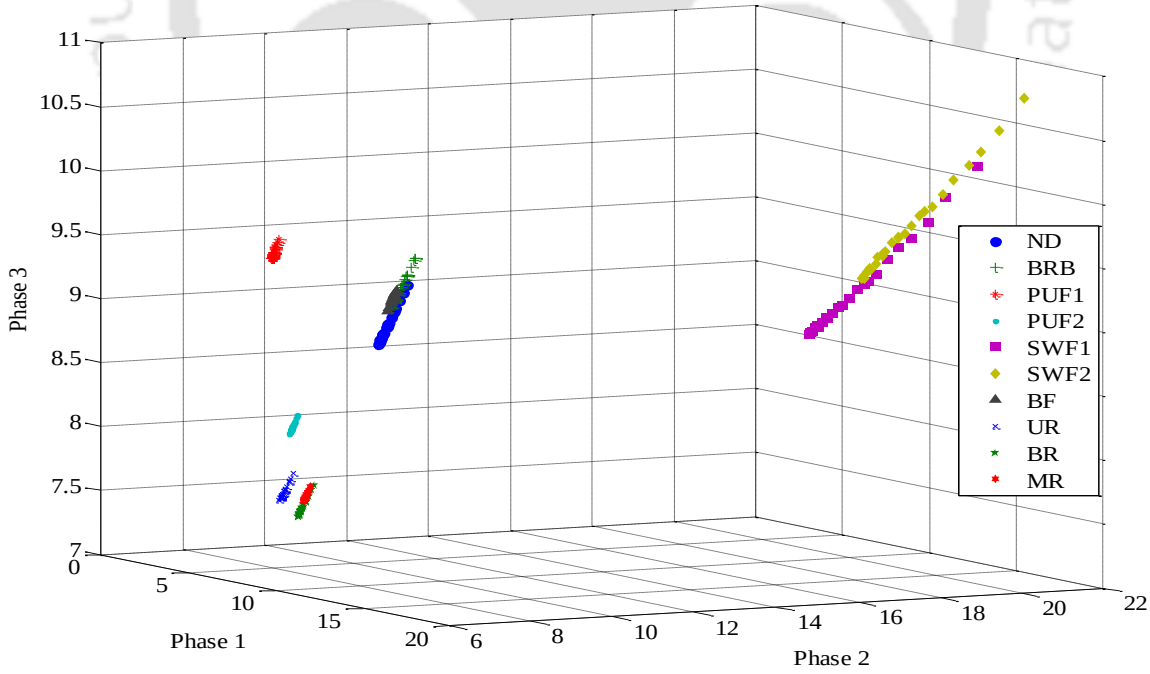

Figure 7.10 Feature distribution (σ) of Shannon wavelet coefficient of current for all IM faults at 40 Hz and T_3

Table 7.5 Features selection by the wrapper model and the SVM at T_3

Statistical features	Average prediction accuracy, %	Statistical features	Average prediction accuracy, %
μ_1	94	μ_8	22.52
μ_2	71.6	R_{pp}	53.33
μ_3	62.28	CF	37.62
μ_4	76.68	R_{msd}	68.67
μ_5	56.14	σ	89.23
μ_6	42.6	χ	36.72
μ_7	33.74	κ	48.52

Fault prediction: Now, the diagnosis for the intermediate speed condition is performed at the no, light and full loads of IMs as shown in Table 7.6. It shows that the average of overall performance is 99.2 % at no load. This is obtained because there is no or little overlapping of selected feature from the vibration as well as the current for all the IM faults at no load as shown in Figure 7.11 and Figure 7.12, respectively. However, the feature of some faults overlaps in vibration signals, but the degree of overlap is very small, so this does not affect much in the fault prediction at no load. The average performance is reduced by 8-9 % in the case of light and full loads as compared to the no load condition. In addition, the individual performance is 100 % at the no load for all fault conditions except two cases, i.e. the MR and the SWF2 with 80 % prediction at intermediate test speeds of 15 Hz and 35 Hz, respectively. However, at the light and full loads, two levels of stator winding fault could not be predicted successfully for all intermediate speed cases. For the

high load, there is no overlap of the feature of vibration of IM faults except the SWF1 and the SWF2 as can be seen in Figure 7.13. This figure shows little variation in vibration features between these two faults. Moreover, Figure 7.14 shows that the current feature obtained from different IM faults gather closely that means large overlapping of the feature occurs at the high load as compared to the no load. In spite of the overlapping, the average performance is high enough, i.e. more than 90 % under loading conditions, and can be considered practically acceptable. In overall, the fault diagnosis for the intermediate case depends upon the external loading on IMs unlike the same speed fault diagnostic case. However, the average performance is more than 90 % regardless of the loading and intermediate speed conditions. The reason for the reduction of prediction performance under loading conditions is due to the fact that the abrupt fluctuation of rotor speed cannot be avoided under loading condition. Therefore, in this case, the features extracted are pertaining to fault signatures at fluctuating speeds. Moreover, here features from three different fluctuating speed ranges are used for the training and the testing; hence, the chances of feature overlap are more. Thus the prediction performances seem to reduce. However, in the same speed case (the prediction was 100 % for all loads), feature obtained at single speed is used so variation in feature due to steady changes of speeds does not affect much. For the same case, the prediction at the high and light loads is increased by 2-3 % as compared to the time and frequency domain analyses; however, the prediction at no load is significantly increased by 6 % and 10 % as compared to the time domain and frequency domain analyses, respectively. The average training and testing time are 6.5 s and 0.97 s, respectively.

Table 7.6 Fault prediction for various operating condition of IM for the intermediate speed case

Train speed (Hz)	Test speed (Hz)	Prediction accuracy (in %)										
		ND	BRB	PUF1	PUF2	SWF1	SWF2	BF	UR	BR	MR	Over.
For no load, T_1												
10,20	15	100	100	100	100	100	100	100	100	100	80	98
15,25	20	100	100	100	100	100	100	100	100	100	100	100
20,30	25	100	100	100	100	100	100	100	100	100	100	100
25,35	30	100	100	100	100	100	100	100	100	100	100	100
30,40	35	100	100	100	100	100	80	100	100	100	100	98
	Avg.	100	100	100	100	100	96	100	100	100	96	99.2
For light load, T_2												
10,20	15	100	100	100	100	40	40	100	80	100	100	86
15,25	20	100	100	100	80	80	60	100	100	100	100	92
20,30	25	100	100	60	100	60	100	100	60	100	100	88
25,35	30	100	100	80	100	100	100	80	100	100	80	94
30,40	35	100	100	60	100	60	100	100	100	100	100	92
	Avg.	100	100	80	96	68	80	96	88	100	96	90.4
For high load, T_3												
10,20	15	100	100	100	100	80	100	100	100	100	100	98
15,25	20	100	100	100	100	100	40	100	100	80	100	92
20,30	25	100	80	100	100	80	40	100	100	40	100	84
25,35	30	100	100	100	100	60	40	80	100	100	100	88
30,40	35	100	80	100	100	60	100	100	100	100	100	94
	Avg.	100	92	100	100	76	64	96	100	84	100	91.2

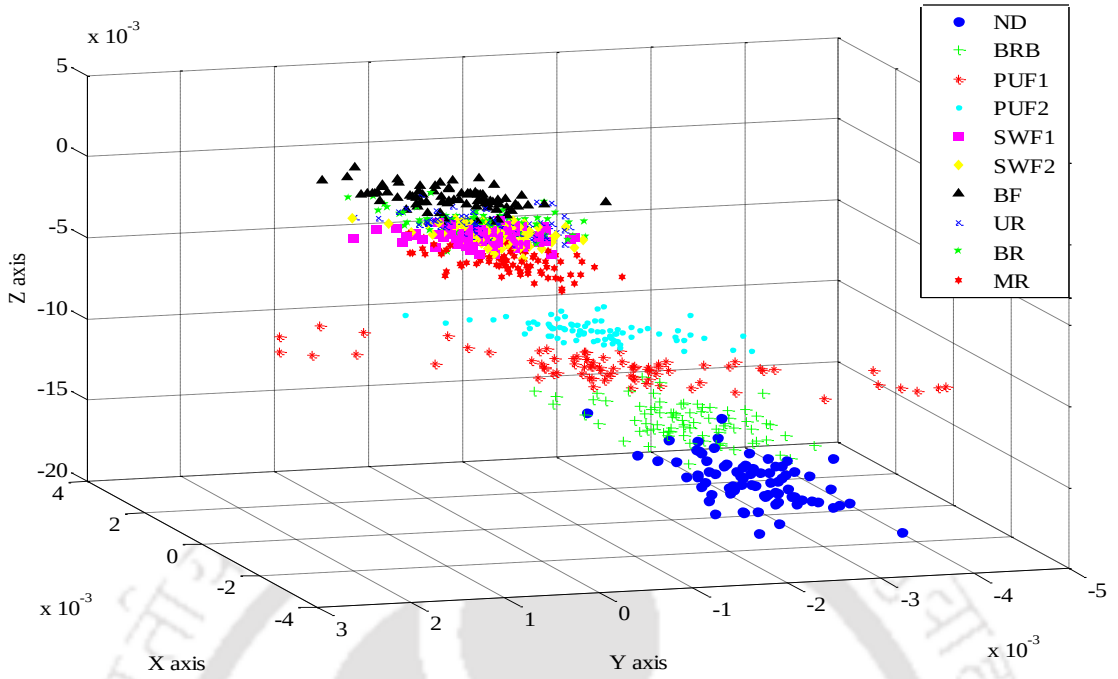

Figure 7.11 Feature distribution (μ_1) of Shannon wavelet coefficient of vibration for all IM faults at 30, 35 and 40 Hz, and T_1

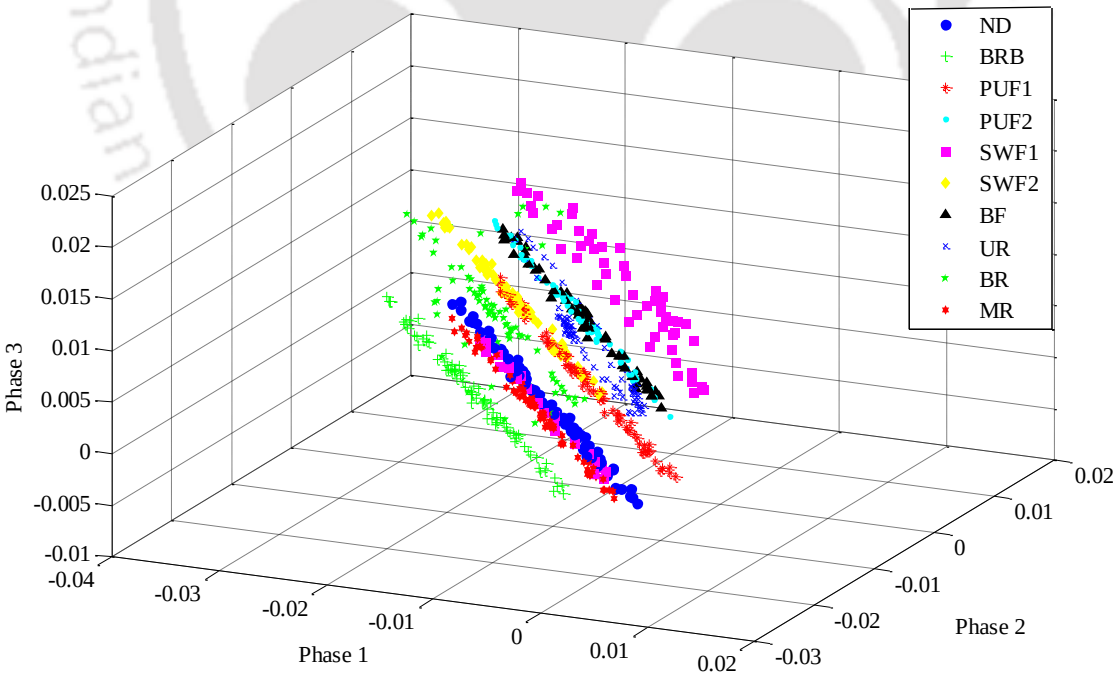

Figure 7.12 Feature distribution (μ_1) of Shannon wavelet coefficient of current for all IM faults at 30, 35 and 40 Hz, and T_1

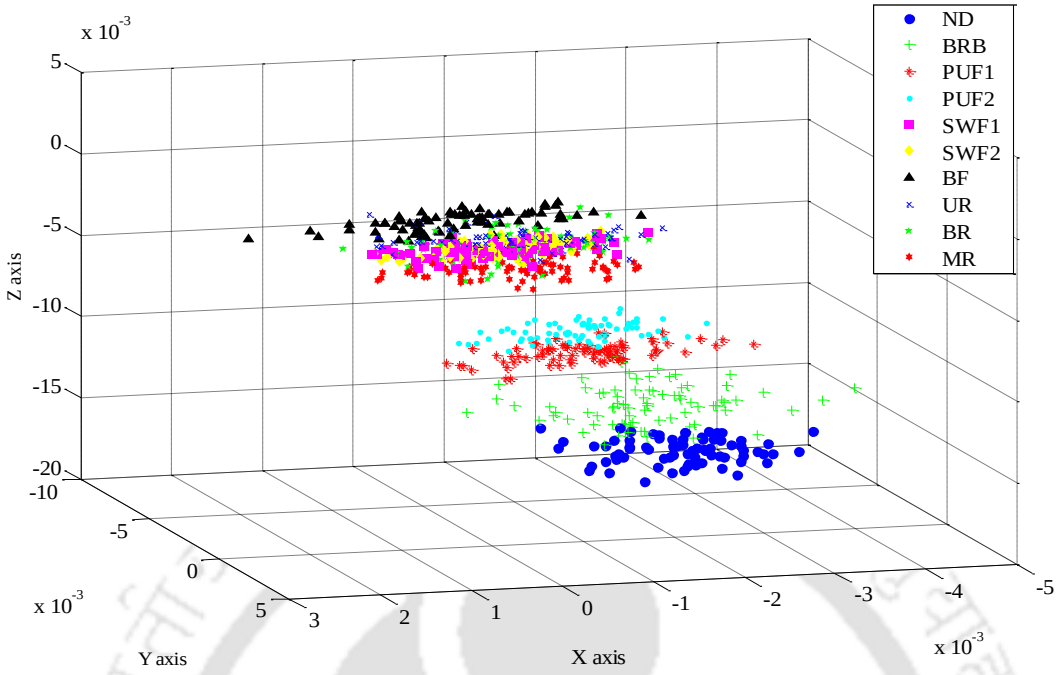

Figure 7.13 Feature distribution (μ_1) of Shannon wavelet coefficient of vibration for all IM faults at 30, 35 and 40 Hz, and T_3

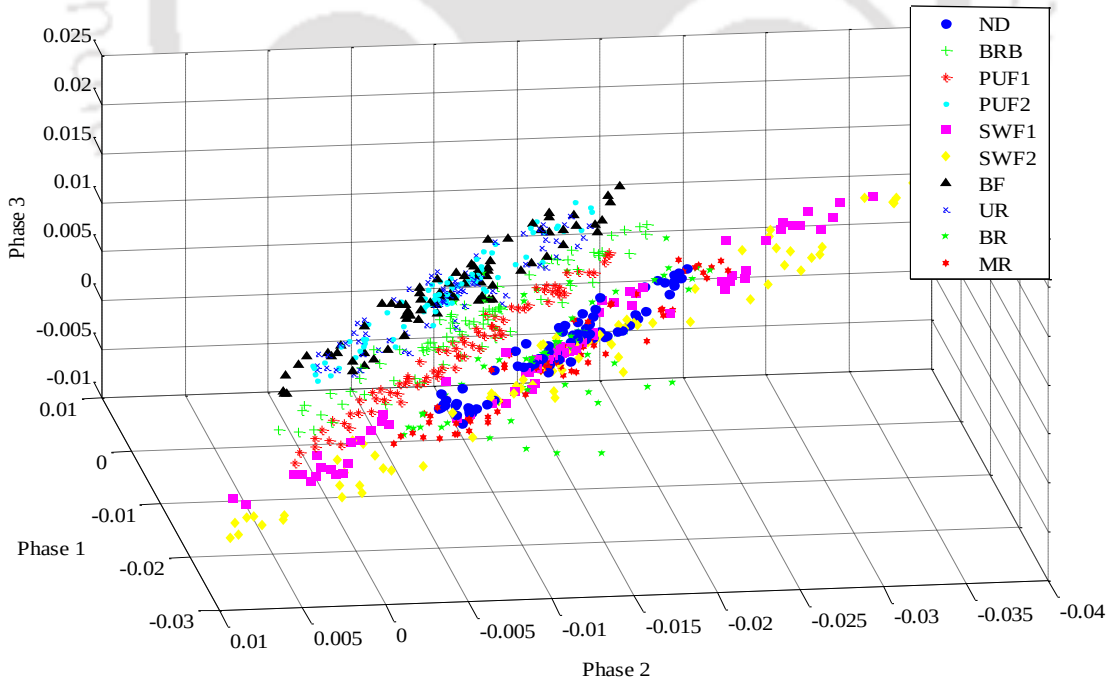

Figure 7.14 Feature distribution (μ_1) of Shannon wavelet coefficient of current for all IM faults at 30, 35 and 40 Hz, and T_3

7.3.5 Fault Diagnosis for the Intermediate Load case

The fault diagnosis is now performed at the intermediate load condition, where the SVM classifier is trained two IM loads and tested at the intermediate load level for which the classifier is not trained. However, for all cases the training and the testing are done at the same speed. Here, σ feature of the Shannon wavelet is used for the fault diagnosis, because the performance of this wavelet feature was better in the same speed and load case as well as in the intermediate speed case. In total, one condition of intermediate load with seven speeds are considered for the fault diagnosis, as shown in Table 5.9.

Fault prediction: The results of the fault diagnosis for this case are tabulated in Table 7.7. It shows that the overall accuracy varies from 90 % (at 10 Hz) to 100 % (at higher speeds). The lowest average of the individual accuracy is 85.7 % for the UR, because this fault condition is not classified at lower speeds, i.e., at 10 Hz (40 %) and 15 Hz (60 %). Besides this fault, all the faults are successfully classified, except ND at 20 Hz (66.6 %), SWF2 at 30 Hz (60 %) and BR at 10 Hz (60 %). It is observed that the average of overall prediction is achieved up to 96.4 %. That means all the fault conditions and their severities can be predicted successfully at all the speeds, even for the intermediate load case. This is obtained because there is no or little overlapping of feature from the vibration as well as the current for all the IM faults as shown in Figure 7.15 and Figure 7.16. These scatter plots are obtained at 20 Hz speeds. Some overlapping occurs between some fault features, still the prediction accuracy achieved up to 94.7 %. However, it is noticed that the overall prediction accuracy is 100 % at higher speeds that means the prediction is performed perfectly at higher speeds unlike the same speed and load case, and intermediate speed case, where the prediction was independent of speeds. The prediction performance is reduced by nearly 3.5 % as

compared to the same speed and 3 % as compared to the no load condition of the intermediate speed case. However, it is increased by 5-6 % in comparison to the light and high load conditions of the intermediate speed case. For the same case, the prediction performance is increased slightly, i.e. 0.4 % as compared to the time domain analysis; however, it is significantly increased, i.e. by 6 % in comparison to the frequency domain analysis.

Table 7.7 Fault diagnosis for various operating conditions of IM for the intermediate load case

Train speed (Hz)	Test speed (Hz)	Prediction accuracy, %										
		ND	BRB	PUF1	PUF2	SWF1	SWF2	BF	UR	BR	RM	Overall
Training at T_1 and T_3, and testing at T_2												
10	10	100	100	100	100	100	100	100	40	60	100	90
15	15	100	100	100	100	100	100	100	60	100	100	96
20	20	66.6	100	100	100	80	100	100	100	100	100	94.7
25	25	100	100	100	100	100	100	100	100	100	80	98
30	30	100	100	100	100	100	60	100	100	100	100	96
35	35	100	100	100	100	100	100	100	100	100	100	100
40	40	100	100	100	100	100	100	100	100	100	100	100
	avg.	95.2	100	100	100	97.2	94.3	100	85.7	94.3	97.2	96.4

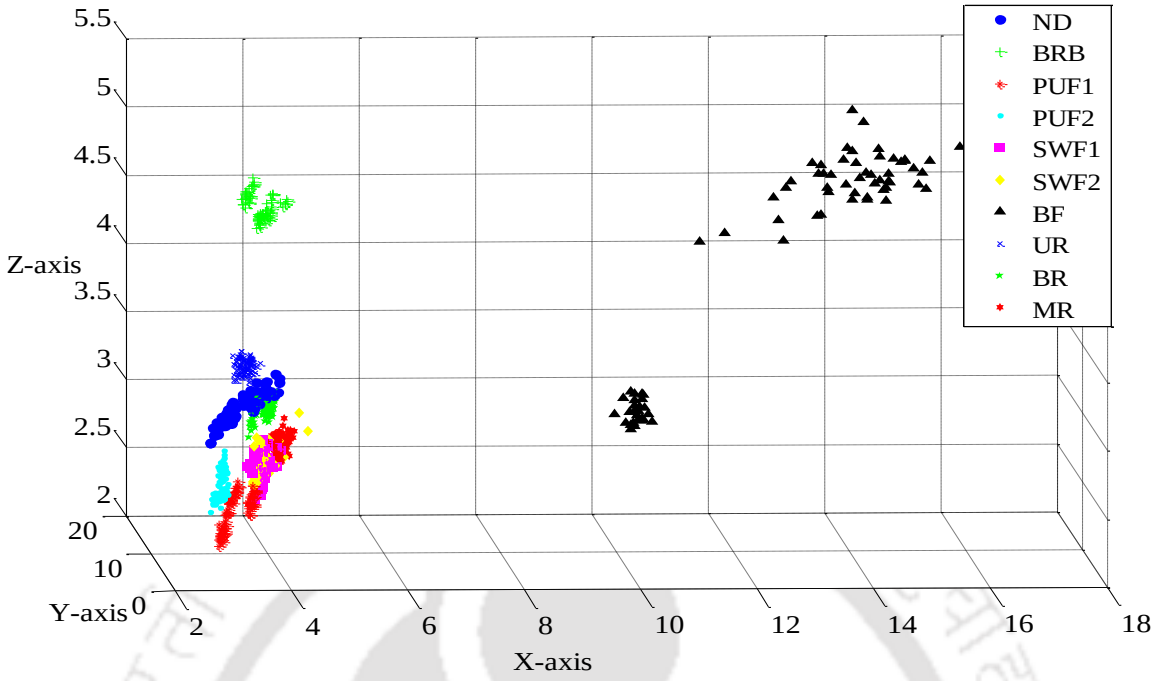

Figure 7.15 Feature distribution (σ) of Shannon wavelet coefficient of vibration for all IM faults at 20 Hz and T_1, T_2 and T_3

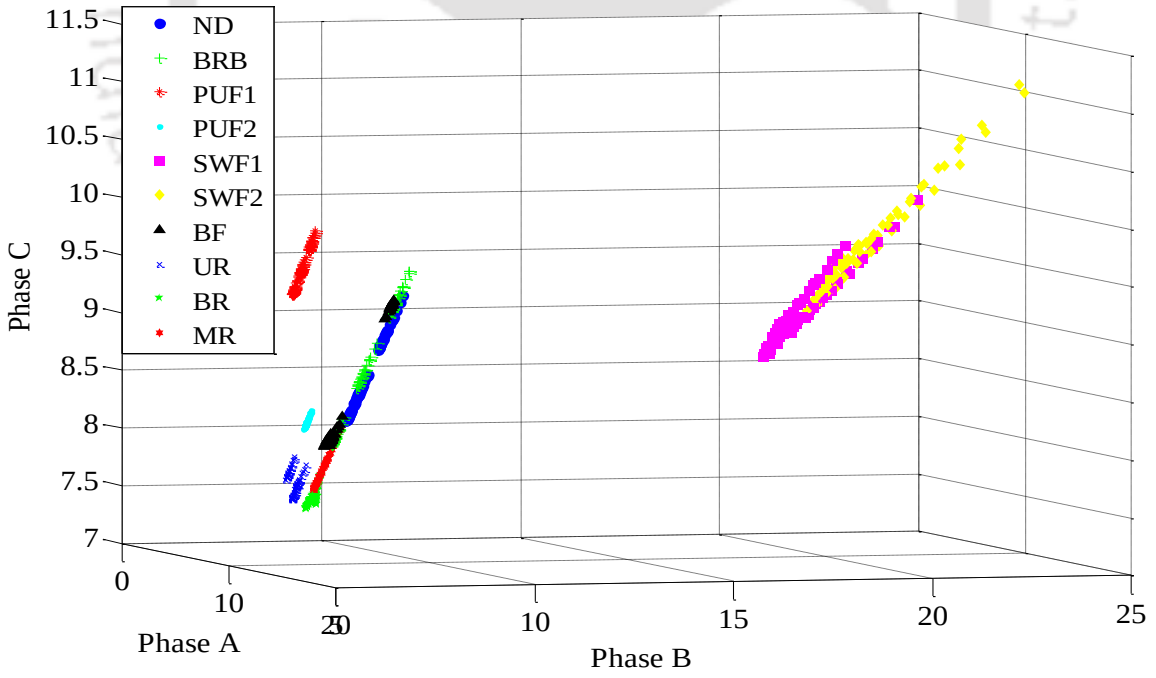

Figure 7.16 Feature distribution (σ) of Shannon wavelet coefficient of vibration for all IM faults at 20 Hz and T_1, T_2 and T_3

7.4 Summary

In this chapter, an attempt has been made to perform the multiple fault diagnosis and isolation in IMs based on CWT features and the SVM, where a combination of various mechanical and electrical faults have been diagnosed under various IM operational conditions. The vibration and current signals acquired under a lower sampling rate of 1 kHz and are used for the feature extraction based on the CWT. Number of features are extracted from wavelet coefficients of best scale which is selected based on RWE criterion. Feature are used as input to SVM and most appropriate features are selected based on the wrapper model and the SVM. The effect of ten different base wavelets on the prediction performance has been investigated and it is found that all the considered mother wavelets are able to diagnose the IM faults. Though, all the wavelets showed good prediction performance, the Shannon wavelet is found to be the most appropriate wavelet for the extraction of significant information from the vibration and current signals for the IM fault prediction.

The observation made from the experimental results show that the proposed diagnosis based on σ as the feature of the Shannon wavelet not only isolate different faults but also diagnose the faults under progression, perfectly. This characteristic is very important to predict the fault at an incipient stage. The proposed fault diagnosis could identify ten different IM fault conditions, simultaneously. It is observed from the results that the proposed fault diagnosis does not depend over the operational conditions of IMs, unlike time domain based diagnosis. It can perfectly (i.e., with 100 % accuracy) diagnose the faults at any considered IM speeds and level of load torques. Such robust fault predictions indicate more acceptability of the CWT based fault diagnosis for a practical application. Furthermore, the diagnosis is attempted for the intermediate speed and load

cases, the prediction performance is found to be very good and significantly increased in comparison to the time and frequency domain analyses. In all the three cases, the diagnosis based on CWT is better as compared to time and frequency domain based features, this is may be due to the ability of joint time and frequency representation of the CWT. The average computational time for the training and the testing is very less, i.e. 4 s for the same speed case and 8 s for the intermediate speed as well as intermediate load cases, which is the vital requirement of an online fault diagnostic.

In this chapter, one variant of WT, i.e. the CWT is used for the fault diagnosis, because it possesses perfect local property in both time space and frequency space. But in order to split the high frequency band, where the modulation information of the machine fault always exist, the other variant of WT, i.e. wavelet packet transform (WPT) should be used. Therefore, the WPT will be used for the fault diagnosis of IM in the following chapter.

CHAPTER 8

Multi-Fault Diagnosis of IM based on Wavelet Packet Transform Data

8.1 Introduction

In this chapter, the multi fault diagnosis in IMs is considered based on the wavelet packet transform (WPT) and the SVM. The wavelet transform is actually a subset of a far more versatile transform, the wavelet packet transform. Wavelet packets are particular linear combinations of wavelets. They form bases, which retain many of the orthogonality, smoothness, and localization properties of their parent wavelets. Coefficients in the linear combinations are computed by a recursive algorithm, making each newly computed sequence of wavelet packet coefficients the root of its own analysis tree. The enhanced signal decomposition capability in the high frequency region makes WPT an attractive tool for detecting and differentiating transient components with high frequency characteristics. The WPT is suitable for analyzing the transient and non-stationary signals because the same frequency bandwidth can provide good resolution regardless of high and low frequencies.

The WPT, the other variant of WT is thus adopted in this chapter to extract the effective features from different IM fault signals. Vibration signals in three orthogonal directions and current signals of the three phases are processed to extract time-frequency domain features based on the wavelet packet decomposition. Wavelet packets are decomposed up to 3rd level and wavelet coefficients are then calculated from each node. Subsequently, the most significant node needs to be selected from resulting nodes of the wavelet tree and for this a Relative Wavelet Energy (RWE) criterion has been used. The signal of the selected node is further processed to extract statistical features.

The most efficient features are chosen from considered features based on the wrapper model of the feature selection. The selected features are used to train the classifier and to produce a knowledgeable model for the diagnosis. A cross-validation along with the grid-search technique is used to optimally select SVM parameters for building an optimal model. To check the performance of different mother wavelets on the fault diagnosis, five wavelets have been used. The fault diagnosis is initially performed when the testing is considered at the same speed and load, then at intermediate speeds, and at intermediate loads as the training. In addition, to check the robustness of the present fault diagnosis, the diagnosis is performed for various operating conditions of the motor, i.e. a range of speeds and load torques.

8.2 Fault Feature Extraction

The classical wavelet transform like the Discrete Wavelet Transform (DWT) can provide good localization in both time domain as well as frequency domain, though it suffers from a poor frequency resolution in the high frequency region. The DWT offers constant *Q*-filtering that permits narrow bandwidth for low frequencies and high bandwidth for high frequencies. Consequently, it is challenging to differentiate the feature that comprises high frequency components. To resolve this problem, Coifman and Wickerhause (1992) generalized the DWT and introduced the WPT, which offers a better resolution in the higher frequency region that means a richer signal analysis. Similar to the DWT, the WPT has framework of the Multi Resolution Analysis (MRA). The main difference is that the WPT provides same frequency bandwidth in each resolution, since it divides the low as well as the high frequency sub-band. In other words, the WPT simultaneously disintegrates approximation and detail versions, unlike the DWT, which disintegrate only the approximation version. Due to this, in case of WPT, the information contained

in the original signal is not increased or lost due to the decomposition. Therefore, WPT is the most suitable for signal processing, particularly of non-stationary signals as the same frequency band can deliver better resolution irrespective of the low and high frequencies. The wavelet packet function is a time-frequency function set and can be defined by the following relationship

$$W_{j,k}^{m} = 2^{\frac{1}{2}} W^{m}\left(2^{j} t - k\right), \tag{8.1}$$

where the variable $m = 0, 1, 2, \ldots$ is the oscillation or the modulation parameter. Integers: j is the scale variable and k is the translation variable. First two wavelet packet functions are the scaling and mother wavelet functions, respectively.

$$W_{0,0}^{0}(t) = \phi(t), \tag{8.2}$$

$$W_{0,0}^{1}(t) = \psi(t), \tag{8.3}$$

The wavelet packet function for $m = 0, 1, 2, \ldots$ can be defined by the following recursive relationships

$$W_{0,0}^{2m}(t) = \sqrt{2}\sum_{k} h(k) W_{1,k}^{m}(2t - k), \tag{8.4}$$

$$W_{0,0}^{2m+1}(t) = \sqrt{2}\sum_{k} g(k) W_{1,k}^{m}(2t - k), \tag{8.5}$$

where $h(k)$ and $g(k)$ are the coefficients of the low pass and high pass filters of the Quadrature Mirror Filter (QMF), which are associated with the predefined scaling and mother wavelet function. The wavelet packet coefficients $W_{j,k}^{m}$ of a function, $f(t)$, can be computed via the inner product $\left\langle f(t), W_{j,k}^{m} \right\rangle$ defined as,

$$W_{j,k}^{m} = \left\langle f(t), W_{j,k}^{m} \right\rangle = \int f(t) W_{j,k}^{m}(t) dt. \tag{8.6}$$

For a signal S, the wavelet packet tree decomposition up to three resolution level is shown in Figure 8.1. Herein, A and D at each node represent the approximation and detail signal obtained by decomposition of a signal in the low and high pass filters, respectively. The approximation and detail signal are then itself divided into a second level approximation and a detail signal, and the process is repeated. Each node in the decomposition tree is the representative of a particular wavelet packet. The last numeric stands for the level of the decomposition tree and the down sampling. It describes that when the signal S (sampling frequency, f_s) is decomposed up to third resolution level, i.e. $j = 3$ with the WPT, the whole scaling space is divided into eight subspaces or also called packets, i.e. 2^j and the frequency interval of each subspace for a frequency interval $(0, 2^{-1} f_s)$ of the whole scaling space, can be calculated by [49]

$$((m-1)2^{-j-1} f_s, m2^{-j-1} f_s), \quad m = 1, 2, ..., 8, \tag{8.7}$$

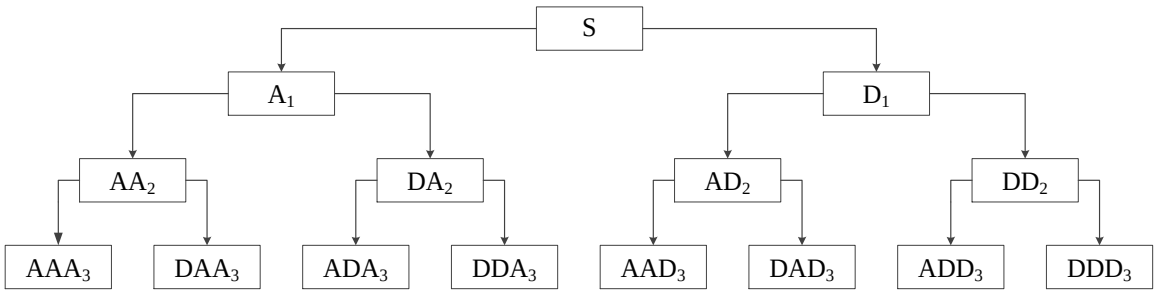

Figure 8.1 Three level wavelet packet decomposition tree

The wavelet has several mother wavelets or families. The most important mother wavelets are the Haar, Daubechies, Coiflet, Symlet and discrete Meyer. The WPT is considered to be useful for the feature extraction and the pattern recognition in many applications. Recently, the WPT as a signal processing technique is being preferred in the intelligent fault diagnosis because of its effectiveness. In a study, Ye et al. (2001) used the wavelet packet based features and the ANN for the fault diagnosis of broken rotor bar and air-gap eccentricity in IMs. Xian and Zeng (2009) have performed an intelligent fault diagnosis of the rotating machinery based on the WPT and the hybrid SVM. They compared the performance of the mother wavelet, like the Daubechies, Symlet and discrete Meyer, and the performance of the hybrid SVM and the BPN. The diagnosis result showed that the discrete Meyer wavelet with the SVM perform the best. Li *et al.* (2012) used the WPT feature for the fault diagnosis of the gearbox and the gasoline engine valve trains through the SVM.

In other works, Keskes *et al.* (2013), Keskes and Braham (2014), and Keskes and Braham (2015) have performed the fault diagnosis of the broken rotor bar in IMs by first combining the stationary WPT with OVO and OVA-SVM, then the pitch synchronous wavelet transform (PSWT) and the directed acyclic graph-SVM, and finally the recursive undecimated WPT and the DAG-SVM. In all these studies, they used different wavelet functions, like the Haar, Daubechies, and Symlet for

kernel functions of the SVM. The classification accuracy was achieved the best with the Daubechies kernel with the stationary WPT and the OVO-SVM, the Symlet kernel with the PSWT, and the RUWPT with the OVO and the DAG-SVM. Moreover, the RUWPT improves the detection time. Vishwakarma *et al.* (2015) proposed a bearing fault diagnosis in IMs based on the wavelet packet decomposition and the SVM, and showed that perfect prediction can be achieved using the energy feature of the 3rd level Daubechies mother wavelet.

In this chapter, five mother wavelets, namely the Haar, Daubechies, Coiflet, Symlet and discrete Meyer, are used to extract appropriate fault features as presented in Table 8.1. Wavelet packets up to three levels is applied to time domain data, which is obtained from experiments as shown in Figure 8.2. Wavelet packet coefficients are thus obtained at each node of the tree. However, the direct use of these coefficients of the nodes as features often reduces the classification performance, because some nodes of the tree do not have useful information for the feature extraction of the faults. Therefore, first an appropriate node of the tree is selected and then the features are extracted from the coefficient of these selected nodes. For the appropriate node selection, two approaches such as the single-level basis selection (SLBS) and the multi-level basis selection (MLBS), and different criterion such as the best basis selection (BBS) based on entropy and the local discriminant basis (LDB) extension of the BBS based on relative entropy can be used (Choi, 2008). The proposed work uses the SLBS approach that restricts the search space for the whole wavelet packet tree to only the lowest level of the decomposed wavelet tree. In order to select the most appropriate node, the relative wavelet energy (RWE) criterion has been used. According to the RWE criterion, the node which is having the maximum RWE is considered as an appropriate node. The RWE depends on the energy concentration of a certain signal and frequency

bands of the particular node. The RWE, which is the probability distribution of energy of each node of decomposed signals can be calculated as

$$\text{RWE}_{\text{m}} = p_m = \frac{E(m)}{E_{overall}} \tag{8.8}$$

where $\sum_m p_m = 1,$ The $E(m)$ is the total energy of decomposed signal at a particular node and is given by

$$E(m) = \sum_{j=1}^{n} \left| C_{m,j} \right|^2 \tag{8.9}$$

where, $C_{m,j}$ denotes j^{th} wavelet coefficients of the m^{th} node, j denotes the number of wavelet coefficients. The $E_{overall}$ is the total energy of the signal corresponding to all the nodes.

$$E_{overall} = \sum_{m=1}^{N} E(m) \tag{8.10}$$

where, $i = 1, 2, \ldots, N$ denotes each node. The RWE is calculated from Eqn. (8.8). Table 8.2 shows the RWE value based on the Haar wavelet for vibration signals in three orthogonal axes and current signals in three phases at 40 Hz speed and T_3 load for the ND and the BF. The table shows that for the vibration signal in the *x*-direction of the ND and the BF, the maximum RWE is for nodes (3, 7) and (3, 0), respectively. Therefore, these nodes are selected as appropriate nodes of the vibration

in *x*-direction. For the vibration signal in other directions and current signals, the appropriate nodes are selected similar to *x*-direction vibration. This process is repeated for all available data sets. After selecting the appropriate node, statistical features are now extracted from coefficients of this selected node. In order to select effective wavelet features for the proposed fault diagnosis, fourteen features, i.e. eight moments (μ_1 to μ_8), peak-to-peak (R_{pp}), crest factor, (CF), mean-to-standard-deviation (R_{msd}), standard deviation (σ), skewness (χ), and kurtosis (κ), have been extracted from each the five wavelet family. The procedure of feature extraction based on the WPT is shown in Figure 8.3. In total 25 raw time domain data sets are available, so 25 sets of wavelet coefficients corresponding to the most appropriate nodes are thus obtained. Now 14×25 feature datasets are extracted from each fault and operating conditions of IMs. In Appendix. A, Figure A.7 and Figure A.8 show the variation of all features obtained from Haar wavelet coefficients of the vibration and current signals, for the BF IM condition, 40 Hz speed and T_3 load. Now these wavelet features would be used as an input to the classifier to perform the fault diagnosis.

Table 8.1 Wavelet packet family and their order considered in this work

S. No.	Wavelet family (short name)	Considered order
1	Haar (db1)	(db1)
2	Daubechies (db)	(db44)
3	Coiflet (coif)	(coif5)
4	Symlet (sym)	(sym15)
5	Discrete Meyer (dmey)	(dmey)

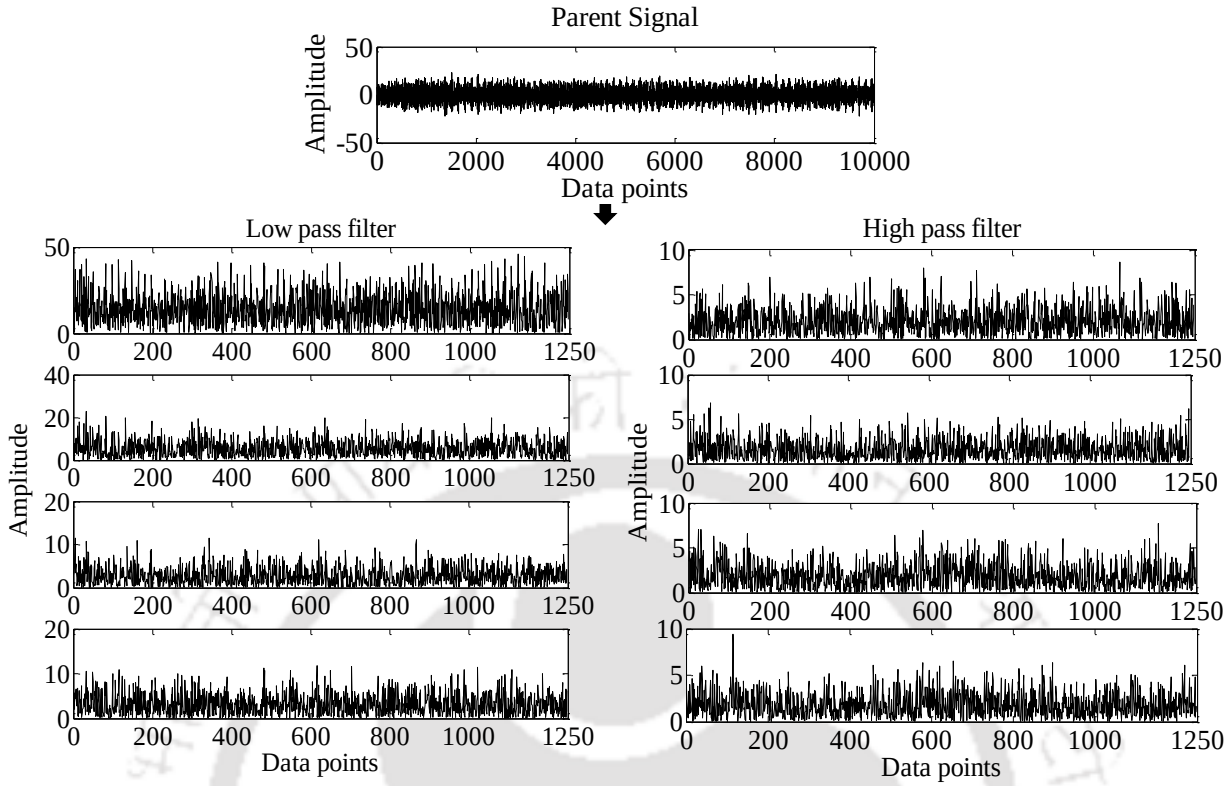

Figure 8.2 Parent signal and the third level of WP decomposition example for vibration signal in x-direction using the Haar family, BF, 40 Hz, T_3

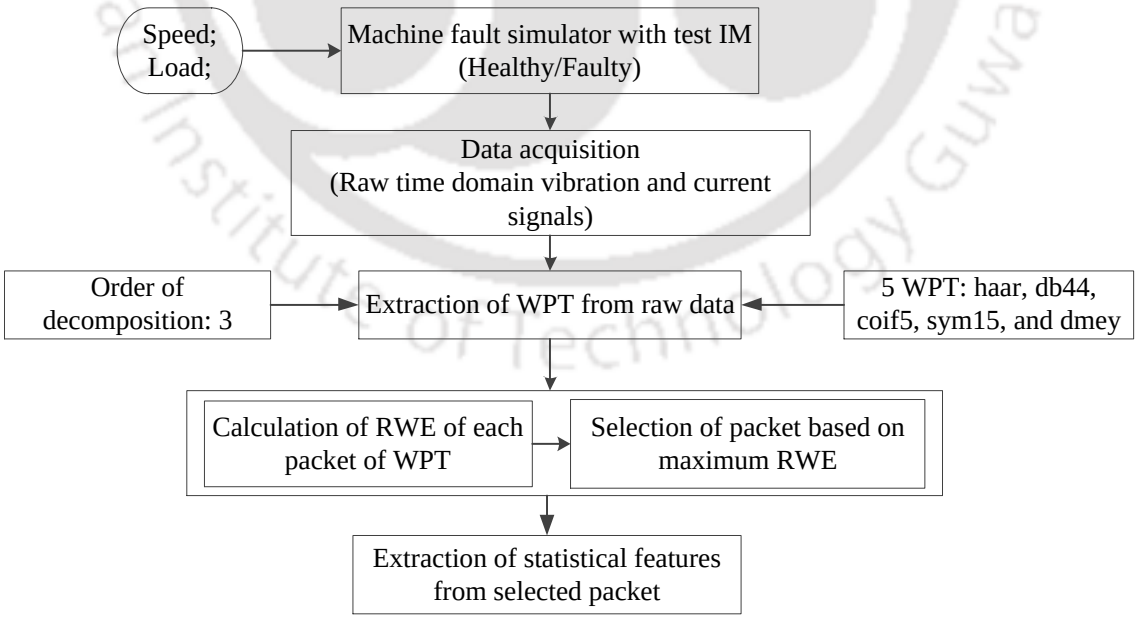

Figure 8. 3 The procedure of feature extraction based on the WPT

Table 8.2 The RWE of the Haar wavelet at third level for the vibration and current signals at 40 Hz and T_3

Wavelet Node	RWE (Vibration signal in *x*-axis)	RWE (Vibration signal in *y*-axis)	RWE (Vibration signal in *z*-axis)	RWE (Current signal in Phase A)	RWE (Current signal in Phase B)	RWE (Current signal in Phase C)
For No defect (ND)						
(3,0)	0.0633	0.0160	0.0274	0.0114	0.0114	0.0114
(3,1)	0.1201	0.0461	0.0646	0.0036	0.0036	0.0036
(3,2)	0.1389	0.0694	0.0896	0.0004	0.0004	0.0004
(3,3)	0.1264	0.0620	0.0702	0.0010	0.0009	0.0010
(3,4)	0.1306	0.1143	0.0962	0.0472	0.0471	0.0473
(3,5)	0.1021	0.2476	**0.2308**	0.0149	0.0148	0.0149
(3,6)	**0.1601**	**0.2840**	0.2233	0.2157	0.2157	0.2161
(3,7)	0.1585	0.1605	0.1978	**0.7059**	**0.7062**	**0.7054**
For Bearing Fault (BF)						
(3,0)	**0.7558**	**0.5569**	0.1217	0.0113	0.0113	0.0114
(3,1)	0.1170	0.0628	0.0653	0.0035	0.0035	0.0035
(3,2)	0.0310	0.0303	0.0914	0.0004	0.0003	0.0004
(3,3)	0.0410	0.0396	0.0779	0.0009	0.0009	0.0009
(3,4)	0.0167	0.0455	0.1024	0.0469	0.0469	0.0470
(3,5)	0.0104	0.0927	**0.2579**	0.0145	0.0145	0.0146
(3,6)	0.0144	0.1123	0.2330	0.2146	0.2145	0.2144
(3,7)	0.0136	0.0600	0.0503	**0.7079**	**0.7081**	**0.7078**

8.3 Fault Diagnosis based on SVMs

After the feature extraction based on the WPT, the SVM using one-versus-one multi-class technique has been applied to perform the IM fault diagnosis in this section. Three cases, i.e. the

same speed and same load case, the intermediate speed, and the intermediate load, are considered for the fault diagnosis.

8.3.1 SVM Parameters Selection and Training

A grid-search technique along with cross-validation is used for the training to realize the parameter selection of the SVM. The training of SVM is performed for each feature of all wavelet functions at all considered operating conditions of IMs. Results of the training, for all features of a Haar wavelet for a typical case of 40 Hz and *T3,* are shown in Figure 8.4 and Figure 8.5. The Figure 8.4 (a) shows that the CV accuracy is achieved up to 100 % using μ_1 only. That means the classifier is well learned with this feature. In addition, the classifier is successfully learned for the second to fifth moments, however, the CV accuracy is significantly decreased with higher moments, i.e. μ_6-μ_8. Other features like, *CF*, R_{msd} also does not give the good training accuracy as shown in Figure 8.5. In this case, with the skewness and the kurtosis, the training accuracy is significantly decreased as compared to the time, frequency and CWT analyses. However, the standard deviation gives very good CV accuracy (99.47 %), similar to other analyses. Two features which give the best CV accuracy (i.e., μ_1 and σ) is now tries in combination and the accuracy is found to be 100 % as shown in Figure 8.5 (g). That means the classifier is well learned with this feature set. Now, SVM parameters that are selected corresponding to the highest CV accuracy, would be used as an input to the SVM in order to build the final model, for each feature. The final prediction will be done using the final model to predict the unknown data that are not used in the training phase.

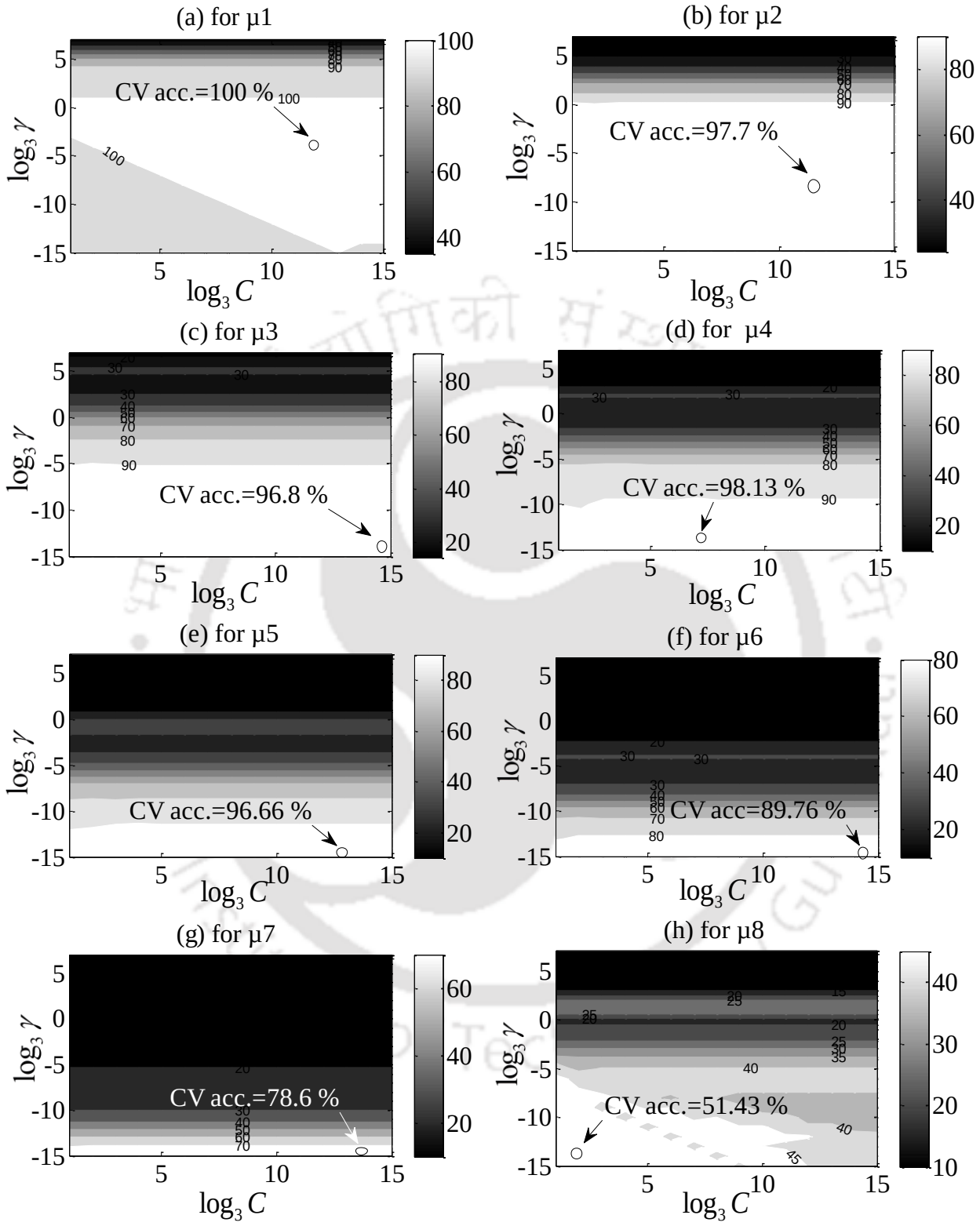

Figure 8.4 Cross-validation accuracy at 40 Hz and T_3, for the Haar wavelet

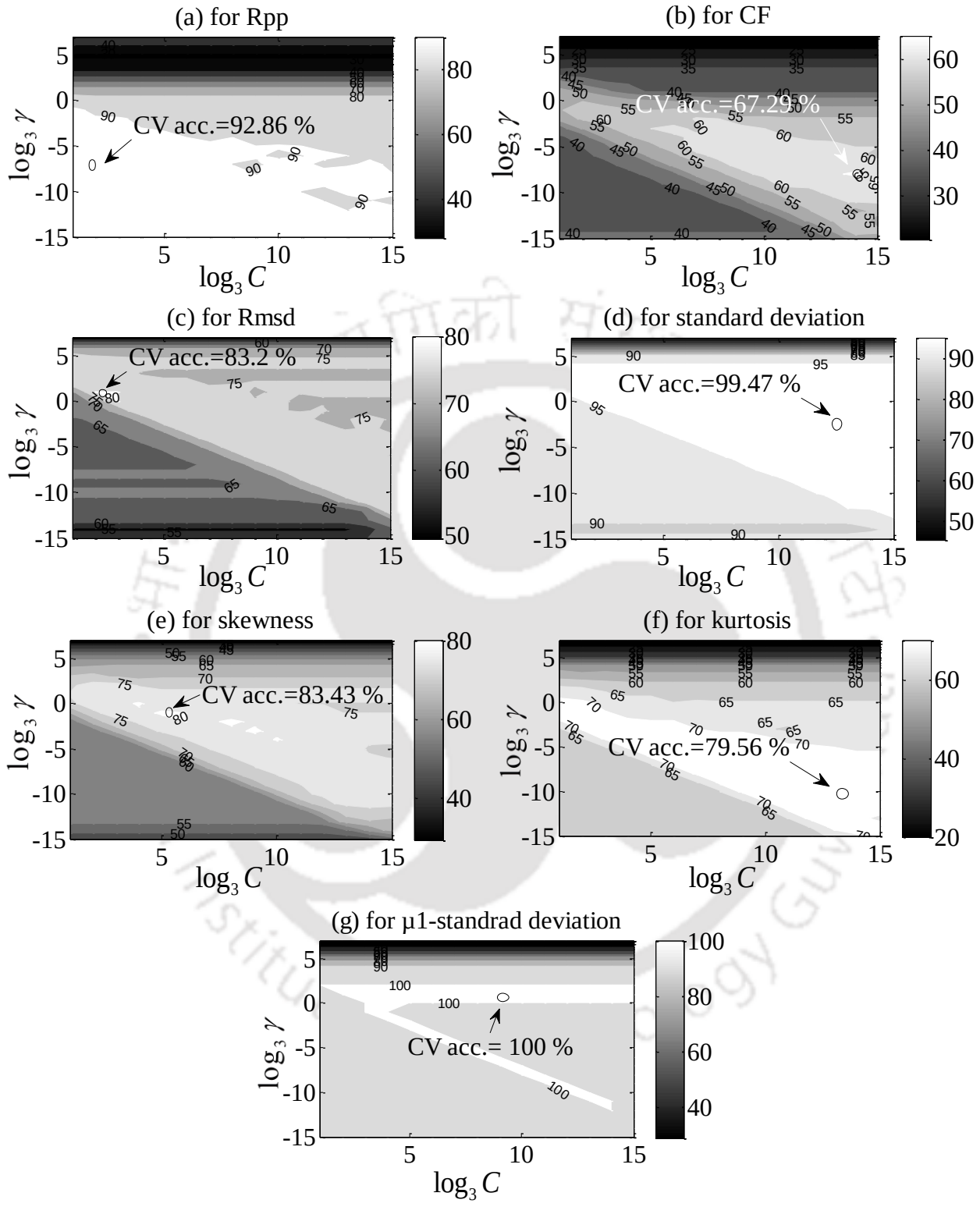

Figure 8.5 Cross-validation accuracy at 40 Hz and T_3, for the Haar wavelet

8.3.2 Fault Feature Selection

All fourteen features, obtained from the Haar, Daubechies, Coiflet, Symlet, and discrete Meyer, are initially used for the fault diagnosis, then the appropriate feature(s) is/are selected based on the wrapper model. In order to choose the best features, the fault diagnosis is performed for the high-load condition. For effectiveness, overall prediction accuracies for seven motor speeds are obtained and average results are presented in Table 8.3. It shows that for all WPTs, some features such as initial five moments (μ_1 to μ_5) and the standard deviation perform satisfactorily with a minimum accuracy of about 95 %; however, remaining features such as last three higher moments (μ_6 to μ_8), R_{pp}, CF, R_{msd}, χ and κ do not perform satisfactory. Consequently, extracted features based on WPTs are not all useful for diagnosing IM fault conditions. That means they contain redundant and irrelevant information, hence do not significantly represent different IM faults. These features are thus discarded from the fault diagnosis. Among the remaining effective features (i.e., μ_1 to μ_5 and σ), μ_1 and σ performs with the maximum average prediction accuracy, i.e. 98.14 % and 97.03 %, respectively. According to the wrapper model, WPT features, i.e., μ_1 and σ are selected as the most suitable individual features for the present fault diagnosis. Therefore, a combination of these features (i.e., μ_1 and σ) is tried based on all five WPTs. The performance of each wavelet increases with this feature set as compared to μ_1 and σ alone. All WPTs with the feature combination of μ_1 and σ are performed excellently, and nearly comparable for the present fault diagnosis. This feature set is selected as the most suitable feature based on the WPT. Now this feature set will be used for further fault diagnosis in this chapter.

Table 8.3 Statistical features selection by the wrapper model for T_3 load

	Average of overall prediction accuracy, %							
WPT	μ_1	μ_2	μ_3	μ_4	μ_5	μ_6	μ_7	μ_8
haar	98.57	95.71	94.28	95.61	95.95	90.94	72.8	42.85
db44	98.09	96.9	95.75	95.95	95.8	89.5	71.09	39.71
coif5	97.85	97.14	95.14	94.9	95.6	90.33	70.95	45.85
sym15	98.33	97.14	96.18	95.95	94.66	89.14	72.57	41.18
dmey	97.84	96.9	96.42	94.9	94.33	89.84	75.71	42.14
avg	98.14	96.76	95.55	95.46	95.27	89.95	72.62	42.35
	R_{pp}	CF	R_{msd}	σ	χ	K	σ-χ-κ	μ_1-σ
haar	93.95	71.6	89.02	96.41	86.71	83.32	97.14	98.57
db44	88.33	56.42	77.14	97.85	81.66	69.04	98.33	98.33
coif5	93.74	62.33	85.74	96.65	80.23	74.9	98.56	98.57
sym15	95.55	66.1	83.66	96.66	84.75	68.74	97.85	98.57
dmey	92.84	68.74	81.85	97.6	83.32	66.66	96.1	99.43
avg	92.88	65.04	83.48	97.03	83.33	72.53	97.60	98.69

8.3.3 Fault Diagnosis for the Same Speed and Load Case

After selecting the best wavelet features, the fault diagnosis is now performed for various operating conditions of the same speed and load case. However, Table 8.3 shows that all the considered mother wavelet with μ_1 and σ can perform the fault diagnosis of IMs effectively; however, the discrete Mayer wavelet performs the best with the prediction accuracy of 99.43 %. That means this wavelet with the mean and the standard deviation characterized all IM faults, effectively. Therefore, this feature-wavelet combination is now used for the fault diagnosis for various operating conditions of IM. The various operating conditions of IMs that are considered in the same speed and load case is shown in Table 5.4. The diagnosis results in the form of the individual and overall prediction accuracy are listed in Table 8.4.

Fault prediction: The fault diagnosis is first performed for seven different motor speeds when there is no load applied on IM externally. Table 8.4 shows that the average of overall prediction accuracy is obtained as 99.52 %. It is noted that, the overall prediction accuracy is obtained as 100 % at all considered speeds except 40 Hz, where the prediction is 96.66 %. That means all IM faults and their severity are perfectly classified at all speeds except the stator winding fault for its second severity level (or SWF2) at 40 Hz (66.66 %). To show the misclassification of SWF2 data at 40 Hz, a confusion matrix has been obtained as shown in Table 8.5. It shows that 33.33 % of the SWF2 data are misclassified with the SWF1 data. Now, the fault diagnosis is performed for all considered speeds when the IM is lightly loaded. Results in Table 8.4 show that the average of overall prediction accuracy is equal to 99.05 %. It is noted that overall prediction accuracies are obtained as 100 %, except at 25 Hz (98.33 %), 35 Hz (98.33 %) and 40 Hz (96.66 %). Thus, it can be concluded that all fault conditions are perfectly classified except two conditions, i.e. the phase unbalance for its second severity level (or PUF2) for 25 Hz (83.33 %) and the stator winding fault at the second severity level (or SWF2) for 35 Hz (83.33 %) and 40 Hz (66.66 %). To show the misclassification of the data, a confusion matrix at 25 Hz has been obtained as shown in Table 8.5. It shows that 16.66 % of the PUF2 data are misclassified with PUF1 data. It is noted that the PUF1 and the PUF2 are two severity levels of the same faults. At the end, the fault diagnosis is performed when there is high load on IMs. Results in Table 8.4 show that the average of overall prediction accuracy achieved is 99.43 %. Moreover, the overall prediction accuracy is 100 %, except 40 Hz (96 %), similar to no load case. All fault conditions are perfectly classified except SWF2 (60 %) at 40 Hz. To show the misclassification of the SWF2 data at 40 Hz, a confusion matrix has been obtained as shown in Table 8.5. It illustrates that the individual prediction accuracy for SWF2 is 60 %, and 40 % of its data are misclassified with the SWF1.

Table 8.4 Fault diagnosis for various operating conditions of IM for the same speed and load case

Train speed (Hz)	Test speed (Hz)	Prediction accuracy, %										
		ND	BRB	PUF1	PUF2	SWF1	SWF2	BF	UR	BR	MR	Over.
For no load, T_1												
10	10	100	100	100	100	100	100	100	100	100	100	100
15	15	100	100	100	100	100	100	100	100	100	100	100
20	20	100	100	100	100	100	100	100	100	100	100	100
25	25	100	100	100	100	100	100	100	100	100	100	100
30	30	100	100	100	100	100	100	100	100	100	100	100
35	35	100	100	100	100	100	100	100	100	100	100	100
40	40	100	100	100	100	100	66.66	100	100	100	100	96.66
	Avg.	100	100	100	100	100	95.24	100	100	100	100	99.52
For light load, T_2												
10	10	100	100	100	100	100	100	100	100	100	100	100
15	15	100	100	100	100	100	100	100	100	100	100	100
20	20	100	100	100	100	100	100	100	100	100	100	100
25	25	100	100	100	83.3	100	100	100	100	100	100	98.33
30	30	100	100	100	100	100	100	100	100	100	100	100
35	35	100	100	100	100	100	83.33	100	100	100	100	98.33
40	40	100	100	100	100	100	66.67	100	100	100	100	96.66
	Avg.	100	100	100	97.6	100	92.86	100	100	100	100	99.05
For high load, T_3												
10	10	100	100	100	100	100	100	100	100	100	100	100
15	15	100	100	100	100	100	100	100	100	100	100	100
20	20	100	100	100	100	100	100	100	100	100	100	100
25	25	100	100	100	100	100	100	100	100	100	100	100
30	30	100	100	100	100	100	100	100	100	100	100	100
35	35	100	100	100	100	100	100	100	100	100	100	100
40	40	100	100	100	100	100	60	100	100	100	100	96
	Avg.	100	100	100	100	100	94.29	100	100	100	100	99.43

Table 8.4 shows that out of twenty-one cases of fault diagnosis, (i.e., 3 loads × 7 speeds), only in five cases, some misclassification (maximum up to 4 %) are there. In these five cases, either the PUF2 data or SWF2 data are misclassified with the data of PUF1 and SWF1, respectively. The reason is that PUF1 and PUF2 are two severity levels of the same fault, i.e. the phase unbalance. Similarly, SWF1 and SWF2 are also two severity levels of the stator winding fault. So if there is no large difference between two severity levels of the fault, then it is less chances of producing distinct features. These features can be misclassified with each other. However, in the most of the cases, all IM faults and their severity levels are classified perfectly, i.e. with 100 % prediction accuracy at all operating conditions of IMs. This is because the selected feature set of μ_1 and σ of discrete Mayer wavelet has the capability to clearly distinguish the ten IM fault conditions in the feature space. These can be seen in feature clusters in Figure 8.6 and Figure 8.7. However, these feature clusters are obtained for 40 Hz and T_1 load, where due to little overlapping of features of some faults, the diagnosis accuracy is reduced to 96.66 %.

Table 8.5 Confusion matrix of fault diagnosis for the same speed and load case

Operating conditions	Misca-sified fault	Classification percentage									
		ND	BRB	PUF1	PUF2	SWF1	SWF2	BF	UR	BR	MR
T_1, 40 Hz	SWF2	0	0	0	0	33.33	66.67	0	0	0	0
T_2, 25 Hz	PUF2	0	0	16.67	83.33	0	0	0	0	0	0
T_2, 35 Hz	SWF2	0	0	0	0	16.67	83.33	0	0	0	0
T_2, 40 Hz	SWF2	0	0	0	0	33.33	66.67	0	0	0	0
T_3, 40 Hz	SWF2	0	0	0	0	40	60	0	0	0	0

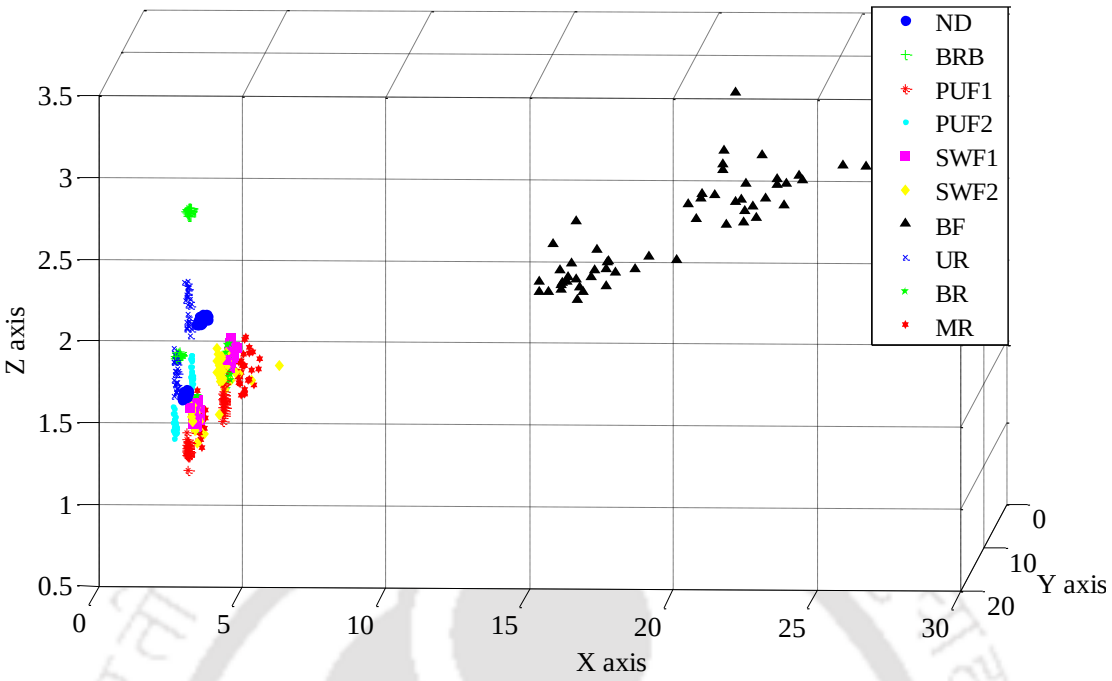

Figure 8.6 Feature distribution (μ_1, σ) of discrete Meyer wavelet coefficient of vibration signal for all IM faults at 40 Hz and T_1

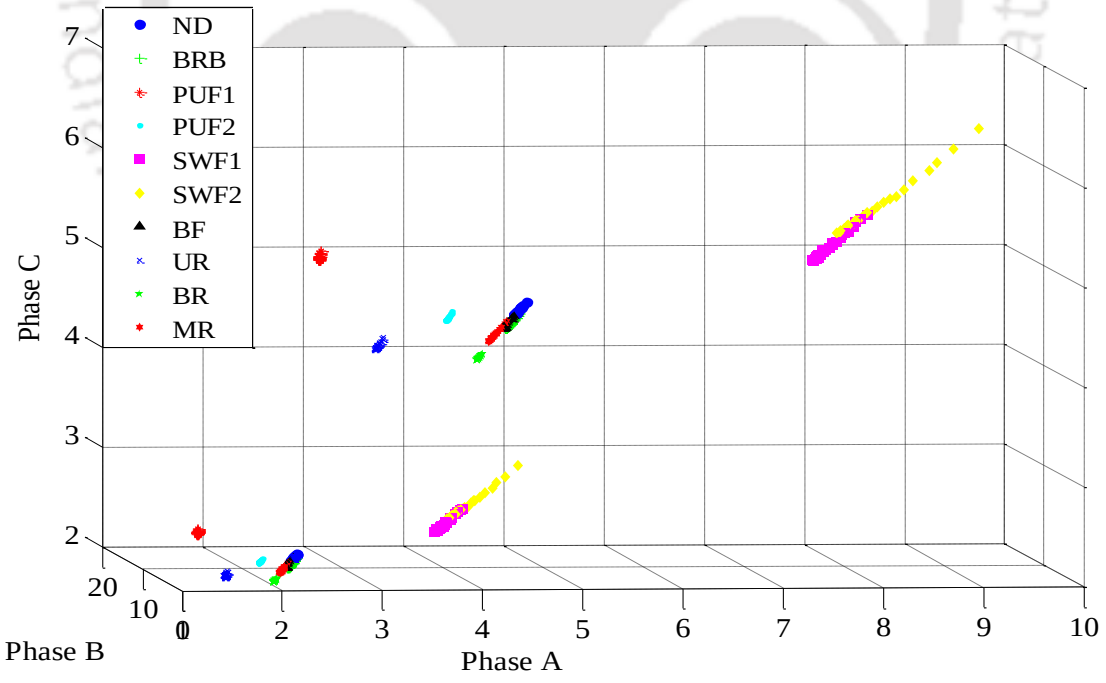

Figure 8.7 Feature distribution (μ_1, σ) of discrete Meyer wavelet coefficient of the current signal for all IM faults at 40 Hz and T_1

8.3.4 Fault Diagnosis for the Intermediate Speed Case

The fault diagnosis is now performed by training the SVM at two rotational speeds and tested at an intermediate speed for which the SVM is not trained. However, the training and the testing are done at same loads. Here, μ_1 and σ of the Discrete Meyer wavelet is selected for the fault diagnosis, because the performance of this wavelet feature combination was better in the same speed and load case. In total, five condition of intermediate speeds for each load are considered for the fault diagnosis, as shown in Table 5.7.

***Fault prediction*:** The results of the fault diagnosis for this case are tabulated in Table 8.6. When the fault diagnosis is performed at no load, the lowest overall accuracy is 85.6 % (at 35 Hz), and it increases up to 100 % (at 25 Hz). The lowest average of individual accuracy is 79.2 % for the MR since this fault is not classified at 30 Hz (40 %) and 35 Hz (56.14 %). Other faults are successfully classified at all the speeds, except for some cases, i.e. the BRB at 35 Hz (60 %), and the SWF2 at 15 Hz (60 %) and 35 Hz (60 %). When the diagnosis is performed at the light load, the overall accuracy is varied from 78.66 % (at 35 Hz) to 100 % (at 20 Hz). In this case, the BR is not successfully classified at higher speeds, i.e. the speed more than 25 Hz; however, it is perfectly classified at lower speeds. All fault conditions are successfully classified here, except few cases, i.e. the BRB at 35 Hz (60 %), the SWF2 at 15 Hz (40 %) and 35 Hz (60 %), and the MR at 30 Hz (40 %) and 35 Hz (60 %). When the diagnosis is performed with heavily loaded motor, the overall accuracy varies from 83.03 % (30 Hz) to 96.66 % (15 Hz). The lowest individual accuracy is found to be around 76 % for the BRB and the SWF2 since these two faults are not classified at the most of intermediate speeds. However, other faults are classified successfully almost all speeds except, the ND at 25 Hz (60 %) and 30 Hz (60 %), the BF at 30 Hz (66 %), the UR at 35 Hz (60 %), the

BR at 30 Hz (68.3 %), and the MR at 30 Hz (76 %) and 35 Hz (68.12 %). It is also noted that at all load conditions, prediction performances are better at lower speeds and the most of the misclassification occurs at higher speeds like in the time domain analysis.

It is observed from Table 8.6 that the average of overall accuracies are 94.32 %, 91.33 % and 90.03 %, corresponding to the no, light and high loads, respectively. That means the diagnosis is better at no load than other load, it is similar to the time domain and CWT analyses. This is due to little overlapping of vibration features of some faults (i.e., ND and BRB, SWF1 and SWF2, also BR and MR) at no load as compared to high load; however, at both load conditions the current features are well separated for all ten IM faults, as shown in Figure 8.8 to Figure 8.11. In spite of overlapping of vibration features, average predictions are achieved more than 90 % at all load conditions, even when the fault information is limited. Overall performances for the same case are increased by 1-3 % as compared to time domain analyses, 3-6 % as compared to frequency domain analyses. However, it is decreased by around 5 % at the no load, similar at the light and high loads as compared to the CWT analysis. Performances for the intermediate speed cases are decreased by 5-9 % in comparison to the same speed and load case. This is due to high range of speeds that are considered for the training, i.e. 10 Hz range. The performance can be further improved if a narrow range of training speeds or multiple speed case is considered for the training.

Table 8.6 Fault diagnosis for various operating conditions of IM for intermediate speed case

Train speed (Hz)	Test speed (Hz)	Prediction accuracy, %										
		ND	BRB	PUF1	PUF2	SWF1	SWF2	BF	UR	BR	MR	Over.
For no load, T_1												
10,20	15	100	100	100	100	100	60	100	100	100	100	96
15,25	20	100	80	100	100	100	100	100	100	100	100	98
20,30	25	100	100	100	100	100	100	100	100	100	100	100
25,35	30	100	100	100	100	100	100	80	100	100	40	92
30,40	35	80	60	100	100	100	60	100	100	100	56.14	85.61
	Avg.	96	88	100	100	100	84	96	100	100	79.2	94.32
For light load, T_2												
10,20	15	100	100	100	100	100	40	100	100	100	100	94
15,25	20	100	100	100	100	100	100	100	100	100	100	100
20,30	25	100	100	100	100	100	100	100	100	40	100	94
25,35	30	100	100	100	100	100	100	100	100	60	40	90
30,40	35	80	60	100	100	100	60	100	80	46.6	60	78.66
	Avg.	96	92	100	100	100	80	100	96	69.3	80	91.33
For high load, T_3												
10,20	15	100	100	100	100	100	66.6	100	100	100	100	96.66
15,25	20	100	60	100	100	100	100	100	100	100	100	96
20,30	25	60	40	100	100	100	60	100	100	100	100	86
25,35	30	60	80	100	100	80	100	66	100	68.3	76	83.03
30,40	35	100	100	100	100	100	56.28	100	60	100	68.12	88.44
	Avg.	84	76	100	100	96	76.6	93.2	92	93.7	88.8	90.03

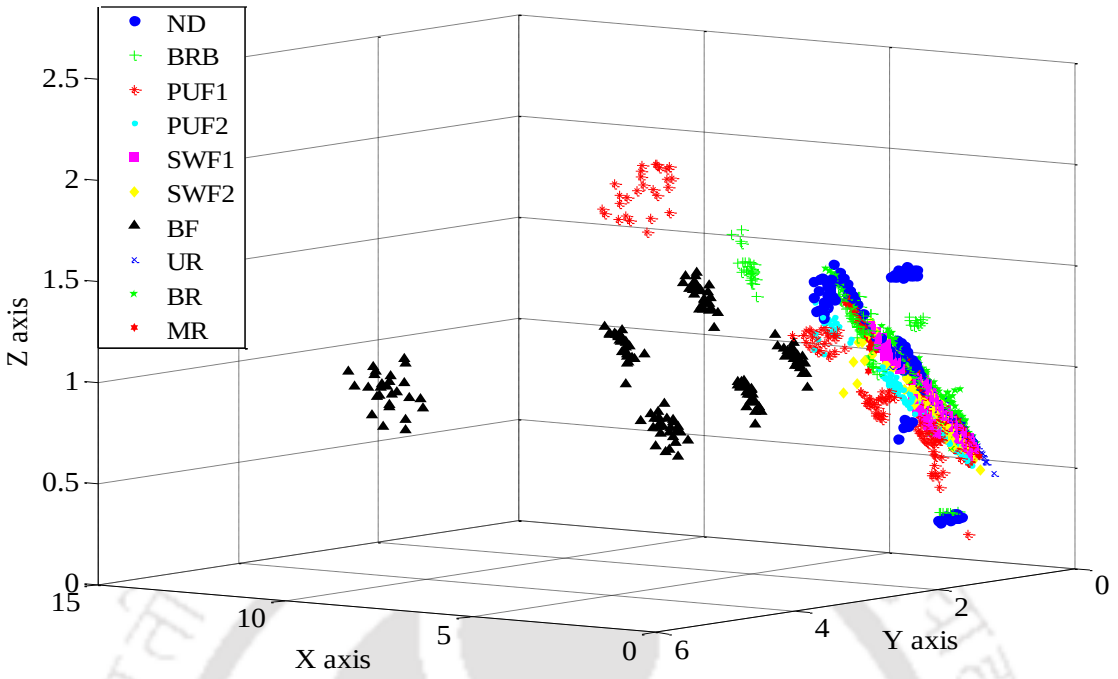

Figure 8.8 Feature distribution (μ_1, σ) of the discrete Meyer wavelet coefficient of vibration signals for all IM faults at 30, 35, 40 Hz and T_1

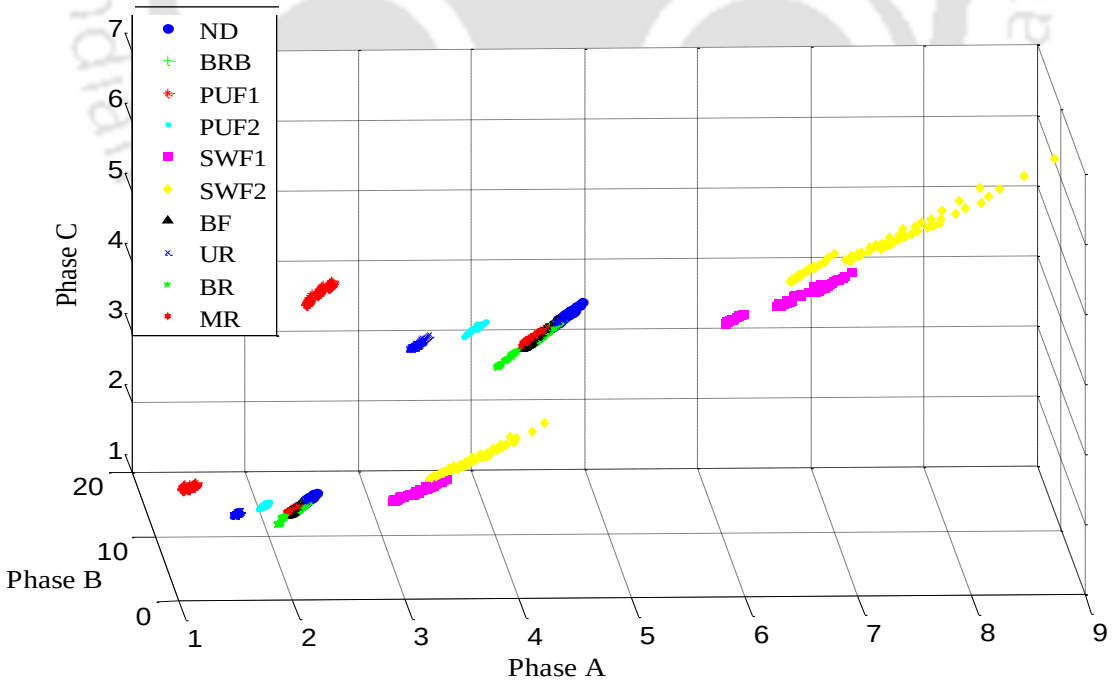

Figure 8.9 Feature distribution (μ_1- σ) of the discrete Meyer wavelet coefficient of vibration signals for all IM faults at 30, 35, 40 Hz and T_1

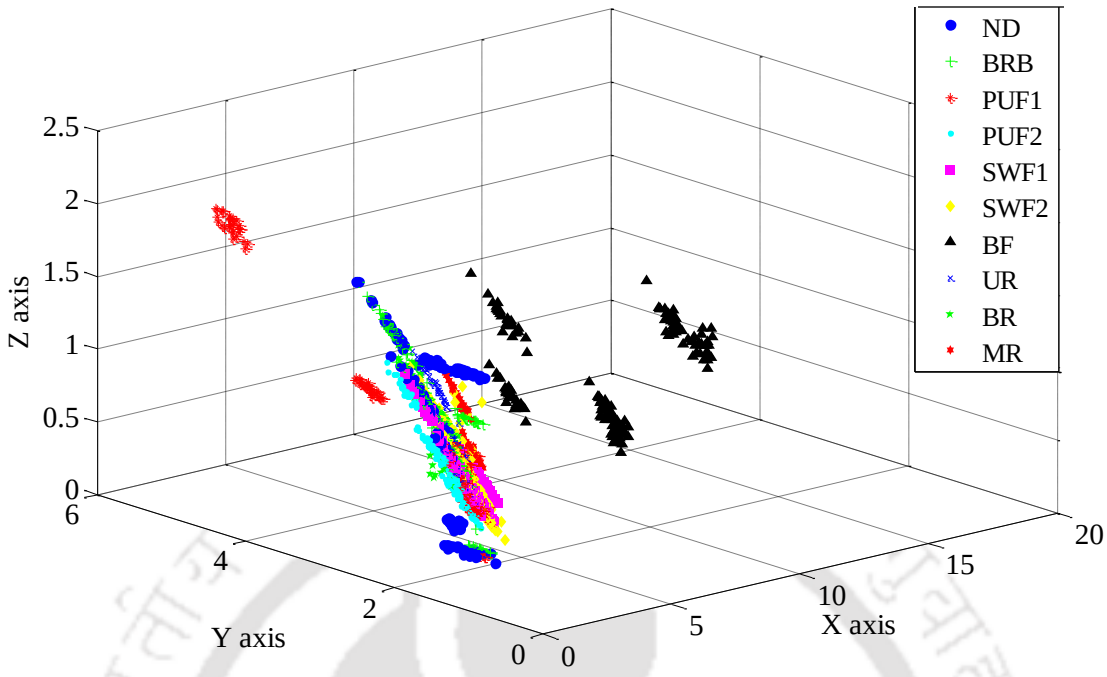

Figure 8.10 Feature distribution (μ_1, σ) of the discrete Meyer wavelet coefficient of vibration signals for all IM faults at 30, 35, 40 Hz and T_3

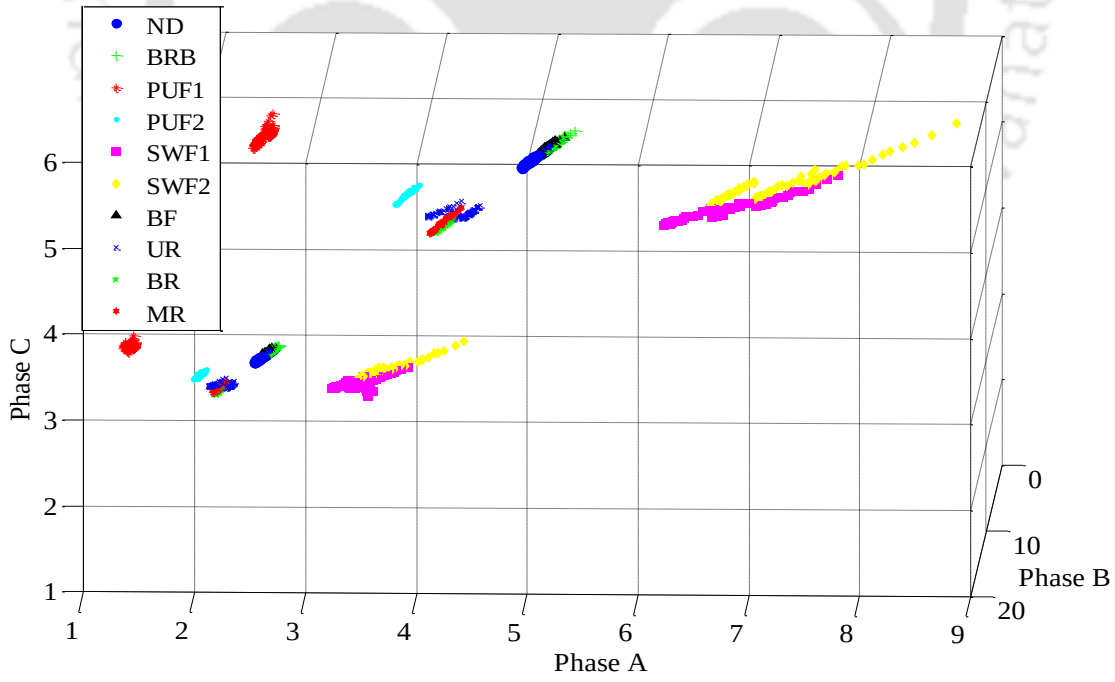

Figure 8.11 Feature distribution (μ_1, σ) of the discrete Meyer wavelet coefficient of current signals for all IM faults at 30, 35, 40 Hz and T_3

8.3.5 Fault diagnosis for the intermediate load case

Now the fault diagnosis is performed for the intermediate load case. One condition of intermediate load with seven speeds are considered for the fault diagnosis, as shown in Table 5.9.

Fault prediction: The results of the fault diagnosis for the case of intermediate load are shown in Table 8.7. It is observed the overall accuracy varies from 94.9 % (at 10 Hz and 30 Hz) to 100 % (at 25 and 35 Hz). That means the fault diagnosis for this case is independent of speeds. In addition, the lowest average of individual accuracy is 89.9 % for the SWF2 since this fault is not predicted at 30 Hz (66.6 %). However, this fault is successfully predicted at all other speeds. All other fault conditions are successfully predicted at all speeds, except the PUF2 at 10 Hz (76.66 %) and the UR at 20 Hz (56.6 %). All ND, BRB, BF, BR and RM are perfectly predicted (i.e., 100 %) at all the speeds. From Table 8.7, it is observed that the average of overall accuracy is 97.7 %. That means the fault diagnosis can be effectively performed for any motor speeds even for the limited information about the load. This is obtained because the clusters of vibration and current signal features for all the IM faults are well separated as shown in Figure 8.12 and Figure 8.13. However, these figures show little overlapping of features and that is why the accuracy, reduced to 94.9 % for 10 Hz. It is noted that the fault diagnosis performance is increased by 3-7 % as compared to intermediate speed cases; however, it is reduced by about 2 % as compared to the same speed and same load case. For this case, when the performance is compared with the time domain, frequency domain and CWT analyses, the highest prediction is achieved with the WPT. The performance is increased by 7 % as compared to frequency domain, 1.7 % as compared to time domain, and about 1 % as compared to CWT analyses.

Table 8.7 Fault diagnosis for various operating conditions of IM for the intermediate load case

Train speed (Hz)	Test speed (Hz)	Prediction accuracy, %										
		ND	BRB	PUF1	PUF2	SWF1	SWF2	BF	UR	BR	RM	Overall
Training at T_1 and T_3, and testing at T_2												
10	10	100	100	92.3	76.7	100	80	100	100	100	100	94.9
15	15	100	100	100	100	100	100	100	100	100	100	100
20	20	100	100	100	100	100	100	100	56.6	100	100	95.6
25	25	100	100	100	100	100	100	100	100	100	100	100
30	30	100	100	100	100	83.18	66.6	100	100	100	100	94.9
35	35	100	100	100	100	100	100	100	100	100	100	100
40	40	100	100	100	100	100	83.3	100	100	100	100	98.3
	Avg.	100	100	98.9	96.7	97.6	89.9	100	93.8	100	100	97.7

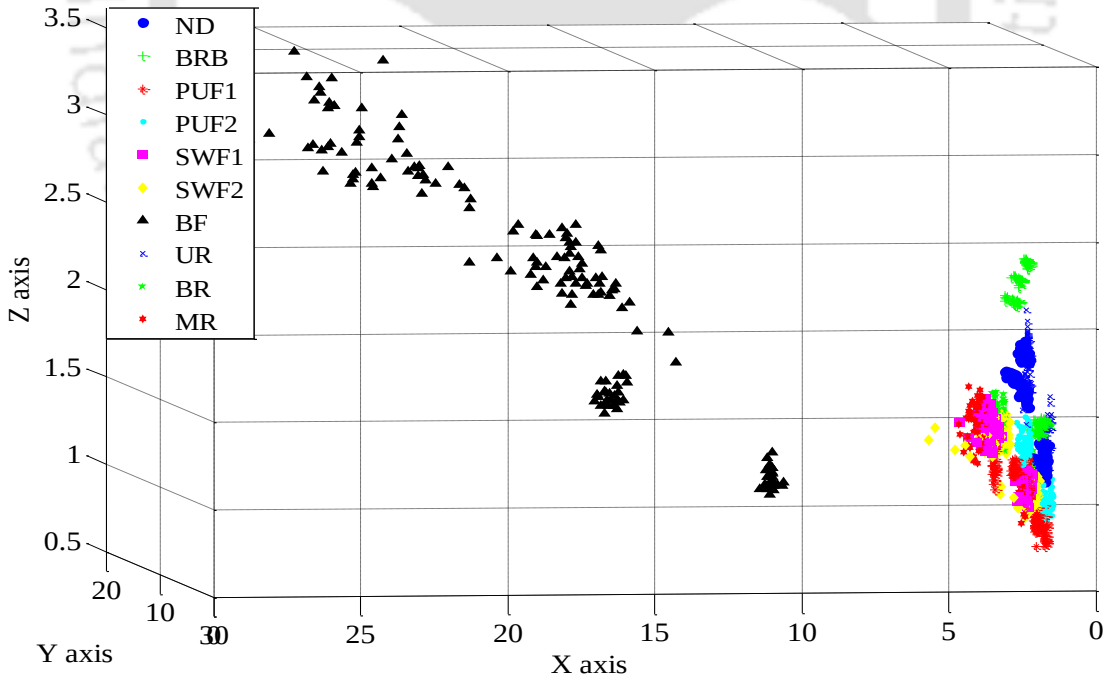

Figure 8.12 Feature distribution (μ_1, σ) of the discrete Meyer wavelet coefficient of vibration signals for all IM faults at 10 Hz and T_1, T_2 and T_3

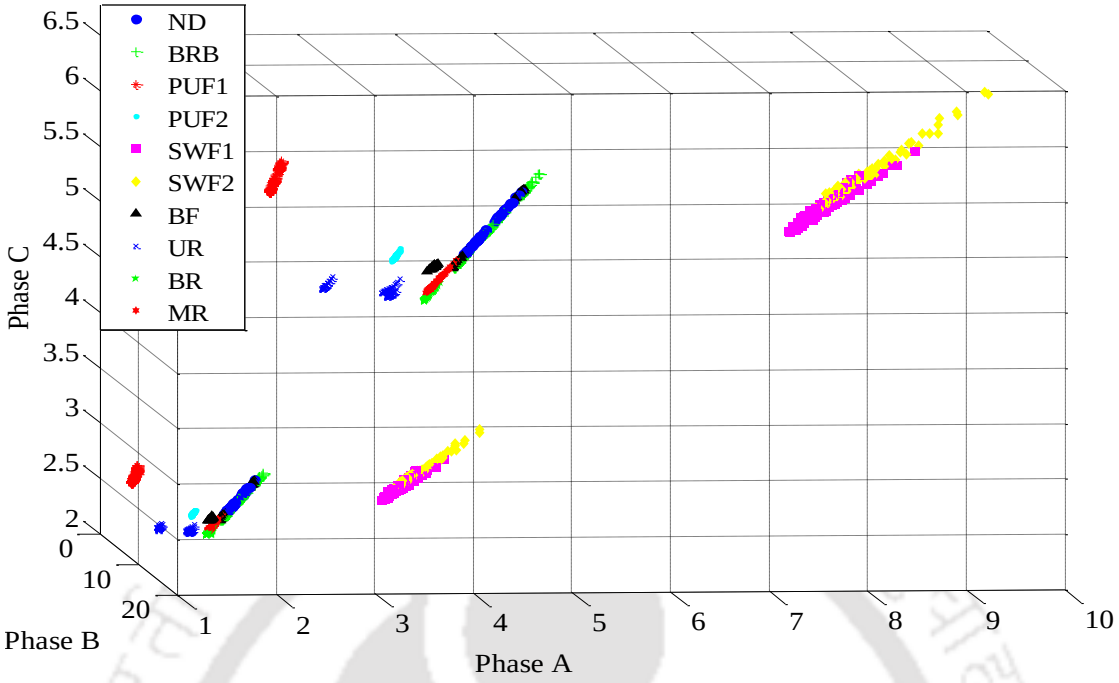

Figure 8.13 Feature distribution (μ_1, σ) of the discrete Meyer wavelet coefficient of current signals for all IM faults at 10 Hz and T_1, T_2 and T_3

8.4 Summary

In this chapter, the multiple fault diagnosis is performed to detect the mechanical as well as electrical faults and also their severity levels in induction motor based on the WPT and the multiclass SVM. To obtain effective fault features, the wavelet packet decomposition up to level three is applied to time domain data of the vibration and current signals acquired at a sampling accuracy of 1 kHz. In order to select the most appropriate node of the wavelet tree, the SLBS approach with (RWE criteria have been used. A number of statistical features are extracted using wavelet coefficients of the selected node and these are further used as the SVM input. The most appropriate features are selected based on the wrapper model and the SVM. It is shown that with appropriate feature the classifier improves the prediction performance significantly. The effect of five different mother wavelets on the prediction is investigated.

Experiments have demonstrated that all the considered mother wavelets with the mean and standard deviation features performed successfully in the IM fault prediction. That means any of the considered mother wavelets in the WPT can be used for the IM fault diagnosis. However, the Discrete Meyer with these features is found to be the best mother wavelet and shows a highest average prediction accuracy up to 99.43 % (when motor is heavily loaded) for the same speed and load case. That is why the Discrete Meyer wavelet is chosen for further study in this chapter. Moreover, in order to check the robustness of the proposed method the diagnosis is performed for a wide range of operating conditions (i.e., the speed and the load) of IMs and the results illustrate that diagnosis does not depend on IM operating conditions. The observation made from experimental results that the present method based on the WPT not only diagnose the different IM faults, but also detect severity levels of faults, even when ten IM fault cases are considered, simultaneously. Furthermore, the diagnosis is extended to the intermediate load and speed conditions and results are found to be promising for both conditions. Fault prediction results in intermediate operating conditions cases show that even when there is incomplete knowledge (signals) about faults, the proposed diagnostics provide the successful prediction of each fault. In both the cases, the prediction performance is significantly increased as compared to the time and frequency domain analyses; however, it is approximately similar to the CWT analysis. The average computational time is 4.9 s for the same speed and load cases, and 8.5 s for the intermediate speed as well as intermediate load cases, which is very less and the vital requirement of the on-line intelligent fault diagnostics.

CHAPTER 9

Conclusions and Scopes of Future Work

9.1 Overview of the Present Work

In order to overcome the limitation of traditional condition monitoring and fault diagnosis, a multi-fault diagnosis is performed to detect the mechanical as well as electrical faults and also their severity levels in IMs based on the multiclass SVM. The vibration and current signals are used here, which are acquired from experiments performed in the laboratory. The fault diagnosis is performed in time domain, frequency domain, and time-frequency domain (CWT and WPT). A comparative investigation of the vibration and current signals has been done in time domain in order to find out which signal(s) (i.e., vibration or/and current) is/are required for an effective diagnosis of the mechanical and/or electrical faults in IM. The fault prediction performances have been checked for the time domain data of high and low sampling rate.

Thereafter, in all three domains, in order to select the optimal statistical features for the proposed fault diagnosis, a number of features are considered and finally selection is done using a simple and timesaving technique of the features section, i.e. the wrapper model. In order to build a best SVM model for the final prediction, SVM parameters are optimally selected based on the grid-search technique along with the cross-validation method. In case of the CWT and the WPT, various mother wavelets are considered to study the impact of different wavelet functions on the fault diagnosis. Initially, the fault diagnosis is attempted for the same IM speed and load case, then it is extended to the intermediate speed and load cases in order to take care of the practical problem of un-availability of data continuously at all operational conditions. To check the robustness of

proposed fault diagnostics, the prediction is performed for various operating conditions of IMs. Fault prediction performances are noted using the time, frequency, CWT and WPT based features using the developed methodology.

9.2 Major Conclusions from the Present Work

- The investigation, based on SVM concludes that to diagnose mechanical faults, the vibration signal is good and sufficient. To diagnose electrical faults, the current signal is sufficient; however, when the current signal is not available, the diagnosis can be performed successfully with the vibration signal alone. To diagnose mechanical and electrical fault simultaneously, the vibration signal can be successfully used, however the performance reduces when only the current signal is used. When these faults are considered with vibration and current signal simultaneously, the prediction performance improves significantly as compared to the case when the vibration or current signal is used alone.
- In order to study the effect of sampling rate and data points (or frequency resolution) on the fault diagnosis of IMs based on the SVM, the data of high sampling rate (i.e., sampling rate of 20,000 S/s and 2,000 sampling points) and the data of low sampling rate (i.e., sampling rate of 1000 S/s and 10,000 sampling points) are used for the diagnosis. It is found that fault predictions are slightly increased with the data of low sampling rate as compared to the data of high sampling rate.
- The fault diagnostics of IM based on SVM is performed in all three domains, i.e. time, frequency and time-frequency domain. In all three domains, three cases of fault diagnosis (i.e., the same speed and load case, the intermediate speed case, and the intermediate load case) are considered. The results from three domains show that for the same speed and load case, the

developed fault diagnostic has the ability to nearly perfectly predict the IM faults, viz. both mechanical as well as electrical faults and their severity. In addition, the fault predictions in the case of intermediate speed are found to be satisfactory. However, fault predictions in the case of intermediate load are found to be effective.

- In all three domains, although, the most of considered features (μ_1- μ_8, R_{pp}, CF, R_{msd}, σ, χ and κ) have performed the fault diagnosis successfully, but the highest prediction accuracy is achieved with the set of standard deviation, skewness and kurtosis in the time domain as well as the frequency domain, the standard deviation alone in case of the CWT, and the set of standard deviation and mean in case of the WPT.
- In the case of CWT and WPT, all considered mother wavelets with appropriate features are effectively performed the IM fault diagnosis. However, the Shannon wavelet using the standard deviation in the case of CWT, and the discrete Meyer wavelet using the set of standard deviation and mean in the case of WPT showed the highest prediction.
- For the same speed and load case, and the intermediate speed case, the fault predictions are merely found better with the CWT data as compared to the time, frequency and WPT data. However, for the intermediate load case, the fault prediction is slightly better with the WPT data as compared to time, frequency and CWT data. In overall, the wavelet (CWT and WPT) based feature is more effective for practical point of view (especially for the intermediate speed and load cases of fault diagnosis).
- In order to check the robustness of the proposed method the diagnosis is performed for a wide range of operating conditions of IMs. It is found that for the same speed and load case, and the intermediate load case in all three domains, the diagnosis does not depend on the load. However, for the intermediate speed case in all domains, the fault diagnosis reduces at higher

load. This may be due to unavoidable fluctuation of speeds under loading conditions. In addition, for all the cases in the time and time-frequency domain, the diagnosis does not depend over the speed. However, for all the cases in frequency domain, the diagnosis reduces at lower speeds. This may be due to low signal-to-noise levels at lower speeds in frequency domain signals.

- The average CPU time for the training as well as the testing is very less, i.e. 3-5 seconds for the same speed and same load case, and 6-8 seconds for the intermediate speed and load cases, which is the vital requirement of a fault diagnostics.

9.3 Main Contribution of the Present Work

- The SVM based fault diagnostic is developed using cross-validation method along with a grid search, and wrapper model, in order to detect various mechanical faults, electrical faults and their severities in IMs.
- A number of statistical features are considered based on time, frequency and time-frequency domain. Further appropriate features are selected based on the wrapper model for effective diagnosis.
- The effect of various mother wavelets based on the CWT and the WPT on the fault diagnosis are studied. All considered mother wavelets with appropriate features are effectively performed the IM fault diagnosis.
- The fault diagnostic has been performed with both the low and high sampling rate data and achieved better prediction accuracy using data of low sampling rate.
- The fault diagnosis is performed for the same speed and load case, when the data or information is available at the required operating conditions. The present diagnosis can predict ten different

mechanical and electrical fault conditions of IMs, simultaneously. The severity of the faults can also be predicted successfully.

- The fault diagnosis is also performed for the intermediate speed and the intermediate load cases in order to take care of the practical situations of unavailability of data at the required operating conditions. The prediction accuracies are slightly reduced as compared to the same speed and load case because of the use of higher range of speed and load for the training. The fault prediction can be further improved if a narrow range of the training speeds and loads are considered.
- The developed methodology has also been checked for various operating conditions of IMs (i.e., no load-0 N-m, light load-0.113 N-m, and high load-0.565 N-m, and speeds ranging from 10 Hz to 40 Hz in interval of 5 Hz)

9.4 Overall Recommendations from the Present Work

The fault diagnostic based on the SVM is developed and successfully used to detect various faults in IMs. It can be used for the fault diagnosis of other kind of motors, and machines like centrifugal pump, compressor, gearbox, engines, and generator. As the fault diagnostic is highly dependent over the signal processing, so the feature extraction and selection should be done carefully for different systems. Moreover, for the selection of effective features, the wrapper model is used in this work, however, other techniques like principal component analysis, independent component analysis, genetic algorithm, distance evaluation technique, and etc. can also be used and compared.

In the present study the training and testing data are collected from the same source and environment are used for the diagnosis. However, if the same fault diagnosis problem is considered for an industrial setting, there is almost always some difference between the training and testing

distributions, even in the large-sample limit. These differences can be due to variations in operating conditions, changes in environment conditions, variations of fault types of same class, sensor noise and etc. Therefore, generalization is one of the most important tasks in machine learning to handle such kind of situation. It gives ability to produce to produce outputs for inputs not encountered during training for the cases where variance is high and information is low. To make a machine learning system more generalize, the pre-processing of the signal is one of the most necessary task to do. It is noted that even if there is the uncertain signal observations (may be due to additional extraneous inputs and variation of parametric condition), the basic features of all the faults would remain same in dynamics or electrodynamics. In addition, the present study suggests that having an appropriate feature or input set is more effective for a fault diagnosis problem, which improves the diagnosis accuracy and reduces the computational burden. Therefore, in order to solve the same problem in an industrial setting, identification of the crucial feature(s) for a particular system is compulsory. After it is expected that, using the suitable features the algorithm would be able to successfully classify the IM faults. In addition, the input parameters of machine learning system have to be optimized before building the optimal system for final prediction. In order to check the robustness of the classifier, the diagnosis can also be performed at different operating conditions.

9.5 Limitations of the Present Work

The data of faulty and healthy IMs used for the fault diagnosis are generated from measurements through artificially created faults in IMs in the laboratory environment. The data from naturally developing faults in IMs in the industry may degrade the diagnostic performance. In the present work, IMs with a single fault in it at a time, is considered for the fault diagnosis, however, the

more complex situation of simultaneous fault occurrence in IMs was not considered for the study. In addition, this thesis did not cover the mathematical modeling of different IM faults for virtual data generation rather than through experimentation for the fault diagnosis. However, the accurate mathematical modelling of the IM faults is still a challenging issue.

9.6 Scopes of Future Work

- The performance of developed fault diagnostics can be checked when the training of algorithm is performed with data obtained from a particular IM and the testing is performed with data obtained from a different configuration IM. This would allow the enlargement of the nature of the classes of IM faults to be analyzed and diagnosed.
- Furthermore, it will be interesting to use the training data that are generated by numerical models of IMs based on multi-physics and the testing data from signals, which are acquired using an experimental measurement. However, it will be a great challenge to make an accurate numerical model for each possible fault in IMs.
- In the present study, the vibration and current signals are processed for the features extractions. Other signal like acoustics can be used for data fusion with the vibration and current signals for the IM fault diagnosis.
- In the present study, the fault diagnosis is performed for the intermediate speed and load cases by considering a wide range of speed and load (which is obtained from the experiments) during the training. The fault diagnosis can be performed and checked for a narrow range of speeds and loads used during the training.

- The motors could have all of the faults considered at the same time is quite farfetched. That would have a vanishingly low probability. However, it would be interesting to consider this challenging problem of simultaneous fault occurrence in IMs in Future.
- The fault diagnosis of different systems can be tried simultaneously for the combined rotating systems such as IM attached with a pump, IM attached with a gearbox, IM attached with the rotor system, etc., using measurement at one location.

Bibliography

Akcay, H., & Germen, E. (2013, September). Identification of acoustic spectra for fault detection in induction motors. In AFRICON, 2013 (pp. 1-5). IEEE.

Albrecht, P. F., Appiarius, J. C., Cornell, E. P., Houghtaling, D. W., McCoy, R. M., Owen, E. L., & Sharma, D. K. (1987). Assessment of the reliability of motors in utility applications. IEEE transactions on energy conversion, (3), 396-406.

Alsaedi, M. A. (2015). Fault Diagnosis of Three-Phase Induction Motor: A Review‖. Optics. Special Issue: Applied Optics and Signal Processing, 4(1-1), 1-8.

Antonino-Daviu, J. A., Riera-Guasp, M., Folch, J. R., & Palomares, M. P. M. (2006). Validation of a new method for the diagnosis of rotor bar failures via wavelet transform in industrial induction machines. IEEE Transactions on Industry Applications, 42(4), 990-996.

Awadallah, M. A., & Morcos, M. M. (2006). Automatic diagnosis and location of open-switch fault in brushless DC motor drives using wavelets and neuro-fuzzy systems. IEEE Transactions on Energy conversion, 21(1), 104-111.

Ayhan, B., Chow, M. Y., & Song, M. H. (2006). Multiple discriminant analysis and neural-network-based monolith and partition fault-detection schemes for broken rotor bar in induction motors. IEEE Transactions on Industrial Electronics, 53(4), 1298-1308.

Ayoubi, M., & Isermann, R. (1997). Neuro-fuzzy systems for diagnosis. Fuzzy sets and Systems, 89(3), 289-307.

Baccarini, L. M. R., e Silva, V. V. R., De Menezes, B. R., & Caminhas, W. M. (2011). SVM practical industrial application for mechanical faults diagnostic. Expert Systems with Applications, 38(6), 6980-6984.

Bacha, K., Henao, H., Gossa, M., & Capolino, G. A. (2008). Induction machine fault detection using stray flux EMF measurement and neural network-based decision. Electric Power Systems Research, 78(7), 1247-1255.

Bacha, K., Salem, S. Ben, & Chaari, A. (2012). An improved combination of Hilbert and Park transforms for fault detection and identification in three-phase induction motors. International Journal of Electrical Power and Energy Systems, 43(1), 1006–1016.

Bazzi, A. M., & Krein, P. T. (2010). Review of methods for real-time loss minimization in induction machines. IEEE Transactions on Industry Applications, 46(6), 2319-2328.

Benbouzid, M. E. H. & Kliman, G. B. (2003). What stator current processing-based technique to use for induction motor rotor faults diagnosis?. IEEE Transactions on Energy Conversion, 18(2), 238-244.

Benbouzid, M. E. H. (2000). A review of induction motors signature analysis as a medium for faults detection. IEEE transactions on industrial electronics, 47(5), 984-993.

Benbouzid, M. E. H., Vieira, M., & Theys, C. (1999). Induction motors' faults detection and localization using stator current advanced signal processing techniques. IEEE Transactions on power electronics, 14(1), 14-22.

Bilski, P. (2014). Application of Support Vector Machines to the induction motor parameters identification. Measurement, 51, 377-386.

Blodt, M., Granjon, P., Raison, B., & Rostaing, G. (2008). Models for bearing damage detection in induction motors using stator current monitoring. IEEE transactions on industrial electronics, 55(4), 1813-1822.

Bordoloi, D. J., & Tiwari, R. (2014). Optimum multi-fault classification of gears with integration of evolutionary and SVM algorithms. Mechanism and Machine Theory, 73, 49-60.

Bordoloi, D. J., & Tiwari, R. (2014). Support vector machine based optimization of multi-fault classification of gears with evolutionary algorithms from time–frequency vibration data. Measurement, 55, 1-14.

Boser B.E., Guyon I.M. and Vapnik V.N. (1992). A training algorithm for optimal margin classifiers. In Proceedings of the Fifth Annual Workshop on Computational Learning Theory (pp. 144-152). ACM.

Burges, C. J. (1998). A tutorial on support vector machines for pattern recognition. Data mining and knowledge discovery, 2(2), 121-167.

Chang, C. C. & Lin, C. J. (2011). LIBSVM: A library for support vector machines. ACM Transactions on Intelligent Systems and Technology (TIST), 2(3), 27:1–27:27.

Chang, S. C. & Yacamini, R. (1996). Experimental study of the vibrational behaviour of machine stators. IEE Proceedings-Electric Power Applications, 143(3), 242-250.

Chang, S. H., Kang, K. S., Choi, S. S., Kim, H. G., Jeong, H. K., & Yi, C. U. (1995). Development of the on-line operator aid system OASYS using a rule-based expert system and fuzzy logic for nuclear power plants. Nuclear Technology, 112(2), 266-294.

Chattopadhyay P. and Konar P. (2014). Feature extraction using wavelet transform for multi-class fault detection of induction motor. Journal of the Institution of Engineers (India): Series B, 1-9.

Choi, S. (2008). Detection of valvular heart disorders using wavelet packet decomposition and support vector machine. Expert Systems with Applications, 35(4), 1679-1687.

Chow, M. Y., Mangum, P. M., & Yee, S. O. (1991). A neural network approach to real-time condition monitoring of induction motors. IEEE Transactions on industrial electronics, 38(6), 448-453.

Chow, T. W. S., & Fei, G. (1995). Three phase induction machines asymmetrical faults identification using bispectrum. IEEE Transactions on Energy Conversion, 10(4), 688-693.

Chow, T. W., & Hai, S. (2004). Induction machine fault diagnostic analysis with wavelet technique. IEEE Transactions on Industrial Electronics, 51(3), 558-565.

Coifman, R. R., & Wickerhauser, M. V. (1992). Entropy-based algorithms for best basis selection. IEEE Transactions on information theory, 38(2), 713-718.

Combastel, C., Lesecq, S., Petropol, S., & Gentil, S. (2002). Model-based and wavelet approaches to induction motor on-line fault detection. Control Engineering Practice, 10(5), 493-509.

Cortes, C., & Vapnik, V. (1995). Support-vector networks. Machine learning, 20(3), 273-297.

CusidOCusido, J., Romeral, L., Ortega, J. A., Rosero, J. A., & Espinosa, A. G. (2008). Fault detection in induction machines using power spectral density in wavelet decomposition. IEEE Transactions on Industrial Electronics, 55(2), 633-643.

D Dyer, R.M Stewart Detection of rolling element bearing damage by statistical vibration analysis Trans. ASME, J. Mech. Design, 100 (2) (1978), pp. 229-235

Da Silva, A. M., Povinelli, R. J., & Demerdash, N. A. (2008). Induction machine broken bar and stator short-circuit fault diagnostics based on three-phase stator current envelopes. IEEE Transactions on Industrial Electronics, 55(3), 1310-1318.

Da Silva, A. M., Povinelli, R. J., & Demerdash, N. A. (2008). Induction machine broken bar and stator short-circuit fault diagnostics based on three-phase stator current envelopes. IEEE Transactions on Industrial Electronics, 55(3), 1310-1318.

Das, S., Purkait, P., Koley, C., & Chakravorti, S. (2014). Performance of a load-immune classifier for robust identification of minor faults in induction motor stator winding. IEEE Transactions on Dielectrics and Electrical Insulation, 21(1), 33-44.

Didier, G., Ternisien, E., Caspary, O. & Razik, H. (2007). A new approach to detect broken rotor bars in induction machines by current spectrum analysis. Mechanical Systems and Signal Processing, 21(2), 1127-1142. DOI 10.1007/978-1-4899-7502-7, 101-1.

Douglas, H., Pillay, P., & Ziarani, A. K. (2004). A new algorithm for transient motor current signature analysis using wavelets. IEEE Transactions on industry applications, 40(5), 1361-1368.

El-Shafei, A., & Rieger, N. (2003). Automated diagnostics of rotating machinery. ASME Turbo Expo, vol. 4, Atlanta, GA, USA, pp. 491-498

Ergin, S., Uzuntas, A., & Gulmezoglu, M. B. (2012). Detection of Stator, Bearing and Rotor Faults in Induction Motors. Procedia Engineering, 30, 1103-1109.

Esfahani, E. T., Wang, S., & Sundararajan, V. (2014). Multisensor wireless system for eccentricity and bearing fault detection in induction motors. IEEE/ASME Transactions on Mechatronics, 19(3), 818-826.

Filippetti, F., Franceschini, G., Tassoni, C., & Vas, P. (2000). Recent developments of induction motor drives fault diagnosis using AI techniques. IEEE transactions on industrial electronics, 47(5), 994-1004.

Gangsar, P., & Tiwari, R. (2014). Multiclass Fault Taxonomy in Rolling Bearings at Interpolated and Extrapolated Speeds Based on Time Domain Vibration Data by SVM Algorithms. Journal of Failure Analysis and Prevention, 14(6), 826-837.

Gao, R. X., & Yan, R. (2006). Non-stationary signal processing for bearing health monitoring. International Journal of Manufacturing Research, 1(1), 18-40.

Garcia-Perez, A., de Jesus Romero-Troncoso, R., Cabal-Yepez, E., & Osornio-Rios, R. A. (2011). The application of high-resolution spectral analysis for identifying multiple combined faults in induction motors. Industrial Electronics, IEEE Transactions, 58(5), 2002-2010.

Ghate, V. N., & Dudul, S. V. (2011). Cascade neural-network-based fault classifier for three-phase induction motor. IEEE Transactions on Industrial Electronics, 58(5), 1555-1563.

Gunal, S., & Gerek, O. N. (2009). Induction machine condition monitoring using notch-filtered motor current. Mechanical Systems and Signal Processing, 23(8), 2658-2670.

Gunn S.R. (1998). Support vector machines for classification and regression. (Department of Electronics and Computer Science of University of Southampton, Southampton), pp. 1–28.

Gyftakis, K. N., Spyropoulos, D. V., Kappatou, J. C., & Mitronikas, E. D. (2013). A novel approach for broken bar fault diagnosis in induction motors through torque monitoring. IEEE Transactions on Energy Conversion, 28(2), 267-277.

Haji, M., & Toliyat, H. A. (2001). Pattern recognition-a technique for induction machines rotor broken bar detection. IEEE Transactions on Energy Conversion, 16(4), 312-317.

Halme, J. (2002, December). Condition monitoring of oil lubricated ball bearing using wear debris and vibration analysis. In Proceedings of the International Tribology Conference (AUSTRIB'02), Frontiers in tribology, Perth, University of Western Australia (pp. 2-5).

Han, T., Yang, B. S., & Lee, J. M. (2005, May). A new condition monitoring and fault diagnosis system of induction motors using artificial intelligence algorithms. In Electric Machines and Drives, 2005 IEEE International Conference on(pp. 1967-1974). IEEE.

Henao, H., Capolino, G. A., Fernandez-Cabanas, M., Filippetti, F., Bruzzese, C., Strangas, E., ... & Hedayati-Kia, S. (2014). Trends in fault diagnosis for electrical machines: A review of diagnostic techniques. IEEE industrial electronics magazine, 8(2), 31-42.

Hsu C.W. and Lin C.J. (2002). A comparison of methods for multiclass support vector machines. Neural Networks, IEEE Transactions on, 13(2), 415-425.

Hsu, C. W., Chang, C. C., & Lin, C. J. (2003). A practical guide to support vector classification.

Hsu, C.W., & Lin, C.J. (2002). A comparison of methods for multiclass support vector machines. Neural Networks, IEEE Transactions on, 13(2), 415-425.

Hsu, J. S. (1995). Monitoring of defects in induction motors through air-gap torque observation. IEEE Transactions on Industry Applications, 31(5), 1016-1021.

Hu, Q., He, Z., Zhang, Z., & Zi, Y. (2007). Fault diagnosis of rotating machinery based on improved wavelet package transform and SVMs ensemble. Mechanical Systems and Signal Processing, 21(2), 688-705.

Huang, Y. C., & Huang, C. M. (2002). Evolving wavelet networks for power transformer condition monitoring. IEEE Transactions on Power Delivery, 17(2), 412-416.

Huang, Y. C., Huang, C. M., & Huang, K. Y. (2012). Fuzzy logic applications to power transformer fault diagnosis using dissolved gas analysis. Procedia Engineering, 50, 195-200.

Iorgulescu, M. & Beloiu, R. (2008). Vibration and current monitoring for fault's diagnosis of induction motors. Annals of the University of Craiova, electrical engineering series, (32), 102-107.

Jack, L. B., & Nandi, A. K. (2002). Fault detection using support vector machines and artificial neural networks, augmented by genetic algorithms. Mechanical systems and signal processing, 16(2-3), 373-390.

Jardine, A. K., Lin, D., & Banjevic, D. (2006). A review on machinery diagnostics and prognostics implementing condition-based maintenance. Mechanical systems and signal processing, 20(7), 1483-1510.

Kankar, P. K., Sharma, S. C., & Harsha, S. P. (2011). Fault diagnosis of ball bearings using continuous wavelet transform. Applied Soft Computing, 11(2), 2300-2312.

Kanovic, Z., Matic, D., Jelicic, Z., Rapaic, M., Jakovljevic, B., & Kapetina, M. (2013, August). Induction motor broken rotor bar detection using vibration analysis—A case study. In Diagnostics for Electric Machines, Power Electronics and Drives (SDEMPED), 2013 9th IEEE International Symposium on (pp. 64-68). IEEE.

Keskes, H., & Braham, A. (2014, April). DAG SVM and pitch synchronous wavelet transform for induction motor diagnosis. In Power Electronics, Machines and Drives (PEMD 2014), 7th IET International Conference on (pp. 1-6). IET.

Keskes, H., & Braham, A. (2015). Recursive undecimated wavelet packet transform and DAG SVM for induction motor diagnosis. IEEE Transactions on Industrial Informatics, 11(5), 1059-1066.

Keskes, H., Braham, A., & Lachiri, Z. (2013). Broken rotor bar diagnosis in induction machines through stationary wavelet packet transform and multiclass wavelet SVM. Electric Power Systems Research, 97, 151-157.

Kim, K., & Parlos, A. G. (2002). Induction motor fault diagnosis based on neuropredictors and wavelet signal processing. IEEE/ASME Transactions on mechatronics, 7(2), 201-219.

Kohavi, R., & John, G. H. (1997). Wrappers for feature subset selection. Artificial intelligence, 97(1-2), 273-324.

Konar, P., & Chattopadhyay, P. (2011). Bearing fault detection of induction motor using wavelet and Support Vector Machines (SVMs). Applied Soft Computing, 11(6), 4203-4211.

Kral, C., Habetler, T. G., & Harley, R. G. (2004). Detection of mechanical imbalances of induction machines without spectral analysis of time-domain signals. IEEE Transactions on Industry Applications, 40(4), 1101-1106.

Kral, C., Habetler, T. G., Harley, R. G., Pirker, F., Pascoli, G., Oberguggenberger, H., & Fenz, C. J. M. (2003, August). A comparison of rotor fault detection techniques with respect to the assessment of fault severity. In Diagnostics for Electric Machines, Power Electronics and Drives, 2003. SDEMPED 2003. 4th IEEE International Symposium on (pp. 265-270). IEEE.

Kressel, U. H. G. (1999, February). Pairwise classification and support vector machines. In Advances in kernel methods (pp. 255-268). MIT press.

Kurek, J., & Osowski, S. (2010). Support vector machine for fault diagnosis of the broken rotor bars of squirrel-cage induction motor. Neural Computing and Applications, 19(4), 557-564.

Lasurt, I., Stronach, A. F., & Penman, J. (2000). A fuzzy logic approach to the interpretation of higher order spectra applied to fault diagnosis in electrical machines. In Fuzzy Information Processing Society, 2000. NAFIPS. 19th International Conference of the North American (pp. 158-162). IEEE.

Lee, S. H., Cheon, S. P., Kim, Y., & Kim, S. (2006, August). Fourier and wavelet transformations for the fault detection of induction motor with stator current. In International Conference on Intelligent Computing (pp. 557-569). Springer, Berlin, Heidelberg.

Lee, S., Bryant, M. D., & Karlapalem, L. (2006). Model-and information theory-based diagnostic method for induction motors. Journal of dynamic systems, measurement, and control, 128(3), 584-591.

Lei, Y., He, Z., & Zi, Y. (2008). A new approach to intelligent fault diagnosis of rotating machinery. Expert Systems with applications, 35(4), 1593-1600.

Li X., Zheng A., Zhang X., Li C. and Zhang L. (2013). Rolling element bearing fault detection using support vector machine with improved ant colony optimization. Measurement, 46, 2726-2734.

Li, B., Chow, M. Y., Tipsuwan, Y., & Hung, J. C. (2000). Neural-network-based motor rolling bearing fault diagnosis. IEEE transactions on industrial electronics, 47(5), 1060-1069.

Li, C., Sánchez, R. V., Zurita, G., Cerrada, M., & Cabrera, D. (2016). Fault diagnosis for rotating machinery using vibration measurement deep statistical feature learning. Sensors, 16(6), 895.

Li, N., Zhou, R., Hu, Q., & Liu, X. (2012). Mechanical fault diagnosis based on redundant second generation wavelet packet transform, neighborhood rough set and support vector machine. Mechanical systems and signal processing, 28, 608-621.

Lim, G. M., Bae, D. M., & Kim, J. H. (2014). Fault diagnosis of rotating machine by thermography method on support vector machine. Journal of Mechanical Science and Technology, 28(8), 2947-2952.

Lin, J. (2009, July). An integrated time domain averaging scheme for gearbox diagnosis. In Reliability, Maintainability and Safety, 2009. ICRMS 2009. 8th International Conference on (pp. 808-812). IEEE.

Liu, T. I., Singonahalli, J. H., & Iyer, N. R. (1996). Detection of roller bearing defects using expert system and fuzzy logic. Mechanical Systems and Signal Processing, 10(5), 595-614.

Liu, Y., & Bazzi, A. M. (2017). A review and comparison of fault detection and diagnosis methods for squirrel-cage induction motors: State of the art. ISA transactions, 70, 400-409.

Liu, Z., Cao, H., Chen, X., He, Z., & Shen, Z. (2013). Multi-fault classification based on wavelet SVM with PSO algorithm to analyze vibration signals from rolling element bearings. Neurocomputing, 99, 399-410.

Martin, K. F. (1994). A review by discussion of condition monitoring and fault diagnosis in machine tools. International Journal of Machine Tools and Manufacture, 34(4), 527-551.

Martinez-Morales, J. D., Palacios, E., & Campos-Delgado, D. U. (2010, September). Data fusion for multiple mechanical fault diagnosis in induction motors at variable operating conditions. In Electrical Engineering Computing Science and Automatic Control (CCE), 2010 7th International Conference on (pp. 176-181). IEEE.

Martins, J. F., Pires, V. F., & Pires, A. J. (2007). Unsupervised neural-network-based algorithm for an on-line diagnosis of three-phase induction motor stator fault. IEEE Transactions on Industrial Electronics, 54(1), 259-264.

Maruthi, G. S. & Vittal, K. P. (2005, November). Electrical fault detection in three phase squirrel cage induction motor by vibration analysis using MEMS accelerometer. In 2005 International Conference on Power Electronics and Drives Systems (Vol. 2, pp. 838-843). IEEE.

Mechefske, C. K. (1998). Objective machinery fault diagnosis using fuzzy logic. Mechanical systems and signal processing, 12(6), 855-862.

Mehrjou, M. R., Mariun, N., Marhaban, M. H. & Misron, N. (2011). Rotor fault condition monitoring techniques for squirrel-cage induction machine-A review. Mechanical Systems and Signal Processing, 25(8), 2827-2848.

Meng, L., Miao, W., & Chunguang, W. (2010, May). Research on SVM classification performance in rolling bearing diagnosis. In Intelligent Computation Technology and Automation (ICICTA), 2010 International Conference on (Vol. 3, pp. 132-135). IEEE.

Nakamura, H., Yamamoto, Y., & Mizuno, Y. (2006). Diagnosis of electrical and mechanical faults of induction motor. In Electrical Insulation and Dielectric Phenomena, 2006 IEEE Conference, (pp. 521-524). IEEE.

Nguyen, N. T., & Lee, H. H. (2008). An Application of Support Vector Machines for Induction Motor Fault Diagnosis with Using Genetic Algorithm. In Advanced Intelligent Computing Theories and Applications. With Aspects of Artificial Intelligence (pp. 190-200). Springer Berlin Heidelberg.

Nguyen, N. T., Lee, H. H., & Kwon, J. M. (2008). Optimal feature selection using genetic algorithm for mechanical fault detection of induction motor. Journal of Mechanical Science and Technology, 22(3), 490-496.

Nikranjbar, A., Ebrahimi, M., & Wood, A. S. (2009). Model-based fault diagnosis of induction motor eccentricity using particle swarm optimization. Proceedings of the Institution of Mechanical Engineers, Part C: Journal of Mechanical Engineering Science, 223(3), 607-615.

Park, W. J., Lee, S. H., Joo, W. K., & Song, J. I. (2007). A mixed algorithm of PCA and LDA for fault diagnosis of induction motor. In Advanced Intelligent Computing Theories and Applications. With Aspects of Artificial Intelligence (pp. 934-942). Springer Berlin Heidelberg.

Peng, Z. K., & Chu, F. L. (2004). Application of the wavelet transform in machine condition monitoring and fault diagnostics: a review with bibliography. Mechanical systems and signal processing, 18(2), 199-221.

Penman, J., Sedding, H. G., Lloyd, B. A., & Fink, W. T. (1994). Detection and location of interturn short circuits in the stator windings of operating motors. IEEE Transactions on Energy Conversion, 9(4), 652-658.

Puche-Panadero, R., Pineda-Sanchez, M., Riera-Guasp, M., Roger-Folch, J., Hurtado-Perez, E., & Perez-Cruz, J. (2009). Improved resolution of the MCSA method via Hilbert transform, enabling the diagnosis of rotor asymmetries at very low slip. IEEE Transactions on Energy Conversion, 24(1), 52-59.

Qingling, D., Xiuqing, H., & Haibo, L. (2001). Fault model identification of rotating machines based on fuzzy back propagation. Transactions of the Chinese Society of Agriculture Machinery, 32(4), 92-95.

Rafiee, J., Rafiee, M. A., & Tse, P. W. (2010). Application of mother wavelet functions for automatic gear and bearing fault diagnosis. Expert Systems with Applications, 37(6), 4568-4579.

Rafiee, J., Rafiee, M. A., Prause, N., & Tse, P. W. (2009, February). Application of Daubechies 44 in machine fault diagnostics. In Computer, Control and Communication, 2009. IC4 2009. 2nd International Conference on (pp. 1-6). IEEE.

Randall, R. B. (2011). Vibration-based condition monitoring: industrial, aerospace and automotive applications. Willey-Blackwell, Hoboken, New Jersey, USA.

Randall, R. B., & Antoni, J. (2011). Rolling element bearing diagnostics—a tutorial. Mechanical systems and signal processing, 25(2), 485-520.

Rojas, A., & Nandi, A. K. (2005, September). Detection and classification of rolling-element bearing faults using support vector machines. In Machine Learning for Signal Processing, 2005 IEEE Workshop on (pp. 153-158). IEEE.

Romero-Troncoso, R. J., Saucedo-Gallaga, R., Cabal-Yepez, E., Garcia-Perez, A., Osornio-Rios, R. A., Alvarez-Salas, R., ... & Huber, N. (2011). FPGA-based online detection of multiple combined faults in induction motors through information entropy and fuzzy inference. IEEE Transactions on Industrial Electronics, 58(11), 5263-5270.

Sadeghian, A., Ye, Z., & Wu, B. (2009). Online detection of broken rotor bars in induction motors by wavelet packet decomposition and artificial neural networks. IEEE Transactions on Instrumentation and Measurement, 58(7), 2253-2263.

Salem, S. B., Bacha, K. & Chaari, A. (2012). Support vector machine based decision for mechanical fault condition monitoring in induction motor using an advanced Hilbert-Park transform. ISA transactions, 51(5), 566-572.

Samanta B. (2004). Gear fault detection using artificial neural networks and support vector machines with genetic algorithms. Mechanical Systems and Signal Processing, 18(3), 625-644.

Samanta, B., & Al-Balushi, K. R. (2003). Artificial neural network based fault diagnostics of rolling element bearings using time-domain features. Mechanical systems and signal processing, 17(2), 317-328.

Sammut, C., & Webb, G.I. (2017). Encyclopedia of Machine Learning and Data Mining,

Saravanan, N., & Ramachandran, K. I. (2010). Incipient gear box fault diagnosis using discrete wavelet transform (DWT) for feature extraction and classification using artificial neural network (ANN). Expert Systems with Applications, 37(6), 4168-4181.

Schoen, R. R., Lin, B. K., Habetler, T. G., Schlag, J. H., & Farag, S. (1995). An unsupervised, on-line system for induction motor fault detection using stator current monitoring. IEEE Transactions on Industry Applications, 31(6), 1280-1286.

Seera, M., & Lim, C. P. (2014). Online motor fault detection and diagnosis using a hybrid FMM-CART model. IEEE transactions on neural networks and learning systems, 25(4), 806-812.

Seera, M., Lim, C. P., Ishak, D., & Singh, H. (2012). Fault detection and diagnosis of induction motors using motor current signature analysis and a hybrid FMM–CART model. IEEE transactions on neural networks and learning systems, 23(1), 97-108.

Seshadrinath, J., Singh, B., & Panigrahi, B. K. (2014). Incipient turn fault detection and condition monitoring of induction machine using analytical wavelet transform. IEEE Transactions on Industry Applications, 50(3), 2235-2242.

Siddique, A., Yadava, G. S., & Singh, B. (2003, August). Applications of artificial intelligence techniques for induction machine stator fault diagnostics: review. In Diagnostics for Electric Machines, Power Electronics and Drives, 2003. SDEMPED 2003. 4th IEEE International Symposium on (pp. 29-34). IEEE.

Siddique, A., Yadava, G. S., & Singh, B. (2005). A review of stator fault monitoring techniques of induction motors. IEEE transactions on energy conversion, 20(1), 106-114.

Silva, V. A. D. & Pederiva, R. (2013). Fault detection in induction motors based on artificial intelligence. Surveillance 7, International Conference - October 29-30, 2013, Institute of Technology of Chartres, France.

Singh, G. K., & Ahmed, S. A. K. S. A. (2004). Vibration signal analysis using wavelet transform for isolation and identification of electrical faults in induction machine. Electric Power Systems Research, 68(2), 119-136.

Soualhi, A., Clerc, G., & Razik, H. (2013). Detection and diagnosis of faults in induction motor using an improved artificial ant clustering technique. IEEE Transactions on Industrial Electronics, 60(9), 4053-4062.

Stone, G. C., Sedding, H. G., & Costello, M. J. (1996). Application of partial discharge testing to motor and generator stator winding maintenance. IEEE Transactions on Industry Applications, 32(2), 459-464.

Su, H., & Chong, K. T. (2007). Induction machine condition monitoring using neural network modeling. IEEE Transactions on Industrial Electronics, 54(1), 241-249.

Sugumaran, V., Ramachandran, K., (2011). Effect of number of features on classification of roller bearing faults using svm and psvm. Expert Systems with Applications, 38(4), 4088-4096.

Sugumaran, V., Sabareesh, G.R., Ramachandran K.I., (2008). Fault diagnostics of roller bearing using kernel based neighborhood score multi-class support vector machine. Expert Systems with Applications: An International Journal, 34(4), 3090-3098.

Sui, W.T., Zhang, D., (2009). Rolling element bearings fault classification based on svm and feature evaluation. Machine Learning and Cybernetics, International Conference on, IEEE, 1, 450-453.

Tan, W. W., & Huo, H. (2005). A generic neurofuzzy model-based approach for detecting faults in induction motors. IEEE Transactions on Industrial Electronics, 52(5), 1420-1427.

Tandon, N., & Choudhury, A. (1999). A review of vibration and acoustic measurement methods for the detection of defects in rolling element bearings. Tribology international, 32(8), 469-480.

Tavner, P. J., Gaydon, B. G., & Ward, D. M. (1986, May). Monitoring generators and large motors. In IEE Proceedings B (Electric Power Applications) (Vol. 133, No. 3, pp. 169-180). IET Digital Library.

Tetrault, S. M., Stone, G. C., & Sedding, H. G. (1999). Monitoring partial discharges on 4-kV motor windings. IEEE Transactions on Industry Applications, 35(3), 682-688

Thomson, W. T. & Orpin, P. (2002, September). Current and vibration monitoring for fault diagnosis and root cause analysis of induction motor drives. In Proceedings of the thirty-first turbomachinery symposium (pp. 61-67).

Timusk M., Lipsett M. and Mechefske C.K. (2008). Fault detection using transient machine signals. Mechanical Systems and Signal Processing, 22(7), 1724-1749.

Tran, V. T., Althobiani, F., Ball, A., & Choi, B. (2013). Expert Systems with Applications An application to transient current signal based induction motor fault diagnosis of Fourier – Bessel expansion and simplified fuzzy ARTMAP. Expert Systems with Applications, 40(13), 5372–5384.

Tran, V. T., Yang, B., Oh, M., Chit, A., & Tan, C. (2009). Fault diagnosis of induction motor based on decision trees and adaptive neuro-fuzzy inference. Expert Systems With Applications, 36(2), 1840–1849.

Vapnik V.N. (1999). An overview of statistical learning theory. Neural Networks, IEEE Transactions on, 10(5), 988-999.

Vapnik, V. N. (1995). The nature of statistical learning theory. New York, Springer.

Vishwakarma, H. O., Sajan, K. S., Maheshwari, B., & Dhiman, Y. D. (2015, August). Intelligent bearing fault monitoring system using support vector machine and wavelet packet decomposition for induction motors. In Power and Advanced Control Engineering (ICPACE), 2015 International Conference on (pp. 339-343). IEEE.

Wang, Z., & Chang, C. S. (2011, June). Online fault detection of induction motors using frequency domain independent components analysis. In Industrial Electronics (ISIE), 2011 IEEE International Symposium on (pp. 2132-2137). IEEE.

Widodo, A., & Yang, B. S. (2007). Application of nonlinear feature extraction and support vector machines for fault diagnosis of induction motors. Expert Systems with Applications, 33(1), 241-250.

Widodo, A., & Yang, B. S. (2007). Support vector machine in machine condition monitoring and fault diagnosis. Mechanical systems and signal processing, 21(6), 2560-2574.

Widodo, A., & Yang, B. S. (2008). Wavelet support vector machine for induction machine fault diagnosis based on transient current signal. Expert Systems with Applications, 35(1), 307-316.

Widodo, A., Yang, B. S., & Han, T. (2007). Combination of independent component analysis and support vector machines for intelligent faults diagnosis of induction motors. Expert Systems with Applications, 32(2), 299-312.

Wu, C., Chen, T., Jiang, R., Ning, L., & Jiang, Z. (2015). ANN Based Multi-classification Using Various Signal Processing Techniques for Bearing Fault Diagnosis. International Journal of Control and Automation, 8(7), 113-124.

Xian, G. M., & Zeng, B. Q. (2009). An intelligent fault diagnosis method based on wavelet packer analysis and hybrid support vector machines. Expert Systems with applications, 36(10), 12131-12136.

Yan, R., Gao, R. X., & Chen, X. (2014). Wavelets for fault diagnosis of rotary machines: A review with applications. Signal Processing, 96, 1-15.

Yang, B. S., & Kim, K. J. (2006). Application of Dempster–Shafer theory in fault diagnosis of induction motors using vibration and current signals. Mechanical Systems and Signal Processing, 20(2), 403-420.

Yang, Y., Yu D., Cheng, J., (2007). A fault diagnosis approach for roller bearing based on imf envelope spectrum and svm. Measurement, 40(9), 943-950.

Ye, Z., Wu, B., & Sadeghian, A. (2003). Current signature analysis of induction motor mechanical faults by wavelet packet decomposition. IEEE transactions on industrial electronics, 50(6), 1217-1228.

Ye, Z., Wu, B., & Zargari, N. (2000). Online mechanical fault diagnosis of induction motor by wavelet artificial neural network using stator current. In Industrial Electronics Society, 2000. IECON 2000. 26th Annual Conference of the IEEE (Vol. 2, pp. 1183-1188). IEEE.

Yen, G. G., & Lin, K. C. (2000). Wavelet packet feature extraction for vibration monitoring. IEEE transactions on industrial electronics, 47(3), 650-667.

Younus, A. M., & Yang, B. S. (2010, January). Wavelet co-efficient of thermal image analysis for machine fault diagnosis. In Prognostics and Health Management Conference, 2010. PHM'10. (pp. 1-6). IEEE.

Zarei, J., & Poshtan, J. (2007). Bearing fault detection using wavelet packet transform of induction motor stator current. Tribology International, 40(5), 763-769.

Zarei, J., Tajeddini, M. A., & Karimi, H. R. (2014). Vibration analysis for bearing fault detection and classification using an intelligent filter. Mechatronics, 24(2), 151-157.

Zhang, L., Xiong, G., Liu, H., Zou, H., & Guo, W. (2010). Fault diagnosis based on optimized node entropy using lifting wavelet packet transform and genetic algorithms. Proceedings of the Institution of Mechanical Engineers, Part I: Journal of Systems and Control Engineering, 224(5), 557-573.

Zhang, P., Du, Y., Habetler, T. G., & Lu, B. (2011). A survey of condition monitoring and protection methods for medium-voltage induction motors. IEEE Transactions on Industry Applications, 47(1), 34-46.

Zhang, R., & Wang, X. (2008). On-line broken-bar fault diagnosis system of induction motor. Transactions of Tianjin University, 14(2), 144-147.

Zhang, S., Asakura, T., Xu, X., & Xu, B. (2003). Fault diagnosis system for rotary machine based on fuzzy neural networks. JSME International Journal Series C Mechanical Systems, Machine Elements and Manufacturing, 46(3), 1035-1041.

Zheng, H., Zhou, L., (2012). Rolling element bearing fault diagnosis based on support vector machine. Consumer Electronics, Communications and Networks (CECNet), 2nd International Conference on. IEEE, 544-547.

Zhitong, C., Hongping, C., Guoguang, H., & Ritchie, E. (2001). Rotor fault diagnosis of induction motor based on wavelet reconstruction. In Electrical Machines and Systems, 2001. ICEMS 2001. Proceedings of the Fifth International Conference on (Vol. 1, pp. 374-377). IEEE.

Zhongming, Y., & Bin, W. (2000). A review on induction motor online fault diagnosis. In Power Electronics and Motion Control Conference, 2000. Proceedings. IPEMC 2000. The Third International (Vol. 3, pp. 1353-1358). IEEE.

Zhou, H., Chen, J., Dong, G., & Wang, R. (2016). Detection and diagnosis of bearing faults using shift-invariant dictionary learning and hidden Markov model. Mechanical Systems and Signal Processing, 72, 65-79.

Zhou, Z., Zhao, J., & Cao, F. (2014). A novel approach for fault diagnosis of induction motor with invariant character vectors. Information Sciences, 281, 496-506.

Zhu, K., Song, X., (2014). A roller bearing fault diagnosis method based on hierarchical entropy and support vector machine with particle swarm optimization algorithm. Measurement, 47, 669–67.

Zolfaghari, S., Noor, S. B. M., Mariun, N., Marhaban, M. H., Mehrjou, M. R., & Karami, M. (2014, December). Broken rotor bar detection of induction machine using wavelet packet coefficient-

related features. In Research and Development (SCOReD), 2014 IEEE Student Conference on (pp. 1-5). IEEE.

Appendix. A

Statistical Feature Plot of Vibration and Current for Time, Frequency, CWT and WPT Data

---

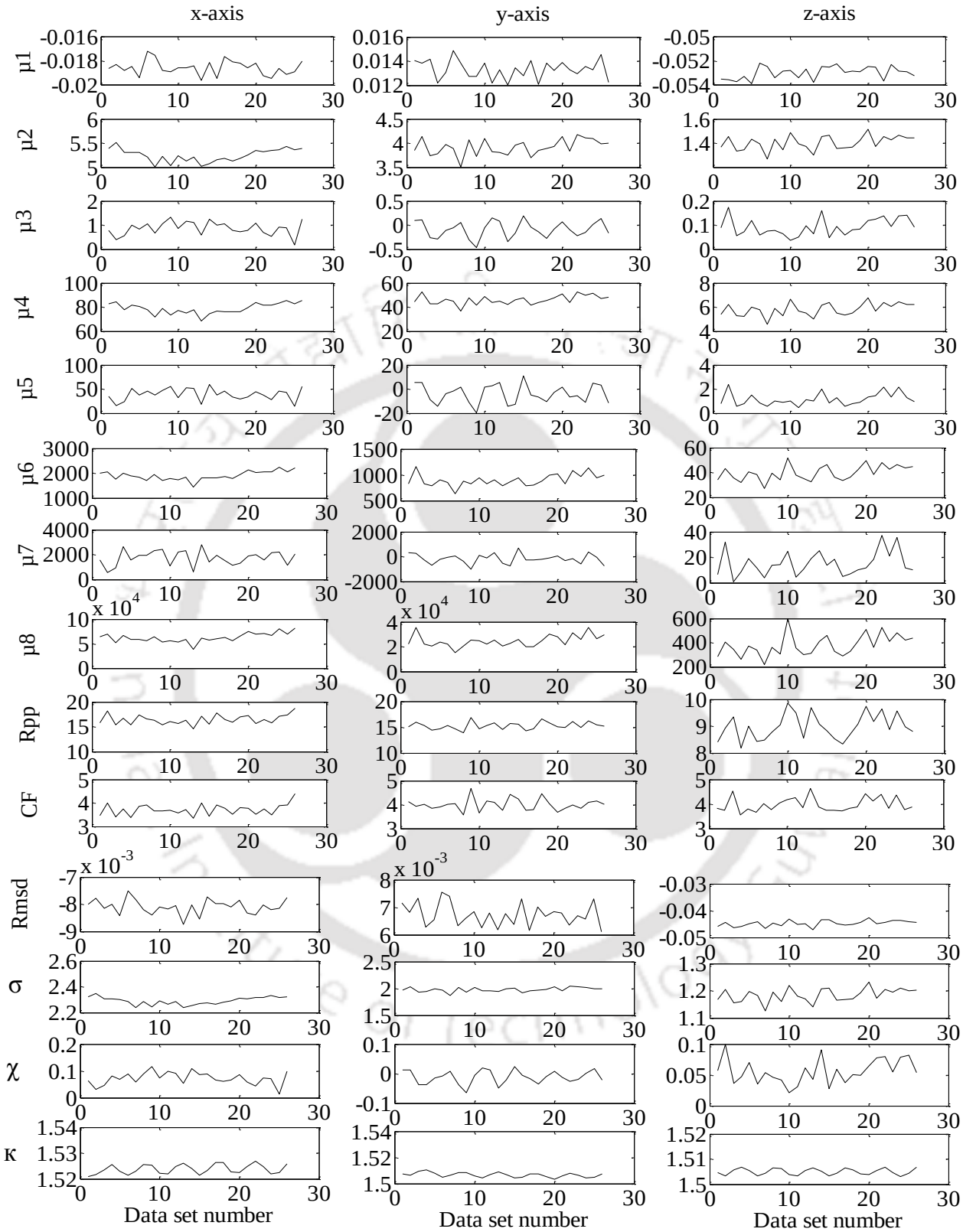

Figure A.1 Time domain features of acquired vibration signals for BF at 40 Hz and T_3

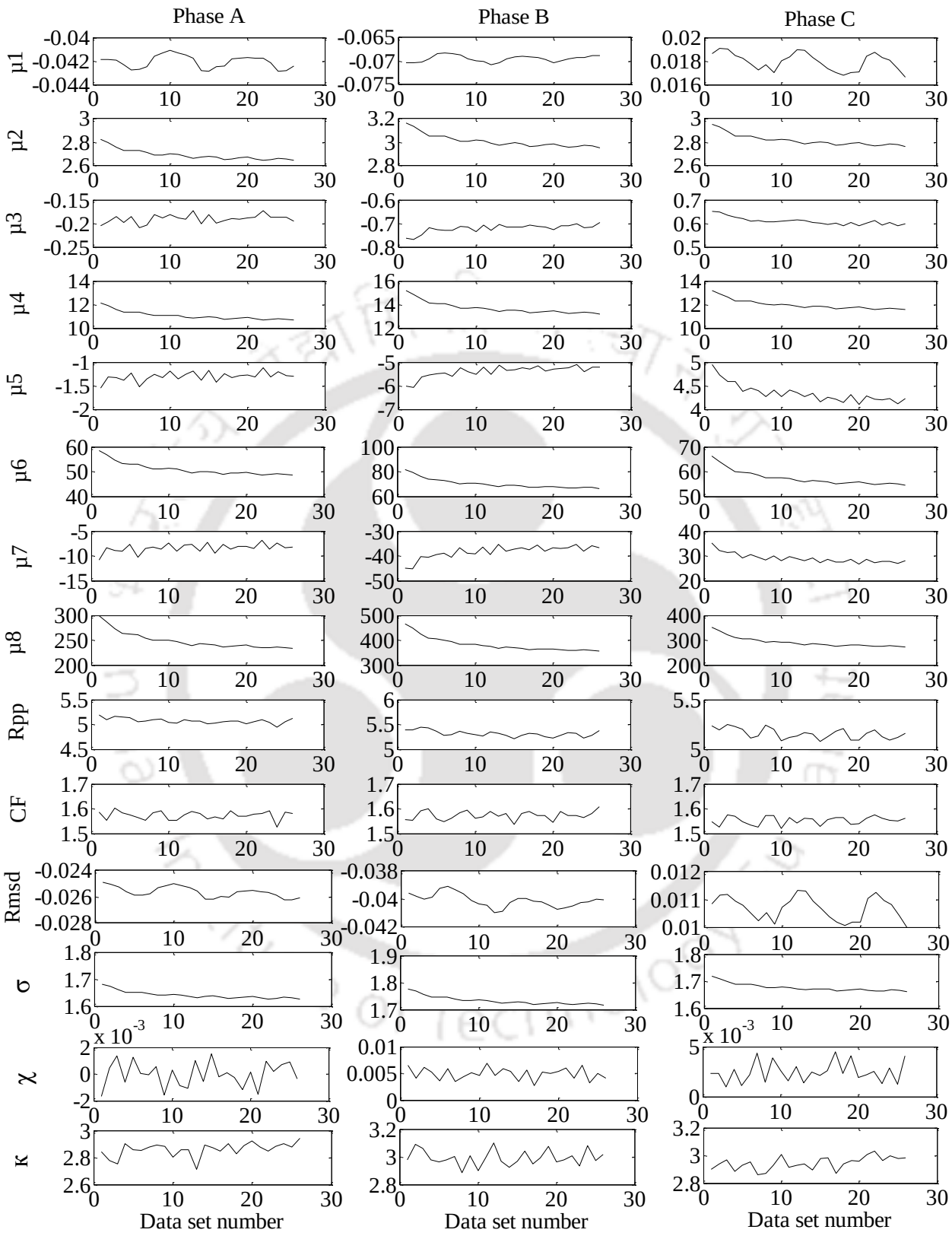

Figure A.2 Time domain features of acquired current signals for BF at 40 Hz and T_3

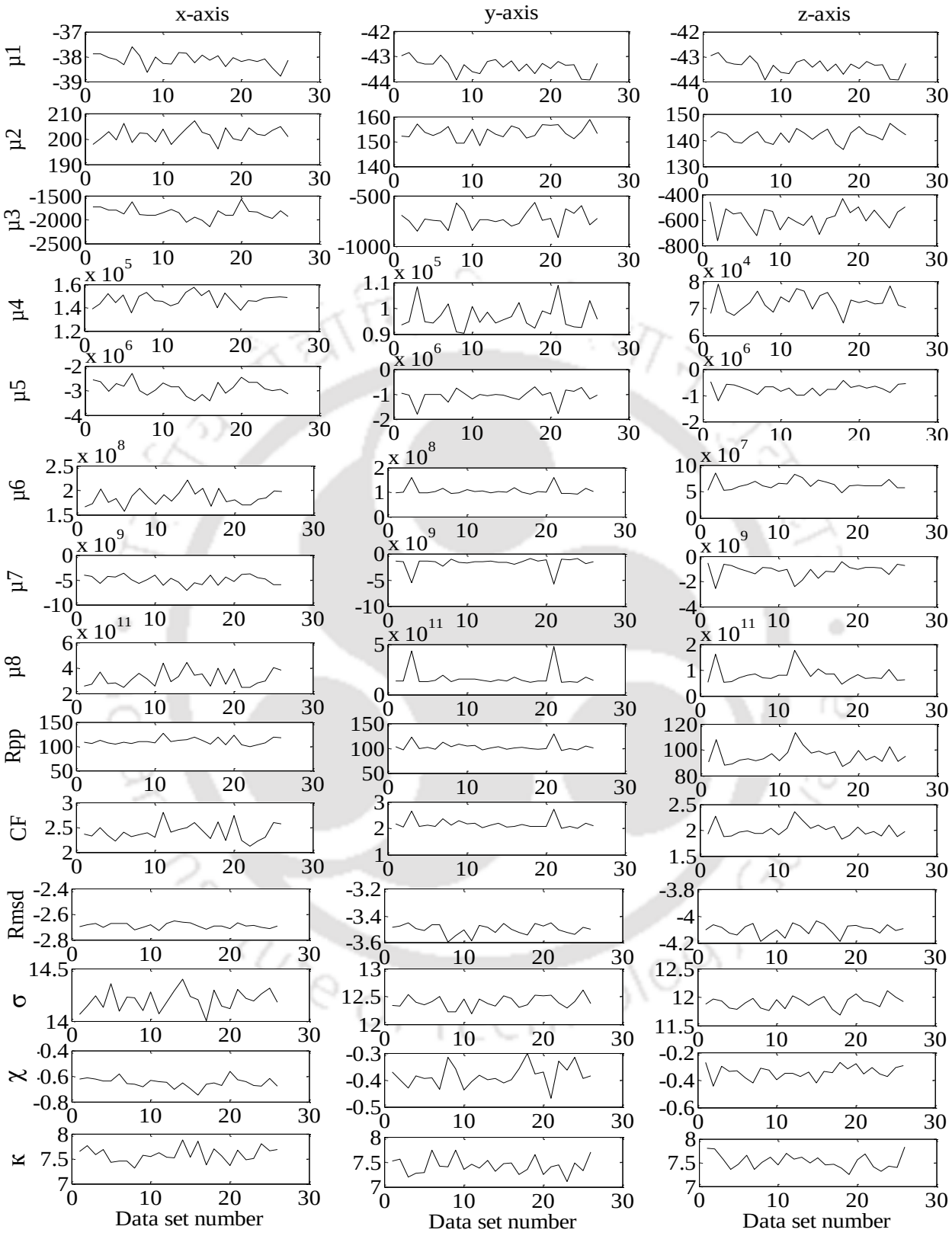

Figure A.3 Frequency domain features of acquired vibration signals for BF at 40 Hz and T_3

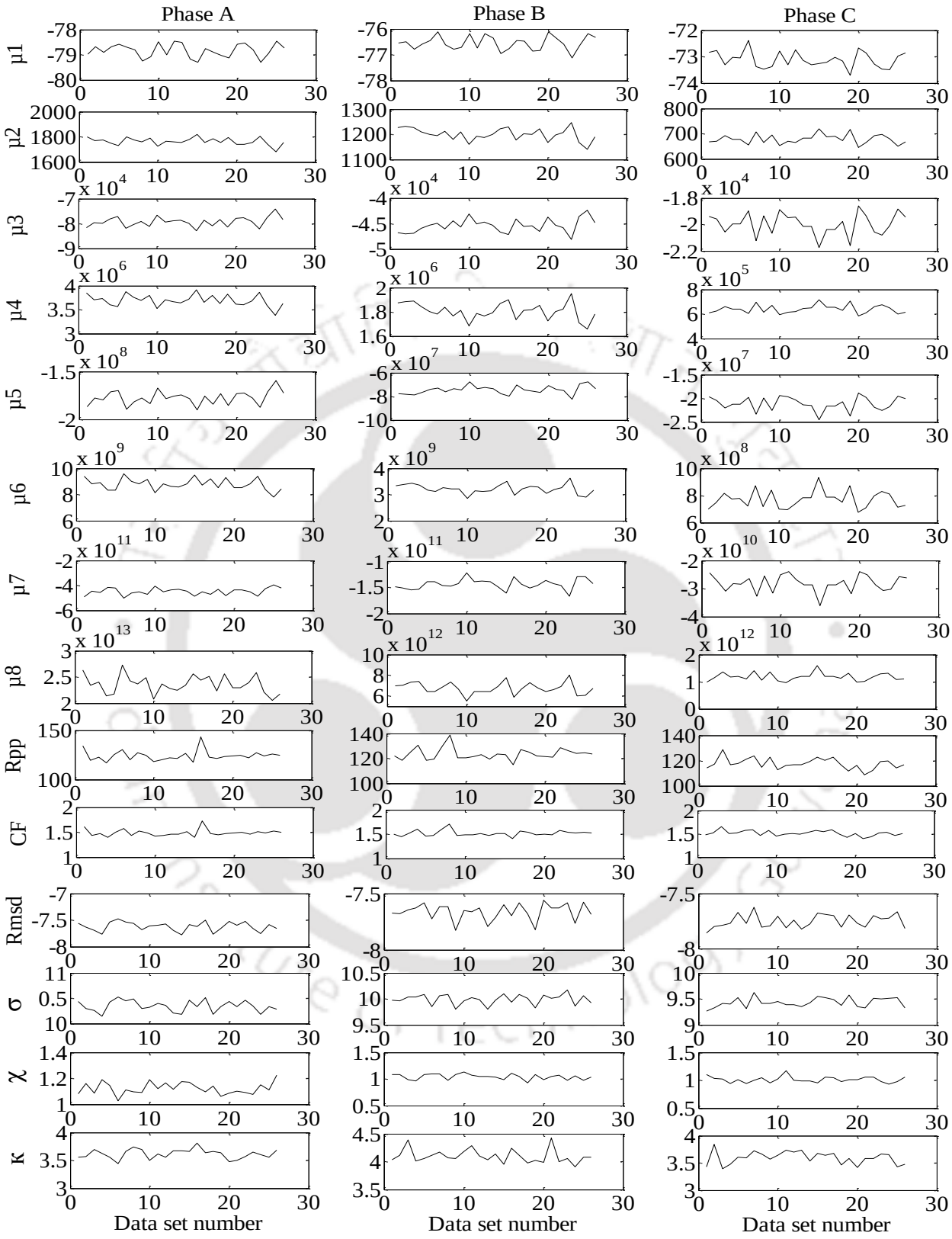

Figure A.4 Frequency domain features of acquired current signals for BF at 40 Hz and T_3

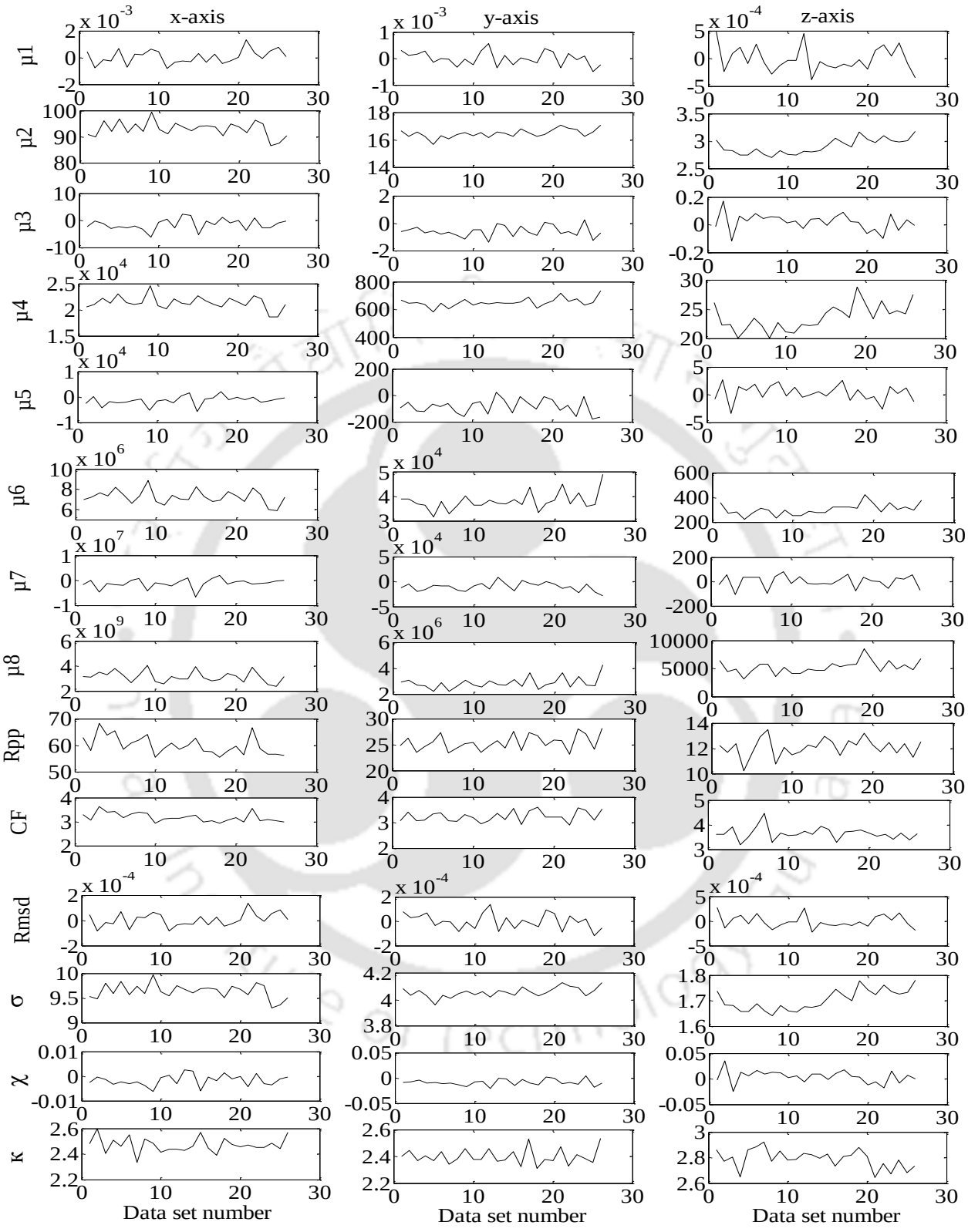

Figure A.5 Features from Haar wavelet coefficients of vibration signal from BF at 40 Hz and T_3

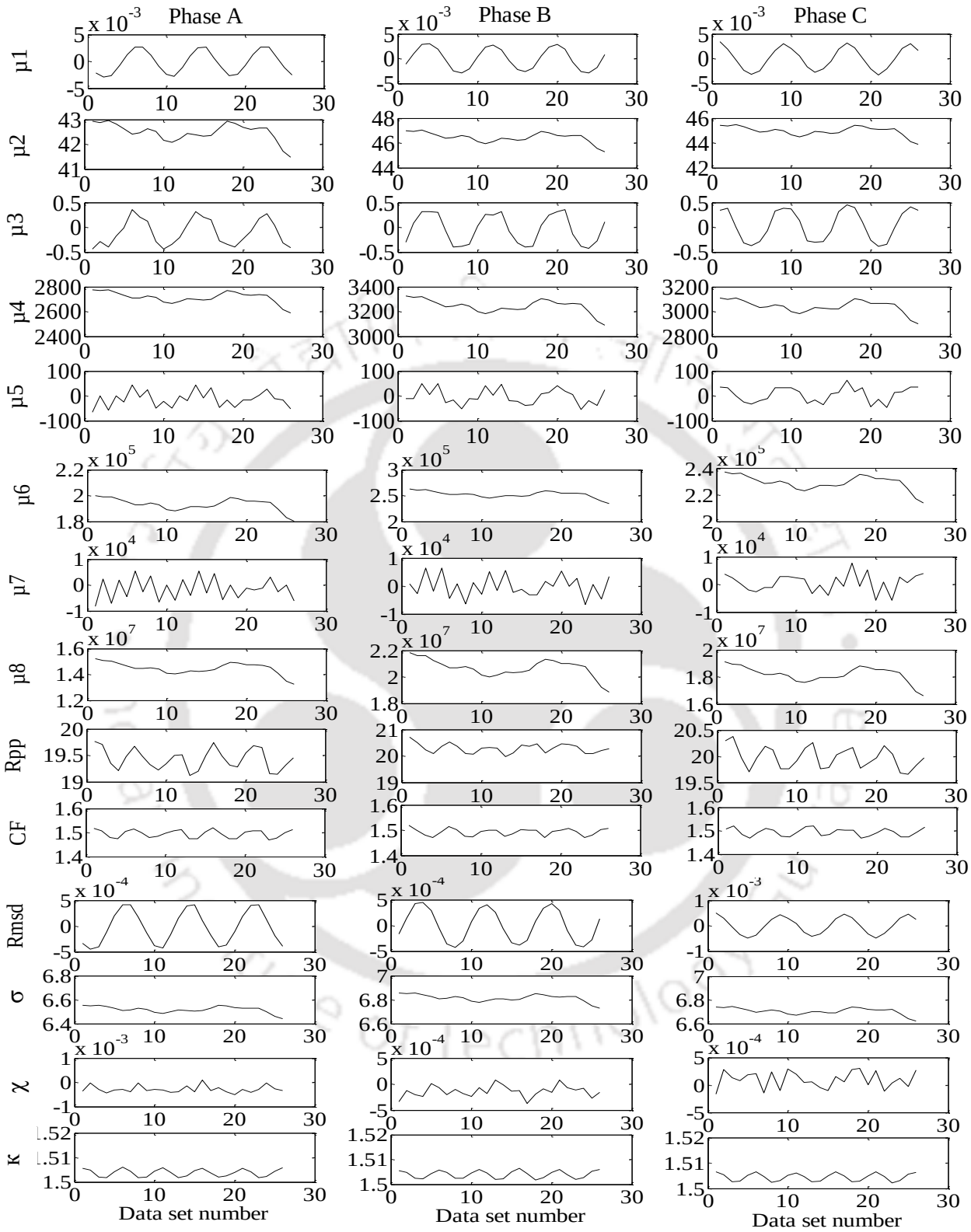

Figure A.6 Features from Haar wavelet coefficients of current signal from BF at 40 Hz and T_3

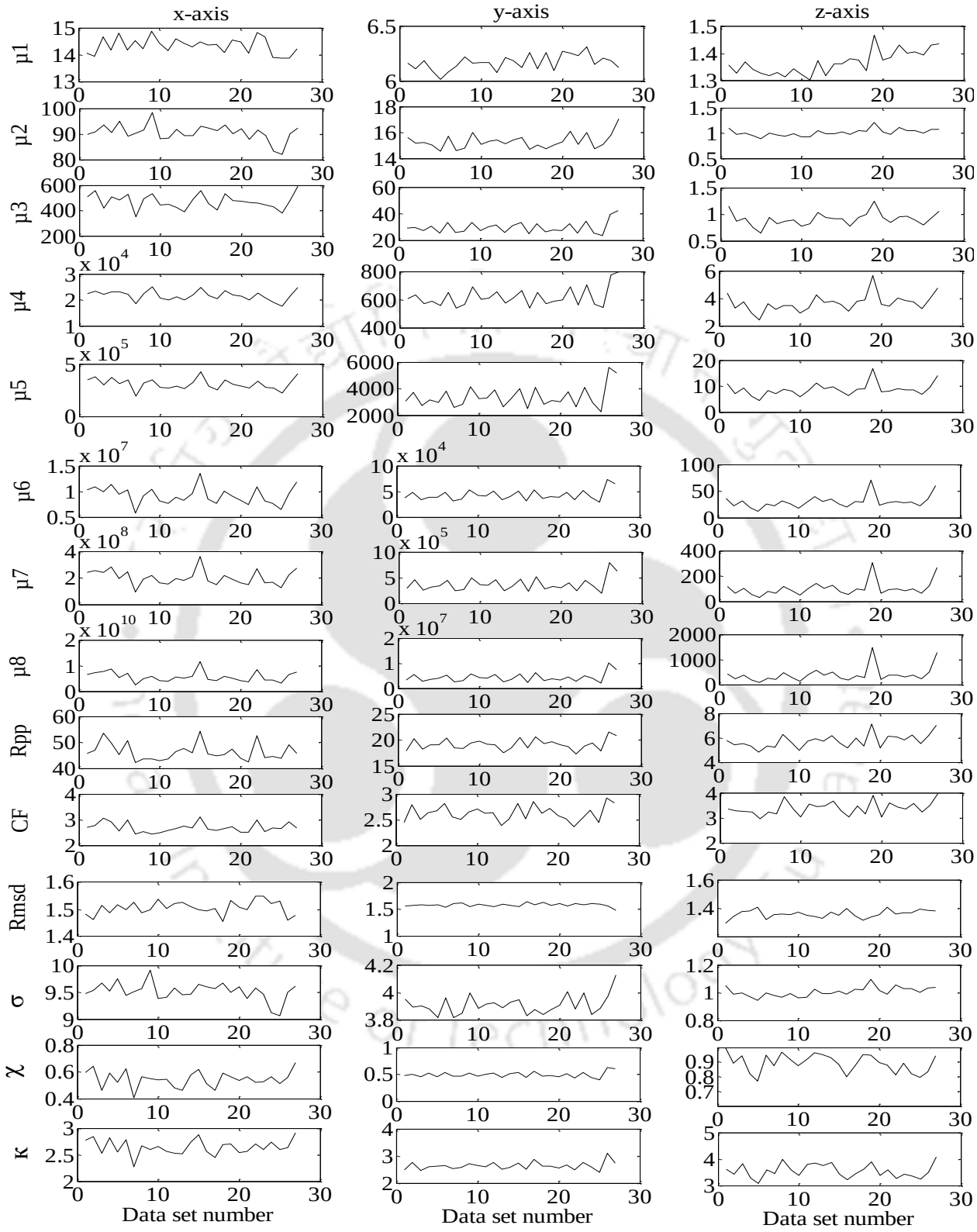

Figure A.7 Features from Haar wavelet coefficients of vibration signal from BF at 40 Hz and T_3

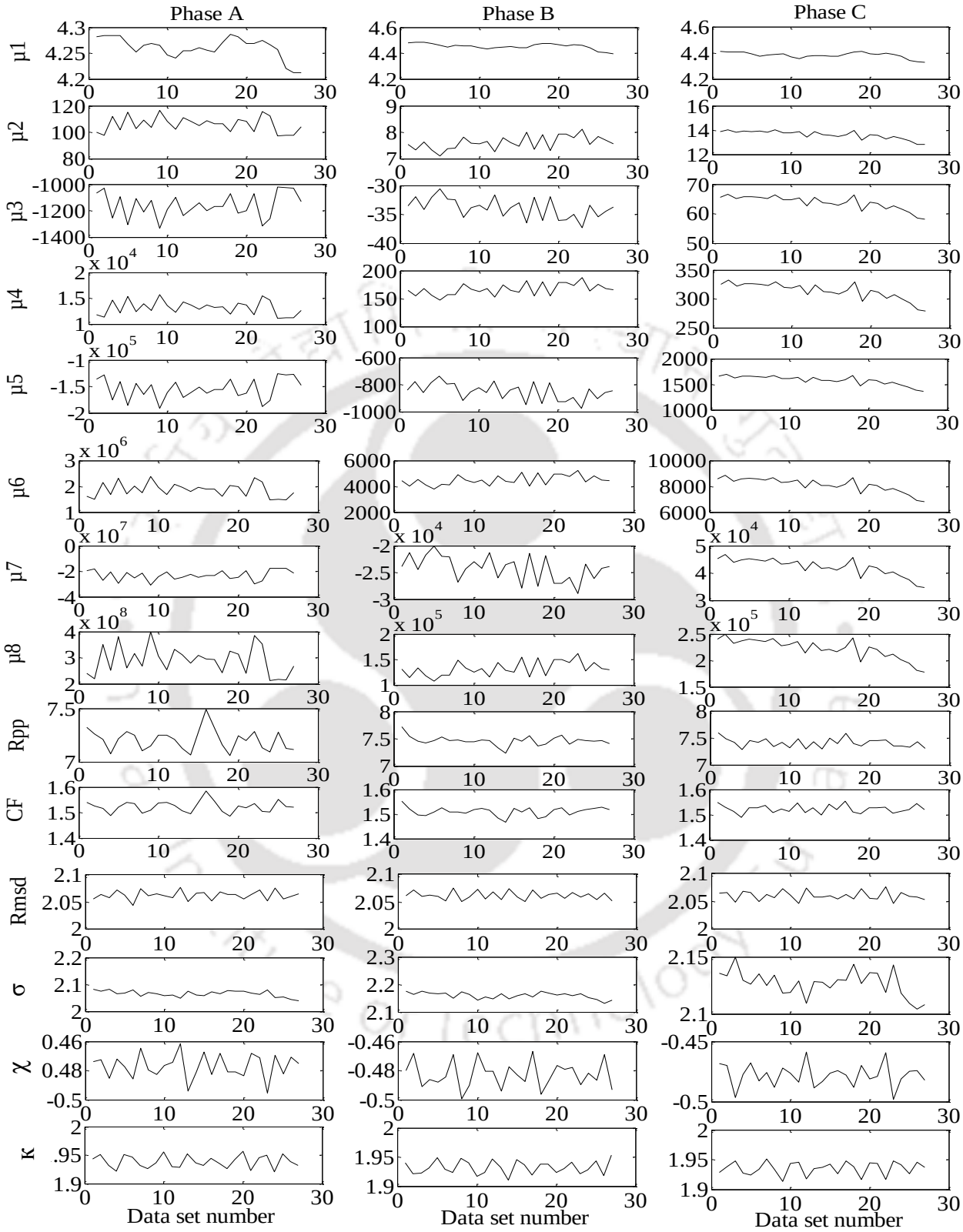

Figure A.8 Features from Haar wavelet coefficients of current signal from BF at 40 Hz and T_3

Publication from the Present Thesis

Journals:

1. Gangsar, P., and Tiwari, R (2016). "Taxonomy of induction-motor mechanical-fault based on time-domain vibration signals by multiclass SVM classifiers". Intelligent Industrial Systems, 2(3), 269-281.

2. Gangsar, P., and Tiwari, R. (2017). "Comparative investigation of vibration and current monitoring for prediction of mechanical and electrical faults in induction motor based on multiclass-support vector machine algorithms". Mechanical Systems and Signal Processing, 94, 464-481.

3. Gangsar, P., & Tiwari, R. (2018). "Multi-fault diagnosis of induction motor at intermediate operating conditions using wavelet packet transform and support vector machine". Journal of Dynamic Systems, Measurement, and Control, 140(8), 081014.

4. Gangsar, P., and Tiwari, R. (2016) "On-line diagnostics of mechanical and electrical faults in induction motor using multiclass support vector machine algorithms based on frequency domain vibration and current signals". ASCE-ASME Journal of Risk and Uncertainty in Engineering Systems, Part B: Mechanical Engineering/Doc. ID: 1000838144/RISK-16-1141. (Communicated).

5. Gangsar, P., and Tiwari, R. (2017). "Diagnostics of mechanical and electrical faults in induction motors using wavelet based features of vibration and current through support vector machine algorithms". Journal of the Brazilian Society of Mechanical Sciences and Engineering, BMSE-D-18-00199. (Communicated).

6. Gangsar, P., and Tiwari, R. (2018). “A review of condition monitoring and fault diagnosis methods for induction motors: - state of the art”. (under preparation).

Conferences:

1. Gangsar, P., and Tiwari, R. (January 2016). “Diagnosis of multiple faults in induction motors based on Gram-Charlier orthogonal expansion coefficients of vibration signals using support vector machine algorithms”. National Symposium on Rotor Dynamics- NSRD, January 5-6, 2016, NIT Rourkela, Odisha, India.

2. Gangsar, P., and Tiwari, R. (September 2016). “Induction motor electrical-fault identification based on vibration monitoring and one-verses-one multiclass SVM”. Vibrations in Rotating Machinery - VIRM 11, September 13-15, 2016, University of Manchester, United Kingdom.

3. Gangsar, P., and Tiwari, R. (October 2016). “Load independent fault classification of induction motor based on vibration and current signals using SVM algorithm”. International Conference in Condition Monitoring-ICCM, October 25-26, 2016, GITAM University, Visakhapatnam, AP, India

4. Gangsar, P., and Tiwari, R. (December 2017). “Analysis of time, frequency and wavelet based features of vibration and current signals for multi-fault diagnosis of induction motors using SVM”. Gas Turbine India Conference- GTIndia 2017, December 7-8, 2017, Bangalore, India.

5. Gangsar, P., and Tiwari, R. (November-December 2017). “Effect of frequency resolution on intelligent multiple fault diagnosis of induction motor based on support vector machine algorithm”. 13th International Conference on Vibration Problems-ICOVP 2017, 29th November-2nd December, 2017, Indian Institute of Technology Guwahati, Assam, India.

6. Gangsar, P., and Tiwari, R. (December 2017). “Intelligent mechanical and electrical fault diagnosis in induction motor using wavelet packet and support vector machine”. National Symposium on Rotor Dynamics- NSRD 2017, December 12th to 13th, 2017, IIT Patna, India.

7. Gangsar, P., and Tiwari, R. (September 2018). “Performance analysis of support vector machine and wavelet packet transform based fault diagnostics of induction motor at various operating conditions”. International Federation for the Promotion of Mechanism and Machine Science- IFToMM 2018, September 23th to 27th, 2018, Rio de Janeiro, Brazil. (submitted)